Targeted delivery of spironolactone for the treatment of cutaneous and ocular diseases involving mineralocorticoid receptor over-activation

Dahmana, Naoual

UNIVERSITÉ DE GENÈVE
FACULTÉ DES SCIENCES
Section de Sciences Pharmaceutiques
Laboratoire de Biochimie Pharmaceutique
Professeur Yogeshvar N. Kalia

Targeted delivery of spironolactone for the treatment of cutaneous and ocular diseases involving mineralocorticoid receptor over-activation

THÈSE

présentée à la Faculté des sciences de l'Université de Genève pour obtenir le grade de Docteur ès sciences, mention sciences pharmaceutiques

par

Naoual Dahmana
de
Béjaïa (Algérie)

Thèse N° 5234

Genève
Atelier de reproduction Repromail
2018

UNIVERSITÉ DE GENÈVE

FACULTÉ DES SCIENCES

DOCTORAT ÈS SCIENCES, MENTION SCIENCES PHARMACEUTIQUES

Thèse de Madame Naoual DAHMANA

intitulée :

«Targeted Delivery of Spironolactone for the Treatment of Cutaneous and Ocular Diseases Involving Mineralocorticoid Receptor Over-activation»

La Faculté des sciences, sur le préavis de Monsieur Y. KALIA, professeur associé et directeur de thèse (Section des sciences pharmaceutiques), Monsieur E. ALLÉMANN, professeur ordinaire (Section des sciences pharmaceutiques), Monsieur B. VERRIER, professeur (Institut de Biologie et de Chimie des Protéines, Université de Lyon, Lyon, France) et Monsieur G. SCHWACH, docteur (Pharmaceutical Development & Supplies, P T D Biologics Europe, F. Hoffmann-La Roche, Phamaceuticals Division, Basel, Switzerland,), autorise l'impression de la présente thèse, sans exprimer d'opinion sur les propositions qui y sont énoncées.

Genève, le 22 juin 2018

Thèse - 5234 -

Le Décanat

N.B. - La thèse doit porter la déclaration précédente et remplir les conditions énumérées dans les "Informations relatives aux thèses de doctorat à l'Université de Genève".

A mon père, parti trop tôt.

A mon oncle qui m'a donné l'amour d'un père.

A mon grand-père sans qui je ne serais pas arrivée là.

“Ne perdez pas confiance durant les périodes de stagnation et de frustration. Il y a un temps pour chaque chose et chaque chose se fait en son temps…
Gardez confiance même si c’est le calme plat en surface, car dans les profondeurs invisibles, votre avenir est en train de se tramer.”
A.C. Ping

“Once you realize that the road is the goal and that you are always on the road, not to reach a goal, but to enjoy its beauty and its wisdom, life ceases to be a task and becomes natural and simple, in itself an ecstasy.”
Nisargadatta Maharaj

“It always seems impossible until it’s done.”
Nelson Mandela

Table of contents

ABBREVIATIONS

11β-HSD2	11β-hydroxysteroid dehydrogenase type II
BSA	Bovine serum albumin
CAN	Canrenone
CANK	Potassium canrenoate
CLSM	Confocal laser scanning microscopy
CMC	Critical micelle concentration
d_n	Number weighted particle diameter
DXM	Dexamethasone
FDA	Food and drug administration
GC	Glucocorticoid
GR	Glucocorticoid receptor
H_2O	Water
HexPLA	Hexyl-substituted-poly(lactic acid)
IC_{50}	Half maximal inhibitory concentration
ICH	International conference of harmonisation
K_d	Dissociation constant at equilibrium
LOD	Limit of determination
LOQ	Limit of quantification
LLOQ	Lower limit of quantification
MC	Mineralocorticoid
MeOH	Methanol
MeT	17α-methyltestosterone
mPEG-dihexPLA	Methoxy-poly(ethylene glycol)-di-hexyl-substituted-poly(lactic acid)
MR	Mineralocorticoid receptor
MRA	Mineralocorticoid receptor antagonist
MRM	Multiple reaction monitoring
PBS	Phosphate buffered saline
PDI	Polydispersity index
PON	Paraoxonase
PSU	Pilosebaceous unit
rpm	Revolution per minute
RSD	Relative standard deviation
RT	Room temperature
SC	Stratum corneum
SD	Standard deviation
SIR	Selected ion recording
SPL	Spironolactone
TEM	Transmission Electron Microscopy
TMSPL	7α-thiomethylspironolactone
UHPLC-UV	Ultra-High Performance Liquid Chromatography coupled with UV detection
UHPLC-ESI-MS	Ultra-High Performance Liquid Chromatography tandem Electrospray Ionization Mass Spectroscopy
UV	Ultra violet
Z_{av}	Intensity weighted mean hydrodynamic particle diameter

RÉSUMÉ

Le récepteur minéralocorticoïde (RM) et son ligand physiologique, l'aldostérone, jouent un rôle important dans l'équilibre hydrosodé de l'organisme. Les glucocorticoïdes (GC ; synthétiques ou l'hormone physiologique, le cortisol) ont aussi une affinité aux RM. Dans les organes tel que le rein et le colon où le RM exerce sa fonction principale, il existe une enzyme qui protège son l'activation par d'autres hormones stéroïdiennes, appelée 11β-hydroxystéroïde déshydrogénase type 2 (11β-HSD2), en revanche dans d'autres organes où le RM est aussi exprimé tel que le cœur, les vaisseaux sanguins, l'œil et la peau ; cette enzyme n'est que très peu exprimée ne protégeant plus le RM contre l'occupation indésirable des glucocorticoïdes. Par conséquent, le RM dans ces organes est susceptible d'être occupé en permanence par des glucocorticoïdes ce qui conduit à sa suractivation. Des études récentes ont démontré que la suractivation du RM par les GC induit différentes maladies oculaires et cutanées notamment chez les patients qui sont sous un traitement prolongé avec les glucocorticoïdes. De plus, plusieurs études ont montré l'intérêt de l'utilisation des antagonistes du récepteur minéralocorticoïde (ARM) comme stratégie thérapeutique pour prévenir l'occupation des RM par les GC.

Le but de cette thèse était de développer des nouvelles formulations du puissant antagoniste du récepteur minéralocorticoïde, la spironolactone, en utilisant des polymères biodégradables et biocompatibles pour une administration ciblée de la spironolactone dans l'œil et dans la peau afin de traiter des maladies liées à la suractivation du récepteur minéralocorticoïde induite par les glucocorticoïdes ; tel que la choriorétinopathie séreuse centrale et le retard dans la cicatrisation des plaies cornéennes et cutanées.

Le chapitre I décrit le développement d'une méthode bio-analytique UHPLC-MS rapide et sensible pour la détection simultanée de la spironolactone (SPL) et de ses métabolites actifs ; La 7α-thiométhylspironolactone (TMSPL) et la canrénone (CAN), conjointement avec un autre ARM ; le canrénoate de potassium (CANK), la dexaméthasone (DXM) comme glucocorticoïde et un étalon interne, la 17α-méthyltestostérone (MeT). La détection simultanée de la SPL et de ses métabolites est cruciale pour comprendre l'effet pharmacologique observé suite à l'administration de la SPL puisque cette dernière exerce son action anti-minéralocorticoïde en soi mais aussi via ses deux principaux métabolites actifs ; TMSPL et CAN. Bien que plusieurs méthodes UHPLC-MS aient été décrites pour la détection de la SPL et / ou de ses métabolites, elles ne nous convenaient pas car elles ne permettaient pas la détermination simultanée de la SPL, TMSPL et CAN, manquaient de sensibilité ou encore étaient trop longues. Nous avons décrit pour la première fois le développement et la validation d'une nouvelle méthode bio-

analytique UHPLC-MS pour la détection simultanée de la spironolactone et de ses métabolites actifs ; du canrénoate de potassium et de la dexaméthasone dans les tissus oculaires. Cette méthode a été validée selon les directives de la FDA et a permis la séparation des six analytes dans un temps relativement court de 5 min et a montré une spécificité par rapport aux composants de la matrice cornéenne. La méthode était linéaire entre 5 et 1000 ng/mL et une limite inférieure de quantification de 5 ng/mL. Une méthode simple d'extraction des analytes de la cornée a également été validée.

L'un des domaines où les GC sont largement prescrits est l'ophtalmologie. Ils sont principalement administrés par voie topique pour prévenir et supprimer l'inflammation post-opératoire ; cependant, ils sont connus pour provoquer un retard dans la cicatrisation (ré-épithélialisation) des plaies cornéennes. Par conséquent, la co-administration topique de la spironolactone avec les glucocorticoïdes pourrait aider le patient à bénéficier des effets anti-inflammatoires des GC tout en évitant leurs effets secondaires délétères sur le processus de cicatrisation de la cornée. Les gouttes ophthalmiques sont la forme la plus pratique pour l'administration topique des médicaments dans l'œil ; cependant, la spironolactone est un composé peu soluble dans l'eau. La stratégie utilisée pour développer et optimiser les gouttes ophtalmiques de spironolactone basée sur des micelles polymériques (mPEG-dihexPLA) est décrite dans le **chapitre II**. L'étude de tolérance et d'efficacité *in vivo* des micelles de spironolactone (0,1%, p/v) pour traiter le retard de cicatrisation de la cornée induit par la dexaméthasone a été étudiée chez des lapins blancs de Nouvelle-Zélande. La taille des micelles de spironolactone était d'environ 20 nm et la formulation avaient une stabilité préliminaire d'au moins 12 mois à 5°C. L'étude préclinique a démontré que la formulation micellaire à 0,1% de spironolactone était bien tolérée par la cornée du lapin ; aucune réaction n'ayant été observée après une instillation quotidienne multiple pendant 5 jours. L'étude a également démontré de façon significative l'efficacité de la co-administration des micelles à 0,1% de spironolactone sur le rétablissement de la cicatrisation retardé de la cornée induite par la dexaméthasone avec un pourcentage de ré-épithélialisation statistiquement équivalent au contrôle (96,9 ± 7,3% *versus* 99,5 ± 1,0%, p> 0,05). La comparaison des efficacités de la spironolactone et du canrénoate de potassium (un précurseur hydrosoluble de la canrénone) pour rétablir la cicatrisation retardée induite par la dexaméthasone a confirmé que la première était plus efficace. Les résultats ont mis en évidence la supériorité du metabolite 7α-thiométhylspironolactone sur la canrenone en tant qu'antagoniste du récepteur minéralocorticoïde, ce qui explique l'efficacité supérieure de la spironolactone par rapport au canrénoate de potassium pour contrer la suractivation du RM induite par les glucocorticoïdes. Enfin, les résultats préliminaires soutenaient que

l'administration concomitante d'antagonistes du récepteur minéralocorticoïde à des patients sous un traitement prolongé avec des glucocorticoïdes pourrait prévenir les effets délétères des glucocorticoïdes sur les processus de cicatrisation des plaies cornéennes.

Un autre effet secondaire des GC dans l'œil est la choriorétinopathie séreuse centrale (CRSC), caractérisée par une accumulation de fluide sous-rétinien suivie d'un décollement de la rétine dans la macula, provoquant des troubles de la vision. La CRSC peut devenir chronique et conduire à une cécité vu qu'il n'existe pas de traitement de référence. Des études récentes ont montré que la CRSC pourrait être due à l'activation inappropriée des récepteurs des minéralocorticoïdes par les glucocorticoïdes (le cortisol ou les médicaments de synthèse couramment utilisés en ophtalmologie) dans les vaisseaux choroïdiens, entraînant une dilatation et une fuite de liquide. Des études pilotes ont montré que l'administration d'ARM entraînait la résorption du liquide sous-rétinien ; Cependant, la plupart des ARM sont administrés par voie orale à des doses élevées pour obtenir un effet thérapeutique dans l'œil, ce qui provoque des effets secondaires dus à l'exposition systémique. Par conséquent, le développement d'une formulation de spironolactone basée sur un polymère à libération prolongée pour une injection intravitréenne dans l'œil pourrait être une stratégie thérapeutique prometteuse avec une amélioration de l'observance et de la sécurité du patient. **Le chapitre III** traite du développement et de l'optimisation d'une formulation à libération prolongée de la spironolactone basée sur un polymère biodégradable et biocompatible (hexPLA) pour injection intravitréenne (IVT) et l'étude *in vivo* chez le rat de la tolérance et de la biodistribution de la spironolactone et de ses métabolites dans les différents tissus oculaires durant un mois après une seule injection intravitréenne d'une gouttelette de 5 µL de la formulation SPL-hexPLA (5% p/p). L'évaluation de la tolérance a été réalisée en utilisant l'imagerie rétinienne *in vivo* et l'histologie. Le profil de libération *in vitro* de la formulation SPL-hexPLA (5% p/p) a montré une libération prolongée de la SPL jusqu'à 65 jours, avec une libération rapide durant la première semaine suivie d'un profil de libération du premier ordre. La biodistribution *in vivo* de la SPL et de ses métabolites dans les tissus oculaires a montré une corrélation avec le profil de libération obtenu *in vitro*. La SPL et ses métabolites ont été détectés dans tous les tissus oculaires 3 jours et 7 jours après l'IVT ; alors que 31 jours après l'IVT, la spironolactone et la canrénone étaient principalement détectées dans la choriorétine. Les résultats ont également mis en évidence la voie de clairance de la spironolactone et de ses métabolites de l'œil impliquant les voies antérieure et postérieure au cours de la première semaine, puis principalement le segment postérieur au cours des dernières semaines. Cette étude a montré

qu'une seule IVT de la formulation SPL-hexPLA (5% p/p) chez le rat entraîne une libération prolongée jusqu'à un mois de quantités thérapeutiques de la spironolactone dans la rétine et à la choroïde où le RM est situé, et ce sans exposition systémique. Cette formulation pourrait donc être d'un intérêt clinique pour le traitement de la choriorétinopathie séreuse centrale.

L'effet délétère des CG sur le processus de cicatrisation des plaies affecte également la peau. Etant donné les résultats positifs sur la cicatrisation des plaies cornéennes obtenus avec la co-administration des micelles de spironolactone avec la dexaméthasone chez le lapin, nous avons voulu tester l'efficacité de cette formulation pour traiter le retard de cicatrisation des plaies cutanées. Le **chapitre IV** décrit le développement de la forme hydrogel des micelles de spironolactone pour une application topique sur la peau et les études *ex vivo* de déposition et de perméation utilisant des cellules de Franz. Tout d'abord, le récepteur minéralocorticoïde a été localisé dans la peau en utilisant un marquage par immunofluorescence. Celui-ci s'est révélé être situé dans les follicules pileux et dans les glandes sudoripares de la peau porcine. La taille des micelles de SPL était d'environ 20 nm et la viscosité de l'hydrogel était de 20 Pa.s. Les études de biodistribution ont montré l'apport de quantités thérapeutiques de SPL à l'épiderme et au derme supérieur (jusqu'à une profondeur de peau de 400 μm). D'autre part, ces micelles ont montré de manière significative une déposition ciblée de SPL dans l'unité pilosébacé (UPS) avec une déposition jusqu'à 5 fois plus élevée dans l'UPS par rapport aux biopsies cutanées qui ne contenaient pas d'UPS. L'administration folliculaire ciblée de SPL par les micelles permet l'antagonisme spécifique du RM situé dans la peau, améliorant ainsi le rapport bénéfice/risque en évitant les effets secondaires liés à l'exposition systémique. La co-administration de cette formulation avec les glucocorticoïdes pourrait donc être d'un grand bénéfice clinique aussi pour le traitement du retard de la cicatrisation des plaies cutanées impliquant la suractivation du RM par les GC. Cette formulation peut également être considérée comme une stratégie prometteuse pour traiter les diverses maladies cutanées associées au récepteur androgène, aussi situé dans l'UPS, telles que l'acné, l'alopécie androgénique et l'hirsutisme, puisque la SPL est également un puissant anti-androgène.

En conclusion, différentes formulations de spironolactone à base de polymères biodégradables ont été développées pour une administration ciblée dans l'œil et sur la peau, évitant ainsi les effets secondaires associés à l'exposition systémique. Aux vues de la libération prolongée de la spironolactone pendant au moins un mois après une seule injection intravitréenne du polymère biodégradable hexPLA chargé de spironolactone, cette formulation pourrait être considérée comme un potentiel traitement de la choriorétinopathie séreuse centrale ; toutefois, davantage

d’études précliniques sont nécessaires pour évaluer son efficacité. L'administration concomitante des micelles de spironolactone avec les glucocorticoïdes pourrait être d’un intérêt clinique pour le traitement des retards de la cicatrisation cornéenne induits par les glucocorticoïdes. L'efficacité de cette formulation pour améliorer la cicatrisation des plaies cutanées, notamment chez les patients diabétiques, est prévue d’être évaluée *in vivo*.

SUMMARY

The mineralocorticoid receptor (MR) and its physiological ligand, aldosterone, play an important role in the extracellular fluid volume homeostasis in the body. Glucocorticoids (GC, synthetic or the physiological hormone, cortisol) also have an affinity for the MR. In organs such as the kidney and the colon where MR exerts its main function, GC binding to the MR is prevented by the enzyme 11β-hydroxysteroid dehydrogenase type 2 (11β-HSD2); however, in other organs where the MR is also expressed such as the heart, the vessels, the eye and the skin; this enzyme is poorly expressed, hence no longer protecting the MR against illicit occupation by the glucocorticoids. Therefore, the MR in these organs is likely to be permanently occupied by glucocorticoids which leads to its overactivation. Recently, MR was found to mediate different ocular and skin diseases due to off-target binding of the glucocorticoids to the MR, particularly in patients who are undergoing prolonged glucocorticoid therapy. Several recent studies have shown the benefit of the use of mineralocorticoid receptor antagonists (MRA) as a therapeutic strategy to off-set the illicit occupancy of the MR by the GC.

The aim of this thesis was to develop novel formulations of the potent mineralocorticoid receptor antagonist, spironolactone, using biodegradable and biocompatible polymers for the site-specific delivery of spironolactone to the eye and to the skin for the treatment of diseases related to overactivation of the mineralocorticoid receptor induced by glucocorticoids, such as central serous chorioretinopathy, corneal and cutaneous delayed wound healing.

Chapter I describes the development of a fast and sensitive UHPLC-MS bio-analytical method for the simultaneous detection of spironolactone (SPL) and its active metabolites; 7α-thiomethylspironolactone (TMSPL) and canrenone (CAN), together with the water-soluble precursor of CAN; potassium canrenoate (CANK), the glucocorticoid dexamethasone (DXM) and an internal standard, 17α-methyltestosterone (MeT). Simultaneous detection of SPL and its metabolites is crucial for understanding the pharmacological effect observed following administration of SPL since the later exerts its anti-mineralocorticoid action *per se* but also via its two major active metabolites; TMSPL and CAN. Although several UHPLC-MS methods have been reported for the detection of SPL and/or its metabolites, they were not suitable for our use since they either did not allow the simultaneous determination of SPL, TMSPL and CAN, lacked sensitivity or were time consuming. We have reported for the first time the development and validation a novel UHPLC-MS bio-analytical method for the simultaneous detection of spironolactone and its active metabolites; potassium canrenoate and dexamethasone in ocular tissues. This method was validated according to the FDA guidelines and allowed the separation of the six analytes within a relatively short-time of 5 min and showed

specificity with regards to corneal matrix components. The method displayed linearity within the range of 5-1000 ng/mL and sensitivity with lower limit of quantification (LLOQ) of 5 ng/mL. A simple one-step extraction method of the analytes from the cornea was also validated.

One of the fields where GC are widely prescribed is ophthalmology. They are mostly applied topically to prevent and suppress post-operative inflammation; however, they are associated with delayed corneal re-epithelialization. Hence, topical co-administration of spironolactone together with the glucocorticoid therapy might help patient to still benefit from the anti-inflammatory effects of GC while preventing their deleterious side effects on the corneal wound healing process. Eye drops are the most convenient form for topical delivery to the eye; however, spironolactone is a poorly-water soluble compound. The strategy used to develop and optimize spironolactone eye drops based on polymeric micelles (mPEG-dihexPLA) is reported in **Chapter II.** The tolerance and efficacy study of the spironolactone micelles (0.1%, w/v) to prevent the dexamethasone-induced corneal delayed wound healing was investigated in New Zealand white rabbits. Spironolactone micelle size was around 20 nm and showed a preliminary stability of at least 12 months at 5°C. The preclinical study demonstrated a good tolerance of the 0.1% spironolactone micellar formulation by the rabbit cornea since no reaction was observed following multiple daily instillation over 5 days. The study also significantly demonstrated the efficacy of the co-administration of the 0.1% spironolactone micelles on off-setting the dexamethasone-induced corneal delayed wound healing with a percentage re-epithelialization that was statistically equivalent to the control (96.9 ± 7.3% versus 99.5 ± 1.0%, $p>0.05$). Comparison of the efficacies of spironolactone and potassium canrenoate (a water-soluble precursor of canrenone) in overcoming the dexamethasone-induced delayed wound healing confirmed that the former had greater efficacy. The results pointed to the greater potency of the metabolite 7α-thiomethylspironolactone over canrenone as a mineralocorticoid receptor antagonist, which explained the superior ability of spironolactone over potassium canrenoate in countering the glucocorticoid-induced over-activation of the MR responsible for the delayed wound healing. Finally, the preliminary results supported that co-administration of mineralocorticoid receptor antagonists to patients under glucocorticoid therapy might prevent the deleterious effects of glucocorticoids on corneal wound healing process.

Another known ocular side effect of the GC is central serous chorioretinopathy (CSRC), characterized by accumulation of subretinal fluid followed by retinal detachment in the macula causing visual disturbance. CSCR may become chronic and may lead to blindness since there is no gold standard treatment. Recent studies showed that CSRC could be due to

mineralocorticoid receptor inappropriate activation by glucocorticoids (physiological cortisol or synthetic drugs routinely used in ophthalmology) in the choroidal vessels, leading to dilatation and fluid leakage. Pilot studies showed that administration of MRA resulted in the resorption of the subretinal fluid; however, most of the MRA are administered orally and high doses are needed to achieve therapeutic effect in the eye. Hence, development of a spironolactone formulation based on a sustained release polymer for intravitreal injection to the eye might be a promising therapeutic strategy for an improved patient compliance and safety. **Chapter III** deals with the development and optimization of spironolactone sustained release formulation based on a biodegradable and biocompatible polymer (hexPLA) for intravitreal injection to the eye and the *in vivo* tolerance and biodistribution study of spironolactone and its metabolites in the rat ocular tissues over one month following single intravitreal injection (IVT) of 5 µL droplet of the formulation SPL-hexPLA (5%, w/w). Tolerance evaluation was performed using *in vivo* retinal imaging and histology. *In vitro* release profile of 5% SPL-hexPLA showed a sustained release of SPL up to 65 days and was characterized by a burst release in the first week followed by a first-order release profile. The *in vivo* biodistribution of SPL and its metabolites in the ocular tissues showed a correlation with the release profile obtained *in vitro*. SPL and its metabolites were detected in all the ocular tissues at 3 days and 7 days post-IVT. At 31 days post-IVT, spironolactone and canrenone were mainly detected in the chorioretina. Results also suggested the clearance pathway of spironolactone and its metabolites from the eye involving the anterior and posterior routes in the first week, then mainly the posterior segment in the last weeks. This study showed that single IVT of SPL-hexPLA (5%, w/w) in rats leads to the sustained delivery of therapeutic amounts of spironolactone up to one month to the retina and the choroid where the MR is located, without systemic exposure, hence this formulation may be of interest for the treatment of central serous chorioretinopathy.

The deleterious effects of the CG on the wound healing process also affects the skin. Given the positive results on the corneal wound healing obtained with the co-administration of the spironolactone micelles together with the GC therapy, we wanted to investigate whether this formulation could be beneficial for patient suffering from cutaneous delayed wound-healing. **Chapter IV** describes the development of hydrogel form of the spironolactone micelles for topical application to the skin and the *ex vivo* skin deposition and permeation studies using Franz cells. First, the mineralocorticoid receptor was localized in the skin using immunofluorescence labelling and was shown to be located in the hair follicles and in the sweat glands of the porcine skin. SPL nanomicelles size was around 20 nm and the viscosity of the

nanomicellar hydrogel was 20 Pa. s. The biodistribution studies showed the delivery of therapeutic amounts of SPL to the epidermis and the upper dermis (up to 400 µm skin depth). More importantly, SPL nanomicelles have shown to significantly target the pilosebaceous unit (PSU) with up to 5-folds higher delivery to the PSU compared to the PSU-free skin biopsies. The targeted transfollicular delivery of SPL by the micelles allows the site-specific antagonism of the MR in the skin, hence improving the benefice/risk balance. Co-administration of this formulation with the glucocorticoid therapy may be of a great clinical benefit for the treatment of cutaneous delayed wound healing involving the overactivation of the MR by the GC. This formulation may also be considered as a promising strategy to treat the various pilosebaceous androgenic-related skin diseases including acne vulgaris, androgenic alopecia and hirsutism, since SPL is also a potent anti-androgenic.

To conclude, different spironolactone formulations based on biodegradable polymers were developed to be site-specifically delivered to the eye and to the skin, thus avoiding the side effects associated with the systemic exposure. Given the prolonged release of spironolactone for at least one month following single intravitreal injection of the biodegradable polymer hexPLA loaded with spironolactone, this formulation could be considered as a potential treatment for central serous chorioretinopathy; However, more preclinical studies are needed to evaluate its efficacy. Co-administration of spironolactone micelles with the glucocorticoids may be of clinical interest for the treatment of the glucocorticoid-induced delayed corneal wound healing. The efficacy of this formulation to improve the cutaneous wound healing, particularly in diabetics, will be evaluated *in vivo*.

INTRODUCTION

1. The mineralocorticoid receptor

The mineralocorticoid receptor (MR) and its physiological ligand aldosterone, the main endogenous mineralocorticoid hormone, are responsible for extracellular fluid homeostasis in the body, and thus blood pressure, by promoting sodium reabsorption in the kidney through upregulation of the epithelial sodium channel (ENaC) and the Na^+-K^+-ATPase pump. Aldosterone is synthesized and secreted from the adrenal cortex in response to hyponatremia (sodium depletion), and a decrease in blood pressure, and is the end-point of the activation of the renin-angiotensin-aldosterone system (RAAS). Increasing aldosterone promotes sodium and water reabsorption in the renal tubules resulting in an increase in blood pressure [1-3].

1.1.Mineralocorticoid receptor-associated diseases

The mineralocorticoid receptor shares structural and functional homology with the glucocorticoid receptor (GR). Aldosterone is the physiological mineralocorticoid ligand for the MR, and cortisol (corticosterone in rodents) is the physiological glucocorticoid ligand for the GR (**Figure 1**). Given the closely related structure of both receptors, cortisol also binds to the MR with high affinity similar to that for GR. However, aldosterone has a lower affinity for the GR [4].

Moreover, the circulating glucocorticoids are 100- to 1000-fold more abundant than aldosterone; hence, off-target and permanent occupancy of the MR by glucocorticoids may occur leading to abnormal MR activity and diseases related to MR overactivation [2].

Off-target occupancy of the MR by glucocorticoids is prevented in mineralocorticoid-sensitive tissues such as the kidney by the enzyme 11β-hydroxysteroid dehydrogenase type 2 (11β-HSD2), which converts the 11β-hydroxy-glucocorticoids into their inactive 11-keto metabolites (cortisone in humans, 11-dehydrocorticosterone in rodents), preventing their binding to MR, which is therefore selectively activated by aldosterone [5, 6]

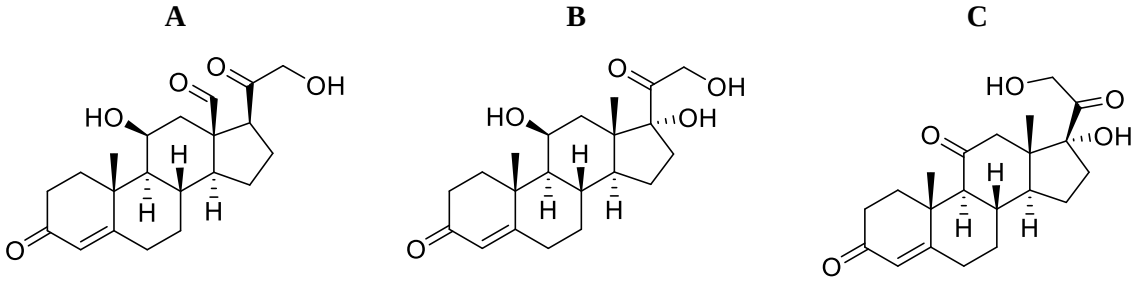

Figure 1. Chemical structure of (A) aldosterone, (B) cortisol and (C) cortisone.

Although the principal physiological functions of the MR are in the kidney and the colon where it is most abundant, it is also expressed to a lower extent in other organs including the heart, blood vessels, skin and the eye [2]. Unlike in the kidney, the enzyme 11β-HSD2 is less co-expressed with the MR in those organs; hence, the specificity of the MR for aldosterone is not ensured, opening the way for GC binding to the MR. Illicit occupancy of the MR is even more likely to occur when circulating GC levels are in excess in the body, which is the case in patients receiving prolonged GC therapy [2, 4].

Synthetic glucocorticoids are among the most widely prescribed drugs in the world. They are given systemically or topically to treat a wide number of inflammatory and autoimmune diseases, allergies and ocular disorders. Apart from their undeniable beneficial anti-inflammatory effects exerted via binding to the glucocorticoid receptor, GC can induce different side effects. Illicit occupancy of the MR in organs where 11β-HSD2 co-expression is low, can lead to cardiovascular, metabolic, renal, ocular and skin diseases [2, 7-13].

1.1.1. Mineralocorticoid receptor-associated ocular diseases

In clinical ophthalmology, synthetic glucocorticoids are routinely used to treat a wide range of ocular diseases. In the anterior segment of the eye, GC are mostly administered topically to prevent and to treat post-operative inflammation of the cornea, keratitis, anterior uveitis, graft rejection and corneal neovascularization. In the posterior segment of the eye, GC are commonly injected into the vitreous for the treatment of macular edema, diabetic retinopathy resistant to anti-VEGF therapy, posterior uveitis and retinal inflammation [14].

Besides their beneficial effects, chronic use of synthetic GC is associated with side effects leading to ocular diseases. In the anterior segment, GC are known to delay corneal wound healing and re-epithelialization [9, 10, 15-19].

Delayed corneal wound healing is a major concern in ophthalmology since it can cause chronic infection and ulceration resulting in corneal opacity and scarring responsible for major visual disturbance that may ultimately lead to blindness [15, 17].

In the posterior segment, in addition to intraocular hypertension (glaucoma) and cataract associated with high doses and frequent intravitreal injections of GC, recent studies have reported that excess GC leads to retinal pathologies including central serous chorioretinopathy (CSCR) [2, 11, 20]. These GC-induced ocular diseases have been attributed to off-target over-activation of the MR by the GC, particularly when they are in excess in the body, combined with the low expression of the enzyme 11β-HSD2 in the eye [11, 12, 21].

Central serous chorioretinopathy (CSCR) is characterized by accumulation of subretinal fluid followed by retinal detachment in the macula causing visual disturbance. This disease affects middle-aged patients with men affected more commonly than women and may be triggered by or aggravated by glucocorticoids. CSCR can become chronic in the non-resolving form and lead to blindness since there is no gold standard treatment. Recent studies showed that CSCR may result from inappropriate activation of the MR by GC (the physiological cortisol or synthetic drugs routinely used in ophthalmology) in the choroidal vessels, leading to their dilatation and fluid leakage [11, 20, 22, 23]. Both MR and 11β-HSD2 are expressed in the retina (Muller glial cells, ganglion cells, retinal pigment epithelium (RPE)) and in the choroid (vascular endothelial cells); however, 11β-HSD2 was found to be approximately 24-fold lower in retina than in rat kidney [11, 12, 21]. Hence, MR antagonists such as spironolactone and eplerenone are being increasingly prescribed "off-label" for the treatment of central serous chorioretinopathy and their use induced significant resorption of the subretinal fluid, which improved visual acuity in patients [22-30] .

1.1.2. Mineralocorticoid receptor-associated skin diseases

Impaired wound healing is a significant clinical problem encountered as a complication of certain chronic conditions such as diabetes, sickle cell disease and Cushing syndrome [31].

Wound healing is a complex and highly organized process implying successive and overlapping phases including the inflammatory phase marked by platelet accumulation, coagulation and leukocyte migration, followed by the proliferative phase where re-epithelialization, angiogenesis, fibroplasia and wound contraction occur; finally, the remodelling phase characterized by production of collagen and matrix proteins. The whole process is orchestrated by a precise and complex interplay of various factors involving cells, growth factors, cytokines and components of the extracellular matrix. Even if the wound healing process follows a uniform pattern all over the body, local specificities exist resulting from tissue-specific differences, for example, lack of vessels in the cornea compared to the skin [31].

The critical phase of wound healing is re-epithelialization. Restoration of the epithelial barrier is a key step in preventing exogenous agents from entering to the body; hence, protecting it from external infections. During this process, epithelial cells proliferate at the wound edge, migrate to cover the lesioned area and differentiate to form the new tissue. Absence of cell migration is related to the clinical phenotype of chronic non-healing wounds [19, 32, 33].

In addition to the delayed corneal wound healing described above, studies have also shown that prolonged glucocorticoid therapy causes delayed cutaneous wound healing via illicit occupancy on the mineralocorticoid receptor, non-prevented by the 11β-HSD2 enzyme given its low expression in the skin [8, 34]. Hence, co-administration of a mineralocorticoid receptor antagonist, such as spironolactone together with a glucocorticoid was suggested as a therapeutic strategy to block the off-target glucocorticoid binding to the MR and indeed *in vivo* studies showed a significant improvement in the wound closure compared to the control, which was further confirmed in a pilot study involving 23 volunteers [35-38].

1.2.Mineralocorticoid receptor antagonists

Spironolactone (Aldactone®; Pfizer, Switzerland) was the first synthetic steroidal MR antagonist (MRA) that competes with the endogenous hormone aldosterone blocking the final step of the RAAS. Spironolactone (SPL; **Figure 2A**) was developed by Searle laboratories (Skokie, USA) in 1960 and was first marketed as a potassium-sparing diuretic and natriuretic. Spironolactone was indicated for the treatment of primary hyperaldosteronism (Conn's syndrome) including essential hypertension and hypokalaemia and later, for the treatment of secondary aldosteronism including various oedematous conditions such as congestive heart failure, cirrhosis with ascites and nephrotic syndrome [39-41].

In addition to its own anti-MR activity, spironolactone is also a pharmacologically active prodrug with a short half-life (~ 2 h) which is further metabolized in the liver via different pathways including deacetylation, S-methylation and dethioacetylation, into its two main active metabolites 7α-thiomethylspironolactone (TMSPL; **Figure 2B**) and canrenone (CAN; **Figure 2C**), which have longer half-lives (13.8 and 16.5 h, respectively) [42-44].

Previously, CAN was considered to be the sole active metabolite of SPL. This assumption was due to the use of non-specific analytical methods such as fluorometric assays that overestimated CAN concentrations in plasma because of the co-determination of other fluorescing sulphur-containing SPL metabolites such as TMSPL [45]. The use of more specific HPLC methods, capable of distinguishing between the metabolites, confirmed that CAN plasma levels were lower than previously thought and it is now believed that both metabolites contribute to the anti-mineralocorticoid effects of SPL [46]. Some studies have even shown that TMSPL is the main active metabolite in humans due to its higher plasma levels and higher affinity for renal MR [44, 47, 48].

Potassium canrenoate (Soludactone®; Pfizer, Switzerland), which is the potassium salt of the γ-hydroxy acid derivative of canrenone, is the only marketed MR antagonist form for parenteral administration (**Figure 2D**).

A second generation of steroidal MRA including eplerenone (Inspra®; Pfizer, Switzerland), was developed by Ciba-Geigy (Basel, Switzerland) to improve the tolerance of spironolactone and was launched by Pfizer (New York, USA) in 2002 for the treatment of congestive heart failure (**Figure 2E**). Indeed, although spironolactone is a very potent MRA, it lacks selectivity since it also inhibits the androgen and progesterone receptors causing side effects including gynecomastia, impotence and menstrual irregularities. Eplerenone (9-11α-epoxymexrenone) was hence designed to improve the selectivity for MR; however, it showed lower potency (40-fold less) compared to spironolactone. This difference in potency was explained by the fact that spironolactone exerts its anti-MR activity *per se* but also through its two active metabolites, which have a long half-life of around 15 h, whereas eplerenone has no active metabolites and a shorter half-life of 4 h [41, 49, 50].

A common drawback of all the steroid MRA is the risk of hyperkalemia due to their higher accumulation in the kidney compared to other organs, leading to increased plasma potassium levels. Hence, more recently, researchers focused their work on developing a third generation, non-steroidal MRA with improved benefit/risk profile such as finerenone currently in phase III (**Figure 2F**). Clinical trials showed that finerenone led to lower rate of hyperkalemia compared to spironolactone which was explained by the equal distribution of the drug in the heart and the kidney leading to less renal MR blockade and hence reduced K^+ sparing effect [51].

Apart from potassium canrenoate, MR antagonists have a poor aqueous solubility making their formulation quite challenging, particularly for topical delivery. Given the higher potency of spironolactone, the later was selected to be used as the MR antagonist in the formulations. Even if spironolactone lacks selectivity, this drawback has less impact since we aim to develop site specific formulations to avoid the systemic exposure.

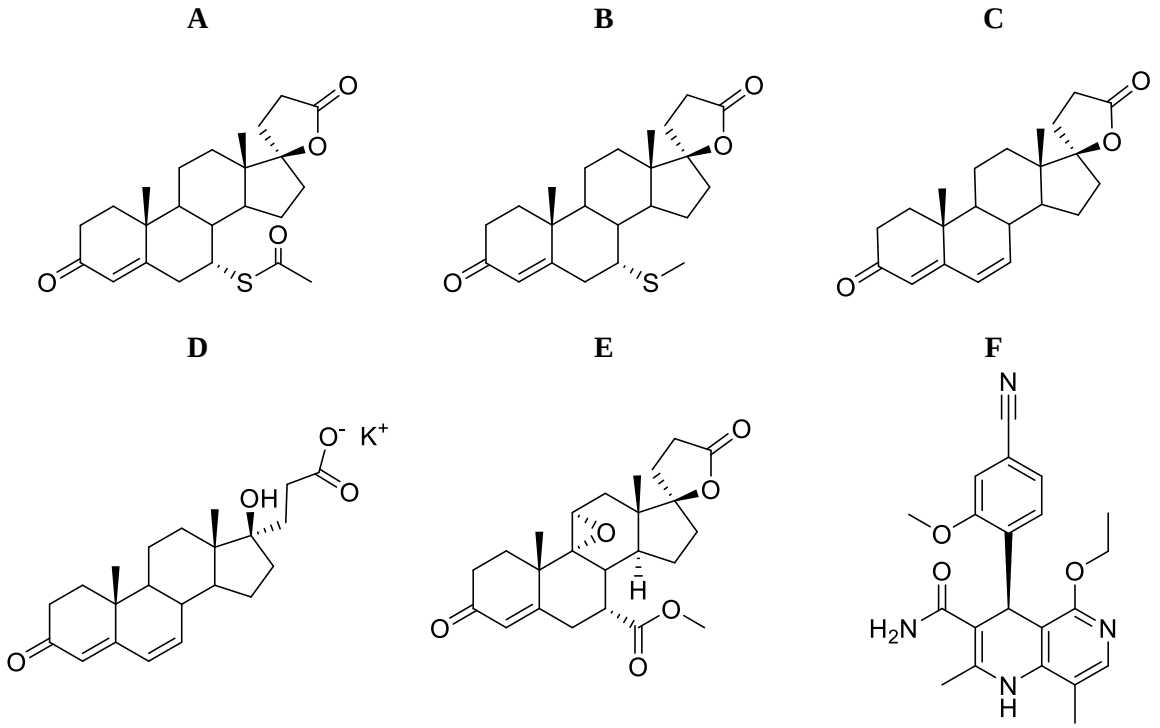

Figure 2. Chemical structure of (A) spironolactone, (B) 7α-thiomethylspironolactone, (C) canrenone, (D) potassium canrenoate, (E) eplerenone and (F) finerenone.

2. Ocular drug delivery

The eye is a subtle and fascinating organ, the most complex after the brain. Thus, ocular drug delivery is one of the most challenging due to various inherent anatomical and physiological barriers that ensure the functionality of this delicate organ.

Anatomically, the eye can be divided into two segments; the anterior segment and the posterior segment. The anterior segment includes the cornea, conjunctiva, sclera and the anterior uvea (iris and ciliary body) (**Figure 3**). The diseases affecting the anterior segment such as dry eye, keratitis and anterior uveitis, are mostly treated with topical eye drops (**Figure 3**) which are rapidly drained from the ocular surface, due to the blinking reflex, tear turnover and the nasolacrimal drainage; limiting the absorption and leading to a very poor bioavailability (5-10%). One strategy to increase the bioavailability of the drug consists of increasing the viscosity of the eye drops in order to prolong the residence time; however, these forms are generally associated with limited patient acceptance. Another obstacle facing the topically applied drug is the corneal barrier (epithelium).

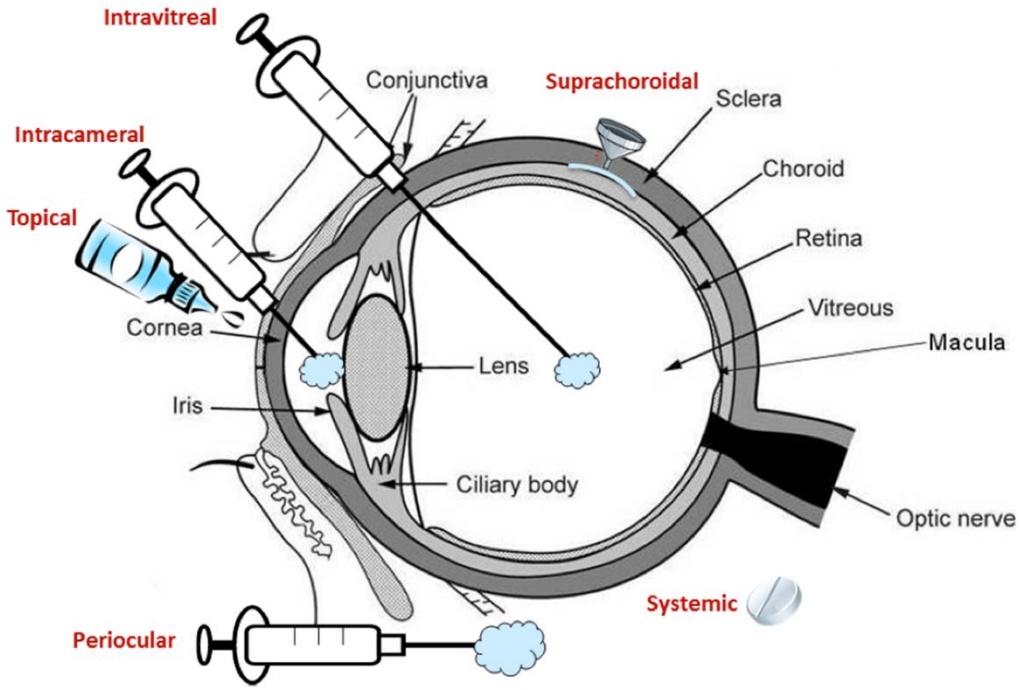

Figure 3. Ocular drug delivery systems. Reproduced with permission from [52].

The posterior segment of the eye is composed of the vitreous, retina, the posterior uvea (choroid) and the sclera (**Figure 3**). Most ocular diseases, and the most vision threatening, are located in the posterior segment, including age related macular degeneration, diabetic retinopathies and glaucoma.

Drug delivery to the posterior segment is even more challenging since topically applied drugs do not reach the posterior segment due to the different anatomical and physiological barriers encountered (**Figure 4**). Indeed, the drug faces static barriers including the cornea, conjunctiva and sclera; the blood-aqueous barrier, as well as dynamic barriers such as nasolacrimal drainage, blood flow and lymphatic clearance [53].

Oral and intravenous route are also used to deliver drugs to the posterior segment, however, they lead to poor penetration into the eye due to the inner (endothelium of retinal vessels) and the outer (retinal pigment epithelium) blood-retinal barriers (**Figure 4**). Therefore, high doses are often necessary to achieve therapeutic concentrations in the eye, which could lead to side effects due to elevated systemic exposure [53-56].

Intravitreal injection (**Figure 3**) has the advantage of enabling direct delivery of the drug to the posterior segment of the eye, avoiding the above-mentioned barriers and side effects given the limited systemic diffusion. However, due to the short half-life of drugs, injections need to be repeated frequently to maintain therapeutic efficacy, which is not very patient-friendly and may

cause some complications, such as cataract, retinal detachment, haemorrhage and endophthalmitis [54, 57].

Therefore, many efforts have been made to develop novel drug delivery systems allowing a sustained drug release into the posterior segment of the eye to improve efficacy and patient compliance. Such systems include erodible polymers, implants, inserts, reservoirs and refillable drug ports based on biodegradable and non-biodegradable polymers [55, 58-64]. Biodegradable polymers are preferred to non-biodegradable since they do not require additional surgery for removal.

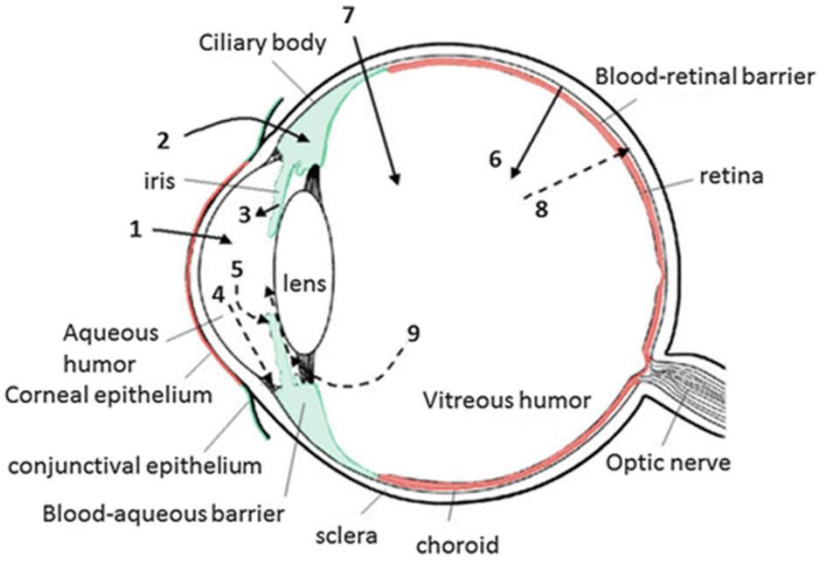

Figure 4. Schematic presentation of the ocular structure with the routes of drug administration and elimination. The numbers refer to following processes: 1) transcorneal permeation from the lacrimal fluid into the anterior chamber, 2) non-corneal drug permeation across the conjunctiva and sclera into the anterior uvea, 3) drug distribution from the blood stream via blood-aqueous barrier into the anterior chamber, 4) elimination of drug from the anterior chamber by the aqueous humor turnover to the trabecular meshwork and Sclemm's canal, 5) drug elimination from the aqueous humor into the systemic circulation across the blood-aqueous barrier, 6) drug distribution from the blood into the posterior segment of the eye across the blood-retina barrier, 7) intravitreal drug administration, 8) drug elimination from the vitreous via posterior route across the blood-retina barrier, and 9) drug elimination from the vitreous via anterior route to the posterior chamber. Reproduced with permission from [54].

3. Topical drug delivery to the skin

The skin plays a major role in protecting the body from external micro-organisms and exogenous molecules through its highly efficient barrier - the stratum corneum (SC). This outermost layer of the epidermis is constituted of layers of flattened corneocytes surrounded by a lipid envelope, which also has a homeostatic function in that it limits transepidermal water loss [65].

Topical drug delivery to the skin for the treatment of cutaneous diseases is the best strategy to achieve a site-specific therapeutic effect with the least possible adverse effects. Thus, to overcome the formidable stratum corneum barrier, an effort has to be made to design the drug delivery system capable of delivering sufficient amounts of the drug to the viable epidermis and dermis. Topically applied drugs mostly penetrate the SC through the lipids surrounding the corneocytes (intercellular route), and some cases via the transcellular route through the corneocytes, depending on their lipophilicity and molecular weight. Diffusion through the SC is usually limited to moderately lipophilic (logP 1-3) compounds with a relatively low molecular weight (<500 Da) [65-68].

Recently, many studies have reported an enhanced drug penetration and bioavailability in the skin following topical application of nanocarrier based systems such as nanoparticles, liposomes and micelles [65]. Although the penetration pathway through the SC depends on the carrier type (**Figure 5**), nanocarriers showed to enhance the drug bioavailability via a common pathway, the transfollicular delivery through the pilosebaceous units (PSU). The PSU is composed of the hair follicle (HF) and the sebaceous gland. These structures are invaginations of epidermis into the dermis. Although the SC acts as an efficient barrier in the superficial interfollicular epidermis, this barrier is disrupted in the epidermis lining the infundibulum part of the hair follicle, located between the middle (isthmus) and the upper (acroinfundibulum or orifice region) part of the hair follicle, where the SC layer is reported to be thinner which makes it more permeable [69, 70]. This feature constitutes an advantage for drug delivery to the viable epidermis and dermis since it allows to circumvent the SC barrier. Even if the orifice area of the HF represents only 0.1% of the total skin area, this delivery route may represent a great advantage to enhance the drug penetration to the skin [71, 72]. Indeed, studies reported that nanocarriers tend to accumulate in the HF forming a reservoir acting as a sustained release system, which allows the drug to diffuse laterally to the viable epidermis and dermis [70, 73-76].

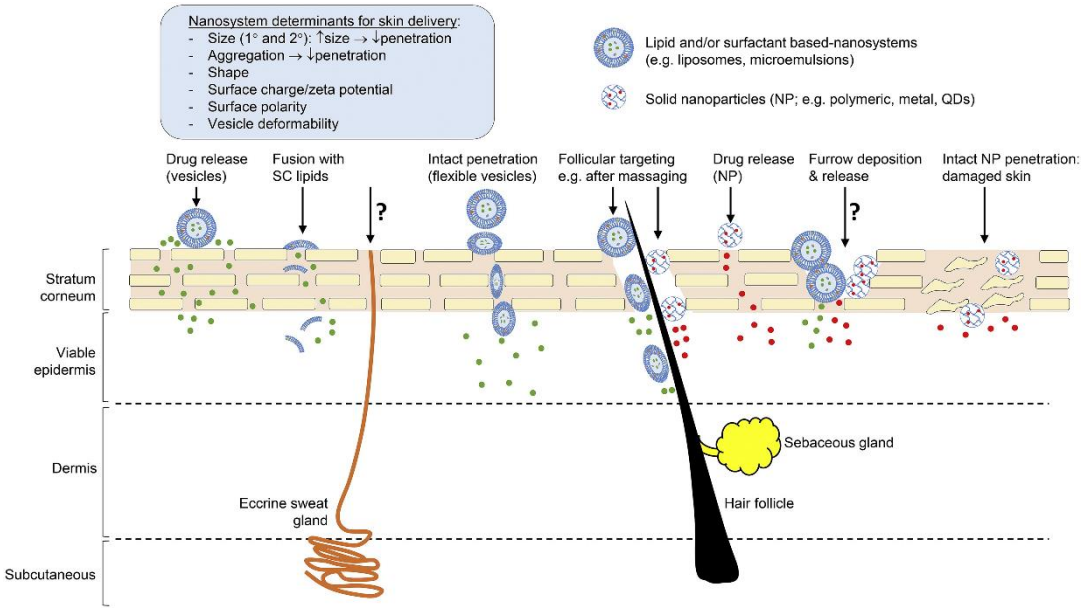

Figure 5. Properties of nanosystems determining skin absorption and potential routes of penetration (skin layer thicknesses not drawn to scale). Reproduced with permission from [65].

Given the poor water-solubility of spironolactone and in order to provide patients with efficient and safe drug delivery systems for the treatment of delayed corneal/cutaneous wound healing and central serous chorioretinopathy, novel formulations of spironolactone for the site-specific delivery to the eye and to the skin are needed. Site specific drug delivery including topical administration to the skin, instillation to the anterior segment of the eye and intravitreal injection to the posterior segment of the eye, allow to deliver therapeutic concentrations to the diseases site, overcoming the above-mentioned barriers and improving the patient safety and compliance by avoiding the side effects associated with systemic exposure.

Recently, nanocarriers including micelles based on amphiphilic copolymers have been shown to increase the aqueous solubility of poorly water-soluble compounds. Moreover, nanocarriers demonstrated an enhanced tissue penetration and bioavailability of the drugs [74, 75, 77, 78]. Hence, the use of a micelle forming biodegradable polymer was suggested as a formulation strategy to increase the aqueous solubility of spironolactone and enhance the bioavailability following topical application the eye and to the skin.

As previously mentioned, intravitreal injection has the advantage of delivering drugs directly to the posterior segment of the eye avoiding the above-mentioned barriers. However, this technique is not patient-friendly and may lead to complications including retinal detachment, haemorrhage and endophthalmitis. The current trend in the drug delivery to the posterior segment of the eye is the use of sustained release systems for a better patient compliance. Such

systems include implants, inserts and refillable reservoir, based on degradable or non-degradable polymers. Biodegradable sustained release systems are of a great interest for intravitreal injection since they don't require surgery for removal. Hence, the use of a biodegradable sustained release polymer for intravitreal injection appeared to the best strategy to deliver therapeutic concentrations of spironolactone to the posterior segment of the eye, and in the same time improve the patient's safety and compliance.

4. Polymeric micelles for topical drug delivery

Amphiphilic copolymers are a combination of a hydrophobic and a hydrophilic segment which have the capacity to self-assemble into micelles in aqueous solution, when the concentration of the copolymer increases above the critical micelle concentration (CMC). At the CMC, hydrophobic segments of the copolymers start to associate to minimize the contact with water molecules leading to the formation of a core-shell structure, entrapping the poorly-water soluble compounds in the core of the micelle. Micelles have proven their utility in drug delivery because of their ability to enhance the aqueous solubility of poorly water-soluble drugs, which represent approximately 70% of the new chemical entities. Moreover, micelles have been gaining interest because of their nano-range size which allows to enhance the drug bioavailability in the tissues, but also for their long circulation properties especially when the hydrophilic shell is constituted of poly(ethylene glycol) [79, 80].

A novel micelle forming amphiphilic diblock copolymer; methoxy-poly(ethylene glycol)-di-hexyl-substituted-poly(lactic acid), (mPEG-dihexPLA) with a CMC of 8 mg/L was previously synthesized and characterized [81]. This biodegradable and biocompatible copolymer showed high efficiencies in incorporating poorly-water soluble drugs, particularly cyclosporin A, tacrolimus and retinoic acid [74, 76, 78, 82, 83]. Moreover, the micelles formed enable an increased drug penetration and drug bioavailability in the skin and the cornea following topical application [74, 76, 78, 83-85].

5. Biodegradable polymer for sustained drug delivery

There is major interest in sustained release polymers since they provide more efficient, safe and patient-friendly drug delivery systems. A novel biodegradable semi-liquid polymer based on hexyl-substituted poly-lactic acid (hexPLA) was developed and showed sustained release properties of the incorporated drug. This biodegradable and biocompatible polymer is hydrolyzed over time in an aqueous environment to 2-hydroxyoctanoic acids monomers which are eliminated from the body.

HexPLA has been designed to control the burst release observed with the poly(lactide) (PLA) and poly(glycolide) (PGA). Moreover, replacing the methyl groups of PLA with more hydrophobic hexyl side-chains resulted in a viscous, injectable polymer in contrast to the solid PLA and PGA, since the hexyl side-chains act as plasticizers.

The formulation process is simple and requires a simple mixing of the active substance with the polymer. The process is solvent free which is a great advantage in terms of safety. The polymer has been tested *in vivo* and after a single subcutaneous injection in rats of 5% triptorelin-hexPLA formulation, hexPLA polymer enabled a sustained delivery of triptorelin up to 6 months [86].

References

[1] E. Bousquet, M. Zhao, A. Ly, G. Leroux Les Jardins, B. Goldenberg, M.C. Naud, L. Jonet, B. Besson-Lescure, F. Jaisser, N. Farman, Y. De Kozak, F. Behar-Cohen, The aldosterone-mineralocorticoid receptor pathway exerts anti-inflammatory effects in endotoxin-induced uveitis, PLoS One 7 (2012) e49036.

[2] F. Jaisser, N. Farman, Emerging Roles of the Mineralocorticoid Receptor in Pathology: Toward New Paradigms in Clinical Pharmacology, Pharmacol. Rev. 68 (2016) 49-75.

[3] B.C. Rossier, M.E. Baker, R.A. Studer, Epithelial sodium transport and its control by aldosterone: the story of our internal environment revisited, Physiol. Rev. 95 (2015) 297-340.

[4] P.J. Fuller, S.S. Lim-Tio, F.E. Brennan, Specificity in mineralocorticoid versus glucocorticoid action, Kidney Int. 57 (2000) 1256-1264.

[5] A. Odermatt, P. Arnold, F.J. Frey, The intracellular localization of the mineralocorticoid receptor is regulated by 11beta-hydroxysteroid dehydrogenase type 2, J. Biol. Chem. 276 (2001) 28484-28492.

[6] Z. Krozowski, K.X. Li, K. Koyama, R.E. Smith, V.R. Obeyesekere, A. Stein-Oakley, H. Sasano, C. Coulter, T. Cole, K.E. Sheppard, The type I and type II 11beta-hydroxysteroid dehydrogenase enzymes, J. Steroid Biochem. Mol. Biol. 69 (1999) 391-401.

[7] H. Schacke, W.D. Docke, K. Asadullah, Mechanisms involved in the side effects of glucocorticoids, Pharmacol. Ther. 96 (2002) 23-43.

[8] N. Farman, V.T. Nguyen, A novel actor in skin biology: the mineralocorticoid receptor, Exp. Dermatol. 25 (2016) 24-25.

[9] G. Petroutsos, R. Guimaraes, J.P. Giraud, Y. Pouliquen, Corticosteroids and corneal epithelial wound healing, Br. J. Ophthalmol. 66 (1982) 705-708.

[10] M. Kadmiel, A. Janoshazi, X. Xu, J.A. Cidlowski, Glucocorticoid action in human corneal epithelial cells establishes roles for corticosteroids in wound healing and barrier function of the eye, Exp. Eye Res. 152 (2016) 10-33.

[11] M. Zhao, I. Celerier, E. Bousquet, J.C. Jeanny, L. Jonet, M. Savoldelli, O. Offret, A. Curan, N. Farman, F. Jaisser, F. Behar-Cohen, Mineralocorticoid receptor is involved in rat and human ocular chorioretinopathy, J. Clin. Invest. 122 (2012) 2672-2679.

[12] M. Zhao, F. Valamanesh, I. Celerier, M. Savoldelli, L. Jonet, J.C. Jeanny, F. Jaisser, N. Farman, F. Behar-Cohen, The neuroretina is a novel mineralocorticoid target: aldosterone up-regulates ion and water channels in Muller glial cells, FASEB J. 24 (2010) 3405-3415.

[13] C.M. Ferrario, E.L. Schiffrin, Role of mineralocorticoid receptor antagonists in cardiovascular disease, Circ. Res. 116 (2015) 206-213.

[14] G.D. Novack, A.L. Robin, Ocular pharmacology, J. Clin. Pharmacol. 56 (2016) 517-527.

[15] M. Srinivasan, P. Lalitha, R. Mahalakshmi, N.V. Prajna, J. Mascarenhas, J.D. Chidambaram, S. Lee, K.C. Hong, M. Zegans, D.V. Glidden, S. McLeod, J.P. Whitcher, T.M. Lietman, N.R. Acharya, Corticosteroids for bacterial corneal ulcers, Br. J. Ophthalmol. 93 (2009) 198-202.

[16] P. Fagerholm, Wound healing after photorefractive keratectomy, J. Cataract Refract. Surg. 26 (2000) 432-447.

[17] S.C. Park, J.H. Kim, Effect of steroids and nonsteroidal anti-inflammatory agents on stromal wound healing following excimer laser keratectomy in rabbits, Ophthalmic Surg. Lasers 27 (1996) S481-486.

[18] A.A. Sarchahi, A. Maimandi, A.K. Tafti, M. Amani, Effects of acetylcysteine and dexamethasone on experimental corneal wounds in rabbits, Ophthalmic Res. 40 (2008) 41-48.

[19] N. Hashizume, S. Saika, Y. Okada, T. Miyamoto, K. Shimizu, Y. Ohnishi, Effects of antiinflammatory drugs on migration of the rabbit corneal epithelium, J. Cataract Refract. Surg. 27 (2001) 1499-1502.

[20] A. Daruich, A. Matet, A. Dirani, E. Bousquet, M. Zhao, N. Farman, F. Jaisser, F. Behar-Cohen, Central serous chorioretinopathy: Recent findings and new physiopathology hypothesis, Prog. Retin. Eye Res. 48 (2015) 82-118.

[21] J.L. Wilkinson-Berka, G. Tan, K. Jaworski, A.G. Miller, Identification of a retinal aldosterone system and the protective effects of mineralocorticoid receptor antagonism on retinal vascular pathology, Circ. Res. 104 (2009) 124-133.

[22] E. Bousquet, T. Beydoun, P.R. Rothschild, C. Bergin, M. Zhao, R. Batista, M.L. Brandely, B. Couraud, N. Farman, A. Gaudric, F. Chast, F. Behar-Cohen, Spironolactone for nonresolving central serous chorioretinopathy: A randomized controlled crossover study, Retina 35 (2015) 2505-2515.

[23] E. Bousquet, T. Beydoun, M. Zhao, L. Hassan, O. Offret, F. Behar-Cohen, Mineralocorticoid receptor antagonism in the treatment of chronic central serous chorioretinopathy: a pilot study, Retina 33 (2013) 2096-2102.

[24] A. Daruich, A. Matet, A. Dirani, M. Gallice, L. Nicholson, S. Sivaprasad, F. Behar-Cohen, Oral mineralocorticoid-receptor antagonists: Real-life experience in clinical subtypes of nonresolving central serous chorioretinopathy with chronic epitheliopathy, Transl. Vis. Sci. Technol. 5 (2016) 2.

[25] Q. Ghadiali, J.J. Jung, S. Yu, S.N. Patel, L.A. Yannuzzi, Central serous chorioretinopathy treated with mineralocorticoid antagonists: A one-year pilot study, Retina 36 (2016) 611-618.

[26] T.R. Herold, K. Rist, S.G. Priglinger, M.W. Ulbig, A. Wolf, Long-term results and recurrence rates after spironolactone treatment in non-resolving central serous chorio-retinopathy (CSCR), Graefes Arch. Clin. Exp. Ophthalmol. DOI 10.1007/s00417-016-3436-5(2016).

[27] E.H. van Dijk, M.F. Nijhoff, E.K. de Jong, O.C. Meijer, A.P. de Vries, C.J. Boon, Central serous chorioretinopathy in primary hyperaldosteronism, Graefes Arch. Clin. Exp. Ophthalmol. 254 (2016) 2033-2042.

[28] E.K. Chin, D.R. Almeida, C.N. Roybal, P.I. Niles, K.M. Gehrs, E.H. Sohn, H.C. Boldt, S.R. Russell, J.C. Folk, Oral mineralocorticoid antagonists for recalcitrant central serous chorioretinopathy, Clin. Ophthalmol. 9 (2015) 1449-1456.

[29] M. Salehi, A.S. Wenick, H.A. Law, J.R. Evans, P. Gehlbach, Interventions for central serous chorioretinopathy: a network meta-analysis, Cochrane Database Syst. Rev. DOI 10.1002/14651858.CD011841.pub2(2015).

[30] T.R. Herold, K. Prause, A. Wolf, W.J. Mayer, M.W. Ulbig, Spironolactone in the treatment of central serous chorioretinopathy - a case series, Graefes Arch. Clin. Exp. Ophthalmol. 252 (2014) 1985-1991.

[31] S. Werner, R. Grose, Regulation of wound healing by growth factors and cytokines, Physiol. Rev. 83 (2003) 835-870.

[32] S. Adams, R.S. Valchanova, B. Munz, RIP2: a novel player in the regulation of keratinocyte proliferation and cutaneous wound repair?, Exp. Cell Res. 316 (2010) 728-736.

[33] M. Liu, K. Saeki, T. Matsunobu, T. Okuno, T. Koga, Y. Sugimoto, C. Yokoyama, S. Nakamizo, K. Kabashima, S. Narumiya, T. Shimizu, T. Yokomizo, 12-Hydroxyheptadecatrienoic acid promotes epidermal wound healing by accelerating keratinocyte migration via the BLT2 receptor, Journal Experimental Medicine 211 (2014) 1063-1078.

[34] N. Farman, E. Maubec, B. Poeggeler, J.E. Klatte, F. Jaisser, R. Paus, The mineralocorticoid receptor as a novel player in skin biology: beyond the renal horizon?, Exp. Dermatol. 19 (2010) 100-107.

[35] V.T. Nguyen, N. Farman, E. Maubec, D. Nassar, D. Desposito, L. Waeckel, S. Aractingi, F. Jaisser, Re-epithelialization of pathological cutaneous wounds is improved by local mineralocorticoid receptor antagonism, J. Invest. Dermatol. DOI 10.1016/j.jid.2016.05.101(2016).

[36] E. Maubec, C. Laouenan, L. Deschamps, V.T. Nguyen, I. Scheer-Senyarich, A.C. Wackenheim-Jacobs, M. Steff, S. Duhamel, S. Tubiana, N. Brahimi, S. Leclerc-Mercier, B. Crickx, C. Perret, S. Aractingi, B. Escoubet, X. Duval, P. Arnaud, F. Jaisser, F. Mentre, N. Farman, Topical mineralocorticoid receptor blockade limits glucocorticoid-induced epidermal atrophy in human skin, J. Invest. Dermatol. 135 (2015) 1781-1789.

[37] J. Boix, L.M. Sevilla, Z. Saez, E. Carceller, P. Perez, Epidermal mineralocorticoid receptor plays beneficial and adverse effects in skin and mediates glucocorticoid responses, J. Invest. Dermatol. DOI 10.1016/j.jid.2016.07.018(2016).

[38] J.K. Youm, K. Park, Y. Uchida, A. Chan, T.M. Mauro, W.M. Holleran, P.M. Elias, Local blockade of glucocorticoid activation reverses stress- and glucocorticoid-induced delays in cutaneous wound healing, Wound Repair Regen. 21 (2013) 715-722.

[39] P. Kolkhof, L. Barfacker, 30 years of the mineralocorticoid receptor: Mineralocorticoid receptor antagonists: 60 years of research and development, J. Endocrinol. 234 (2017) T125-T140.

[40] D.A. Sica, Pharmacokinetics and pharmacodynamics of mineralocorticoid blocking agents and their effects on potassium homeostasis, Heart Fail. Rev. 10 (2005) 23-29.

[41] J. Menard, The 45-year story of the development of an anti-aldosterone more specific than spironolactone, Mol. Cell. Endocrinol. 217 (2004) 45-52.

[42] L.E. Los, A.B. Coddington, H.G. Ramjit, H.D. Colby, Identification of spironolactone metabolites in plasma and target organs of guinea pigs, Drug Metab. Dispos. 21 (1993) 1086-1090.

[43] L.E. Los, H.D. Colby, Binding of spironolactone metabolites in vivo to renal mineralocorticoid receptors in guinea pigs, Pharmacology 48 (1994) 86-92.

[44] H.W. Overdiek, W.A. Hermens, F.W. Merkus, New insights into the pharmacokinetics of spironolactone, Clin. Pharmacol. Ther. 38 (1985) 469-474.

[45] L. Ramsay, J. Shelton, I. Harrison, M. Tidd, M. Asbury, Spironolactone and potassium canrenoate in normal man, Clin. Pharmacol. Ther. 20 (1976) 167-177.

[46] C.G. Dahlof, P. Lundborg, B.A. Persson, C.G. Regardh, Re-evaluation of the antimineralocorticoid effect of the spironolactone metabolite, canrenone, from plasma concentrations determined by a new high-pressure liquid-chromatographic method, Drug Metab. Dispos. 7 (1979) 103-107.

[47] J.M. Sandall, J.S. Millership, P.S. Collier, J.C. McElnay, Development and validation of an HPLC method for the determination of spironolactone and its metabolites in paediatric plasma samples, J. Chromatogr. B 839 (2006) 36-44.

[48] L.E. Los, S.M. Pitzenberger, H.G. Ramjit, A.B. Coddington, H.D. Colby, Hepatic metabolism of spironolactone. Production of 3-hydroxy-thiomethyl metabolites, Drug Metab. Dispos. 22 (1994) 903-908.

[49] P. Kolkhof, S.A. Borden, Molecular pharmacology of the mineralocorticoid receptor: prospects for novel therapeutics, Mol. Cell. Endocrinol. 350 (2012) 310-317.

[50] S.M. Garthwaite, E.G. McMahon, The evolution of aldosterone antagonists, Mol. Cell. Endocrinol. 217 (2004) 27-31.

[51] P. Kolkhof, M. Delbeck, A. Kretschmer, W. Steinke, E. Hartmann, L. Barfacker, F. Eitner, B. Albrecht-Kupper, S. Schafer, Finerenone, a novel selective nonsteroidal mineralocorticoid receptor antagonist protects from rat cardiorenal injury, J. Cardiovasc. Pharmacol. 64 (2014) 69-78.

[52] S.P. Chaplot, I.D. Rupenthal, Dendrimers for gene delivery – a potential approach for ocular therapy?, J. Pharm. Pharmacol. 66 (2014) 542-556.

[53] R. Gaudana, H.K. Ananthula, A. Parenky, A.K. Mitra, Ocular drug delivery, AAPS J 12 (2010) 348-360.

[54] A. Urtti, Challenges and obstacles of ocular pharmacokinetics and drug delivery, Adv Drug Deliv Rev 58 (2006) 1131-1135.

[55] E. Sakurai, H. Ozeki, N. Kunou, Y. Ogura, Effect of particle size of polymeric nanospheres on intravitreal kinetics, Ophthalmic Res. 33 (2001) 31-36.

[56] G. Gough, M. Szapacs, T. Shah, P. Clements, C. Struble, R. Wilson, Ocular tissue distribution and pharmacokinetic study of a small 13kDa domain antibody after intravitreal, subconjuctival and eye drop administration in rabbits, Exp. Eye Res. 167 (2017) 14-17.

[57] V. Agrahari, A. Mandal, V. Agrahari, H.M. Trinh, M. Joseph, A. Ray, H. Hadji, R. Mitra, D. Pal, A.K. Mitra, A comprehensive insight on ocular pharmacokinetics, Drug Deliv Transl Res 6 (2016) 735-754.

[58] U.B. Kompella, A.C. Amrite, R. Pacha Ravi, S.A. Durazo, Nanomedicines for back of the eye drug delivery, gene delivery, and imaging, Prog. Retin. Eye Res. 36 (2013) 172-198.

[59] A. Lambiase, S. Abdolrahimzadeh, S.M. Recupero, An update on intravitreal implants in use for eye disorders, Drugs Today (Barc) 50 (2014) 239-249.

[60] J. Wang, A. Jiang, M. Joshi, J. Christoforidis, Drug delivery implants in the treatment of vitreous inflammation, Mediators Inflamm. 2013 (2013) 780634.

[61] M.N. Yasin, D. Svirskis, A. Seyfoddin, I.D. Rupenthal, Implants for drug delivery to the posterior segment of the eye: A focus on stimuli-responsive and tunable release systems, J. Control. Release 196 (2014) 208-221.

[62] J.J. Kang-Mieler, C.R. Osswald, W.F. Mieler, Advances in ocular drug delivery: emphasis on the posterior segment, Expert Opinion on Drug Delivery 11 (2014) 1647-1660.

[63] W. Pearce, J. Hsu, S. Yeh, Advances in drug delivery to the posterior segment, Curr. Opin. Ophthalmol. 26 (2015) 233-239.

[64] H. Chen, Recent developments in ocular drug delivery, J. Drug Target. 23 (2015) 597-604.

[65] M.S. Roberts, Y. Mohammed, M.N. Pastore, S. Namjoshi, S. Yousef, A. Alinaghi, I.N. Haridass, E. Abd, V.R. Leite-Silva, H.A.E. Benson, J.E. Grice, Topical and cutaneous delivery using nanosystems, J. Control. Release 247 (2017) 86-105.

[66] R.J. Scheuplein, I.H. Blank, Permeability of the skin, Physiol. Rev. 51 (1971) 702-747.

[67] A. Vogt, F. Rancan, S. Ahlberg, B. Nazemi, C.S. Choe, M.E. Darvin, S. Hadam, U. Blume-Peytavi, K. Loza, J. Diendorf, M. Epple, C. Graf, E. Ruhl, M.C. Meinke, J. Lademann, Interaction of dermatologically relevant nanoparticles with skin cells and skin, Beilstein J Nanotechnol 5 (2014) 2363-2373.

[68] G.B. Kasting, N.D. Barai, T.F. Wang, J.M. Nitsche, Mobility of Water in Human Stratum Corneum, J. Pharm. Sci. 92 (2003) 2326-2340.

[69] F. Knorr, J. Lademann, A. Patzelt, W. Sterry, U. Blume-Peytavi, A. Vogt, Follicular transport route--research progress and future perspectives, Eur. J. Pharm. Biopharm. 71 (2009) 173-180.

[70] J. Lademann, F. Knorr, H. Richter, U. Blume-Peytavi, A. Vogt, C. Antoniou, W. Sterry, A. Patzelt, Hair follicles--an efficient storage and penetration pathway for topically applied substances. Summary of recent results obtained at the Center of Experimental and Applied Cutaneous Physiology, Charite - Universitatsmedizin Berlin, Germany, Skin Pharmacol. Physiol. 21 (2008) 150-155.

[71] B. Illel, H. Schaefer, J. Wepierre, O. Doucet, Follicles Play an Important Role in Percutaneous Absorption, J. Pharm. Sci. 80 (1991) 424-427.

[72] A.C. Lauer, L.M. Lieb, C. Ramachandran, G.L. Flynn, N.D. Weiner, Transfollicular Drug Delivery, Pharm. Res. 12 (1995) 179-186.

[73] J. Lademann, H. Richter, U.F. Schaefer, U. Blume-Peytavi, A. Teichmann, N. Otberg, W. Sterry, Hair follicles - a long-term reservoir for drug delivery, Skin Pharmacol. Physiol. 19 (2006) 232-236.

[74] M. Lapteva, K. Mondon, M. Moller, R. Gurny, Y.N. Kalia, Polymeric micelle nanocarriers for the cutaneous delivery of tacrolimus: a targeted approach for the treatment of psoriasis, Mol. Pharm. 11 (2014) 2989-3001.

[75] S.G. Kandekar, S. Del Rio-Sancho, M. Lapteva, Y.N. Kalia, Selective delivery of adapalene to the human hair follicle under finite dose conditions using polymeric micelle nanocarriers, Nanoscale DOI 10.1039/c7nr07706h(2017).

[76] M. Lapteva, M. Moller, R. Gurny, Y.N. Kalia, Self-assembled polymeric nanocarriers for the targeted delivery of retinoic acid to the hair follicle, Nanoscale 7 (2015) 18651-18662.

[77] S. Reimondez-Troitiño, N. Csaba, M.J. Alonso, M. de la Fuente, Nanotherapies for the treatment of ocular diseases, Eur. J. Pharm. Biopharm. 95 (2015) 279-293.

[78] M. Lapteva, V. Santer, K. Mondon, I. Patmanidis, G. Chiriano, L. Scapozza, R. Gurny, M. Moller, Y.N. Kalia, Targeted cutaneous delivery of ciclosporin A using micellar nanocarriers and the possible role of inter-cluster regions as molecular transport pathways, J. Control. Release 196 (2014) 9-18.

[79] W. Xu, P. Ling, T. Zhang, Polymeric micelles, a promising drug delivery system to enhance bioavailability of poorly water-soluble drugs, Journal of drug delivery 2013 (2013) 340315.

[80] H. Cabral, K. Kataoka, Progress of drug-loaded polymeric micelles into clinical studies, J. Control. Release 190 (2014) 465-476.

[81] C. Di Tommaso, A. Torriglia, P. Furrer, F. Behar-Cohen, R. Gurny, M. Moller, Ocular biocompatibility of novel Cyclosporin A formulations based on methoxy poly(ethylene glycol)-hexylsubstituted poly(lactide) micelle carriers, Int. J. Pharm. 416 (2011) 515-524.

[82] C. Di Tommaso, F. Valamanesh, F. Miller, P. Furrer, M. Rodriguez-Aller, F. Behar-Cohen, R. Gurny, M. Moller, A novel cyclosporin a aqueous formulation for dry eye treatment: in vitro and in vivo evaluation, Invest. Ophthalmol. Vis. Sci. 53 (2012) 2292-2299.

[83] C. Di Tommaso, J.L. Bourges, F. Valamanesh, G. Trubitsyn, A. Torriglia, J.C. Jeanny, F. Behar-Cohen, R. Gurny, M. Moller, Novel micelle carriers for cyclosporin A topical ocular delivery: in vivo cornea penetration, ocular distribution and efficacy studies, Eur. J. Pharm. Biopharm. 81 (2012) 257-264.

[84] D. Gabriel, T. Mugnier, H. Courthion, K. Kranidioti, N. Karagianni, M.C. Denis, M. Lapteva, Y. Kalia, M. Moller, R. Gurny, Improved topical delivery of tacrolimus: A novel composite hydrogel formulation for the treatment of psoriasis, J. Control. Release 242 (2016) 16-24.

[85] Y.G. Bachhav, K. Mondon, Y.N. Kalia, R. Gurny, M. Moller, Novel micelle formulations to increase cutaneous bioavailability of azole antifungals, J. Control. Release 153 (2011) 126-132.

[86] L.R. Asmus, J.C. Tille, B. Kaufmann, L. Melander, T. Weiss, K. Vessman, W. Koechling, G. Schwach, R. Gurny, M. Moller, In vivo biocompatibility, sustained-release and stability of triptorelin formulations based on a liquid, degradable polymer, J. Control. Release 165 (2013) 199-206.

CHAPTER I

Development and validation of a fast and sensitive UHPLC-ESI-MS method for the simultaneous quantification of spironolactone and its metabolites in ocular tissues.

Naoual Dahmana[a], Doris Gabriel[b], Robert Gurny[a, b], Yogeshvar N. Kalia[a,]

[a] School of Pharmaceutical Sciences, University of Geneva, University of Lausanne, CMU - 1 rue Michel Servet, 1211 Geneva 4, Switzerland.

[b] Apidel SA, 29 Quai du Mont Blanc, 1201 Geneva, Switzerland.

Published in Biomedical Chromatography *(Biomed. Chromatogr. 2018, e4287).*

Abstract

Glucocorticoids are a mainstay for the treatment of immune-mediated conditions and inflammatory diseases. However, their chronic use causes numerous side-effects including delays in corneal and cutaneous wound healing. This is attributed to off-target agonism of the mineralocorticoid receptor, which can be reduced by co-administration of a mineralocorticoid receptor antagonist such as spironolactone. The aim of this study was to develop a fast, selective and sensitive UHPLC-ESI-MS method for the simultaneous quantification of spironolactone, its active metabolites – 7α-thiomethylspironolactone and canrenone, the latter's water-soluble prodrug potassium canrenoate, and the synthetic glucocorticoid, dexamethasone, in corneal samples (17α-methyltestosterone served as an internal standard). A one-step extraction procedure using MeOH:H_2O (1:1) was validated and employed to recover the analytes from the corneal tissue. Extracts were centrifuged and the supernatant analyzed under isocratic conditions. Compounds were detected using SIR mode. The method satisfied FDA guidelines with respect to selectivity, precision and accuracy and displayed linearity from 5 to 1000 ng/mL for all the analytes. The LLOQ of the method was 5 ng/mL making it sufficiently sensitive for quantification of the analytes in samples from *in vivo* studies.

Keywords: spironolactone, 7α-thiomethylspironolactone, canrenone, potassium canrenoate, ultra-high performance liquid chromatography tandem mass spectrometry.

1. Introduction

Spironolactone (SPL; **Figure 1A**) is a synthetic mineralocorticoid receptor (MR) antagonist that competes with the endogenous hormone aldosterone to bind to the MR [1]. It is indicated for the treatment of (i) primary and secondary hyperaldosteronism and hypokalaemia, (ii) oedematous conditions such as nephrotic syndrome and ascites and (iii) cardiovascular conditions such as congestive heart failure and essential hypertension [1-3].

To-date, it has proved difficult to establish a direct relationship between the extent of the pharmacological effect exerted by SPL and its concentration since the molecule undergoes rapid and extensive metabolism via different pathways – including deacetylation, S-methylation and dethioacetylation. Two of its principal metabolites, 7α-thiomethylspironolactone (TMSPL; **Figure 1B**) and canrenone (CAN; **Figure 1C**) [3], have biological activity in their own right and exert a pharmacological effect. Indeed, for many years, CAN was believed to be the sole active metabolite of SPL and responsible for most of its pharmacological activity. This assumption was due to the use of non-specific analytical methods, such as fluorometric detection [4] that overestimated CAN concentrations in plasma, because of the co-determination of other fluorescing sulphur-containing SPL metabolites such as TMSPL. The use of more specific HPLC methods, capable of distinguishing between the metabolites, confirmed that CAN plasma levels were lower than previously thought [5]. As a result, it is now considered that both metabolites contribute to the anti-mineralocorticoid effects of SPL [3, 6]. Some studies have even suggested that TMSPL is the main active metabolite in humans due to its higher affinity for renal MR and since its plasma concentrations were higher than those of CAN [3, 6-8].

Recent reports have pointed to new therapeutic applications for SPL (and its active metabolites); for example, it is being increasingly prescribed “off-label” in ophthalmology for the treatment of central serous chorioretinopathy [9-16], which involves the accumulation of fluid under the retina and can result in retinal detachment and vision impairment. Other studies have suggested that concomitant administration of MR antagonists might offset glucocorticoid-induced delays in cutaneous wound healing [17-19]. This led to the hypothesis that SPL and its metabolites might also be able to counter the deleterious effects of glucocorticoids on corneal lesions and the delayed wound healing process and so create a new therapeutic application in ophthalmology.

It was decided to test this hypothesis with an *in vivo* study [20]; however, this required the development of a sophisticated analytical method able not only to quantify the biodistribution of SPL and its active metabolites (TMSPL and CAN), but also potassium canrenoate (CANK; **Figure 1D**), a water-soluble CAN prodrug that is of particular clinical interest since it can be administered intravenously (and was used as a control in the *in vivo* study) and dexamethasone (a potent glucocorticoid that was used to induce the delayed wound healing; DXM, **Figure 1E**).

Although several HPLC methods have been reported for the separation and quantification of SPL and/or its metabolites, none satisfied all of the requirements of the *in vivo* study. Some protocols did not enable the simultaneous determination of SPL and its active metabolites, TMSPL and CAN [2, 21, 22], others either lacked sensitivity (limits of quantification above 10 ng/mL) or the runtime was excessively long, ranging from 11 to 36 minutes making them unsuitable for routine or high throughput sample management [3, 6, 23-26]. Furthermore, none of the methods included the simultaneous quantification of CANK and DXM.

Therefore, the aim of the present investigation was to develop and to validate a fast, selective and sensitive analytical method for the simultaneous quantification of spironolactone, its two main metabolites (7α-thiomethylspironolactone and canrenone), potassium canrenoate and dexamethasone concentrations in the cornea that could be used in the planned *in vivo* study. To normalize the matrix effect of the biological tissue, 17α-methyltestosterone (MeT; **Figure 1F**) was used as an internal standard (IS).

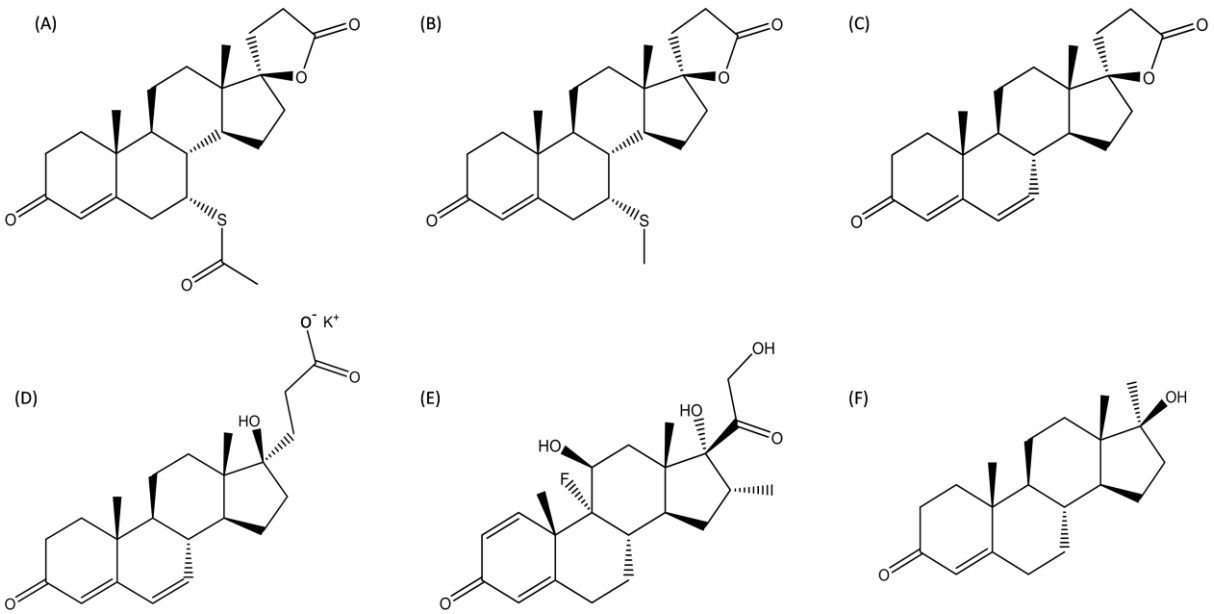

Figure 1. Chemical structures of (A) spironolactone, (B) 7α-thiomethylspironolactone, (C) canrenone, (D) potassium canrenoate, (E) dexamethasone and (F) 17α-methyltestosterone, internal standard.

2. Experimental

2.1. Chemicals and reagents

Spironolactone was purchased from Zhejiang Langhua Pharmaceutical Co., Ltd. (Zhejiang, China). 7α-thiomethylspironolactone was purchased from TLC Pharmaceutical Standards Ltd. (Ontario, Canada). Canrenone, potassium canrenoate and 17α-methyltestosterone were obtained from Sigma-Aldrich (Buchs, Switzerland). Dexamethasone was purchased from Tianjin TianMao Technology Development Corp. Ltd (Tianjin, China). Ultrapure water (H_2O) was obtained from a Milli-Q® water purification system (resistivity > 18 MΩ cm) from Merck Millipore (Darmstadt, Germany). Methanol (MeOH, HPLC grade) was obtained from Fisher Scientific (Waltham, MA, USA) and formic acid (ULC/MS grade) from Biosolve (Dieuze, France). All other chemicals were at least of analytical grade.

2.2. Liquid chromatography set-up

The liquid chromatographic system consisted of a Waters Acquity® ultra-performance liquid chromatography (UPLC®) core system (Baden-Dättwil, Switzerland) including a binary solvent manager, a sample manager with an injection loop volume of 10 µL and a column manager. The reverse phase chromatographic separation of the analytes (SPL, CAN, TMSPL, CANK, DXM) and the internal standard (MeT; IS) was performed using a Waters XBridge® BEH C18 column (50 x 2.1 mm I.D., 2.5 µm) fitted with a Waters XBridge® BEH C18 VanGuard pre-column (5 x 2.1 mm I.D., 2.5 µm). Isocratic elution was carried out using a mobile phase consisting of 0.1% formic acid in H_2O:MeOH (48:52, v/v) with a flow rate of 0.45 mL/min and a runtime of 5 minutes. Column temperature was kept at 40°C and the sample manager was at room temperature. Injection volume was set at 5 µL (partial loop injection mode).

2.3. Mass spectrometry system

The mass spectrometry (MS) system consisted of a Waters XEVO® TQ-MS detector (Baden-Dättwil, Switzerland) fitted with a Z-spray electrospray ionization source. MS detection of the six compounds was performed using electrospray ionization in the positive-ion mode (ESI+) and selected ion recording (SIR) using the pseudo-molecular ion of each compound as the parent ion (hydrogen adduct, $[M + H]^+$). Capillary voltage was set at 2.3 kV, desolvation gas temperature and flow were maintained at 350°C and 650 L/h, respectively, and cone

temperature was set at 150°C. Analyte specific MS parameters were tuned and determined by infusing each compound individually at 1 µg/mL in MeOH:H_2O (1:1) at a flow rate of 5 µL/min. Cone voltages and dwell time were optimized to obtain the best peak intensity for each compound. Data processing was performed using Waters MassLynx software version 4.1.

2.4. Preparation of the corneal matrix

Freshly enucleated porcine eyes were obtained from a local slaughterhouse. After cleaning the eye globes, the corneas were harvested and rinsed in phosphate buffered saline (PBS). Each cornea was then cut into small pieces in a vial containing 2 mL MeOH:H_2O (1:1) and left for extraction overnight under agitation at room temperature. The following day, samples were centrifuged at 12 000 rpm for 20 min, then supernatants were collected and pooled. Fifty corneas harvested from different animals were used to prepare the corneal matrix.

The corneal matrix solution was used to assess the specificity of the method and evaluate the matrix effect. Calibration standards and quality control samples were also prepared in the corneal matrix solution.

2.5. Preparation of stock solutions, calibration standards and quality control samples

A stock solution of each compound (SPL, TMSPL, CAN, CANK, DXM and MeT) was prepared at 1 mg/mL in methanol. All stock solutions were freshly prepared prior to each analysis except for 7α-thiomethylspironolactone and canrenone – for these substances, the stock solutions were stored at -20°C. A working solution was then prepared by mixing SPL, TMSPL, CAN, CANK and DXM stock solutions at 10 µg/mL in corneal matrix (prepared as described above). This solution was further diluted in corneal matrix to obtain the intermediate working solutions at 1 and 0.1 µg/mL, which served to prepare the calibration standards. A working solution of the internal standard (IS) was also prepared at 1 µg/mL by appropriate dilution of the stock solution in corneal matrix.

Calibration standard samples were prepared in corneal matrix by suitable dilution of the working solutions to the desired concentration in the range 5-1000 ng/mL. The appropriate volume of the IS working solution was then used to spike the calibration standard samples so as to obtain a final IS concentration of 100 ng/mL.

Quality control samples were prepared in the same way at 10, 100 and 500 ng/mL in corneal matrix. All the working solutions, calibration standards and quality control samples were

prepared and diluted in corneal matrix in a way so that the final composition in terms of matrix component remains equivalent in each sample at the different analytes concentration.

2.6. Method validation

The method was validated according to FDA guidelines [27] with respect to selectivity and specificity, accuracy and precision, linearity and sensitivity (lower limit of quantification, LLOQ). In addition, the matrix effect of the cornea was evaluated, the extraction procedure of the analytes from the cornea was validated and sample stability was assessed.

2.6.1. Selectivity and specificity

The selectivity of the method was verified by analyzing a sample containing a mixture of the six analytes (SPL, TMSPL, CAN, CANK, DXM and the IS) in MeOH:H_2O (1:1) at different concentrations, in the range of 5-1000 ng/mL, and assessing peak separation and baseline resolution.

The specificity of the method was investigated in two steps. First, the specificity was assessed with respect to signal interferences between the respective SIR signals of the different analytes, where each analyte was injected individually at 100 ng/mL in MeOH:H_2O (1:1) and the resulting signals were compared to the signal obtained after injection of the mixture of the six analytes at the same concentration. Second, the specificity was verified with respect to the endogenous compounds present in the porcine cornea to confirm the absence of interferences between their peaks and the peaks of the different analytes. For that, a blank sample of the corneal matrix (obtained as described in section 2.4) was analyzed and compared to another corneal matrix sample spiked with the six analytes at 100 ng/mL.

2.6.2. Matrix effect evaluation

Ion suppression/enhancement due to a matrix effect was investigated by comparing the signal obtained from the five analytes (SPL, TMSPL, CAN, CANK and DXM) at 50 ng/mL prepared in a standard solution of MeOH:H_2O (1:1) versus the signal obtained of the same five analytes prepared at the same concentration in corneal matrix. All the samples contained IS at 100 ng/mL. The matrix effect was evaluated by calculating the matrix factor and the IS normalized matrix factor using the following equations:

$$\%\ \text{Matrix Factor} = \frac{\text{Analyte area}_{\ \text{spiked matrix}}}{\text{Analyte area}_{\ \text{standard solution}}} \times 100\% \qquad \text{(Eq. 1)}$$

$$\%\ \text{IS Normalized Matrix Factor} = \frac{\text{Matrix Factor}_{\text{Analyte}}}{\text{Matrix Factor}_{\text{IS}}} \times 100\% \quad \text{(Eq. 2)}$$

(% Matrix Factor: 100%, absence of matrix effect; <100%, ion suppression; >100%, ion enhancement).

2.6.3. Linearity

Calibration standards were prepared by spiking the analytes at known concentrations in porcine corneal matrix obtained as described in section 2.4. The concentrations were selected to cover the range of the concentrations expected to be found in the biological samples, i.e. from 5 to 1000 ng/mL. Eight calibration standards containing 100 ng/mL IS (MeT) were prepared at 5, 10, 20, 50, 100, 200, 500 and 1000 ng/mL (n=5) in porcine corneal matrix as described in section 2.5.

To standardize the matrix effect of the cornea, calibration curves of each analyte (SPL, TMSPL, CAN, CANK and DXM) were constructed by plotting the relative peak area, i.e. the ratio between the peak area of each analyte to the peak area of the IS (MeT), versus the concentration of each analyte to the known concentration of the IS (100 ng/mL, Eq. 1). This method was also used for further sample quantification such as the quality control samples.

$$\text{Conc. Analyte} = \left(\frac{\text{Conc. IS}}{\text{Slope}}\right) \text{x} \left(\frac{\text{Area Analyte}}{\text{Area IS}} - \text{Intercept}\right) \quad \text{(Eq. 3)}$$

The slope and the intercept were calculated from the calibration curve obtained the same day as each analysis (Conc. refers to the concentration, IS to the internal standard). The acceptance criterion for the linearity of a calibration curve was a correlation coefficient (R) of at least 0.99 and a RSD below 15% at each calibration standard (below 20% at LLOQ).

2.6.4. Sensitivity (LLOQ)

The lower limit of quantification (LLOQ) was determined by calculating the signal-to-noise ratio for each analyte and assessing at least five times higher area obtained with the lowest calibration standard (5 ng/mL, n=5) of each analyte (SPL, TMSPL, CAN, CANK and DXM) when compared to a blank sample consisting of a blank corneal matrix and verifying accuracy and precision at the LLOQ.

2.6.5. Accuracy and precision

Accuracy and precision were determined by measuring the intra-day and inter-day recovery and variability of each analyte (SPL, TMSPL, CAN, CANK and DXM) at three different concentrations over three days. Samples were prepared by spiking the corneal matrix containing 100 ng/mL IS with a mixture of the five analytes (SPL, TMSPL, CAN, CANK and DXM) at 10, 100 and 500 ng/mL (n=5).

Accuracy (expressed as a percentage recovery) for each analyte was calculated as the ratio of the measured concentration, calculated using the calibration curve obtained on the same day of analysis, to the actual (spiked) concentration, as shown in the following equation:

$$\%\ \text{Recovery} = \frac{\text{Measured concentration}}{\text{Actual concentration}} \times 100\% \qquad \text{(Eq. 4)}$$

Intra-day accuracy was evaluated by calculating the percentage recovery of measurements of the same concentration obtained from 5 independent determinations during the same day. Inter-day accuracy was evaluated by calculating the percentage recovery of measurements of the same concentration obtained from 10 independent determinations over 2 days and 15 independent determinations over 3 days.

Intra-day precision was evaluated by calculating the relative standard deviation (RSD) of measurements of the same concentration obtained from 5 independent determinations during the same day. Inter-day precision was evaluated by calculating the relative standard deviation of measurements of the same concentration obtained from 10 independent determinations over 2 days and 15 independent determinations over 3 days.

2.6.6. Extraction procedure

The efficiency of the extraction procedure to recover the different analytes from the cornea was evaluated and validated using porcine cornea samples, obtained as explained in section 2.4. Corneas (n=3 per concentration) were spiked with 10 µL of an acetone solution containing a mixture of SPL, TMSPL, CAN, CANK and DXM at either 10, 40 or 100 µg/mL then left to evaporate (i.e. resulting in deposition of 100, 400 or 1000 ng of each analyte in the cornea). Acetone is a lipid solvent which partially lyses the epithelium of the cornea allowing the compounds to spread in the tissue. After acetone evaporation, the corneas were carefully cut into small pieces, placed in vials containing 2 mL MeOH:H_2O (1:1) and 100 ng/mL IS then left

under agitation overnight (~ 12 h) for extraction at room temperature. Subsequently, samples were centrifuged at 12 000 rpm for 20 min and the supernatants collected for analysis.

The extraction efficiency (expressed as a percentage) was estimated by calculating the recovered amount to the spiked amount as displayed in the following equation:

$$\%\ \text{Extraction Efficiency} = \frac{\text{Recovered amount}}{\text{Spiked amount}} \times 100\% \qquad \text{(Eq. 5)}$$

2.6.7. Sample stability

Stability of the stock solutions of 7α-thiomethylspironolactone and canrenone at 1 mg/mL stored at -20°C was tested at 10 µg/mL by comparing the IS normalized area obtained from the stored solutions to that obtained from the freshly prepared solutions with acceptable difference being ± 10% and RSD no more than 10%. Stock solutions of the other analytes and the corneal matrix solution were prepared freshly prior to each analysis. Validation of the extraction procedure was also used to test the stability of the analytes in contact with the corneal matrix.

2.7. Statistical analysis

Data were expressed as the Mean ± SD. The Grubbs test was used to test for outliers (none were found).

3. Results and discussion

3.1. Method development

The chromatographic separation of the analytes (SPL, its metabolites TMSPL and CAN, prodrug CANK and DXM) and the IS (MeT) within a reasonable runtime was the most challenging part of the method development. This was especially so with respect to the separation of SPL and its two active metabolites, TMSPL and CAN, due to their very similar chemical structures. Chromatographic conditions were optimized to obtain the best peak resolution, intensity and shape within the shortest possible runtime.

For this purpose, various conditions including column chemistry and temperature, mobile phase composition and flow rate, injection volume and runtime were varied and optimized. First, a Waters Acquity UPLC® BEH C18 column (50 x 2.1 mm I.D., 1.7 µm) was tested but this did not enable the separation of SPL and its metabolites within a relatively short runtime. Interestingly, that was achieved with a Waters XBridge® BEH C18 column (50 x 2.1 mm I.D., 2.5 µm). The only difference between the Acquity® and XBridge® columns is the particle size,

which is smaller in the former; although this should enable better selectivity, in our case, the XBridge® column proved to be more selective. Separation of SPL, its metabolites, CANK, DXM and the IS was achieved with a mobile phase consisting of 0.1% formic acid in H_2O:MeOH (48:52, v/v) with a flow rate of 0.45 mL/min. It was noted that isocratic elution resulted in a better separation of the analytes. These experiments enabled the best chromatographic conditions to be selected and these were used for the subsequent validation of the analytical method.

To maximize the MS signal of the parent ion of the six analytes, some instrument parameters were optimized. Because most of the analytes are protonated at the low pH of the mobile phase, electrospray ionization in the positive mode was selected over the negative mode for better sensitivity. Identification and quantification of each analyte were carried out according to the mass-to-charge ratio (*m/z*) of the pseudo-molecular ion of each compound (hydrogen adduct, $[M + H]^+$). MRM (multiple reaction monitoring) detection is accepted as being more specific than the SIR detection mode; however, as demonstrated by the validation of this method described below, the SIR mode was able to provide the necessary sensitivity and specificity for quantification of the samples to be analyzed in this study.

The pseudo-molecular parent ion *m/z* corresponding to DXM, CANK, SPL/CAN, TMSPL and MeT were 393.1, 359.1, 341.0, 389.0 and 303.0, respectively. SPL was detected with *m/z* of 341.0, which corresponds to the pseudo-molecular parent ion of CAN. This is due to the cleavage of the 7α-thioacetyl group of SPL during the electrospray evaporation and ionization process within the ESI source producing CAN. This was already reported by Sora *et al.* (2010) and Vlase *et al.* (2011). However, the SPL signal can be easily distinguished from the CAN signal since their retention times are 2.4 and 3.0 min, respectively. The capillary voltage was set at 2.3 kV and the optimal cone voltage settings were 15 V for DXM, 32 V for CANK and 35 V for SPL, TMSPL, CAN and MeT. Dwell time was set at 5 ms for all the compounds except for DXM at 328 ms to enhance the sensitivity. The specific detection settings for each of the six compounds are presented in **Table 1**.

Table 1. Specific MS parameters for the detection of each analyte.

Analyte [M]	$[M + H]^+$	Cone voltage (V)	Dwell time (s)
Dexamethasone	393.1	15	0.328
Potassium canrenoate	359.1	32	0.005
Spironolactone	341.0	35	0.005
7α-thiomethylspironolactone	389.0	35	0.005
Canrenone	341.0	35	0.005
17α-methyltestosterone (IS)	303.0	35	0.005

3.2. Method validation

3.2.1. Selectivity and specificity

As mentioned previously, MRM mode is reported to be more specific because of the use of a unique parent-to-daughter transition for the detection of each analyte; however, in this study, we showed that we can achieve sufficient specificity using SIR mode. Individual injection of the standard solution of each analyte in MeOH:H_2O (1:1) showed no interference (**Figure 2 A-F**). Injection of a standard solution containing a mixture of the six compounds at 100 ng/mL in MeOH:H_2O (1:1) confirmed the good peak separation and resolution (**Figure 2G**).

The inter-day relative standard deviations (RSD) of the retention times (t_R) were less than 2% for all the compounds (**Table 2**). Any minor shift (~0.05 min) in the retention time of the six analytes always followed the same trend, *i.e.* all peaks shifted either to shorter or longer retention times and hence did not affect the peak separation and resolution.

Table 2. Retention time (t_R) of each analyte.

Analyte	Inter-day mean tR (min)	RSD
Dexamethasone	1.56 ± 0.01	0.8
Potassium canrenoate	2.03 ± 0.02	1.1
Spironolactone	2.35 ± 0.03	1.2
7α-thiomethyspironolactone	2.64 ± 0.03	1.0
Canrenone	2.93 ± 0.03	1.2
17α-methyltestosterone (IS)	4.02 ± 0.06	1.5

Values are given as mean ± SD of 20 determinations.

Analysis of a blank corneal matrix sample (**Figure 3A**) and a spiked sample with the six compounds (**Figure 3B**) showed no interferences between the corneal matrix components and

the analytes since the endogenous substances from the cornea eluted much earlier (t = 0.34 min) than the analytes confirming the specificity of this method for the identification of DXM, CANK, SPL, TMSPL, CAN and MeT (IS) in the corneal matrix.

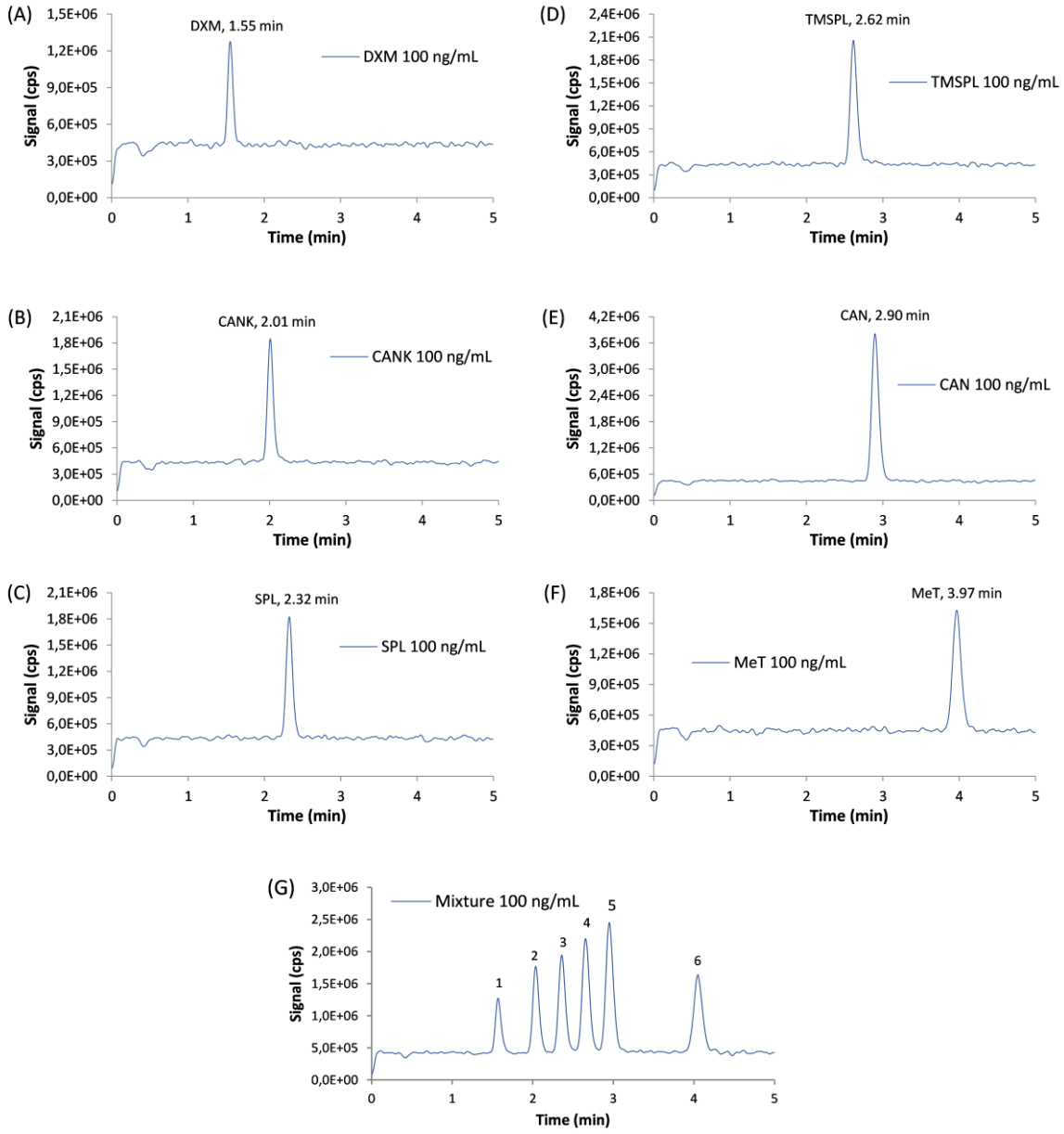

Figure 2. SIR trace of each analyte at 100 ng/mL in methanol:water (1:1); (A) dexamethasone, DXM; (B) potassium canrenoate, CANK; (C) spironolactone, SPL; (D) 7α-thiomethylspironolactone, TMSPL; (E) canrenone, CAN; (F) 17α-methyltestosterone, MeT and (G) SIR trace of a mixture with all six analytes at 100 ng/mL in methanol:water (1:1); 1, DXM; 2, CANK; 3, SPL; 4, TMSPL; 5, CAN and 6, MeT.

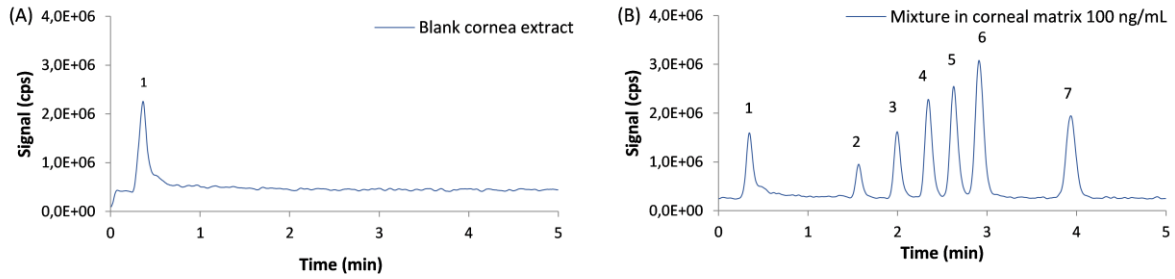

Figure 3. SIR trace of (A) blank porcine corneal matrix and (B) porcine corneal matrix spiked with the six analytes at 100 ng/mL; 1, porcine corneal matrix peak, 2, dexamethasone; 3, potassium canrenoate; 4, spironolactone; 5, 7α-thiomethylspironolactone; 6, canrenone; 7, 17α-methyltestosterone (internal standard).

3.2.2. Matrix effect

Matrix effect was observed for the six analytes (**Table 3**). All the analytes, including the internal standard (IS), underwent ion suppression to a relatively similar extent with percentage matrix factors ranging from 80.4 to 84.2% and RSD from 0.6 to 5.5%. IS normalized matrix factors ranged from 97.3 to 102.0% and RSD from 2.3 to 4.9% supporting the choice of 17α-methyltestosterone as the internal standard.

Table 3. Matrix factor (MF) and IS normalized matrix factor of each analyte.

Analyte	MF (%)	RSD (%)	IS Normalized MF (%)	RSD (%)
Dexamethasone	82.9 ± 3.1	3.7	100.4 ± 4.2	4.2
Canrenoate potassium	80.4 ± 1.4	1.8	97.3 ± 2.3	2.3
Spironolactone	82.6 ± 3.6	4.3	100.0 ± 4.4	4.4
7α-thiomethylspironolactone	83.4 ± 4.6	5.5	101.0 ± 5.0	4.9
Canrenone	84.2 ± 2.9	3.4	102.0 ± 3.2	3.2
17α-methyltestosterone (IS)	82.6 ± 0.5	0.6	-	-

Values are given as mean ± SD of 5 determinations.

3.2.3. Linearity

The method showed linearity over the concentration range of 5 to 1000 ng/mL for all the analytes with RSD of the calibration standards from the nominal concentration ranging from 0.6 to 9.1 (8.0 to 9.7 at LLOQ) which is consistent with FDA guidelines. Moreover, all the calibration curves showed an excellent correlation ($R > 0.99$) between the IS normalized peak area and the IS normalized concentration of each analyte within the test range. Typical equations of the calibration curves of each analyte are displayed in Table 4.

Table 4. Linearity range and typical equation of each analyte.

Analyte	Linearity range (ng/mL)	Typical equation	R
Dexamethasone	05-1000	$y = 0.2908\,x + 0.0262$	1.000
Potassium canrenoate	05-1000	$y = 0.5373\,x + 0.0118$	1.000
Spironolactone	05-1000	$y = 0.7387\,x + 0.0679$	1.000
7α-thiomethylspironolactone	05-1000	$y = 0.5805\,x + 0.0495$	1.000
Canrenone	05-1000	$y = 0.9911\,x + 0.0912$	1.000

y is the ratio between the peak area of each analyte to the peak area of the IS (MeT), x is the ratio of the concentration of each analyte to the known concentration of the IS (100 ng/mL).

3.2.4. Sensitivity (LLOQ)

The lower limit of quantification (LLOQ) of each analyte (DXM, CANK, SPL, TMSPL and CAN) was determined to be 5 ng/mL since the signal-to-noise ratio of each analyte, i. e. the areas obtained from each analyte versus the areas obtained from the blank corneal matrix sample, ranged from 9.6 to 42.9 with RSD ranging from 4.2 to 17.2% which satisfied the FDA guidelines (**Table 5**). Accuracy and precision were also verified at 5 ng/mL for all the analytes since all intra-day and inter-day recovery values (94.6 – 107.1%) and RSD values (3.0 – 11.0%) were within the acceptable range as described in the FDA guidelines for the LLOQ (**Table 5**). Thus, the method was considered to be sufficiently sensitive for the quantification of DXM, CANK, SPL, TMSPL and CAN in the corneal matrix.

Table 5. Signal-to-noise (S/N), accuracy and precision (intra-day, inter-day 1 and 2) at the lower limit of quantification (LLOQ = 5 ng/mL) of each analyte. DXM, dexamethasone; CANK, potassium canrenoate; SPL, spironolactone; TMSPL, 7α-thiomethylspironolactone; CAN, canrenone.

	S/N		Intra-day			Inter-day 1			Inter-day 2		
	$\frac{\text{Area LLOQ}}{\text{Area Blank}}$	RSD (%)	$\text{Conc.}_{\text{meas}}$ (ng/mL)	RSD (%)	Recovery (%)	$\text{Conc.}_{\text{meas}}$ (ng/mL)	RSD (%)	Recovery (%)	$\text{Conc.}_{\text{meas}}$ (ng/mL)	RSD (%)	Recovery (%)
DXM	9.6 ± 1.7	17.2	5.1 ± 0.5	10.2	102.9	5.1 ± 0.6	11.0	101.8	5.0 ± 0.5	11.0	99.4
CANK	12.0 ± 1.9	15.7	5.2 ± 0.5	9.0	103.9	5.4 ± 0.5	8.5	107.1	5.1 ± 0.5	9.5	101.7
SPL	19.3 ± 1.9	9.9	4.7 ± 0.5	10.1	94.7	5.2 ± 0.5	8.9	104.2	5.2 ± 0.5	9.3	103.5
TMSPL	36.2 ± 1.5	4.2	5.1 ± 0.2	3.0	102.9	5.2 ± 0.5	9.6	104.6	5.1 ± 0.5	8.9	102.0
CAN	42.9 ± 5.4	12.6	4.7 ± 0.5	10.0	94.6	5.0 ± 0.4	7.6	99.3	5.0 ± 0.4	8.8	100.5

Values are given as mean ± SD of 5 determinations for S/N and intra-day accuracy and precision, 10 determinations for inter-day 1 and 15 determinations for inter-day 2.

3.2.5. Accuracy and precision

Results of intra-day and inter-day accuracy and precision of the method for the determination of the different analytes are shown in **Table 6**. For intra-day measurements, the mean recoveries (accuracy) were within the range of 85.7 to 103.3% and RSD (precision) ranged from 0.6 to 9.2%. For inter-day measurements, the mean recoveries were within the range of 93.8 to 103.3% and RSD ranged from 1.0 to 11.0%. All intra-day and inter-day recovery values (85.7 – 103.3%) and RSD values (0.6 – 11.0%) were within the acceptable range as described in the FDA guidelines.

3.2.6. Extraction procedure

Given the high water content of the cornea (70 - 80% in the stroma), MeOH:H_2O (1:1) mixture was used as the extraction solvent to improve the extraction efficiency and to enable the simultaneous extraction of the six analytes from the cornea. The mean recovery percentages of the different analytes from the cornea ranged from 91 ± 8% to 107 ± 5% at three different concentrations. The only exception was CAN spiked at 100 ng where the percentage recovery was 116 ± 1%. Recovered concentrations and extraction efficiency (% recovery) of each analyte are presented in **Table 7**. The convenience and simplicity of this one-step extraction method made it ideal for routine sample analysis.

3.2.7. Sample stability

Results of the stability study of the stock solutions of 7α-thiomethylspironolactone and canrenone at 1 mg/mL stored at -20°C showed a stability over a period of at least 6 months since the IS normalized areas of each analyte after 6 months were within ± 10% of the IS normalized areas obtained from the freshly prepared stock solutions (5.5 ± 0.0 and 5.8 ± 0.1 for TMSPL; 8.8 ± 0.0 and 9.3 ± 0.2 for CAN, for the freshly prepared stock solutions and after storage, respectively). RSD ranged from 0.4 to 2.2. Validation of the extraction procedure also confirmed the stability of the six analytes in the presence of the corneal matrix since they were left in contact with the corneal matrix overnight (~12 h) before they were recovered.

Table 6. Intra-day and inter-day precision and accuracy of the method for each analyte. DXM, dexamethasone; CANK, potassium canrenoate; SPL, spironolactone; TMSPL, 7α-thiomethylspironolactone; CAN, canrenone. $Conc._{theo}$: theoretical (true) concentration. $Conc._{meas}$: measured (calculated) concentration.

	Intra-day			**Inter-day 1**			**Inter-day 2**		
$Conc._{theo}$ (ng/mL)	$Conc._{meas}$ (ng/mL)	RSD (%)	Recovery (%)	$Conc._{meas}$ (ng/mL)	RSD (%)	Recovery (%)	$Conc._{meas}$ (ng/mL)	RSD (%)	Recovery (%)
DXM									
10	9.9 ± 0.9	9.2	98.9	10.1 ± 0.9	8.5	100.7	10.2 ± 1.0	10.0	102.1
100	98.8 ± 1.5	1.5	98.8	96.4 ± 3.0	3.1	96.4	97.2 ± 3.4	3.5	97.2
500	511.0 ± 3.1	0.6	102.2	505.3 ± 5.8	1.2	101.1	513.6 ± 13.7	2.7	102.7
CANK									
10	8.6 ± 0.2	2.5	85.7	9.5 ± 1.0	10.0	95.3	9.6 ± 1.1	11.0	96.1
100	98.2 ± 1.0	1.0	98.2	95.3 ± 2.0	2.1	95.3	96.8 ± 4.6	4.8	96.8
500	502.7 ± 6.8	1.3	100.5	494.2 ± 6.2	1.3	98.8	502.2 ± 16.0	3.2	100.4
SPL									
10	9.1 ± 0.4	4.2	90.8	9.4 ± 0.5	5.0	93.8	9.5 ± 0.5	5.2	94.8
100	99.1 ± 1.2	1.2	99.1	97.3 ± 2.4	2.5	97.3	98.1 ± 3.1	3.2	98.1
500	516.7 ± 4.4	0.9	103.3	509.0 ± 4.9	1.0	101.8	516.6 ± 12.4	2.4	103.3
TMSPL									
10	9.5 ± 0.4	4.6	94.7	9.7 ± 0.8	8.1	97.3	9.6 ± 0.8	8.2	95.7
100	99.3 ± 2.1	2.1	99.3	96.8 ± 3.3	3.4	96.8	97.6 ± 3.3	3.3	97.6
500	515.2 ± 3.0	0.6	103.0	507.0 ± 7.5	1.5	101.4	514.8 ± 11.1	2.2	103.0
CAN									
10	8.7 ± 0.4	4.1	87.5	9.6 ± 0.6	6.3	95.7	9.5 ± 0.5	5.7	95.4
100	99.2 ± 2.1	2.1	99.2	96.8 ± 3.0	3.1	96.8	97.9 ± 3.7	3.8	97.9
500	516.1 ± 4.8	0.9	103.2	508.7 ± 7.2	1.4	101.7	515.4 ± 12.0	2.3	103.1

Values are given as mean ± SD of 5 determinations for intra-day, 10 determinations for inter-day 1 and 15 determinations for inter-day 2.

3.3.Novelty of the method

As far as we are aware, there is no available validated UHPLC-MS method in the literature allowing the simultaneous detection and quantification of spironolactone and its main metabolites, 7α-thiomethylspironolactone and canrenone, in corneal tissues, within a relatively short runtime of five min. Indeed, recent LC-MS/MS methods have been published for the quantification of spironolactone and its metabolite, canrenone, in human plasma but these methods did not include 7α-thiomethylspironolactone [2, 21, 29-31] and the run times were relatively long (> 10 min) [2, 21, 32]. Including 7α-thiomethylspironolactone in the analytical method is of great importance especially now that it is recognized as being one of the main active metabolites of spironolactone [3, 6, 21] and contributes significantly to the pharmacological effects observed [3, 6-8]. The method described here enables a more complete characterization of the biotransformation of spironolactone in the cornea, and hence allows for a better understanding of the relative contributions of the different molecules to the underlying mechanism of action of spironolactone and its metabolites as mineralocorticoid receptor antagonists.

Table 7. Recovered amounts and extraction efficiency of the different analytes after extraction from the corneas. DXM, dexamethasone; CANK, potassium canrenoate; SPL, spironolactone; TMSPL, 7α-thiomethylspironolactone; CAN, canrenone.

Spiked amount (ng)	**Recovered amount (ng)**				
	DXM	**CANK**	**SPL**	**TMSPL**	**CAN**
100	96 ± 10	99 ± 6	96 ± 4	103 ± 5	116 ± 1
400	428 ± 21	395 ± 25	365 ± 32	370 ± 32	406 ± 18
1000	982 ± 42	1028 ± 33	939 ± 48	981 ± 26	1039 ± 33
	Extraction recovery (%)				
100	96 ± 10	99 ± 6	96 ± 4	103 ± 5	116 ± 1
400	107 ± 5	99 ± 6	91 ± 8	92 ± 8	101 ± 5
1000	98 ± 4	103 ± 3	94 ± 5	98 ± 3	104 ± 3

Values are given as mean ± SD of 3 different corneas spiked with the same amount of analytes at each concentration level.

4. Conclusion

To the best of our knowledge, this is the first analytical method developed and validated allowing the simultaneous quantification of spironolactone and its two main metabolites i.e. 7α-thiomethylspironolactone and canrenone, potassium canrenoate and dexamethasone in ocular tissues. The sensitivity of this UHPLC-ESI-MS method enables quantification of concentrations below 10 ng/mL with a relative short runtime of five minutes. In addition, the method brings real advantages in terms of high-throughput features given the one-step extraction method combined with a "one-shot" analysis of each sample since all of the analytes are detected and quantified simultaneously within five minutes, which constitutes a real time-saving when analyzing a large number of samples. This method was applied *in vivo* to quantify the corneal penetration and biotransformation of mineralocorticoid receptor antagonists following multiple topical instillation and to relate the concentrations to the observed pharmacological effects [20]. That study showed that co-administration of a mineralocorticoid receptor antagonist together with the glucocorticoid countered the glucocorticoid-induced corneal delayed wound healing with a higher potency of spironolactone over potassium canrenoate. Finally, it should be possible to adapt the method for use with other biological matrices such as the skin to investigate the interplay between glucocorticoids and mineralocorticoid antagonists following different loco-regional applications and so develop novel pharmaceutical formulations.

Acknowledgements

ND and YNK acknowledge financial support from the Swiss Commission for Technology and Innovation (CTI Project 19086.1 PFLS-LS) and Apidel SA (Geneva, Switzerland). YNK would like to thank the University of Geneva, the Fondation Ernst and Lucie Schmidheiny and the Société Académique de Genève for providing financial support to enable the acquisition of the Waters Xevo® TQ-MS detector.

References

[1] D.A. Sica, Pharmacokinetics and pharmacodynamics of mineralocorticoid blocking agents and their effects on potassium homeostasis, Heart Fail. Rev. 10 (2005) 23-29.

[2] H. Dong, F. Xu, Z. Zhang, Y. Tian, Y. Chen, Simultaneous determination of spironolactone and its active metabolite canrenone in human plasma by HPLC-APCI-MS, J. Mass Spectrom. 41 (2006) 477-486.

[3] J.M. Sandall, J.S. Millership, P.S. Collier, J.C. McElnay, Development and validation of an HPLC method for the determination of spironolactone and its metabolites in paediatric plasma samples, J. Chromatogr. B 839 (2006) 36-44.

[4] L. Ramsay, J. Shelton, I. Harrison, M. Tidd, M. Asbury, Spironolactone and potassium canrenoate in normal man, Clin. Pharmacol. Ther. 20 (1976) 167-177.

[5] C.G. Dahlof, P. Lundborg, B.A. Persson, C.G. Regardh, Re-evaluation of the antimineralocorticoid effect of the spironolactone metabolite, canrenone, from plasma concentrations determined by a new high-pressure liquid-chromatographic method, Drug Metab. Dispos. 7 (1979) 103-107.

[6] A.M. Kaukonen, P. Vuorela, H. Vuorela, J.P. Mannermaa, High-performance liquid chromatography methods for the separation and quantitation of spironolactone and its degradation products in aqueous formulations and of its metabolites in rat serum, J. Chromatogr. A 797 (1998) 271-281.

[7] H.W. Overdiek, W.A. Hermens, F.W. Merkus, New insights into the pharmacokinetics of spironolactone, Clin. Pharmacol. Ther. 38 (1985) 469-474.

[8] L.E. Los, S.M. Pitzenberger, H.G. Ramjit, A.B. Coddington, H.D. Colby, Hepatic metabolism of spironolactone. Production of 3-hydroxy-thiomethyl metabolites, Drug Metab. Dispos. 22 (1994) 903-908.

[9] A. Daruich, A. Matet, A. Dirani, M. Gallice, L. Nicholson, S. Sivaprasad, F. Behar-Cohen, Oral mineralocorticoid-receptor antagonists: Real-life experience in clinical subtypes of nonresolving central serous chorioretinopathy with chronic epitheliopathy, Transl. Vis. Sci. Technol. 5 (2016) 2.

[10] Q. Ghadiali, J.J. Jung, S. Yu, S.N. Patel, L.A. Yannuzzi, Central serous chorioretinopathy treated with mineralocorticoid antagonists: A one-year pilot study, Retina 36 (2016) 611-618.

[11] T.R. Herold, K. Rist, S.G. Priglinger, M.W. Ulbig, A. Wolf, Long-term results and recurrence rates after spironolactone treatment in non-resolving central serous chorio-retinopathy (CSCR), Graefes Arch. Clin. Exp. Ophthalmol. DOI 10.1007/s00417-016-3436-5(2016).

[12] E.H. van Dijk, M.F. Nijhoff, E.K. de Jong, O.C. Meijer, A.P. de Vries, C.J. Boon, Central serous chorioretinopathy in primary hyperaldosteronism, Graefes Arch. Clin. Exp. Ophthalmol. 254 (2016) 2033-2042.

[13] E. Bousquet, T. Beydoun, P.R. Rothschild, C. Bergin, M. Zhao, R. Batista, M.L. Brandely, B. Couraud, N. Farman, A. Gaudric, F. Chast, F. Behar-Cohen, Spironolactone for nonresolving central serous chorioretinopathy: A randomized controlled crossover study, Retina 35 (2015) 2505-2515.

[14] E.K. Chin, D.R. Almeida, C.N. Roybal, P.I. Niles, K.M. Gehrs, E.H. Sohn, H.C. Boldt, S.R. Russell, J.C. Folk, Oral mineralocorticoid antagonists for recalcitrant central serous chorioretinopathy, Clin. Ophthalmol. 9 (2015) 1449-1456.

[15] M. Salehi, A.S. Wenick, H.A. Law, J.R. Evans, P. Gehlbach, Interventions for central serous chorioretinopathy: a network meta-analysis, Cochrane Database Syst. Rev. DOI 10.1002/14651858.CD011841.pub2(2015).

[16] T.R. Herold, K. Prause, A. Wolf, W.J. Mayer, M.W. Ulbig, Spironolactone in the treatment of central serous chorioretinopathy - a case series, Graefes Arch. Clin. Exp. Ophthalmol. 252 (2014) 1985-1991.

[17] N. Farman, E. Maubec, B. Poeggeler, J.E. Klatte, F. Jaisser, R. Paus, The mineralocorticoid receptor as a novel player in skin biology: beyond the renal horizon?, Exp. Dermatol. 19 (2010) 100-107.

[18] E. Maubec, C. Laouenan, L. Deschamps, V.T. Nguyen, I. Scheer-Senyarich, A.C. Wackenheim-Jacobs, M. Steff, S. Duhamel, S. Tubiana, N. Brahimi, S. Leclerc-Mercier, B. Crickx, C. Perret, S. Aractingi, B. Escoubet, X. Duval, P. Arnaud, F. Jaisser, F. Mentre, N. Farman, Topical mineralocorticoid receptor blockade limits glucocorticoid-induced epidermal atrophy in human skin, J. Invest. Dermatol. 135 (2015) 1781-1789.

[19] V.T. Nguyen, N. Farman, E. Maubec, D. Nassar, D. Desposito, L. Waeckel, S. Aractingi, F. Jaisser, Re-epithelialization of pathological cutaneous wounds is improved by local mineralocorticoid receptor antagonism, J. Invest. Dermatol. 136 (2016) 2080-2089.

[20] N. Dahmana, T. Mugnier, D. Gabriel, V. Kaltsatos, T. Bertaim, F. Behar-Cohen, R. Gurny, Y.N. Kalia, Topical Administration of Spironolactone-Loaded Nanomicelles Prevents Glucocorticoid-Induced Delayed Corneal Wound Healing in Rabbits, Mol. Pharm. 15 (2018) 1192-1202.

[21] D.I. Sora, S. Udrescu, F. Albu, V. David, A. Medvedovici, Analytical issues in HPLC/MS/MS simultaneous assay of furosemide, spironolactone and canrenone in human plasma samples, J. Pharm. Biomed. Anal. 52 (2010) 734-740.

[22] M.F. Suyagh, P.L. Kole, J. Millership, P. Collier, H. Halliday, J.C. McElnay, Development and validation of a dried blood spot-LC-APCI-MS assay for estimation of canrenone in paediatric samples, J. Chromatogr. B 878 (2010) 769-776.

[23] J.W. Overdiek, W.A. Hermens, F.W. Merkus, Determination of the serum concentration of spironolactone and its metabolites by high-performance liquid chromatography, J. Chromatogr. B 341 (1985) 279-285.

[24] J.H. Sherry, J.P. O'Donnell, H.D. Colby, Separation of spironolactone and its biologically active sulfur-containing metabolites by high-performance liquid chromatography, J. Chromatogr. B 374 (1986) 183-190.

[25] A. Jankowski, A. Skorek-Jankowska, H. Lamparczyk, Simultaneous determination of spironolactone and its metabolites in human plasma, J. Pharm. Biomed. Anal. 14 (1996) 1359-1365.

[26] A.Z. Abosehmah-Albidy, P. York, V. Wong, M.S. Losowsky, H. Chrystyn, Improved bioavailability and clinical response in patients with chronic liver disease following the administration of a spironolactone: beta-cyclodextrin complex, Br. J. Clin. Pharmacol. 44 (1997) 35-39.

[27] FDA, Guidance for Industry Bioanalytical Method Validation DOI (2001).

[28] International Conference on Harmonisation of Technical Requirements for Registration of Pharmaceuticals for Human Use - Validation of Analytical Procedures: Text and Methodology Q2 (R1). 2005.

[29] L. Vlase, S. Imre, D. Muntean, M. Achim, D.-L. Muntean, Determination of Spironolactone and Canrenone in Human Plasma by High-performance Liquid Chromatography with Mass Spectrometry Detection, Croat. Chem. Acta 84 (2011) 361-366.

[30] J.-H. Lee, T.-G. An, S.J. Kim, W.-S. Shim, K.-T. Lee, Development of liquid chromatography tandem mass spectrometry method for determination of spironolactone in human plasma: application to a bioequivalence study of Daewon Spiracton tablet® (spironolactone 50 mg), J. Pharm. Investig. 45 (2015) 601-609.

[31] B.C.H. van der Nagel, J. Versmissen, S. Bahmany, T. van Gelder, B.C.P. Koch, High-throughput quantification of 8 antihypertensive drugs and active metabolites in human plasma using UPLC-MS/MS, J. Chromatogr. B Analyt. Technol. Biomed. Life Sci. 1060 (2017) 367-373.

[32] K. Takkis, R. Aro, L.-T. Kõrgvee, H. Varendi, J. Lass, K. Herodes, K. Kipper, Signal Enhancement in the HPLC-ESI-MS/MS analysis of spironolactone and its metabolites using HFIP and NH4F as eluent additives, Anal. Bioanal. Chem. 409 (2017) 3145-3151.

CHAPTER II

Topical administration of spironolactone-loaded nanomicelles prevents glucocorticoid-induced delayed corneal wound healing in the rabbit

Naoual Dahmana,[†] Thibault Mugnier,[‡] Doris Gabriel,[‡] Vassilios Kaltsatos,[§] Thierry Bertaim,[§] Francine Behar-Cohen,[‖,⊥] Robert Gurny,[†,‡] and Yogeshvar N. Kalia[†]

[†] School of Pharmaceutical Sciences, University of Geneva & University of Lausanne, CMU - 1 rue Michel Servet, 1211 Geneva 4, Switzerland.
[‡] Apidel SA, 29 Quai du Mont Blanc, 1201 Geneva, Switzerland.
[§] CEVA Santé Animal, 10 Avenue de la Ballastière, 33500 Libourne, France.
[‖] Fondation Asile des Aveugles - Hôpital Ophtalmique Jules-Gonin, 15 Avenue de France, 1004 Lausanne, Switzerland.
[⊥] INSERM, UMRS 872 Team 17, Centre de Recherche des Cordeliers, 15 rue de l'Ecole de Médecine, 75006 Paris, France.

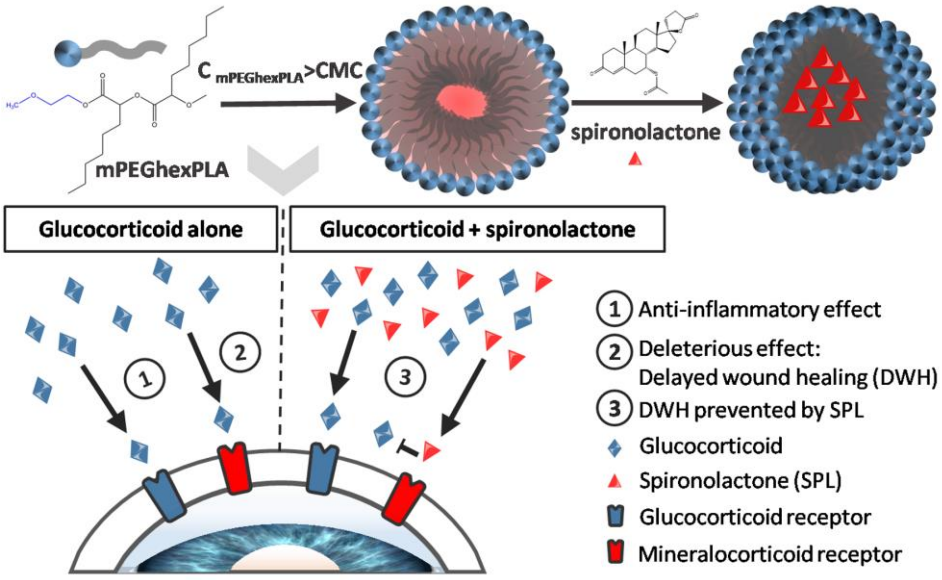

Published in Molecular Pharmaceutics *(Mol. Pharm. 2018, 15, 1192-1202).*

Abstract

The objective was to investigate whether mineralocorticoid receptor antagonism using a novel topical micellar formulation of spironolactone could prevent glucocorticoid-induced delayed corneal wound healing in New Zealand white rabbits. Spironolactone micelles (0.1%, w/v) with a mean number weighted diameter of 20 nm were prepared using a pegylated copolymer (mPEG-dihexPLA) and showed a preliminary stability of at least 12 months at 5°C. Preclinical studies in New Zealand white rabbits demonstrated that the 0.1% spironolactone micellar formulation was well-tolerated since no reaction was observed in the cornea following multiple daily instillation over 5 days. As expected, the preclinical studies also confirmed that dexamethasone significantly delayed epithelial wound healing as compared to untreated control (percentage re-epithelialization after Day 4: 84.6 ± 13.9% versus 99.5 ± 1.0% for the control, $p<0.05$). However, the addition of the 0.1% spironolactone micellar formulation significantly improved the extent of re-epithelialization, countering the dexamethasone induced delayed wound healing with a percentage re-epithelialization that was statistically equivalent to the control (96.9 ± 7.3% versus 99.5 ± 1.0%, $p>0.05$). The biodistribution study provided insight into the ocular metabolism of spironolactone and hence the relative contributions of the parent molecule and its two principal metabolites, 7α-thiomethylspironolactone and canrenone, to the observed pharmacological effects. Comparison of the efficacies of spironolactone and potassium canrenoate (a water-soluble precursor of canrenone) in overcoming the dexamethasone-induced delayed wound healing confirmed that the former had greater efficacy. The results pointed to the greater potency of 7α-thiomethylspironolactone over canrenone as a mineralocorticoid receptor antagonist, which explained its superior ability in countering the glucocorticoid-induced over-activation that was responsible for the delayed wound healing. In conclusion, the preliminary results supported the above-mentioned hypothesis suggesting that co-administration of mineralocorticoid receptor antagonists to patients under glucocorticoid therapy might prevent the deleterious effects of glucocorticoids on complex corneal wound healing processes.

Keywords: Glucocorticoids, corneal wound healing, spironolactone, polymeric micelles, *in vivo* preclinical study, ultra-high performance liquid chromatography – mass spectrometry.

1. Introduction

Impaired wound healing is a significant clinical problem encountered as a complication of certain chronic conditions such as diabetes, sickle cell disease, Cushing syndrome and also in patients receiving prolonged glucocorticoid therapy [1, 2]. Impaired corneal wound healing is a major concern in ophthalmology since it can cause chronic infection and ulceration resulting in corneal opacity and scarring responsible for major visual disturbance that may ultimately lead to blindness [3, 4].

Wound healing is a complex and highly organized process that encompasses successive and overlapping stages including inflammation, granular tissue formation and re-epithelialization, new matrix formation and collagen accumulation. The whole process is tightly controlled by a precise and complex interplay of various factors involving cells, growth factors, cytokines and components of the extracellular matrix [1, 2, 5-8]. Whilst wound healing follows a uniform pattern all over the body, local specificities exist resulting from tissue-specific differences, for example, lack of vessels in the cornea compared to the skin [8]. The critical feature of wound healing is the restoration of the epithelial barrier. Re-epithelialization in the cornea is a key step in preventing abnormal healing and subsequent impaired vision [6]. During this process, corneal epithelial cells proliferate at the wound edge, migrate to cover the lesioned area and differentiate to form the new tissue. Absence of cell migration is related to the clinical phenotype of chronic non-healing wounds. When total re-epithelialization is achieved, the barrier is restored and the eye is again protected from external infections [2, 3, 5, 6, 8].

Synthetic glucocorticoids (GC) are among the most widely prescribed drugs in the world. They are given systemically or topically to treat a wide number of inflammatory and autoimmune diseases, allergies and ocular disorders. In ophthalmology, GC are currently used to prevent and to treat post-operative ocular inflammation, graft rejection and corneal neovascularization; they are also indicated for the treatment of many ocular surface disorders including dry eye [2, 7, 9, 10]. Whilst the pleiotropic anti-inflammatory effects of GC reduce cytotoxic and pro-angiogenic cytokines and metalloproteinase expression [11], they are also associated with delayed wound healing [2, 8, 12]. Several *in vivo* studies have reported that the use of GC such as dexamethasone resulted in delayed corneal wound healing in rabbits [4, 7, 13, 14]. More significantly, GC treatment also leads to reduced and delayed wound re-epithelialization in humans [15]. In a clinical trial, 42 patients who received topical prednisolone phosphate were found to re-epithelialize more slowly than the placebo group [4].

GC bind to the glucocorticoid receptor (GR), but they can also bind with high affinity to the closely related mineralocorticoid receptor (MR) – both receptors are expressed in the corneal epithelium. Recent studies have reported that, in the skin, delayed wound healing might be due to illicit occupancy of the MR by GC. In mineralocorticoid-sensitive tissues like the kidney, GC are inactivated by the enzyme 11β-hydroxysteroid dehydrogenase type II (HSD2), thereby preventing their binding to MR which is therefore selectively activated by aldosterone, the endogenous mineralocorticoid (MC) that binds to the MR and is responsible for sodium homeostasis [2, 9, 12, 16-18]. However, tissues where HSD2 activity is low such as skin, eye, heart, and neurons are susceptible to off-target GC binding to the MR.

Given that the MR might be over-activated by GC in tissues where HSD2 activity is low, the use of a MR antagonist (MRA) was proposed as a potential therapeutic strategy to overcome the negative impact of GC treatment on wound healing. This hypothesis was verified in several studies: (i) in cultured human skin explants where clobetasol-induced epidermal atrophy was significantly limited by the MRA, potassium canrenoate and eplerenone [2, 9], (ii) in mice where potassium canrenoate significantly improved clobetasol-induced delayed wound healing [2] and (iii) in healthy volunteers, where local co-administration of the MRA, spironolactone, with clobetasol significantly improved the clobetasol-induced impairment of skin wound closure [9]. Spironolactone is a potent MRA, which competes with aldosterone to bind to the MR, and is marketed mainly as a diuretic (potassium-sparing) for the treatment of congestive heart failure, essential hypertension and various oedematous conditions [19, 20]. Spironolactone is pharmacologically active, but it also exerts its effect via two main metabolites; 7α-thiomethylspironolactone and canrenone [21-23].

The objective of the present study was to investigate whether, as in the case of the skin, GC-induced delayed corneal wound healing could be reversed by MR antagonists. To test this hypothesis, a novel micellar formulation of spironolactone (0.1%, w/v) was developed and characterized for topical ocular administration and then evaluated to determine whether it was possible to counter the impaired corneal wound healing induced by dexamethasone in New Zealand white rabbits. It was decided to compare the results to those observed after topical application of a lower concentration micellar formulation of spironolactone (0.01%, w/v) and a formulation containing the water-soluble prodrug, potassium canrenoate (0.1%, w/w), which is a precursor of canrenone. In order to provide an insight on the role played by the different aforementioned molecules in the process of re-epithelialization, an analytical method allowing the simultaneous quantification of spironolactone and its two main metabolites; 7α-

thiomethylspironolactone and canrenone; potassium canrenoate and dexamethasone was developed and validated. Although aqueous solutions are the most suitable and convenient dosage form for topical delivery to the eye, spironolactone has a very low aqueous solubility (0.02 mg/mL). Therefore, methoxy-poly(ethylene glycol)-dihexyl-substituted-poly(lactic acid) (mPEG-dihexPLA) diblock copolymer was used to prepare spironolactone micelles in order to increase its aqueous solubility. This biodegradable self-assembling copolymer has proven safety in rabbits and enhanced drug bioavailability following topical application to the eye [24-26].

2. Experimental section

2.1. Materials

Methoxy-poly(ethylene glycol)-di-hexyl-substituted-poly(lactic acid) [27], (mPEG-dihexPLA, 5.5 kDa, **Scheme 1A**) was supplied by Apidel SA (Geneva, Switzerland). Spironolactone (SPL, **Scheme 1B**) was purchased from Zhejiang Langhua pharmaceutical Co., Ltd. (Zhejiang, China). 7α-thiomethylspironolactone (TMSPL) was purchased from TLC Pharmaceutical Standards Ltd. (Ontario, Canada). Canrenone (CAN), potassium canrenoate (CANK) and 17α-methyltestosterone (MeT), used as an internal standard (IS), were purchased from Sigma-Aldrich (Buchs, Switzerland). Dexamethasone (DXM) was purchased from Tianjin TianMao Technology Development Corp. Ltd (Tianjin, China). Maxidex® (dexamethasone 0.1% suspension, Alcon) was purchased from a local pharmacy. Sodium chloride was obtained from Hänseler AG (Herisau, Switzerland). Ultrapure water (H_2O, resistivity > 18 MΩ cm) was prepared using a Merck Millipore Milli-Q water purification system (Darmstadt, Germany). Methanol (MeOH, HPLC grade) was obtained from Fisher Scientific (Waltham, MA, USA), acetonitrile (ACN, HPLC grade) and formic acid (ULC/MS grade) from Biosolve (Dieuze, France). Acetone Chromasolv® (HPLC grade) was purchased from Sigma Aldrich (Buchs, Switzerland) and trifluoroacetic acid was obtained from VWR (Dietikon, Switzerland). All other chemicals were at least of analytical grade. Millex® filters (Durapore PVDF, pore size 0.22 µm, diameter 13 mm) were purchased from Sigma-Aldrich (Buchs, Switzerland). 10 mL sterile eye drop vials were purchased from Müller + Krempel AG (Bülach, Switzerland).

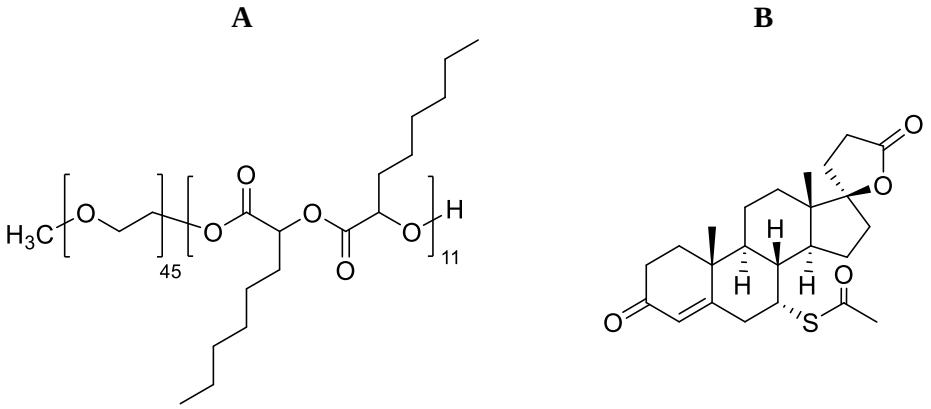

Scheme 1. Chemical structure of (A) mPEG-dihexPLA copolymer and (B) spironolactone.

2.2. Analytical methods

2.2.1. HPLC methods

HPLC methods were developed to support formulation development and stability studies of both spironolactone micelles and the potassium canrenoate solution.

Quantification of spironolactone by HPLC-UV: Spironolactone quantification was performed on an Agilent 1100 HPLC using a reversed phase column (YMC basic, 250 x 3.0 mm, 5 µm) heated to 40°C. The method employed a gradient of acetonitrile and water containing 0.1% trifluoroacetic acid: the acetonitrile percentage was increased from 40% to 80% over 5 min, kept constant for 3 min and then decreased to 40% within half a minute. The mobile phase flow rate was 1.0 mL/min and the UV detector was set to 238 nm.

Quantification of potassium canrenoate by HPLC-UV: Potassium canrenoate quantification was performed on an Agilent 1100 HPLC using a reversed phase column (YMC basic, 250 x 3.0 mm, 5 µm) heated to 40°C. The mobile phase consisted of acetonitrile containing 0.1% trifluoroacetic acid (A) and water containing 0.1% trifluoroacetic acid (B). The analysis was carried out in isocratic mode with 55% eluent A and 45% eluent B. The mobile phase flow rate was 1.0 mL/min and the UV detector was set to 286 nm.

2.2.2. UHPLC-MS method

A UHPLC-MS analytical method was developed and validated to enable the simultaneous quantification of the different analytes in the rabbit corneas obtained from the *in vivo* study. Briefly, the liquid chromatographic system consisted of a Waters Acquity® ultra performance liquid chromatography (UPLC®) system (Baden-Dättwil, Switzerland) including a binary solvent manager, a sample manager with an injection loop volume of 10 µL and a column manager. The reversed phase chromatographic separation of the six compounds was performed

on a Waters XBridge® BEH C18 column (50 x 2.1 mm I.D., 2.5 µm) fitted with a Waters XBridge® BEH C18 Vanguard pre-column (5 x 2.1 mm I.D., 2.5 µm). The elution was carried out in isocratic mode with a mobile phase consisting of 0.1% formic acid in H_2O/MeOH (48/52, v/v) with a flow rate of 0.45 mL/min and a run time of 5 min. Column temperature was held at 40°C and sample manager temperature was kept at room temperature. Injection volume was set at 5 µL. The mass spectrometry (MS) system consisted of a Waters XEVO® TQ-MS detector (Baden-Dättwil, Switzerland) fitted with a Z-spray electrospray ionisation source. MS detection of the six compounds was performed using electrospray ionisation in the positive mode (ESI+) and selected ion recording (SIR) using the pseudo-molecular ion of each compound as the parent ion (hydrogen adduct, $[M + H]^+$). The capillary voltage was set at 2.3 kV, and desolvation gas temperature and flow were maintained at 350°C and 650 L/h, respectively. The specific MS parameters for each analyte were tuned and determined by infusing each compound individually at 1 µg/mL in MeOH:H_2O (1:1) at a flow rate of 5 µL/min. Identification and quantification of each analyte were carried out according to the mass-to-charge ratio (m/z) of the pseudo-molecular ion of each compound (hydrogen adduct, $[M + H]^+$). Cone voltage optimal settings were 15 V for DXM, 32 V for CANK and 35 V for SPL, TMSPL, CAN and MeT. The pseudo-molecular parent ion corresponding to DXM, CANK, SPL/CAN, TMSPL and MeT have an *m/z* of 393.1, 359.1, 341.0, 389.0 and 303.0 respectively. Dwell time was set at 5 ms for all the compounds except for DXM at 328 ms. Data processing was performed using Waters MassLynx software version 4.1 (Baden-Dättwil, Switzerland).

Calibration standards at 10, 20, 50, 100, 200, 500 and 1000 ng/mL were prepared in a corneal matrix obtained from porcine corneas extracted in MeOH:H_2O (1:1). All calibration curves were linear ($r^2 > 0.99$). The limit of detection (LOD) and the limit of quantification (LOQ) for each analyte are summarized in **Table 1**.

Table 1. Limit of determination (LOD) and limit of quantification (LOQ) of each analyte in corneal matrix.

Analyte	LOD (ng/mL)	LOQ (ng/mL)
Dexamethasone	5.4	16.3
Potassium canrenoate	2.4	7.2
Spironolactone	3.8	11.4
7α-thiomethyspironolactone	1.3	3.9
Canrenone	2.9	8.8

2.3. Development and optimization of spironolactone micellar formulation

Spironolactone loaded micelles (0.1%, w/v) were prepared using mPEG-dihexPLA copolymer at different SPL:copolymer ratios; 1:20, 1:40 and 1:60. Two buffers were also evaluated; citrate buffer (10 mM, pH 5.5) and PBS (10 mM, pH 7.4). Formulations were prepared at a batch size of 10 mL. Briefly, 10 mg spironolactone were dissolved in 2 mL acetone. Then 200, 400 or 600 mg mPEG-dihexPLA, corresponding respectively to 1:20, 1:40 and 1:60 SPL:copolymer ratios, were added to the acetone solution containing SPL and dissolved. Subsequently, this solution was added dropwise using a syringe pump (6 mL/h) under sonication (20% amplitude - S 450 D, Branson, USA) to 10 mL of the aqueous phase, consisting of either citrate buffer (10 mM, pH 5.5) or PBS (10 mM, pH 7.4). Then, acetone was removed under reduced pressure (58°C, 180 mbar - Buchi Rotavapor R-210, Switzerland). Finally, the osmolarity was adjusted to 270-300 mOsm with NaCl and the formulations filtered under a laminar flow hood through 0.22 µm PVDF filters into sterilized vials and kept at 5°C. Formulations were characterized in terms of concentration, drug loading, incorporation efficiency and micelle size. Micelles were also visualized using transmission electron microscope (TEM, FEI Tecnai™ G2 Sphera, Oregon, USA). Briefly, the micellar formulation was diluted 1:10 in MilliQ water, then 5 µL were deposited on a grid, left for 30 s and the excess was carefully wiped. Subsequently, one drop of 2% uranyl acetate was applied during 30 s to enhance the contrast and the excess was carefully removed. TEM magnification was set at 25000x.

2.3.1. Determination of drug content and incorporation efficiency

Spironolactone content was quantified by HPLC-UV. Aliquots from spironolactone micellar formulations were diluted with acetonitrile (1:10) prior to HPLC analysis. Drug loading and incorporation efficiency were calculated using the following equations:

$$\text{Drug Loading(mg/g)} = \frac{\text{Mass of drug incorporated in micelles (mg)}}{\text{Mass of copolymer used (g)}} \qquad \textit{Eq. 1}$$

$$\text{Incorporation Efficiency (\%)} = \frac{\text{Actual drug loading}}{\text{Target drug loading}} \text{ x } 100 \qquad \textit{Eq. 2}$$

2.3.2. Size determination

The intensity weighted (Z-average, Z_{av}) and the number weighted (d_n) hydrodynamic diameters and the polydispersity index (PDI) of the micelles were measured by dynamic light scattering

using the Zetasizer Nano-ZS (Malvern Instruments, UK). SPL micellar solutions were diluted 1:1 in MilliQ water and filled into disposable plastic cuvettes for analysis with back scattering light (173 degrees).

2.4. Preparation and characterization of the formulations used *in vivo*

Spironolactone micellar formulations (0.1% and 0.01%, w/v)

Spironolactone loaded micelles (0.1%, w/v) were prepared at a batch scale of 14 mL. Briefly, 616 mg mPEG-dihexPLA and 15.4 mg spironolactone were dissolved in 2 mL of acetone. The organic phase was added dropwise (6 mL/h) to the aqueous phase (10 mM citrate buffer, 0.7% NaCl, pH 5.5) under sonication (20% amplitude - S 450 D, Branson, USA). Subsequently, acetone was removed under reduced pressure (58°C, 180 mbar - Buchi Rotavapor R-210, Switzerland). This formulation was prepared with 10% excess (by weight) to counterbalance the amount of SPL and mPEG-dihexPLA lost in the syringe during the formulation process. The 0.01% (w/v) SPL concentration was obtained by 1:10 dilution of the 0.1% SPL micelles in the aqueous phase. Finally, formulations were filtered through 0.22 µm PVDF filters and stored in sterile eye drop vials. Spare aliquots from both formulations were kept for stability testing.

Potassium canrenoate solution (0.1%, w/w)

Potassium canrenoate solution (0.1%, w/w) was prepared by dissolving 50 mg potassium canrenoate in 50 g of aqueous buffer (5 mM phosphate buffer, 0.9% NaCl, pH 8.0). This solution was filtered through 0.22 µm PVDF filters and stored in sterile eye drop vials. Spare aliquots were kept for stability testing of the formulation.

2.5. *In vivo* tolerability and efficacy study in rabbits

2.5.1. Animals

Fifty male albino New Zealand rabbits, weighing approximately 2.3–3.0 kg, were included in the study (Iris Pharma, France). Animals were housed individually in standard cages, under identical environmental conditions. The temperature was kept at 15-21°C and the relative humidity was >45%. Rooms were continuously ventilated (≥ 15 air volumes per hour). Temperature and relative humidity were continuously controlled and recorded. Animals were routinely exposed (in-cage) to a 10-200 lx light in a 12-hour light/dark cycle (from 7:00 a.m. to 7:00 p.m.). Animals had enrichment and free access to food (150 g/day) and were allowed water *ad libitum*. All animals were healthy and free of clinically observable ocular abnormalities throughout the study. All animals were treated according to the Directive 2010/63/EU – The

European convention on the protection of animals used for scientific purposes – and to the Association for Research in Vision and Ophthalmology (ARVO) Statement for the use of animals in ophthalmic and visual research. The studies were approved by the local veterinary authority for animal experimentation (French governmental platform APAFIS - authorization number 20160212659386).

2.5.2. Induction of the corneal wounds

Animals were anesthetized by intramuscular injection of a ketamine-xylazine mixture. Then, a drop of 0.4% oxybuprocaine was topically applied for local anesthesia. In addition, buprenorphine (20 µg/kg) was administrated, by subcutaneous injection, 30 min prior to wound induction to prevent pain. A scalpel handle was used to keep the right eye out of orbit, then the corneal epithelium was completely removed using a scalpel blade. De-epithelialization was monitored by fluorescein staining. Finally, eyes were washed with physiological saline and swabbed with a dry cotton tip applicator to remove cellular debris.

2.5.3. Study design

Animals were randomized into 5 treatment groups as presented in **Table 2**. Each group included 10 rabbits and the animals were instilled in the right eye every 1.50 ± 0.15 h using an eye-dropper, 3 times daily on Day 0, 6 times daily from Day 1 to Day 4and once on Day 5.

Group 1, 2 and 3: Animals received the formulations containing the mineralocorticoid receptor antagonist (0.1% spironolactone micelles, 0.01% spironolactone micelles and 0.1% potassium canrenoate solution, respectively) – 1 drop (~35 µL) of the formulation, then 5 minutes later, 1 drop of 0.1% dexamethasone (Maxidex®).

Group 4 (positive control): Animals received only PBS (control) - 2 drops of PBS with 5 minutes interval between each administration.

Group 5 (negative control): Animals received 1 drop of PBS, then 5 minutes later, 1 drop of 0.1% dexamethasone (Maxidex®).

On Day 5, 30 minutes after the last assessment of tolerability, animals received the last instillation (1 drop in the right eye). Subsequently, rabbits were euthanized, both eyes were enucleated and corneas were harvested and stored at -80°C until analysis.

Ocular tolerability

An ophthalmoscope was used for accurate examination of the conjunctiva, cornea and iris. Both eyes of each rabbit were examined using the ophthalmoscope during the pre-test period

(baseline), then once daily after the last administration of the day from Day 0 to Day 4. The observations were scored using the Draize scale (**Table S1**).

Table 2. Treatment received per animal group.

Group	Rabbit N°	Left Eye	Right Eye
1	01-10	Control	0.1% spironolactone micelles + 0.1% dexamethasone
2	11-20	Control	0.01% spironolactone micelles + 0.1% dexamethasone
3	21-30	Control	0.1% potassium canrenoate solution + 0.1% dexamethasone
4	31-40	Control	PBS
5	41-50	Control	0.1% dexamethasone

2.5.4. Corneal wound healing

The size of the corneal wound was evaluated using the fluorescein test, immediately after the ocular debridement and once a day before the first instillation. A baseline was recorded before the de-epithelialization (**Table S2**). One drop of fluorescein was instilled to the right (lesioned) eye, then the cornea was illuminated with blue light. Images of the corneal lesion (area stained by fluorescein) were taken using a CCD camera and analyzed using image J software. Percentage of re-epithelialization was calculated as follow:

$$\%\ Re-Epithelialization\ (Day\ x) = \%\ Wounded\ Area\ (Day\ 0) - \%\ Wounded\ Area\ (Day\ x) \quad Eq.\ 3$$

2.5.5. Animal sacrifice and sampling

At the end of the measurement period, animals were euthanized by an intracardiac injection of overdosed pentobarbital following anaesthesia by intramuscular injection of ketamine-xylazine mixture. This method is one of the recommended methods for euthanasia by the European authorities. Immediately after euthanasia, both eyes were enucleated and corneas were dissected and stored at -80°C until analysis.

2.5.6. Extraction and quantification of the drugs in the cornea

The extraction method of the drugs from the cornea was validated prior to use. The 50 treated and 50 control corneas stored at -80°C were thawed at room temperature, weighed and ground manually into small pieces which were placed in a glass vial containing 1 mL of MeOH:H_2O (1:1) and 100 ng/mL internal standard (IS, 17α-methyltestosterone). The vials were left under stirring at 300 rpm overnight for extraction. The following day, samples were centrifuged during 20 min at 12 000 rpm and the supernatants were quantified using the validated UHPLC-MS method.

2.6. Statistical analysis

Statistical analysis on the percentage re-epithelialization of the corneas in the rabbits from the different groups was performed using Kruskal-Wallis one-way analysis of variance on ranks followed by Student-Newman-Keuls post-hoc analysis. Statistical analysis on the mean concentrations found in the left and right corneas was performed using Student t-test or Mann-Whitney rank sum test.

3. Results

3.1. Spironolactone micelles formulation and optimization

The incorporation efficiency of SPL in the mPEG-dihexPLA micelles varied according to the SPL:copolymer ratio and was also influenced by the buffer used. Overall, the formulation containing SPL and mPEG-dihexPLA copolymer at a ratio of 1:40 and citrate buffer (buffer A; 10 mM, pH 5.5) as the aqueous phase (Formulation A40) achieved the best incorporation efficiency of 89.1 ± 0.2% corresponding to a drug loading of 22.3 ± 0.1 mg/g (**Table 3**). In the case of PBS (buffer B; 10 mM, pH 7.4), the highest incorporation efficiency, of 83.6 ± 0.6%, was achieved with SPL:copolymer ratio of 1:60 (Formulation B60) corresponding to a drug loading of 14.0 ± 0.1 mg/g (**Table 3**). The difference of ~5% in incorporation efficiency may have been due to the different ionic strengths of the buffer solutions (citrate 50 mM, PBS buffer, 167 mM). The intensity weighted micelles diameters (Z_{av}) for Formulation A40 and B60 were 50 and 52 nm, respectively and the corresponding number weighted micelles diameters (d_n) were 17 and 19 nm (PDI=0.2) (**Table 3**). The spherical and homogeneous aspect of the spironolactone loaded micellar nanocarriers are clearly discerned in **Figure 1**.

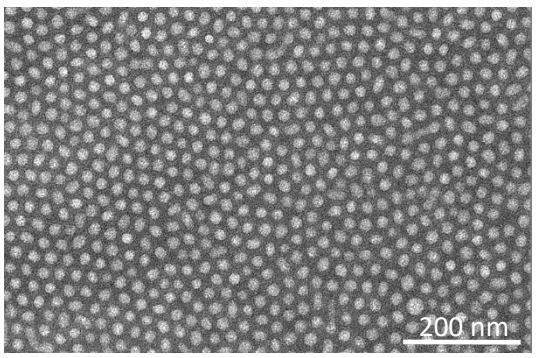

Figure 1. Transmission electron microscopy (TEM) image of the optimized 0.1% spironolactone loaded micelles.

The stability of Formulations A40 and B60 was monitored during one month at 5°C. Results showed that Formulation A40 remained stable over one month with respect to the concentration,

pH and osmolarity versus two weeks for Formulation B60. Micelle size was stable over a period of one month after storage at 5°C for both formulations (d_n, Z_{av} and PDI were 19 nm, 62 nm and 0.2 respectively for Formulation A40 and 25 nm, 55 nm and 0.2 respectively for Formulation B60). Formulation A40 was optimized to achieve 100% incorporation efficiency corresponding to a SPL concentration of 1 mg/mL. During the formulation development, it was noticed that a small amount of SPL and mPEG-dihexPLA was lost in the syringe during addition to the aqueous solution. In order to correct for this loss, it was decided to prepare the formulations with 10% excess (by weight) of spironolactone and mPEG-dihexPLA, corresponding to the amount lost during the formulation process. Given the higher incorporation efficiency and the superior stability, Formulation A40 was selected as the lead formulation to be used in further studies.

Table 3. Characterization of the different formulations of spironolactone.

Buffer	Ratio[a]	Name	Target [SPL][b] (mg/mL)	[SPL] ± SD (mg/mL)	Target DL[c] (mg/g)	Actual DL ± SD (mg/g)	IE[d] ± SD (%)	Size (nm)		
								d_n	Z_{av}	PDI
Citrate	1:20	A20	1	0.49 ± 0.01	50.0	24.5 ± 0.5	49.0 ± 1.0	13	53	0.2
	1:40	**A40**	1	0.89 ± 0.00	25.0	22.3 ± 0.1	89.1 ± 0.2	17	50	0.2
	1:60	A60	1	0.85 ± 0.01	16.7	14.2 ± 0.1	84.8 ± 0.7	16	50	0.2
PBS	1:20	B20	1	0.45 ± 0.02	50.0	22.4 ± 1.0	44.8 ± 2.0	31	55	0.2
	1:40	B40	1	0.73 ± 0.00	25.0	18.2 ± 0.1	72.9 ± 0.3	25	56	0.2
	1:60	B60	1	0.84 ± 0.01	16.7	14.0 ± 0.1	83.6 ± 0.6	19	52	0.2

[a] Spironolactone:copolymer ratio, [b] Spironolactone concentration, [c] Drug loading, [d] Incorporation efficiency.

3.2. Characterization of the formulations used *in vivo*

The stability of the 0.01% and 0.1% spironolactone micellar formulations was assessed over 12 months at 5°C. Concentration, pH and micelles size remained perfectly stable over the 12 months period. The stability of the 0.1% potassium canrenoate solution was assessed over 24 days at 5°C, to ensure product stability for the duration of the animal study. Results showed that the concentration and pH remained stable over the desired study period. Formulation characteristics are summarized in **Table 4**.

Table 4. Characterization of the formulations used during the *in vivo* study.

Formulation	Conc.[a] ± SD (mg/mL)	pH	Size (nm)		
			d_n	Z_{av}	PDI
0.1% spironolactone micelles	1.03 ± 0.00	5.5	20	48	0.2
0.01% spironolactone micelles	0.10 ± 0.00	5.5	26	49	0.2
0.1% potassium canrenoate solution	0.95 ± 0.00	8.0	-	-	-

[a] Measured concentration of spironolactone or potassium canrenoate.

3.3. Tolerability and efficacy study in new zealand white rabbits

3.3.1. Ocular tolerability

Results of the ocular examinations of the animals on Day 4 are reported per treatment group in **Table 5.** Conjunctival redness, chemosis, discharge, iritis and corneal opacities were scored according to the Draize scale (**Table S1**). Most of the ocular reactions observed were slight and transient and were not attributed to the treatment since they are commonly observed in the de-epithelialization model. No ocular reaction was observed on Day 5 for all groups except for one animal treated with 0.1% dexamethasone alone (Group 5) which still displayed a slight conjunctival redness (score 1 on a scale of 0 to 3), a mild chemosis (score 2 on a scale of 0 to 4) associated to a moderate discharge (score 2 on a scale of 0 to 3). Indeed, this animal still exhibited a marked corneal re-epithelialization defect on Day 5 (-42.6%), this having possibly contributed to a persistent ocular reaction.

Table 5. Ocular observations of the animals on Day 4. Score (*italic*) and number of animals concerned.

	0.1% SPL micelles + 0.1% DXM	**0.01% SPL micelles + 0.1% DXM**	**0.1% CANK solution + 0.1% DXM**	**PBS**	**0.1% DXM**
Conjunctival redness	*1/3*** 1/10	*1/3*** 2/10	*1/3*** 5/10	*	*1/3*** 4/10
Chemosis	*1/4* 1/10	*	*	*	*2/4* 1/10
Discharge	*	*	*1-2/3* 5/10	*	*2/3* 1/10
Iritis	*	*	*1/2*** 2/10	*	*
Corneal opacities	***	*Intensity: 1/4 Area: 1-2/4* 4/10	*Intensity: 1-2/4 Area: 1-4/4* 10/10	*Intensity: 1/4 Area: 1/4* 5/10	*Intensity: 1/4 Area: 1/4* 4/10

* No reaction was observed, ** Observation of the right treated eye, *** Corneal opacities were observed but not scored. Conjunctival redness, conjunctival hyperemia; Chemosis, swelling of the bulbar conjunctiva; Discharge, mucus, pus or excessive tearing from the eye; Iritis, inflammation of the

iris; Corneal opacities, loss of the cornea transparency. Scoring according to the Draize scale. SPL, spironolactone; CANK, potassium canrenoate; DXM, dexamethasone.

3.3.2. Corneal wound healing

A significant beneficial effect of the 0.1% spironolactone micelles on corneal re-epithelialization was observed from Day 4. The mean percentages of re-epithelialization achieved on Day 4 according to the treatment received are shown in **Figure 2**.

As expected, re-epithelialization of the wounded corneas treated with 0.1% DXM (Maxidex®) was delayed compared to the corneas treated with PBS alone (control). In this model, we expected a 2-fold delay in the healing of the wounded corneas treated with 0.1% DXM, compared to control, on Day 2 or 3. This difference was observed on Day 3 with a percentage wounded area of 21.2 ± 9.2% for the animals treated with 0.1% DXM versus 9.3 ± 8.3% for the animals treated with PBS in the control group, which validated the model used in this study (**Table S2**).

After multiple topical administration of 0.1% SPL micelles together with 0.1% DXM, a significant suppression of the dexamethasone-induced corneal delayed wound healing was observed on Day 4 with a mean percentage of re-epithelialization of 96.9 ± 7.3% versus 84.6 ± 13.9% with 0.1% DXM alone ($p<0.05$). Moreover, the percentage re-epithelialization achieved with co-administration of 0.1% SPL micelles with 0.1% DXM was statistically equivalent ($p>0.05$) to the positive control (PBS treatment alone – 99.5 ± 1.0%). Thus, 0.1% SPL micelles seemed to completely compensate the negative impact of 0.1% DXM on corneal re-epithelialization (**Figure 2**).

After multiple topical administration of 0.01% SPL micelles or 0.1% CANK solution together with 0.1% DXM, a trend towards a reduction in the negative impact of DXM on re-epithelialization was observed. Although the mean extents of re-epithelialization of the wounded area observed upon co-treatment with either 0.01% SPL micelles or 0.1% CANK solution remained higher than 0.1% DXM alone at Day 4 (91.6 ± 9.5% and 87.6 ± 13.1%, respectively versus 84.6 ± 13.9%), these differences were not statistically significant ($p>0.05$). Therefore, in this model and with these study conditions, effects on re-epithelialization of 0.01% SPL micelles and 0.1% CANK solution treatments did not appear as evident as was the case for 0.1% SPL micelles (**Figure 2**).

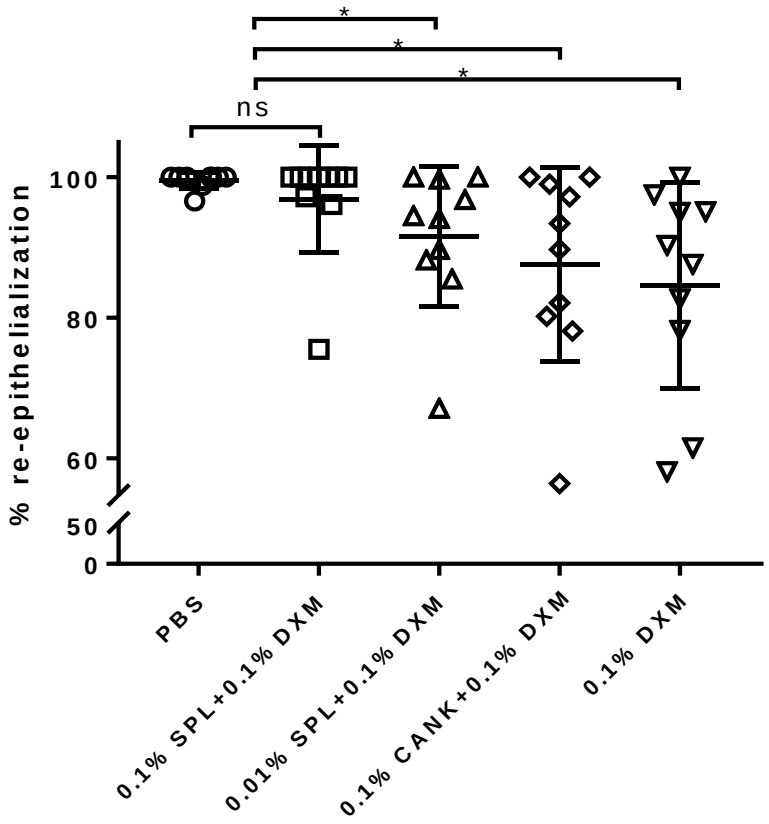

Figure 2. Mean percentage of re-epithelialization of the corneal wounds per treatment group at Day 4. Bars represent means, errors bars represent standard deviation. p-values were calculated using Kruskal-Wallis one-way analysis of variance on ranks followed by Student-Newman-Keuls post-hoc analysis test; ns, non-significant difference ($p>0.05$); *, significant difference ($p<0.05$). SPL, spironolactone; DXM, dexamethasone; CANK, potassium canrenoate.

3.3.3. Biodistribution and quantification of the drugs in the cornea

Group 1: 0.1% spironolactone micelles + 0.1% dexamethasone (Maxidex®)

Multiple ocular instillation of 0.1% SPL micelles and 0.1% DXM to the right eyes of 10 animals during 5 days resulted in the detection in the right corneas of spironolactone and its metabolites, 7α-thiomethylspironolactone and canrenone, with mean concentrations of 7802 ± 4387 ng/g, 114 ± 82 ng/g and 809 ± 180 ng/g, respectively. Dexamethasone was also detected in the right corneas with a concentration of 3233 ± 2190 ng/g (**Figure 3A**). Interestingly, SPL and its metabolites were also detected in the left (control) corneas of all the animals instilled with 0.1% SPL micelles and 0.1% DXM with mean concentrations of 7406 ± 3040 ng/g, 95 ± 75 ng/g and 651 ± 177 ng/g, respectively for SPL, TMSPL and CAN. There was no significant difference in their mean concentrations found in the treated corneas compared to the control corneas

($p>0.05$). However, unlike the aforementioned molecules, DXM was not detected in the left corneas (**Figure 3A**).

Group 2: 0.01% spironolactone micelles + 0.1% dexamethasone (Maxidex®)

Multiple ocular instillation of 0.01% SPL micelles and 0.1% DXM to the right eyes of 9* animals during 5 days resulted in the detection of SPL in the right corneas with a mean concentration of 715 ± 488 ng/g, i.e. 10-fold less than the mean concentration found with 0.1% SPL micelles (7802 ± 4387 ng/g, **Figure 3B**) (*according to Grubbs test, rabbit number 18 was an outlier and was then excluded from the data analysis of Group 2). The metabolites, TMSPL and CAN, were also detected, at concentrations of 36 ± 25 ng/g and 168 ± 57 ng/g, respectively, as was DXM (4542 ± 3428 ng/g). As for the 0.1% SPL formulation, SPL and its metabolites were also detected in the left corneas of all the animals instilled with 0.01% SPL micelles and 0.1% DXM at concentrations of 1148 ± 864 ng/g, 37 ± 19 ng/g and 122 ± 77 ng/g, respectively for SPL, TMSPL and CAN (no significant difference in the mean concentrations found in the treated and control corneas, $p>0.05$). As for the animals in Group 1, DXM was not detected in the left corneas (**Figure 3B**).

Group 3: 0.1% potassium canrenoate solution + 0.1% dexamethasone (Maxidex®)

Multiple ocular instillation of 0.1% CANK solution and 0.1% DXM to the right eyes of 10 animals during 5 days allowed the detection in the right corneas of potassium canrenoate and canrenone at 13440 ± 6346 ng/g and 8596 ± 3097 ng/g, respectively, whereas dexamethasone was detected at 5004 ± 2376 ng/g (**Figure 3C**). CANK and CAN were also detected in the left corneas at 1672 ± 739 ng/g and 6349 ± 2379 ng/g, respectively, with a significant difference compared to the right corneas ($p<0.05$). Unlike in the right corneas, mean concentration of CAN was higher than that of CANK; as for Groups 1 and 2, DXM was not detected in the left corneas (**Figure 3C**).

Group 4: PBS (Positive control)

No drug was detected in the corneas obtained from the PBS treated animals (**Figure S4**).

Group 5: 0.1% dexamethasone (Maxidex® - Negative control)

Multiple ocular instillation of 0.1% DXM to the right eyes of 10 animals during 5 days resulted in the detection of dexamethasone in the right corneas at 19651 ± 13032 ng/g. Interestingly, unlike in Groups 1-3, DXM was also detected in the left corneas at 6337 ± 2603 ng/g (**Figure 3D**) albeit with a significant difference compared to the right corneas ($p<0.05$).

Typical chromatograms obtained from the analysis of both corneas from each group are provided in the Supporting Information (**Figures S1-S5**).

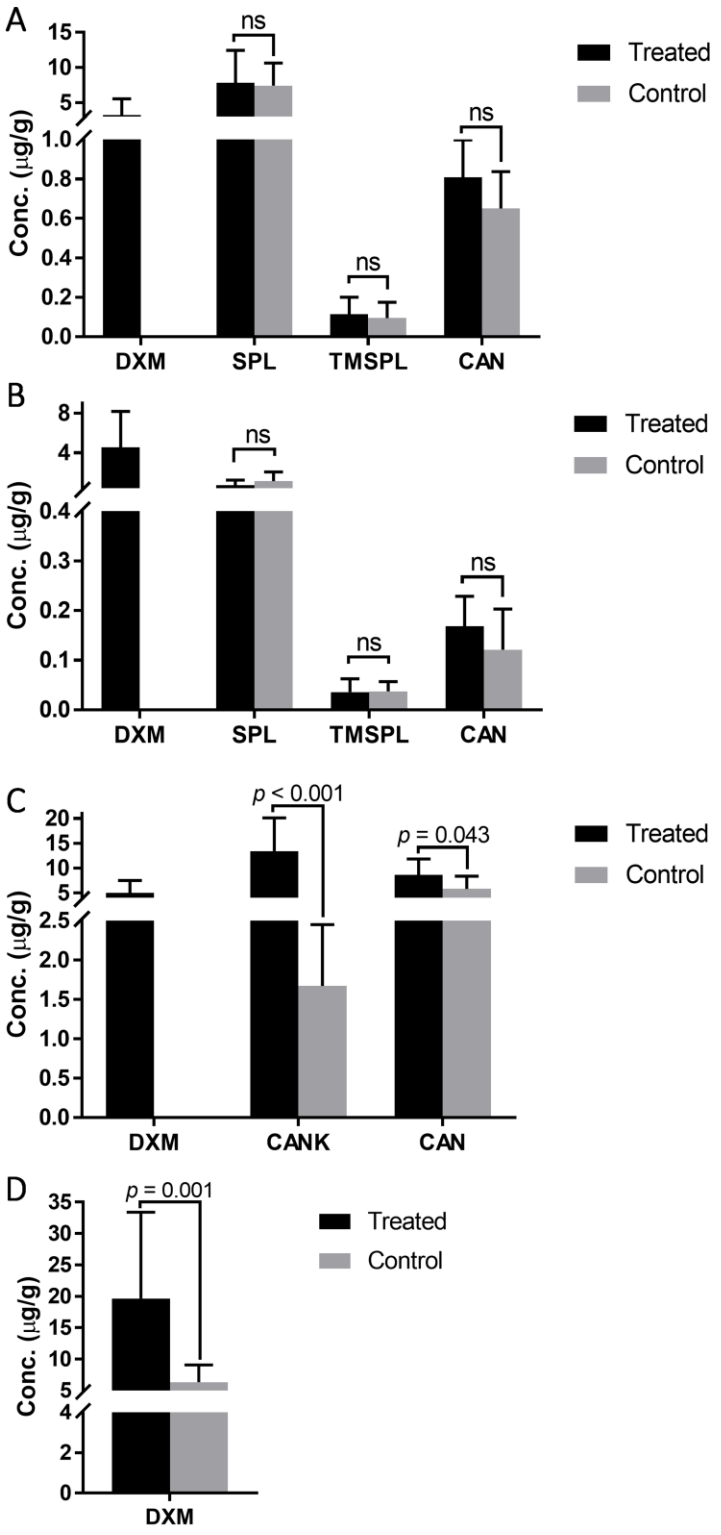

Figure 3. Mean concentrations of the drugs and metabolites found in the right (treated) and left (control) corneas after 5-days multiple instillation of (A) 0.1% spironolactone micelles followed by 0.1% dexamethasone (n=10), (B) 0.01% spironolactone micelles followed by 0.1% dexamethasone (n=9), (C)

0.1% potassium canrenoate solution followed by 0.1% dexamethasone (n=10) and (D) 0.1% dexamethasone (n=10). p-values are obtained with Student t-test; ns, non-significant difference (p>0.99). DXM, dexamethasone; SPL, spironolactone; TMSPL, 7α-thiomethyspironolactone; CAN, canrenone; CANK, potassium canrenoate.

4. Discussion

The results of the *in vivo* study showed a good tolerability of the 0.1% spironolactone micelles following multiple topical instillation into rabbit eye. More interestingly, 0.1% spironolactone micelles showed a significant beneficial effect on the dexamethasone-induced delayed corneal wound healing.

Comparison of the mean SPL concentrations found in the corneas treated either with 0.1% or 0.01% SPL micelles showed a 10-fold difference (7802 ± 4387 ng/g versus 715 ± 488 ng/g, respectively), which is consistent with the 10-fold difference in the applied dose. These results show that there is a correlation between the applied SPL dose and the amount quantified in the corneas pointing to the controlled delivery of SPL by the micelles. In addition to the quantification of the drugs in the corneas, the biodistribution study provided information on their metabolism in the eye, and to a certain extent, on their mechanism of action. Indeed, multiple topical instillation of spironolactone to the eye resulted in the detection of its two main metabolites i.e. 7α-thiomethylspironolactone and canrenone, confirming the presence of thioesterase and thiol methyltransferase activity in the rabbit eye. The detection of canrenone after multiple topical instillation of potassium canrenoate confirmed the *in situ* conversion of canrenoate to canrenone via lactonization of the γ-hydroxy acid group and so confirming the presence of paraoxonase enzyme (PON) in the rabbit eye.

4.1. Mineralocorticoid receptor antagonists improved re-epithelialization

Table 6 summarizes the mean concentrations of SPL, TMSPL and CAN found in the right (treated) corneas following multiple topical instillation of 0.1% SPL micelles, 0.01% SPL micelles or 0.1% CANK solution and their corresponding mean percentage of re-epithelialization. The mean percentage of re-epithelialization obtained with 0.1% SPL micelles was superior and significantly different from that obtained with 0.01% SPL micelles and 0.1% CANK solution ($p<0.05$); however, there was no significant difference in the mean percentage of re-epithelialization obtained between the latter two groups ($p>0.05$). The highest CAN concentration level was found in the corneas treated with 0.1% CANK solution; however, these corneas had the lowest percentage of re-epithelialization, suggesting that CAN is not the main metabolite involved in the mineralocorticoid receptor antagonism. The mean percentages of re-

epithelialization achieved with 0.1% and 0.01% SPL micelles were higher, supporting the higher potency of TMSPL over CAN as a mineralocorticoid receptor antagonist and evidencing its ability to counter-act the GC side effects and thus improve wound healing.

These findings are consistent with previously published data where (i) Corvol et al. [28] pointed out the importance of the C_7 side chain for MR antagonism and reported a 10-fold lower affinity of CAN for the MR as compared to SPL (and its sulphur-containing metabolite, TMSPL), and a very low affinity of CANK for the MR since the negative charge of the carboxylate hinders binding to the receptor as there is no compensatory positive charge in the vicinity; (ii) Sutanto et al. [29] reported the higher potency of SPL as compared to CANK in terms of MR antagonism with half maximal inhibitory concentrations (IC_{50}) of 4.9 nM and >1000 nM, respectively.

Table 6. Mean concentrations of spironolactone (SPL), 7α-thiomethyspironolactone (TMSPL) and canrenone (CAN) found in the treated corneas at Day 5 and their corresponding percentage of re-epithelialization at Day 4, following multiple instillation of 0.1% SPL micelles (n=10), 0.01% SPL micelles (n=9) or 0.1% potassium canrenoate (CANK) solution (n=10).

	Mean concentration in the treated corneas ± SD (ng/g)			**Re-Epithelialization ± SD (%)**
	SPL	**TMSPL**	**CAN**	
0.1% SPL micelles	7802 ± 4387	114 ± 82	809 ± 180	96.9 ± 7.3
0.01% SPL micelles	715 ± 488	36 ± 25	168 ± 57	91.6 ± 9.5
0.1% CANK solution	-	-	8596 ± 3097	87.6 ± 13.1

4.2. Detection of the drugs and their metabolites in the contralateral eye

During this study, animals received the different treatments only in their right eye, the contralateral (control) eye was kept as a control. Interestingly, after multiple instillation of the different treatments, SPL, CANK and their metabolites were detected in the control corneas of all the treated animals. More interestingly, DXM was only detected in the control corneas of the animals that did not receive any MR antagonist (Group 5).

It has been reported that unilateral ocular drug administration leads to its detection in the contralateral eye, [30-33] and this was explained in two different ways. The first involves a local non-hematogenous route where a direct passage from one eye to another can occur, especially in rats and lagomorphs, by interorbital communication either via lymphatic spread or via the lacrimal duct system with retrograde flow into the uninstilled eye [31]. Indeed, a previous study confirmed, clinically and histologically, the conjunctival cross-transfer of an antigen in rabbits using labelled human serum albumin [32]. In another study, iontophoresis of glucocorticoids into rat eyes resulted in the observation of GC effects in the contralateral eye at

levels much higher than those deemed compatible with systemic passage [33]. The second explanation involves the hematogenous route, which involves the return of the drug to the eyes through the general circulation. Indeed, after topical instillation of a drug, there are two main pathways of entry into the anterior segment: (i) across the cornea and (ii) across the conjunctiva. When the drug is crossing the conjunctiva, a fraction of the drug will be lost into the conjunctival blood circulation and the rest will diffuse into the sclera before reaching the heavily vascularized choroid, where another part is also cleared into the general circulation. The possibility of external contact transfer of the molecules from one eye to another with the rabbit paw was excluded regarding the equivalent concentrations of SPL and its metabolites found in both eyes in all the animals.

Another interesting observation was the comparison between the concentrations found in the treated eye versus the contralateral eye following the different treatments and molecules administered. Indeed, in Group 1 and 2, concentrations of SPL, TMSPL and CAN in the treated and control corneas were statistically equivalent; however, DXM was only detected in the treated corneas. In Group 3, concentrations of CANK and CAN in the treated and control corneas were statistically different (13.44 ± 6.35 µg/g vs 1.67 ± 0.74 µg/g and 8.60 ± 3.10 µg/g vs 5.84 ± 2.38 µg/g for CANK and CAN, respectively; Student t-test). It should be noted that the mean concentration of CANK is higher than CAN in the treated eye, whereas the opposite is the case for the contralateral eye. CANK once administered is available in the body as canrenoic acid, which is in equilibrium with its metabolite, canrenone. Indeed, the γ-hydroxy acid on the C_{17} of CANK is converted by cyclization to the γ-lactone present in CAN by the paraoxonase enzyme (PON). Our findings confirm the presence of PON in the rabbit eye; however, the higher mean concentration of CAN compared to CANK found in the contralateral eye suggests that PON in the plasma and/or other tissues play a significant role in the biotransformation of CANK to CAN, resulting in the higher levels of CAN found in the contralateral eye. As in Group 1 and 2, DXM was only detected in the treated corneas of Group 3.

4.3. Mineralocorticoid receptor antagonists prevented dexamethasone binding to the MR

In Group 5, unlike in Groups 1-3, DXM was detected in both the treated and control corneas, although levels in the control corneas were significantly lower (p=0.001). Interestingly, DXM mean concentration in the treated corneas was found to be at least 4-fold higher in the absence

of any MR antagonist (19.65 ± 13.03 µg/g vs 3.23 ± 2.19 µg/g, 4.54 ± 3.43 µg/g and 5.00 ± 2.38 µg/g for Group 5, 1, 2 and 3, respectively). These findings demonstrate that DXM binding to the MR was prevented by the presence of a MR antagonist (SPL, TMSPL, CAN or CANK). This can be explained by the saturation of MR by the MR antagonist (SPL, TMSPL, CAN or CANK) in Groups 1-3, leading to a lower occupancy of the MR by DXM, which is consequently quickly eliminated given its relative short plasma half-life (estimated at 1.9 h in rabbit cf. 1.4, 13.8 and 16.5 h respectively for SPL, TMSPL and CAN) [34-36]. Moreover, Rafestin-Oblin et al. [37, 38] reported a higher affinity of SPL to MR (K_d =3.6 nM) compared to DXM (K_d =10 nM) and Stokes et al. [39] reported that the MR concentration in the human corneal epithelium and endothelium is 3-times higher than the GR concentration. Given the above, the 4-fold higher DXM concentrations found in the treated corneas and its detection only in the contralateral corneas of the animals in Group 5 might be explained by the fact that in this case, there was no competition to bind to MR since there were no MR antagonists. Thus, the mean DXM concentration found in Group 5 was the sum of DXM bound to GR and to MR, whereas the mean concentrations found in Group 1, 2 and 3 corresponded to the unique fraction of DXM bound to GR. These findings confirm: (i) the increased off-target occupancy of MR by DXM in the absence of a MR antagonist and (ii) the resulting delayed wound healing when considering the percentage of re-epithelialization obtained with Group 5. Finally, the results support the rationale of using MR antagonist co-administration in conjunction with a prolonged GC therapy to prevent the delayed wound healing side-effects associated with GC.

In future studies, blood samples will also be taken to quantify the systemic exposure following a topical administration to better understand the roles of hematogenous and non-hematogenous drug transport to the contralateral eye.

5. Conclusion

A stable spironolactone micellar formulation (0.1%, w/v) for topical administration was developed and tested in New Zealand white rabbits *in vivo* with respect to tolerability and efficacy in a corneal wound healing model. The formulation was safe and showed beneficial effects on corneal wound management, i.e. the use of spironolactone micelles countered the delayed wound healing caused by the glucocorticoid therapy. This is the first study showing that MR antagonism can efficiently prevent the glucocorticoid-induced delay in corneal wound re-epithelialization, providing evidence that MR activation by glucocorticoids prevents corneal epithelial growth, differentiation and/or migration.

Mineralocorticoid receptor antagonism may exert beneficial effects through modulation of several mechanisms known to be induced by mineralocorticoid receptor activation such as activation of monocyte/macrophage and polymorphonuclear leukocyte as well as expression of metalloproteinases and pro-fibrotic molecules [11, 17, 40]. Mineralocorticoid receptors could also directly influence the expression of ion channels such as ENAC and therefore influence epithelial cell migration [41]. Additional studies are required to better dissect the exact mechanisms of the effects we have observed *in vivo*.

Successful translation of these preclinical results to the clinic could improve therapeutic outcomes for glucocorticoid-treated patients since topical instillation of the spironolactone micelles might counter the impaired wound healing associated with routine glucocorticoid therapy.

6. Supporting information

6.1. Draize scale

Ocular reactions following instillation of the different treatment were scored according to Draize scale (Table S1).

Table S1. Draize scale for ocular observations scoring.

CONJUNCTIVA		
Chemosis (lids and/or nictitating membrane)	No swelling	**0**
	Slight swelling (incl. Nictitating membrane)	**1**
	Obvious visible swelling with eversion of lids	**2**
	Swelling which leads to half closed lids	**3**
	Swelling which leads to half closed lids, up to totally closed lids	**4**
Discharge	No discharge	**0**
	Slight discharge (not including normal secretions)	**1**
	Discharge with moistening of lids and hairs just adjacent to lids	**2**
	Discharge with moistening of lids and hairs just adjacent to lids on a considerable area around the eye	**3**
Redness	Vessels normal	**0**
	Hyperaemia	**1**
	Diffuse redness, individual vessels not discernible	**2**
	Massive redness of all sections	**3**
IRIS		
Iritis	Normal	**0**
	Markedly deepened folds, congestion, swelling moderate circumcorneal injection (any of these or combination of any thereof), iris still reacting to light	**1**
	No reaction to light, haemorrhage, gross destruction (any or all these)	**2**
CORNEA		
Opacity	No opacity	**0**
	Scattered or diffuse areas of opacity, details of iris clearly visible	**1**
	Not completely translucent areas, details of iris slightly obscured	**2**
	Nacreous areas, details of iris not visible, size of pupil barely discernible	**3**
	Complete corneal opacity, iris not discernible	**4**
Involvement of opacities	No involvement	**0**
	One quarter or less, but not 0	**1**
	Exceeding one quarter, but less than half	**2**
	Exceeding one half, but less than three quarters	**3**
	Exceeding three quarters up to whole area	**4**

6.2. Corneal wound healing

Percentage of re-epithelialization of the cornea was calculated from day 1 to day 5 by measuring the percentage of the wounded area and compared to the baseline (day 0, Table S2).

$$\% \text{ Re-Epithelialization}_{DayX} = \% \text{ Wounded Area}_{Day0} - \% \text{ Wounded Area}_{DayX}$$

Table S2. Mean percentage of the corneal wounded area per treatment group.

		Wounded area (%)					
Treatment		**Day 0***	**Day 1**	**Day 2**	**Day 3**	**Day 4**	**Day 5**
0.1% spironolactone micelles	**Mean**	**100**	**81.0**	**37.9**	**11.9**	**3.1**	**1.8**
	SD	100	8.2	6.6	12.2	7.6	4.1
0.01% spironolactone micelles	**Mean**	**100**	**84.6**	**35.3**	**13.1**	**8.4**	**3.7**
	SD	100	6.6	9.0	9.2	10.0	5.0
0.1% potassium canrenoate solution	**Mean**	**100**	**79.4**	**37.9**	**13.9**	**12.4**	**8.0**
	SD	100	7.6	10.4	10.0	13.8	9.1
PBS	**Mean**	**100**	**80.7**	**38.0**	**9.3**	**0.5**	**0.0**
	SD	100	6.9	10.2	8.3	1.1	0.0
0.1% dexamethasone (Maxidex®)	**Mean**	**100**	**86.4**	**45.9**	**21.2**	**15.4**	**11.7**
	SD	100	6.9	10.0	9.2	14.7	15.1

* measured right after the induction of the wound.

6.3. Analysis of the Cornea

Chromatograms were obtained from the UHPLC-MS analysis of the treated and control corneas of the rabbits involved in the study.

Group 1: 0.1% spironolactone micelles + 0.1% dexamethasone

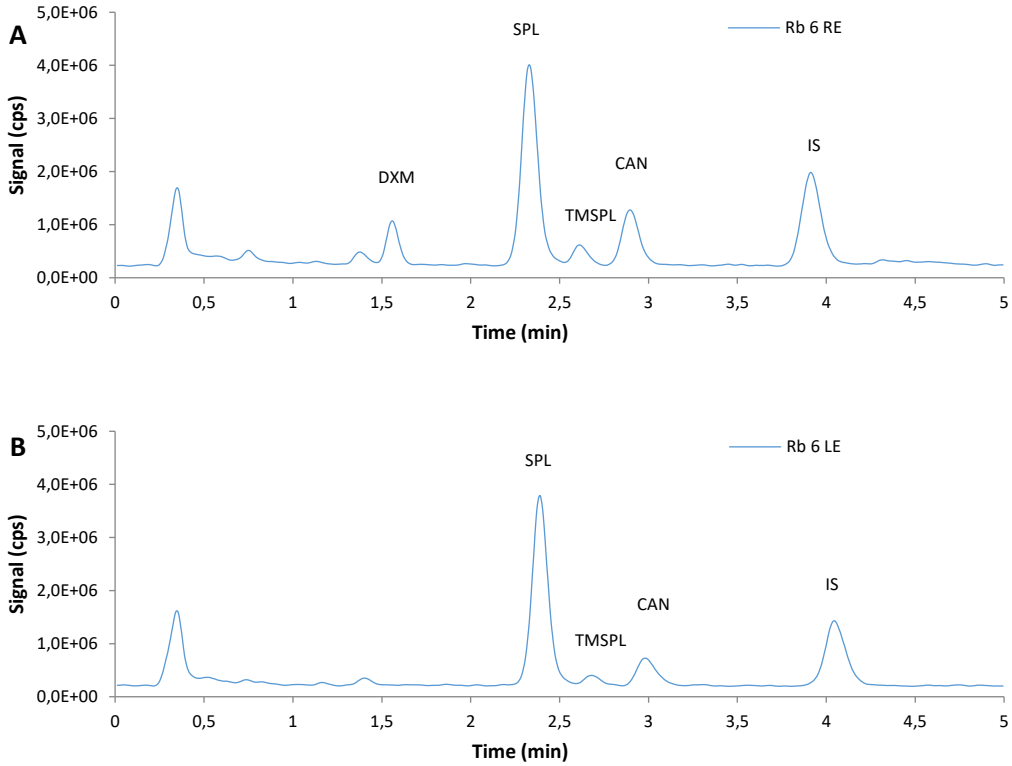

Figure S4. Typical SIR traces obtained from rabbit #6 treated with 0.1% spironolactone micelles and 0.1% dexamethasone (Group 1). A, right treated cornea. B, left control (untreated) cornea.

Group 2: 0.01% spironolactone micelles + 0.1% dexamethasone

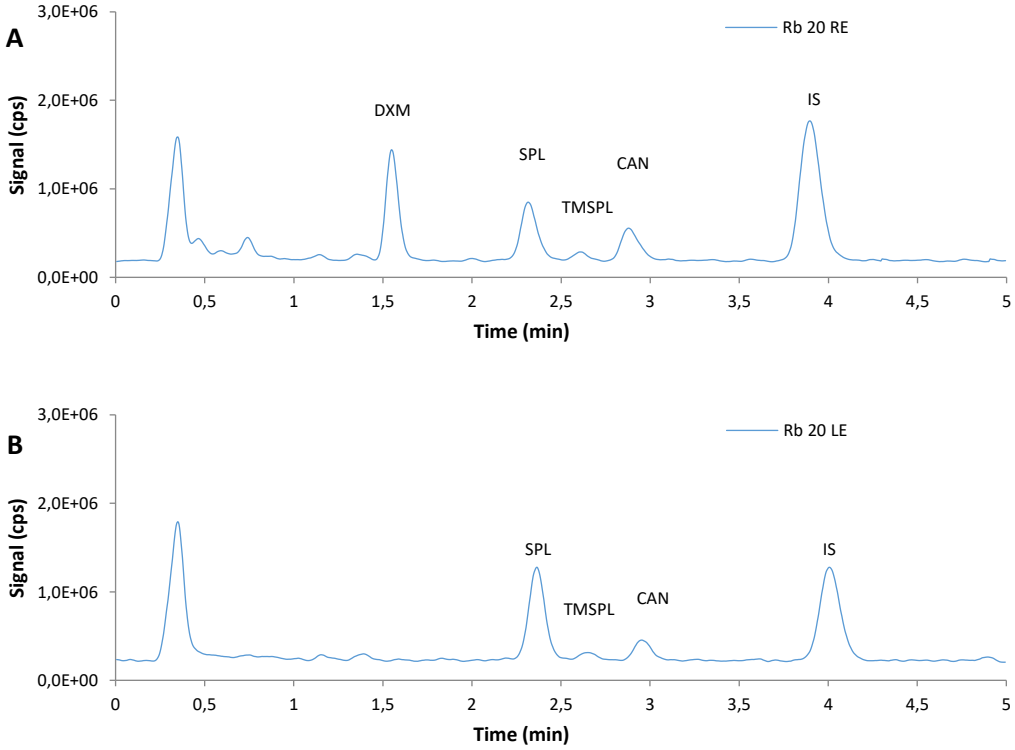

Figure S5. Typical SIR traces obtained from rabbit #20 treated with 0.01% spironolactone micelles and 0.1% dexamethasone (Group 2). A, right treated cornea. B, left control (untreated) cornea.

Group 3: 0.1% potassium canrenoate solution + 0.1% dexamethasone

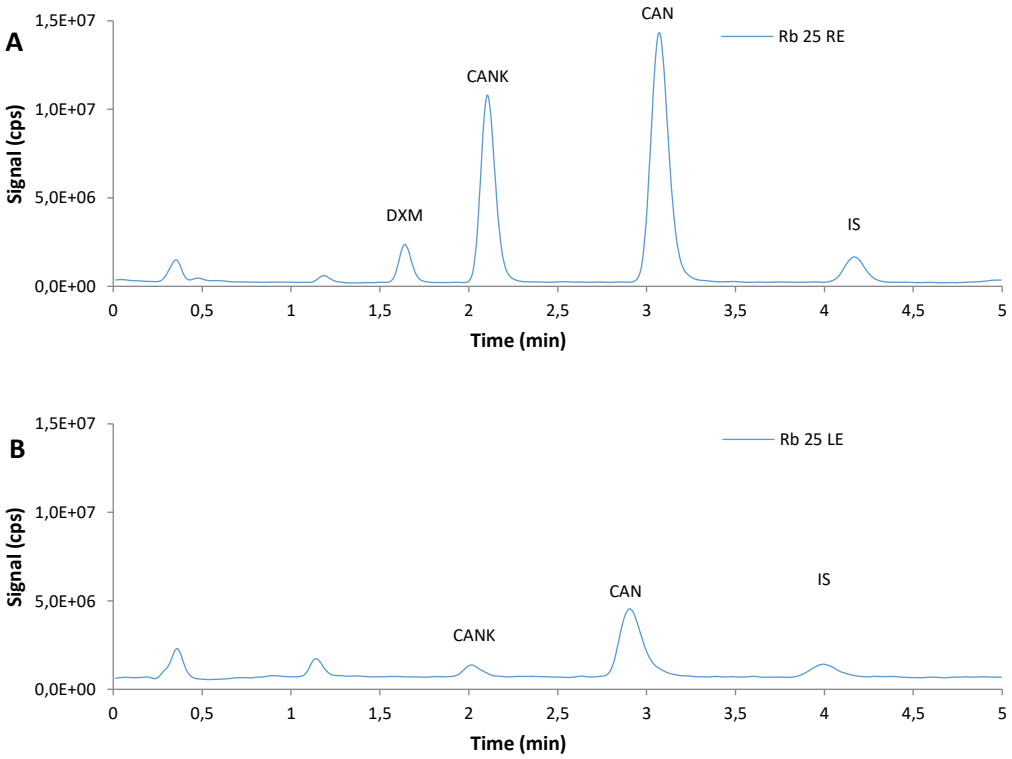

Figure S6. Typical SIR traces obtained from rabbit #25 treated with 0.1% potassium canrenoate solution and 0.1% dexamethasone (Group 3). A, right treated cornea. B, left control (untreated) cornea.

Group 4: PBS (positive control)

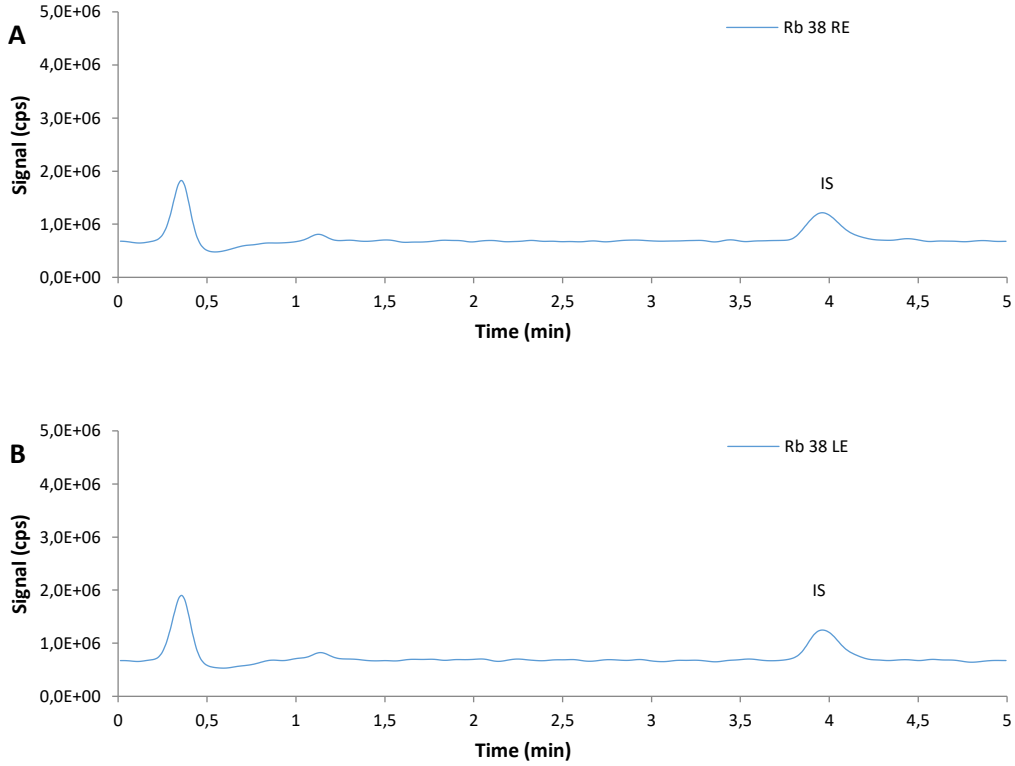

Figure S7. Typical SIR traces obtained from rabbit #38 treated with PBS (Group 4). A, right treated cornea. B, left control (untreated) cornea.

Group 5: 0.1% dexamethasone (negative control)

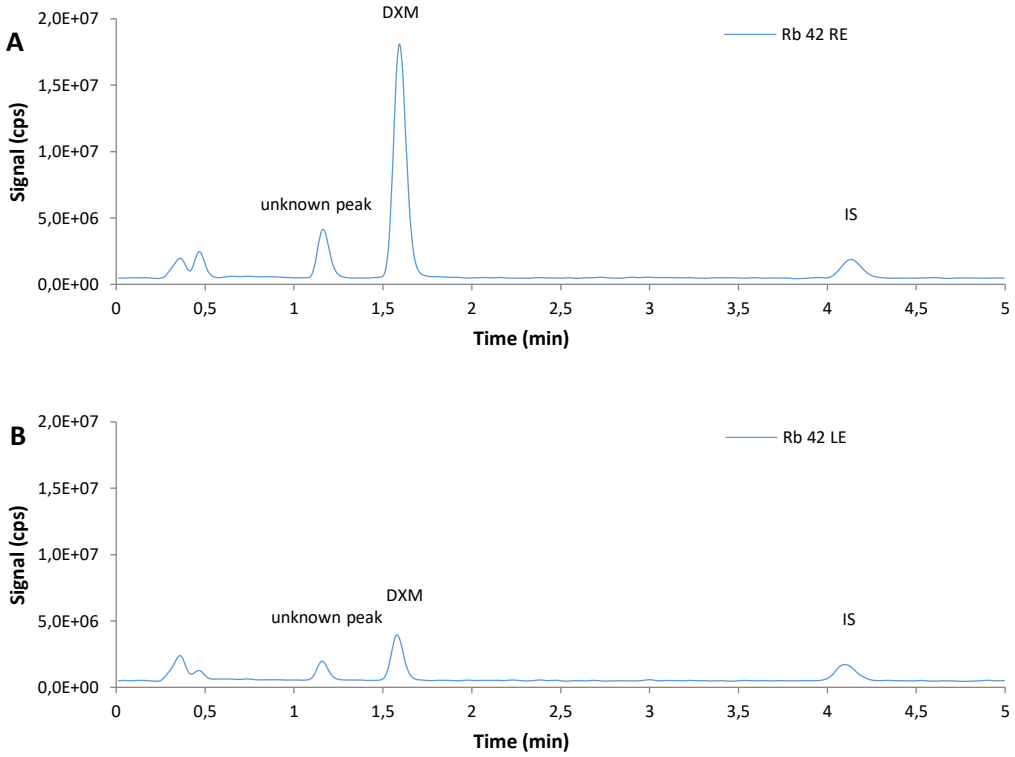

Figure S8. Typical SIR traces obtained from rabbit #42 treated with 0.1% dexamethasone (Group 5). A, right treated cornea. B, left control (untreated) cornea.

Acknowledgement

ND and YNK acknowledge financial support from the Swiss Commission for Technology and Innovation (CTI Project 19086.1 PFLS-LS) and Apidel SA (Geneva, Switzerland). We also acknowledge the support from CEVA Animal Health (Libourne, France) for the *in vivo* study. YNK would like to thank the University of Geneva, the Fondation Ernst and Lucie Schmidheiny and the Société Académique de Genève for providing financial support to enable the acquisition of the Waters Xevo® TQ-MS detector.

References

[1] S. Werner, R. Grose, Regulation of wound healing by growth factors and cytokines, Physiol. Rev. 83 (2003) 835-870.

[2] V.T. Nguyen, N. Farman, E. Maubec, D. Nassar, D. Desposito, L. Waeckel, S. Aractingi, F. Jaisser, Re-epithelialization of pathological cutaneous wounds is improved by local mineralocorticoid receptor antagonism, J. Invest. Dermatol. 136 (2016) 2080-2089.

[3] S.C. Park, J.H. Kim, Effect of steroids and nonsteroidal anti-inflammatory agents on stromal wound healing following excimer laser keratectomy in rabbits, Ophthalmic Surg. Lasers 27 (1996) S481-486.

[4] M. Srinivasan, P. Lalitha, R. Mahalakshmi, N.V. Prajna, J. Mascarenhas, J.D. Chidambaram, S. Lee, K.C. Hong, M. Zegans, D.V. Glidden, S. McLeod, J.P. Whitcher, T.M. Lietman, N.R. Acharya, Corticosteroids for bacterial corneal ulcers, Br. J. Ophthalmol. 93 (2009) 198-202.

[5] S. Adams, R.S. Valchanova, B. Munz, RIP2: a novel player in the regulation of keratinocyte proliferation and cutaneous wound repair?, Exp. Cell Res. 316 (2010) 728-736.

[6] M. Liu, K. Saeki, T. Matsunobu, T. Okuno, T. Koga, Y. Sugimoto, C. Yokoyama, S. Nakamizo, K. Kabashima, S. Narumiya, T. Shimizu, T. Yokomizo, 12-Hydroxyheptadecatrienoic acid promotes epidermal wound healing by accelerating keratinocyte migration via the BLT2 receptor, Journal Experimental Medicine 211 (2014) 1063-1078.

[7] M. Kadmiel, A. Janoshazi, X. Xu, J.A. Cidlowski, Glucocorticoid action in human corneal epithelial cells establishes roles for corticosteroids in wound healing and barrier function of the eye, Exp. Eye Res. 152 (2016) 10-33.

[8] N. Hashizume, S. Saika, Y. Okada, T. Miyamoto, K. Shimizu, Y. Ohnishi, Effects of antiinflammatory drugs on migration of the rabbit corneal epithelium, J. Cataract Refract. Surg. 27 (2001) 1499-1502.

[9] E. Maubec, C. Laouenan, L. Deschamps, V.T. Nguyen, I. Scheer-Senyarich, A.C. Wackenheim-Jacobs, M. Steff, S. Duhamel, S. Tubiana, N. Brahimi, S. Leclerc-Mercier, B. Crickx, C. Perret, S. Aractingi, B. Escoubet, X. Duval, P. Arnaud, F. Jaisser, F. Mentre, N. Farman, Topical mineralocorticoid receptor blockade limits glucocorticoid-induced epidermal atrophy in human skin, J. Invest. Dermatol. 135 (2015) 1781-1789.

[10] A.A. Sarchahi, A. Maimandi, A.K. Tafti, M. Amani, Effects of acetylcysteine and dexamethasone on experimental corneal wounds in rabbits, Ophthalmic Res. 40 (2008) 41-48.

[11] C.S. De Paiva, R.M. Corrales, A.L. Villarreal, W.J. Farley, D.Q. Li, M.E. Stern, S.C. Pflugfelder, Corticosteroid and doxycycline suppress MMP-9 and inflammatory cytokine expression, MAPK activation in the corneal epithelium in experimental dry eye, Exp. Eye Res. 83 (2006) 526-535.

[12] O. Stojadinovic, L.E. Lindley, I. Jozic, M. Tomic-Canic, Mineralocorticoid Receptor Antagonists-A New Sprinkle of Salt and Youth, J. Invest. Dermatol. 136 (2016) 1938-1941.

[13] G. Petroutsos, R. Guimaraes, J.P. Giraud, Y. Pouliquen, Corticosteroids and corneal epithelial wound healing, Br. J. Ophthalmol. 66 (1982) 705-708.

[14] P. Fagerholm, Wound healing after photorefractive keratectomy, J. Cataract Refract. Surg. 26 (2000) 432-447.

[15] A.S. Wang, E.J. Armstrong, A.W. Armstrong, Corticosteroids and wound healing: clinical considerations in the perioperative period, Am. J. Surg. 206 (2013) 410-417.

[16] J.K. Youm, K. Park, Y. Uchida, A. Chan, T.M. Mauro, W.M. Holleran, P.M. Elias, Local blockade of glucocorticoid activation reverses stress- and glucocorticoid-induced delays in cutaneous wound healing, Wound Repair Regen. 21 (2013) 715-722.

[17] N. Farman, V.T. Nguyen, A novel actor in skin biology: the mineralocorticoid receptor, Exp. Dermatol. 25 (2016) 24-25.

[18] J. Boix, L.M. Sevilla, Z. Saez, E. Carceller, P. Perez, Epidermal mineralocorticoid receptor plays beneficial and adverse effects in skin and mediates glucocorticoid responses, J. Invest. Dermatol. DOI 10.1016/j.jid.2016.07.018(2016).

[19] D.A. Sica, Pharmacokinetics and pharmacodynamics of mineralocorticoid blocking agents and their effects on potassium homeostasis, Heart Fail. Rev. 10 (2005) 23-29.

[20] C.M. Ferrario, E.L. Schiffrin, Role of mineralocorticoid receptor antagonists in cardiovascular disease, Circ. Res. 116 (2015) 206-213.

[21] H. Dong, F. Xu, Z. Zhang, Y. Tian, Y. Chen, Simultaneous determination of spironolactone and its active metabolite canrenone in human plasma by HPLC-APCI-MS, J. Mass Spectrom. 41 (2006) 477-486.

[22] J.M. Sandall, J.S. Millership, P.S. Collier, J.C. McElnay, Development and validation of an HPLC method for the determination of spironolactone and its metabolites in paediatric plasma samples, J. Chromatogr. B 839 (2006) 36-44.

[23] A.M. Kaukonen, P. Vuorela, H. Vuorela, J.P. Mannermaa, High-performance liquid chromatography methods for the separation and quantitation of spironolactone and its degradation products in aqueous formulations and of its metabolites in rat serum, J. Chromatogr. A 797 (1998) 271-281.

[24] C. Di Tommaso, J.L. Bourges, F. Valamanesh, G. Trubitsyn, A. Torriglia, J.C. Jeanny, F. Behar-Cohen, R. Gurny, M. Moller, Novel micelle carriers for cyclosporin A topical ocular delivery: in vivo cornea penetration, ocular distribution and efficacy studies, Eur. J. Pharm. Biopharm. 81 (2012) 257-264.

[25] C. Di Tommaso, A. Torriglia, P. Furrer, F. Behar-Cohen, R. Gurny, M. Moller, Ocular biocompatibility of novel Cyclosporin A formulations based on methoxy poly(ethylene glycol)-hexylsubstituted poly(lactide) micelle carriers, Int. J. Pharm. 416 (2011) 515-524.

[26] C. Di Tommaso, F. Valamanesh, F. Miller, P. Furrer, M. Rodriguez-Aller, F. Behar-Cohen, R. Gurny, M. Moller, A novel cyclosporin a aqueous formulation for dry eye treatment: in vitro and in vivo evaluation, Invest. Ophthalmol. Vis. Sci. 53 (2012) 2292-2299.

[27] T. Trimaille, K. Mondon, R. Gurny, M. Moller, Novel polymeric micelles for hydrophobic drug delivery based on biodegradable poly(hexyl-substituted lactides), Int. J. Pharm. 319 (2006) 147-154.

[28] P. Corvol, M. Claire, M.E. Oblin, K. Geering, B. Rossier, Mechanism of the antimineralocorticoid effects of spirolactones, Kidney Int. 20 (1981) 1-6.

[29] W. Sutanto, E.R. de Kloet, Mineralocorticoid receptor ligands: biochemical, pharmacological, and clinical aspects, Med. Res. Rev. 11 (1991) 617-639.

[30] D.M. Maurice, S. Mishima, Ocular Pharmacokinetics, in: M.L. Sears (Ed.) Pharmacology of the Eye, Springer Berlin Heidelberg, Berlin, Heidelberg, 1984, pp. 19-116.

[31] P.R. Jensen, S.B. Aronson, M. Pollycove, E. Yamamoto, Mechanisms of host response in the eye. 3. Interocular protein transfer, Arch. Ophthalmol. 77 (1967) 814-817.

[32] P. Jensen, M. Pollycove, S.B. Aronso, E. Yamamoto, Radioisotopic measurements of protein transfer between the eyes, Invest. Ophthalmol. Vis. Sci. 3 (1964) 676.

[33] F. Behar-Cohen, J.M. Parel, Y. Pouliquen, B. Thillaye-Goldenberg, O. Goureau, S. Heydolph, Y. Courtois, Y. De Kozak, Iontophoresis of dexamethasone in the treatment of endotoxin-induced-uveitis in rats, Exp. Eye Res. 65 (1997) 533-545.

[34] P.E. Stokes, P.M. Stoll, J.H. Schluger, B. Lasley, Hypercortisolemia decreases dexamethasone half-life in rabbit, J. Psychiatr. Res. 36 (2002) 423-428.

[35] B.A. Maron, J.A. Leopold, Mineralocorticoid receptor antagonists and endothelial function, Curr Opin Investig Drugs 9 (2008) 963-969.

[36] J. Beyer, A. Bierl, F.T. Peters, H.H. Maurer, Screening procedure for detection of diuretics and uricosurics and/or their metabolites in human urine using gas chromatography-mass spectrometry after extractive methylation, Ther. Drug Monit. 27 (2005) 509-520.

[37] M.E. Rafestin-Oblin, M. Lombes, B. Couette, E.E. Baulieu, Differences between aldosterone and its antagonists in binding kinetics and ligand-induced hsp90 release from mineralocorticosteroid receptor, J. Steroid Biochem. Mol. Biol. 41 (1992) 815-821.

[38] M.E. Rafestin-Oblin, M. Lombes, P. Lustenberger, P. Blanchardie, A. Michaud, G. Cornu, M. Claire, Affinity of corticosteroids for mineralocorticoid and glucocorticoid receptors of the rabbit kidney: effect of steroid substitution, J. Steroid Biochem. 25 (1986) 527-534.

[39] J. Stokes, J. Noble, L. Brett, C. Phillips, J.R. Seckl, C. O'Brien, R. Andrew, Distribution of glucocorticoid and mineralocorticoid receptors and 11beta-hydroxysteroid dehydrogenases in human and rat ocular tissues, Invest. Ophthalmol. Vis. Sci. 41 (2000) 1629-1638.

[40] F. Jaisser, N. Farman, Emerging Roles of the Mineralocorticoid Receptor in Pathology: Toward New Paradigms in Clinical Pharmacology, Pharmacol. Rev. 68 (2016) 49-75.

[41] H.Y. Yang, R.P. Charles, E. Hummler, D.L. Baines, R.R. Isseroff, The epithelial sodium channel mediates the directionality of galvanotaxis in human keratinocytes, J. Cell Sci. 126 (2013) 1942-1951.

CHAPTER III

Ocular biodistribution of spironolactone after single intravitreal injection of a biodegradable sustained release polymer in rats

Naoual Dahmana[a, *], Laura Kowalczuk[b, c, *], Doris Gabriel[d], Francine Behar-Cohen[b, e], Robert Gurny[a, d], Yogeshvar N. Kalia[a]

[a] School of Pharmaceutical Sciences, University of Geneva & University of Lausanne, CMU - Rue Michel Servet 1, 1211 Geneva 4, Switzerland.
[b] Faculty of Biology and Medicine, University of Lausanne, Rue du Bugnon 21, 1011 Lausanne, Switzerland
[c] Jules-Gonin Eye Hospital, Fondation Asile des aveugles, Avenue de France 15, 1004 Lausanne, Switzerland.
[d] Apidel SA, Quai du Mont Blanc 29, 1201 Geneva, Switzerland.
[e] Inserm, U1138, Team 17, From physiopathology of ocular diseases to clinical development, Paris Descartes University, Sorbonne Paris Cité, Centre de Recherche des Cordeliers, 15 rue de l'Ecole de Médecine, 75006 Paris, France.

([*] contributed equally to the work)

Manuscript in preparation.

Abstract:

The objectives of this study were to develop a sustained release formulation of spironolactone (SPL) using a biodegradable and biocompatible polymer based on hexyl-substituted polylactic acid (hexPLA) and investigate the biodistribution of spironolactone (SPL) and its metabolites *in vivo* in rat ocular tissues over one month following a single intravitreal injection (IVT) of a 5% (w/w) SPL-hexPLA formulation. The concentrations of SPL and its two principal active metabolites, 7α-thiomethylspironolactone and canrenone, in the different ocular compartments were determined using a validated UHPLC-ESI-MS method, at different time points (3, 7 and 31 days after IVT). Systemic exposure following single IVT of 5% SPL-hexPLA was evaluated by quantifying the plasma levels of SPL and its metabolites. Ocular tolerability of the formulation was evaluated using *in vivo* retinal imaging and histology.

In vitro release profile of 5% SPL-hexPLA showed a sustained release of SPL for up to 65 days and was characterized by a burst release in the first week followed by a first-order release profile. SPL and its metabolites were detected in all the ocular tissues at 3 days and 7 days post-IVT. At 31 days post-IVT, spironolactone and canrenone were mainly detected in the retina. These results also suggested the clearance pathway of spironolactone and its metabolites involving the anterior and posterior routes in the first week, then mainly the posterior segment in the last weeks.

This study confirmed that single IVT of 5% SPL-hexPLA in rats enabled sustained delivery of therapeutic amounts of SPL up to one month to the retina and the choroid, without systemic exposure. This formulation may be of interest for the treatment of diseases involving over-activation of the mineralocorticoid receptor in the chorioretina such as central serous chorioretinopathy; where a targeted once-monthly injection might improve efficacy, patient compliance and safety.

Keywords: Central serous chorioretinopathy, spironolactone, sustained release polymer, intravitreal injection, ocular biodistribution, optical coherence tomography.

1. Introduction

Central serous chorioretinopathy (CSCR) is a posterior segment eye disease characterized by accumulation of subretinal fluid following focal alterations of the retinal pigment epithelium barrier, associated with vascular choroidal deregulation. CSCR is the only macular edema that is aggravated instead of being improved by glucocorticoids [1].

Recent studies proposed that CSCR could result from the inappropriate activation of the mineralocorticoid receptor (MR) pathway by glucocorticoids (the physiological cortisol or synthetic drugs routinely used in ophthalmology) in the choroidal vessels and the retina, leading to choroidal vessels dilatation and fluid leakage through the retinal pigment epithelium [1-4]. Therefore, MR antagonists such as spironolactone and eplerenone have been tested for the treatment of CSCR and elicited in most studies, a significant reduction of the subretinal fluid which improved visual acuity in patients [2, 3, 5-8].

MR is known to be involved in the regulation of the extracellular fluid volume and blood pressure through sodium absorption and potassium excretion in the kidney [9]. This receptor is activated by aldosterone; however, glucocorticoids also can bind to it with similar affinity. This off-target activation of the MR by glucocorticoids is prevented in mineralocorticoid-sensitive tissues by the enzyme 11β-hydroxysteroid dehydrogenase type 2 (11β-HSD2) which converts the 11β-hydroxy-glucocorticoids into their inactive 11β-keto metabolites, thereby providing specificity to the MR for aldosterone [10]. MR and 11β-HSD2 are expressed in the retina (ganglion cells, inner nuclear layer, retinal pigment epithelium (RPE)) and in the choroid (vascular endothelial cells). However, 11β-HSD2 levels were found to be approximately 24-fold lower in rat retina than in rat kidney [4, 11, 12].

Other studies found that MR and aldosterone influence retinal vasculopathy, which may involve inflammatory mechanisms and that blockade of the renin–angiotensin–aldosterone system may be relevant as a treatment for diabetic retinopathy. In an oxygen-induced retinopathy animal model, SPL showed antiangiogenic effects on retinal neovascularization [12].

Ocular drug delivery is extremely challenging due to various inherent anatomical and physiological barriers. Indeed, once administered, and depending on the administration route, the drug faces static barriers such as the cornea, the sclera, the blood-aqueous barrier and the blood-retinal barrier, as well as dynamic barriers such as tear drainage, blood flow and lymphatic surface clearance [13]. Given these anatomical and physiological barriers, it is difficult to achieve effective drug concentrations in the posterior segment after topical or

systemic administration. Indeed, after instillation of eye drops, gels or suspensions, only 5-10% of the applied dose penetrates into the anterior chamber due to precorneal drainage and to the corneal barrier (epithelium). Systemic administration leads to poor penetration into the eye due to the inner (endothelium of retinal vessels) and the outer (RPE) blood-ocular barriers. Therefore, systemic (intravenous or oral) administration of high doses is necessary to achieve therapeutic concentrations into the eye, which often leads to severe side effects [13-16]. Intravitreal injection (IVT) enables direct delivery to the posterior segment of the eye, avoiding the above-mentioned barriers and side effects given the limited entry to the systemic circulation. However, due to the short half-life of drugs, injections need to be repeated frequently to maintain therapeutic concentration, this is not very patient-friendly and may cause some rare but severe complications, such as retinal detachment, haemorrhage and endophthalmitis [14, 17]. In recent years, much work has been done to develop new drug delivery systems for sustained drug release into the posterior segment of the eye. Such systems include nanoparticles, liposomes, micelles, microspheres, dendrimers, hydrogels, matrix films, as well as various implants, inserts, reservoirs and refillable drug ports based on biodegradable and non-biodegradable polymers [15, 18-24].

With regards to patient compliance, biodegradable polymers have the advantage that they do not require additional surgery for removal. Recently, a biodegradable liquid polymer based on hexyl-substituted poly-lactic acid (hexPLA) was developed and showed *in vivo* biocompatibility and sustained release properties [25]. After a single subcutaneous injection in rats of 5% triptorelin-hexPLA formulation, hexPLA polymer enabled a sustained delivery of triptorelin for up to 6 months. This biodegradable polymer is hydrolyzed in aqueous environments into 2-hydroxyoctanoic acid monomers which are subsequently eliminated from the body [26].

The aim of this study was to evaluate a novel biodegradable sustained release polymer as drug delivery system for intravitreal injection of spironolactone (SPL). Drug release *in vitro* from the polymer was evaluated over a period of two months and over one month *in vivo* using a novel ultra-performance liquid chromatography-mass spectrometry (UHPLC-ESI-MS) analytical method. Finally, the ocular distribution of spironolactone and its metabolites (canrenone and 7α-thiomethylspironolactone) *in vivo* was also determined in rats over one month following a single intravitreal injection of a 5% (w/w) SPL-hexPLA formulation.

2. Material and methods

2.1. Material

Hexyl-substituted poly-lactic acid (hexPLA, **Scheme 1**), polymer was supplied by Apidel SA (Geneva, Switzerland). Spironolactone (SPL) was purchased from Zhejiang Langhua pharmaceutical Co., Ltd. (Zhejiang, China). 7α-thiomethylspironolactone (TMSPL) was purchased from TLC Pharmaceutical Standards Ltd. (Ontario, Canada). Canrenone (CAN) and 17α-methyltestosterone (MeT), used as an internal standard (IS), were purchased from Sigma-Aldrich (Buchs, Switzerland). Ultrapure water (H_2O, resistivity > 18 MΩ cm) was prepared using a Merck Millipore Milli-Q water purification system (Darmstadt, Germany). Methanol (MeOH, HPLC grade) was obtained from Fisher Scientific (Waltham, MA, USA), formic acid (ULC/MS grade) from Biosolve (Dieuze, France) and dimethylformamide (DMF) from Sigma Aldrich (Buchs, Switzerland). All other chemicals were at least of analytical grade.

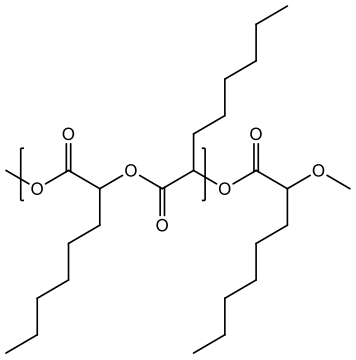

Scheme 1. Chemical structure of hexPLA polymer.

2.2. Analytics

2.2.1. UHPLC-UV method

An ultra-performance liquid chromatography coupled to UV spectroscopy (UHPLC-UV) method was developed to support the formulation development and the drug release studies of spironolactone from hexPLA polymer.

The liquid chromatographic system consisted of a Waters Acquity® UPLC® H-Class system (Baden-Dättwil, Switzerland) including a binary solvent manager, a sample manager and a column manager. Reverse phase chromatography was performed using a Waters XBridge® BEH C18 column (50 x 2.1 mm I.D., 2.5 µm) fitted with a Waters XBridge® BEH C18 VanGuard pre-column (5 x 2.1 mm I.D., 2.5 µm). Isocratic elution was carried out using a mobile phase consisting of 0.1% formic acid in H_2O:MeOH (45:55, v/v) with a flow rate of 0.35 mL/min and a runtime of 5 min. Column temperature was held at 40°C and the sample

manager was kept at room temperature. Injection volume was set at 10 µL and the UV detector was set at 240 nm.

Stock solution of spironolactone (SPL) was prepared in MeOH at 1 mg/mL then calibration standards were prepared in MeOH:H_2O (1:1) or MeOH:PBS (1:1) at 0.1, 0.5, 1, 5, 10, 25, 50 and 100 µg/mL. Calibration curves were constructed by plotting the area versus the concentration of each analyte. All the calibration curves were linear with correlation coefficient $R > 0.99$.

2.2.2. UHPLC-ESI-MS bioanalytical method

An ultra-performance liquid chromatography coupled to a tandem quadruple mass spectrometer (UHPLC-ESI-MS) was used to quantify spironolactone (SPL) and its metabolites, 7α-thiomethylspironolactone (TMSPL) and canrenone (CAN), in the ocular tissues and the plasma obtained from the *in vivo* study. 17α-methyltestosterone (MeT) was used as an internal standard (IS). Briefly, the liquid chromatographic system consisted of a Waters Acquity® UPLC® system (Baden-Dättwil, Switzerland) including a binary solvent manager, a sample manager with an injection loop volume of 10 µL and a column manager. The reversed phase chromatographic separation of the four compounds was performed using a Waters XBridge® BEH C18 column (50 x 2.1 mm I.D., 2.5 µm) fitted with a Waters XBridge® BEH C18 Vanguard pre-column (5 x 2.1 mm I.D., 2.5 µm). The elution was carried out in isocratic mode with a mobile phase consisting of 0.1% formic acid in H_2O/MeOH (48/52, v/v) with a flow rate of 0.45 mL/min and a run time of 5 min. Column temperature was held at 40°C and sample manager temperature was kept at room temperature. Injection volume was set at 5 µL. The mass spectrometry (MS) system consisted of a Waters XEVO® TQ-MS detector (Baden-Dättwil, Switzerland) fitted with a Z-spray electrospray ionisation source. MS detection of the 4 compounds was performed using electrospray ionisation in the positive mode (ESI+) and selected ion recording (SIR) using the pseudo-molecular ion of each compound as the parent ion (hydrogen adduct, $[M + H]^+$). The capillary voltage was set at 2.3 kV, and desolvation gas temperature and flow were maintained at 350 °C and 650 L/h, respectively. The specific MS parameters for each analyte were tuned and determined by infusing each compound individually at 1 µg/mL in MeOH:H_2O (1:1) at a flow rate of 5 µL/min. Identification and quantification of each analyte were carried out according to the mass-to-charge ratio (m/z) of the pseudo-molecular ion of each compound (hydrogen adduct, $[M + H]^+$). Cone voltage optimal setting was 35 V for all the analytes. The pseudo-molecular parent ion corresponding to SPL/CAN, TMSPL and MeT have an m/z of 341.0, 389.0 and 303.0 respectively. Dwell time was set at 5 ms for all the compounds. Data

processing was performed using Waters MassLynx software version 4.1 (Baden-Dättwil, Switzerland). Calibration standards were prepared at 10, 20, 50, 100, 200, 500 and 1000 ng/mL in MeOH:H_2O (1:1). All calibration curves showed linearity over the range of 10 to 1000 ng/mL ($R > 0.99$). The limit of quantification (LLOQ) was 5.0 ng/mL, for all analytes.

2.3. Development and characterization of SPL-hexPLA formulations

Spironolactone-hexPLA formulations (3 g) were prepared at 1, 2, 3 and 5% (w/w). Briefly, 30, 60, 90 or 150 mg SPL were added to 2970, 2940, 2910 or 2850 mg hexPLA and left under magnetic stirring at 40°C for 2 h, then the preparations were stored at 5°C. Formulations were characterized in terms of concentration and drug release profile. The particle size distribution in the formulations was analysed using a microscope (Zeiss Axioskop 2 plus) and the mean particle size was calculated using ImageJ software.

2.3.1. Quantification of SPL-hexPLA formulations

Quantification of spironolactone in SPL-hexPLA formulations was performed using the UHPLC-UV method described above. SPL calibration standards were prepared in MeOH:H_2O (1:1) from 0.01 to 100 µg/mL. First, 100 µL of SPL-hexPLA formulations at 1, 2, 3 or 5% were dissolved in 900 uL DMF, then 10 µL of this solution were diluted in 990 µL MeOH:H_2O (1:1) to precipitate hexPLA polymer. This solution was then filtered through PTFE 0.22 µm filter and injected for quantification.

2.3.2. *In vitro* drug release studies

In vitro release profile of SPL from the hexPLA polymer was assessed by placing a 50 µL droplet of SPL-hexPLA formulation in a vial containing 4 mL PBS 10 mM. Samples containing SPL-hexPLA formulations (1, 2, 3 or 5%; n=5/group) or blank hexPLA were prepared then the vials were sealed and placed in a shaking incubator maintained at 37°C and set at 15 rpm. One millilitre buffer was sampled at day 9, 16, 23, 30, 51 and 65 to quantify the amount of the drug released, then replaced with a fresh PBS solution.

Quantification of the drug release from SPL-hexPLA formulations

To quantify the amount of spironolactone released in PBS from the hexPLA polymer, SPL calibration standards were prepared in MeOH:PBS (1:1) from 0.01 to 100 ug/mL. One mL PBS was withdrawn from each sample at 9, 16, 23, 30, 51 and 65 days incubations then diluted in MeOH (1:1) and injected for quantification. The amount of SPL released in the buffer was calculated as the difference between the initial content and the actual content at each time point.

2.4. *In vivo* ocular biodistribution study in rats

2.4.1. Animals

All experiments were performed in accordance with the European convention on the protection of animals used for scientific purposes (Directive 2010/63/EU) and to the Association for Research in Vision and Ophthalmology (ARVO) Statement for the use of animals in ophthalmic and visual research and were approved by the local veterinary authority for animal experimentation (Authorization N° VD2928). Fifteen adult Wistar rats (7-10 weeks old) weighing approximately 230-370 g were obtained from Charles-River Laboratories (L'Arbresle, France). Animals were housed per pair in standard cages and kept in pathogen-free environmental conditions with a 12-hour light/12-hour dark cycle. Animals had enrichment and free access to food and were allowed water ad libitum. All animals were healthy and free of clinically observable ocular abnormalities. Animals were randomized into 5 groups as described in **Table 1.** Two groups received hexPLA placebo IVT and were followed 7 days and 31 days after IVT. Three groups received SPL-hexPLA and were followed 3 days, 7 days and 31 days after IVT.

Table 1. Study plan.

Group #	Formulation	Duration	# Eyes	# Histology	# Quantification
1	hexPLA placebo	7 days	2	2	-
2	hexPLA placebo	31 days	4	4	-
3	5% SPL-hexPLA	3 days	6	0	6
4	5% SPL-hexPLA	7 days	8	1	6
5	5% SPL-hexPLA	31 days	10	4	6

2.4.2. Intravitreal injection of hexPLA and SPL-hexPLA

Animals were anaesthetised by intramuscular injection of ketamine (Ketalar®, Parke-Davis, USA) / xylazine (Rompun®, Bayer, Switzerland) (80 mg/kg / 8 mg/kg). After pupillary dilation using topical tropicamide 0.5% (Théa, Switzerland) and phenylephrine hydrochloride 2.5% (Bausch & Lomb, USA), animals received instillation of tetracaine hydrochloride 1% (Bausch & Lomb, USA) for local anaesthesia and moisturising gel (Genteal®, Alcon, Switzerland) to avoid eye dryness during the intervention. Subsequently, animals were injected in both eyes with 5 µL of either 5% SPL-hexPLA formulation or blank hexPLA polymer through the temporal sclera into the vitreous cavity using a sterile insulin syringe with a 29G needle (29G x ½'', 0.3 mL, Terumo, Japan). The injection was performed under direct visualisation through a surgical microscope to avoid damaging the eye structures especially the lens given its

relatively large size in the rat eye. Immediately after the IVT, the droplet was visualised with the microscope SteREO Discovery.V12 (Zeiss, Germany), then the eyes were rinsed with BSS® solution (Alcon, Switzerland).

2.4.3. Eye fundus examination

Eye fundus and polymer imaging were performed *in vivo* using a retinal camera specially designed for mouse/rat retinal imaging (Micron III, Phoenix Research Labs', USA) at 3, 7, 14 and 31 days after the polymer IVT. After anaesthesia and pupillary dilation, animals were placed on a specific support and received a drop of a moisturizing gel (Genteal, Alcon) to allow contact with the camera lens.

2.4.4. Optical Coherence Tomography

Retinal morphology was examined *in vivo* using a spectral domain optical coherence tomography (SD-OCT) system adapted for rat eyes (Bioptigen, Leica microsystems, Buffalo Grove, IL, USA), at day 14 after IVT of hexPLA placebo (Group 2) and 5% SPL-hexPLA (Group 5). For each eye, two volume acquisitions (3 mm x 3 mm) were performed, one centred on the optic nerve, one toward the nasal side (the opposite side of the IVT site).

2.4.5. Sampling

At each time point as indicated in **Table 1** (3, 7 or 31 days post IVT), Immediately after the last examination, blood samples were collected by cardiac puncture in heparin-coated tubes immediately stored at 5°C, then animals were euthanized by pentobarbital overdose. For histology, both eyes were enucleated then immediately placed in 5 mL of Bouin's solution. For quantification, eyes were kept on dry ice before microdissection. First, fluids (aqueous humour and vitreous humour) were collected, then cornea, iris, neuroretina, sclera-choroid-RPE complex were carefully separated, weighed and stored at -80°C until analysis. The collected blood samples were centrifuged at 4°C (3000 rpm, 10 min) then the plasma samples were kept at -80°C until analysis.

2.4.6. Histology

Enucleated eyes were fixed in Bouin's solution for 24 hours at room temperature then dehydrated using an automatic system (Histokinette 2000, Reichert-Jung) in graded alcohol solutions (70% to 100%) followed by xylol, finally, eyes were embedded in paraffin. Samples were further mounted on a microtome (Hyrax M55, Carl Zeiss) and cut into 5 µm thickness serial sections. Subsequently, sections were mounted on glass slides and stained with haematoxylin-eosin. Further, all sections were examined with light microscopy (Zeiss, Oberkochen, Germany).

2.4.7. Biodistribution of SPL and its metabolites in ocular tissues

Bioavailability of spironolactone and its metabolites, 7α-thiomethylspironolactone and canrenone, in the ocular tissues and plasma of the rats following single intravitreal injection of 5% SPL-hexPLA formulation was determined at different time points; 3, 7 and 31 days post-IVT. The different ocular tissues, fluids and the plasma were extracted and quantified using a validated UHPLC-ESI-MS method.

Samples were thawed at room temperature, then the corneas and sclera-choroid-RPE complexes were cut into small pieces and placed into individual vials containing 300 µL MeOH:H_2O (1:1) and 100 ng/mL internal standard. Iris, neuroretina and fluids were directly placed in individual vials containing 200 µL MeOH:H_2O (1:1) and 100 ng/mL internal standard. Plasma samples were diluted 1:1 with 300 µL methanol, containing 200 ng/mL internal standard, to precipitate proteins. Ocular and plasma samples were then left under stirring overnight for extraction. The following day, samples were centrifuged during 20 min at 12 000 rpm and the supernatants were quantified using the validated UHPLC-MS method.

3. Results

3.1. Spironolactone-hexPLA formulations

Formulations of SPL mixed with hexPLA polymer resulted in injectable viscous solutions or suspensions **(Figure 1A**). At low concentrations (1 and 2%, w/w), SPL-hexPLA formulations were transparent solutions, like hexPLA placebo, whereas SPL-hexPLA formulations at 3 and 5% (w/w) were suspensions. This is due to the solubilization of SPL within the hexPLA polymer up to 20 mg/g, which is the case in the formulations at 1 and 2%, while in formulations at 3 and 5%, SPL is in a saturated form, with a solubilized and a suspended fraction. **Figure 1B** shows the droplets formed once SPL-hexPLA formulations are in contact with the aqueous buffer (PBS 10 mM). These samples were used to evaluate the *in vitro* release profile of SPL from hexPLA. Particle size in the SPL-hexPLA suspensions at 3% and 5% ranged from 1 to 10 µm (**Figure 1C**).

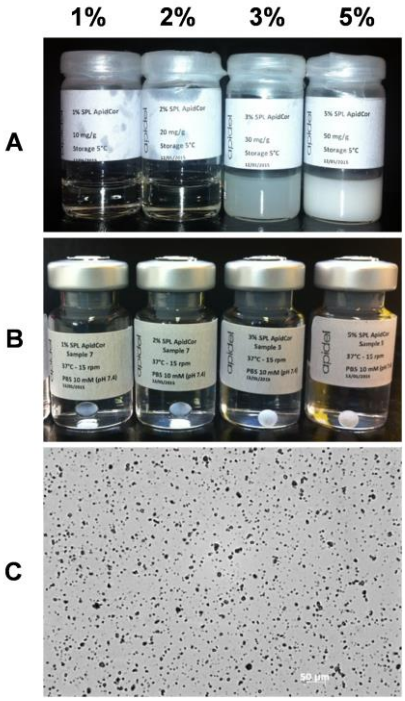

Figure 1. Spironolactone-hexPLA formulations. (A) Visual aspect of the solutions and suspensions of spironolactone (SPL) mixed with hexPLA polymer at 1, 2, 3 and 5% w/w; (B) Pictures of the SPL-hexPLA droplets in aqueous buffer (PBS 10 mM) used to assess the in vitro release profile; (C) Microscopic image of 5% SPL-hexPLA. Particle size ranged from 1 to 10 µm.

3.2. *In vitro* release profile of spironolactone

The amount of SPL released per week from SPL-hexPLA formulations and the cumulative percentage release over time at the different drug loadings are shown in **Figure 2**.

Although the amounts of SPL released from hexPLA into the buffer and the release period varied depending on the amount of SPL loaded in the polymer, the release profile obtained with the different concentrations of SPL was similar and characterized by two phases; a burst release in the first week, followed by a more gradual decrease in the amounts released by the different formulations (**Figure 2A**). The initial burst release may be due to the rapid degradation of the outer surface of the polymer releasing the surface associated SPL molecules. The higher burst observed in the 3% and 5% suspensions may be due to the release of both the solubilized fraction and the suspended fraction of SPL, *versus* only a solubilized fraction in the case of the 1% and 2% solutions. The gradual decrease in the amounts of SPL released by the different formulations may be due to a slower erosion of the polymer. The cumulative release profile (**Figure 2B**) showed that formulations at 1 and 2% reached a plateau and that there was no further release from Day 9, whereas formulation at 3% stopped releasing SPL from Day 30 and the 5% formulation continuously released SPL up to 65 days. The release profile of the 5% SPL-hexPLA formulation is characterized by an initial burst during the first week, followed by a first-order phase (**Figure 2C**).

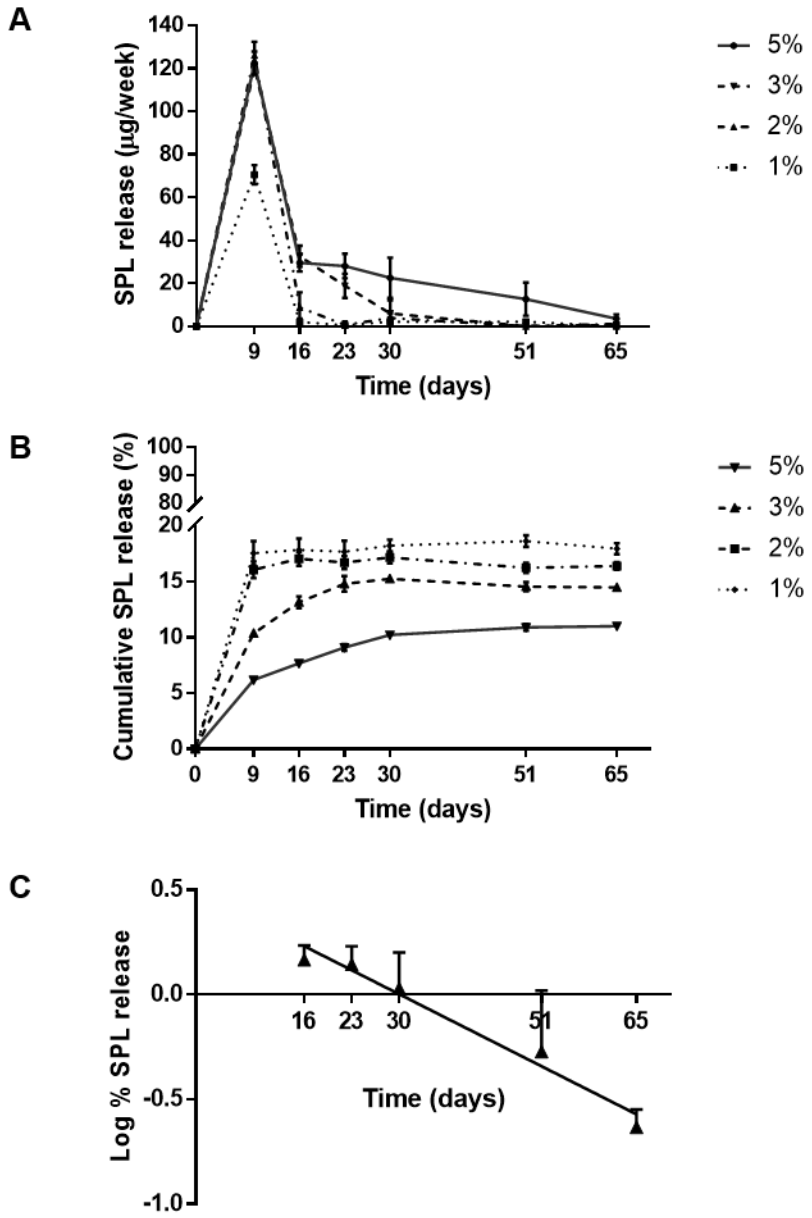

Figure 2. *in vitro* release profile of spironolactone from the SPL-hexPLA formulations at 1, 2, 3 and 5% (w/w). (A) SPL amount released weekly (n=5, mean ± SD); (B) SPL cumulative release over time (n=5, mean ± SD); (C) Phase 2 of the release profile of 5% SPL-hexPLA formulation following a first-order kinetics (n=5, mean ± SD, R^2=0.96).

Given the sustained release period achieved with the 5% SPL-hexPLA, it was selected for the subsequent *in vivo* studies. This formulation was stable for at least 10 weeks at 5°C.

3.3. *In vivo* eye fundus and Optical Coherence Tomography

The polymer shape and its position in the eye were followed up at Day 7 (Group 1), Day 14 and Day 28 (Group 2) after hexPLA placebo IVT, and at Day 3 (Group 3), Day 7 (Group 4), Day 14 and Day 28 (Group 5) after SPL-hexPLA IVT. **Table 2** presents a summary of the observations of each group, at each time point, which are illustrated in **Figure 3.**

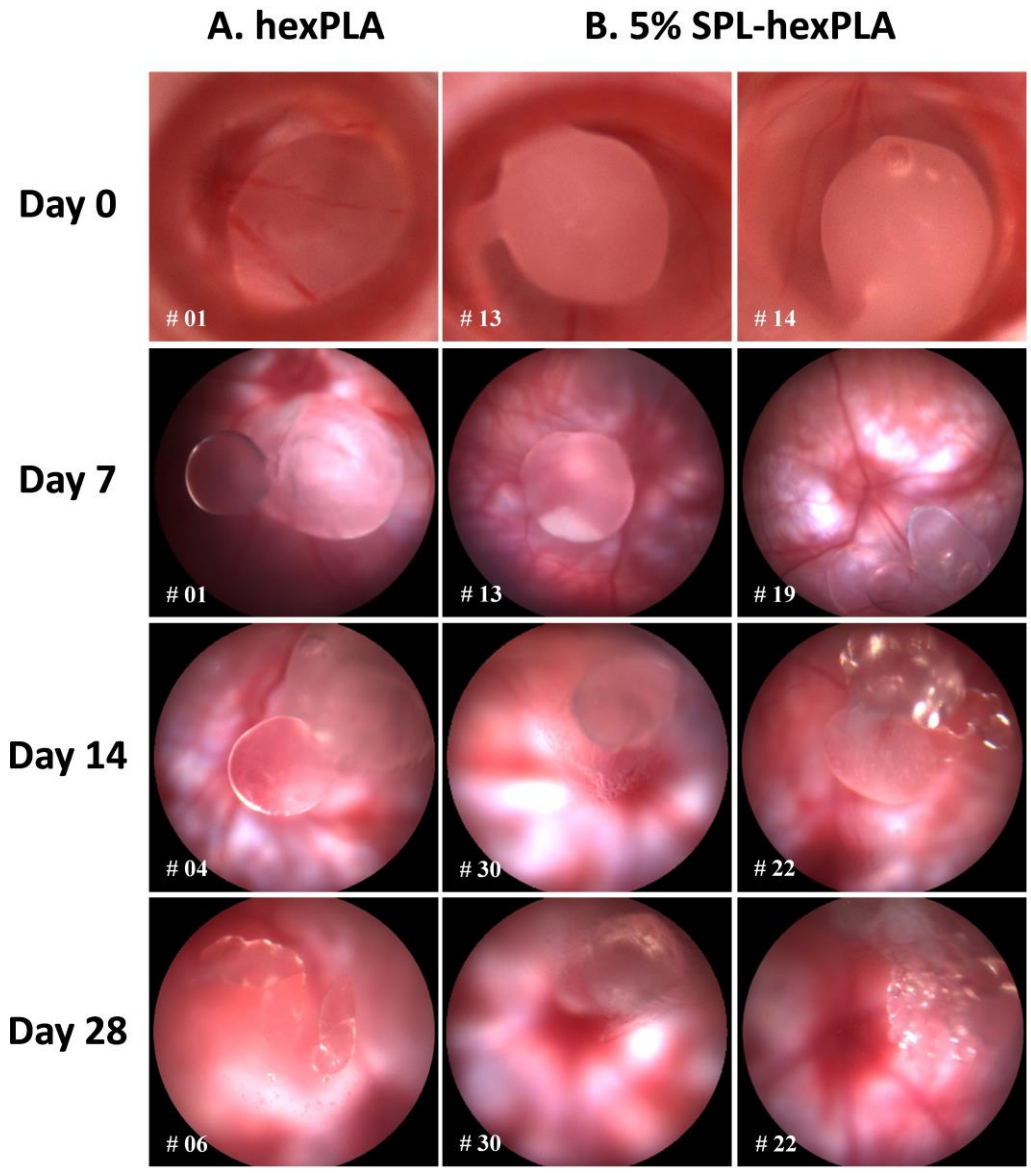

Figure 3. *in vivo* eye fundus of rat eyes injected with hexPLA placebo polymer (A, First column) and 5% SPL-hexPLA formulation (B, second and last columns) at day 0, day 7, day 14 and day 28 after intravitreal injection (IVT). The eye fundus at day 0 were observed under the microscope STEREO Discovery v12 (Zeiss). All the other eye fundus were examined using the retinal camera Micron III (Phoenix Research Labs'). Eye fundus illustrate the visualization of droplets floating in the vitreous (#01 days 0 and 7, #4 day 14; #13 days 0 and 7, #14 day 0), droplets stuck on the lens (#06 day 28; #30 days 14 and 28, #22 day 28) and droplets with clustered bubbles (#06 day 28; #19 day7, #22 days 14 and 28).

At Day 0, IVT of the polymer resulted in the formation of transparent droplets of hexPLA placebo and opaque droplets of SPL-hexPLA suspended in the vitreous. One week after IVT, most of the droplets retained this shape and were still floating in the vitreous. Two weeks after IVT, in both groups, half of the polymers had the aspect of a droplet floating in the vitreous or stuck to the lens, and the other half formed bubbles and were either floating in the vitreous or stuck to the lens. At the end of the follow up, two thirds of the droplets formed bubbles and 80% of the polymers were stuck to the lens. This change of location of the polymer was probably due to the saccadic motion of the eye, combined to the movements of the rats.

Table 2. Follow up of the polymer shape and site on eye fundus.

Formulation	Time (days)	Eyes (#)	Polymer Shape		Polymer Site	
			Droplet	Droplet with bubbles	Floating in the vitreous	Stuck to the lens
hexPLA placebo	7	2	2	0	2	0
	14	4	2	2	2	2
	28	4	1	3	0	4
5% SPL-hexPLA	3	6	5	1	6	0
	7	7	6	1	6	1
	14	10	4	6	4	6
	28	10	3	6	2	8

At Day 14, retinal examinations using SD-OCT of the eyes injected with hexPLA (**Figure 4A**) and with 5% SPL-hexPLA (**Figure 4B**) were performed *in vivo* sections OCT images of the retina taken through the optic nerve and near the polymer showed some intravitreal hyper-reflective dots in both groups, suggesting the presence of inflammatory cells. However, these intravitreal hyper-reflective dots were absent in retinal sections imaged far from the polymer. No retinal degeneration was observed in any of the sections.

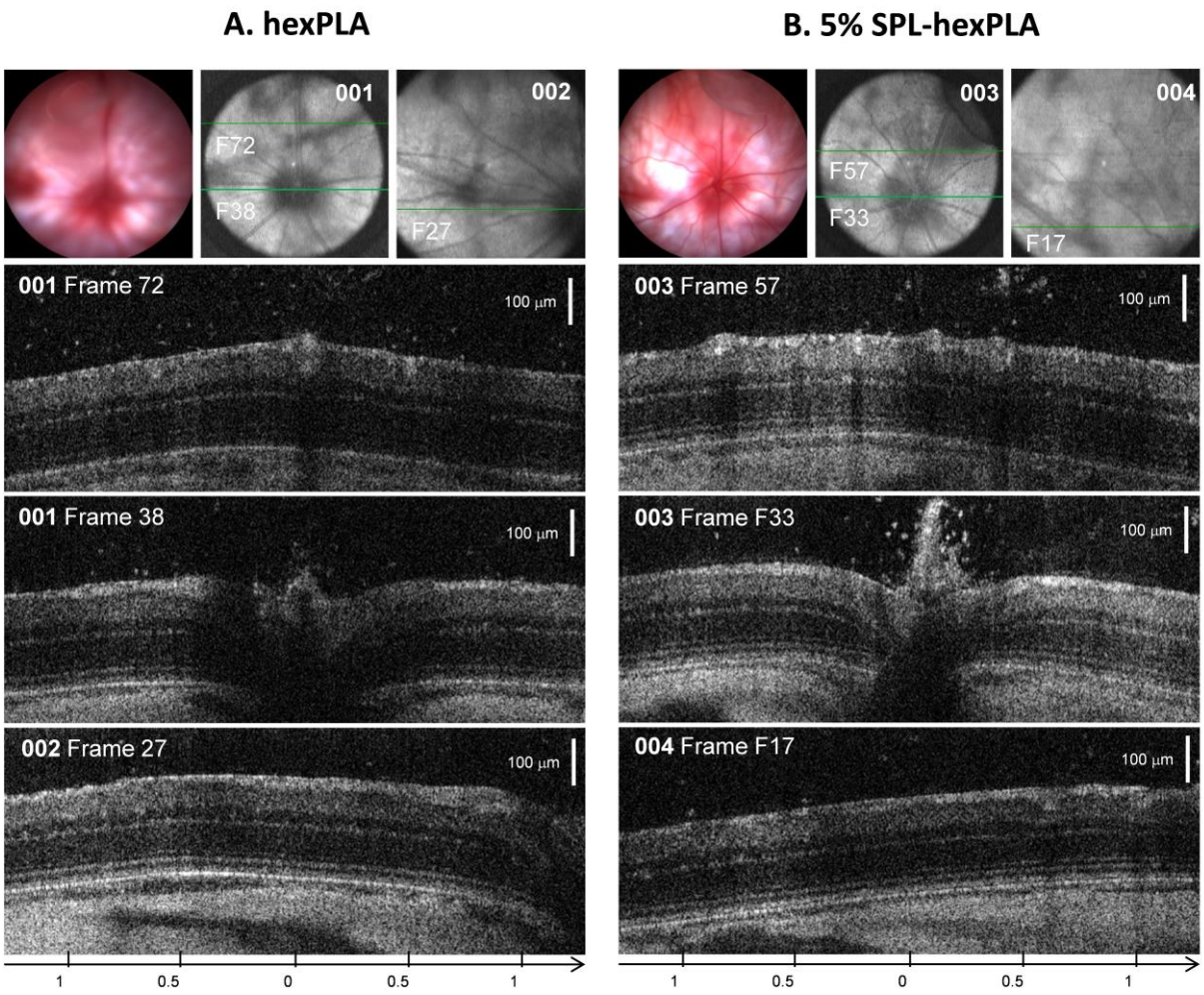

Figure 4. Optical coherence tomography (OCT) images showing retinal sections of rat eyes, 14 days after intravitreal injection of hexPLA placebo polymer (A) or 5% SPL-hexPLA (B). For each group, the first line represents color eye fundus (Micron III) and infrared eye fundus generated during OCT acquisitions (Bioptigen). The second line represents the retinal sections observed near the polymer (001 F72 and 003 F57). The third line represents the retinal sections observed through the optic nerve (001 F38 and 003 F33). The fourth line represents the retinal sections observed far from the polymer (002 F27 and 004 F17).

3.4. Histology

Histological analyses were performed at Day 7 (Group 1 and 4) and Day 31 (Group 2 and 5) after IVT (**Figure 5**). All sections observed through the center of the IVT site revealed that the placebo polymer (hexPLA), as well as the polymer loaded with SPL (5% SPL-hexPLA) remained in the injection hole formed by the needle which hindered its closure and healing leading to a subsequent inflammatory reaction at the IVT site. Consistent with the *in vivo* OCT examination, the architecture of the retina was well preserved near the IVT site and at the opposite side of the IVT, showing that the inflammatory reaction was not caused by the polymer

itself or by its degradation products but was a consequence of the non-healed injection site clogged by the polymer.

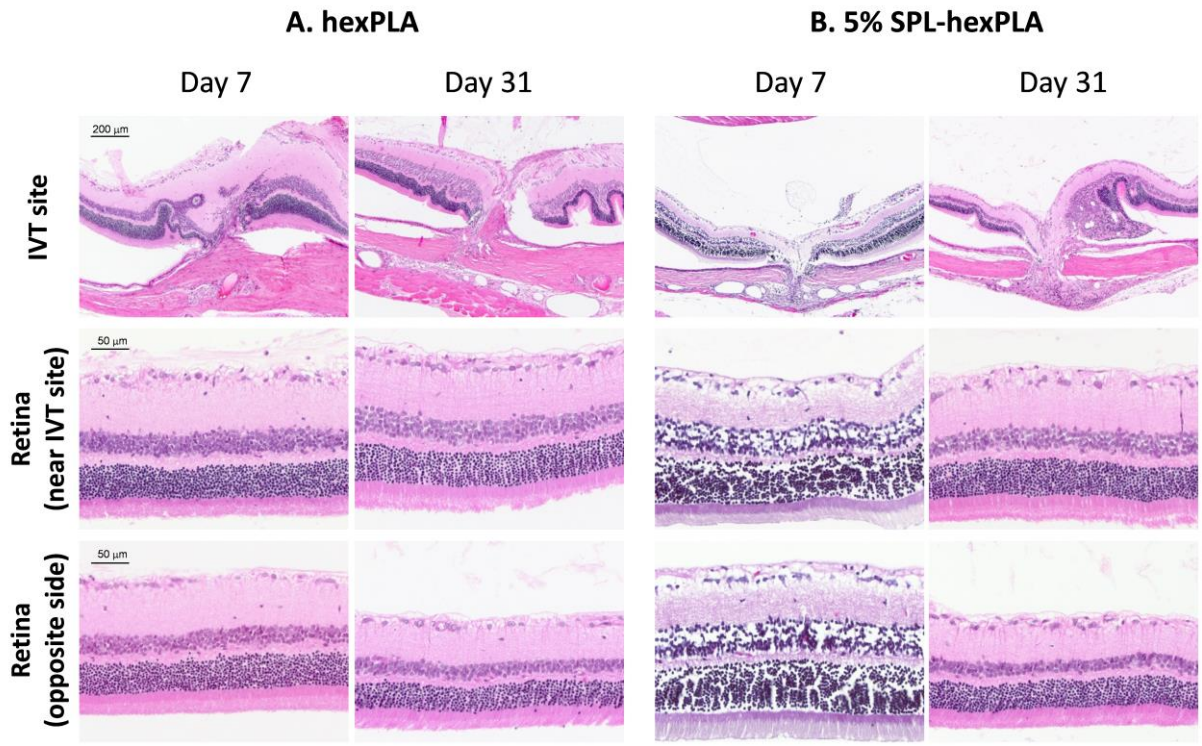

Figure 5. Histology of rat eyes 7 days and 31 days after intravitreal injection (IVT) of hexPLA placebo polymer (A) or 5% SPL-hexPLA (B). The eye injected with 5% SPL-hexPLA and observed at day 7 was fixed in a solution of formalin, explaining the lower quality of the image. The other samples were fixed in Bouin's solution. All the sections were stained with Hematoxylin-Eosin. All the images were taken on the section through the center of the IVT site.

3.5. Ocular biodistribution of SPL and its metabolites

The biodistribution of spironolactone (SPL) and its main metabolites in ocular tissues was determined at Day 3 (Group 3, **Figure 6A**), at Day 7 (Group 4, **Figure 6B**) and day 31 (Group 5, **Figure 6C**) after single IVT of 5% SPL-hexPLA. At each time point, 6 eyes were dissected to isolate the cornea, iris, neuroretina, sclera-choroid-RPE complex and fluids and analyzed using UHPLC-ESI-MS.

At Day 3, SPL concentration was 491 ± 347 ng/g in the cornea, 422 ± 357 ng/g in the iris, 96814 ± 85039 ng/g in the neuroretina, 2338 ± 972 ng/g in the sclera-choroid-RPE complex and 452 ± 142 ng/g in the fluids. At Day 7, SPL concentration was 978 ± 816 ng/g in the cornea, 723 ± 603 ng/g in the iris, 3769 ± 1393 ng/g in the neuroretina, 1228 ± 1194 ng/g in the sclera-choroid-RPE complex and 437 ± 359 ng/g in the fluids. In ocular fluids (aqueous humor + vitreous), SPL concentrations found at Day 3 and Day 7 correspond respectively to 0.55 and 0.43 µM. At

Day 31, SPL was only detected in the neuroretina and in the sclera-choroid-RPE complex at respectively 45 ± 27 ng/g and 29 ± 8 ng/g.

At Day 3, canrenone (CAN) concentration was 164 ± 71 ng/g in the cornea, 186 ± 52 ng/g in the iris, 4292 ± 3557 ng/g in the neuroretina, 417 ± 145 ng/g in the sclera-choroid-RPE complex and 121 ± 68 ng/g in the fluids. At Day 7, CAN concentration was 245 ± 227 ng/g in the cornea, 355 ± 311 ng/g in the iris, 388 ± 142 ng/g in the neuroretina, 354 ± 238 ng/g in the sclera-choroid-RPE complex and 134 ± 96 ng/g in the fluids. At Day 31, consistent with the SPL levels detected, CAN was only detected in the neuroretina and in the sclera-choroid-RPE complex at respectively 15 ± 5 ng/g and 11 ± 5 ng/g.

At day 3, 7α-thiomethylspironolactone (TMSPL) concentration was 137 ± 77 ng/g in the cornea, 954 ± 441 ng/g in the iris, 827 ± 381 ng/g in the neuroretina, 474 ± 217 ng/g in the sclera-choroid-RPE complex and 25 ± 18 ng/g in the fluids. At day 7, TMSPL concentration was 224 ± 156 ng/g in the cornea, 1232 ± 776 ng/g in the iris, 434 ± 343 ng/g in the neuroretina, 355 ± 302 ng/g in the sclera-choroid-RPE complex and 30 ± 19 ng/g in the fluids. At day 31, TMSPL was not detected in any of the ocular tissues.

The biodistribution of SPL, CAN and TMSPL over time in ocular tissues is represented in **Figure 6**.

One month after a single IVT of 5% SPL-hexPLA, neither spironolactone nor its metabolites were detected in rat plasmas, demonstrating that there was no systemic exposure induced by the IVT of formulation after 31 days. Whether there was systemic exposure during the first weeks remains unknown since we did not sample the plasma at Day 3 neither at Day 7.

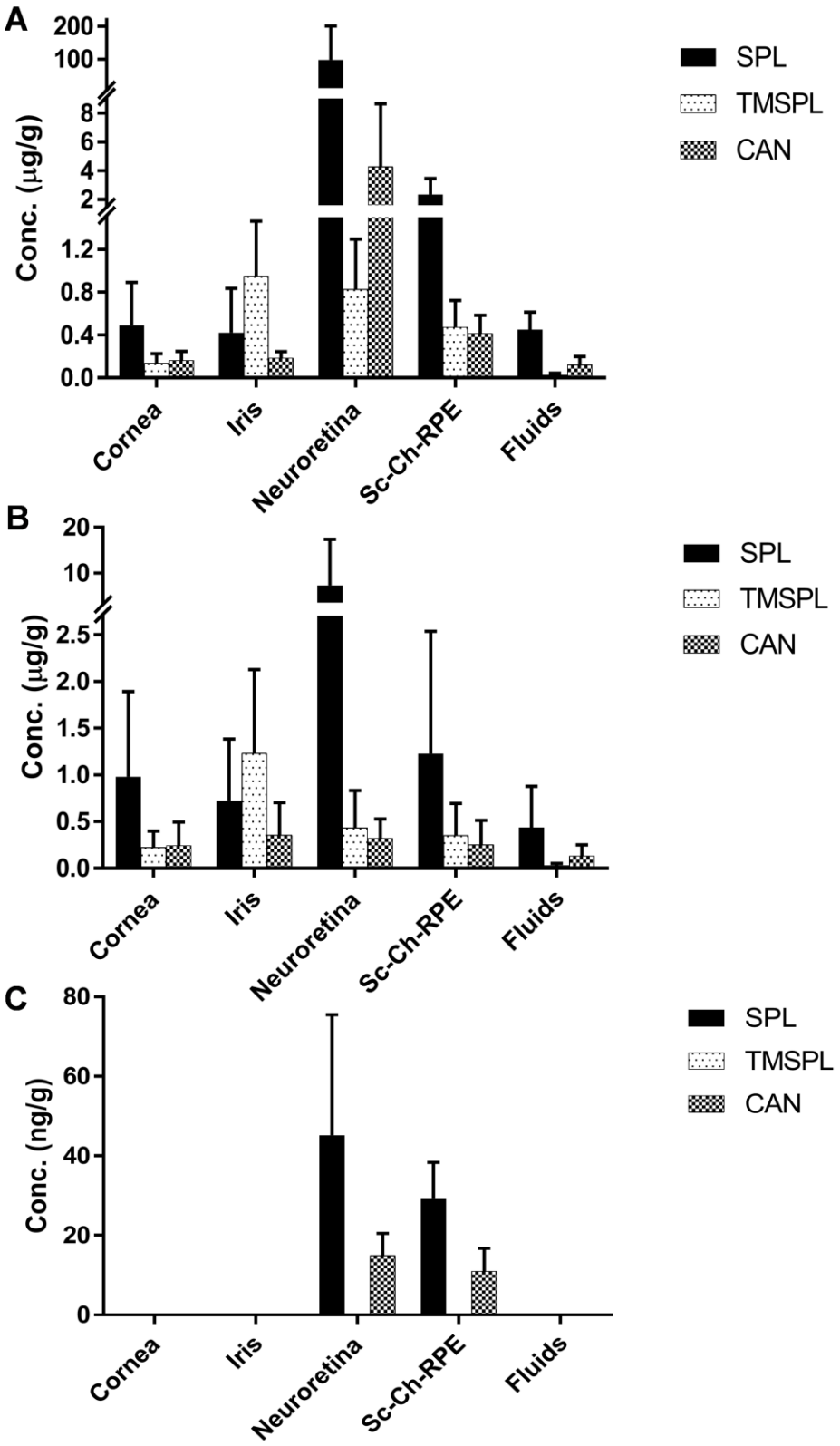

Figure 6. Mean concentrations of spironolactone and of its main metabolites found in ocular tissues after 3 days (A, n=6), 7 days (B, n=6) and 31 days (C, n=6) following single intravitreal injection of 5% SPL-hexPLA formulation. CAN, canrenone; SPL, spironolactone; TMSPL, 7α-thiomethylspironolactone. Fluids, aqueous and vitreous humour; Sc-Ch-RPE, Sclera-choroid-retinal pigment epithelium complex.

4. Discussion

MR antagonists (MRa) are increasingly gaining interest for the treatment of CSCR [3, 27-30]. However, long-term treatment is required in chronic forms of CSCR [27, 28, 31], which is partly due to the reduced bioavailability of MRa in ocular tissues after systemic administration. In a previous study, we have demonstrated the tolerance of intravitreal injection of the only commercial intravenous preparation of potassium canrenoate (Soludactone®, Pfizer), the water-soluble precursor of the active metabolite of spironolactone, canrenone [32]. However, due to the short half-life of spironolactone and canrenone in the vitreous, frequent injections are necessary to maintain the therapeutic effect. In this study, after the evaluation of the *in vitro* release profile of spironolactone from hexPLA, a biodegradable and biocompatible sustained release polymer, we evaluated the *in vivo* ocular biodistribution of spironolactone and its metabolites after a single intravitreal injection of this polymer loaded with 5% spironolactone.

Pharmacokinetic of MRa after oral administration is widely reported, however, the fate of MRa following intravitreal injection is lacking. To our knowledge, this study provides for the first-time insight on the intraocular biodistribution of spironolactone and its metabolites after a single intravitreal injection. In our previous study [32], it was not possible to perform an *in vivo* ocular biodistribution of spironolactone after intravitreal injection of spironolactone-loaded PLGA-microspheres due to the lack of a highly sensitive analytical method. The analytical methods described in the literature for the detection of spironolactone are not suitable for this study due to several reasons: (i) lack of sensitivity, (ii) excessively long run time required, (iii) do not allow simultaneous detection of spironolactone and its metabolites [33-36]. In this study, we report the application of a novel sensitive UHPLC-MS analytical method allowing the simultaneous quantification of spironolactone and its metabolites in small volumes of ocular samples, with low limits of quantification (5 ng/mL) and within a short run time of 5 min. The simultaneous detection of canrenone and 7α-thiomethylspironolactone was necessary because, in the contrary to what was previously thought, not only CAN but also TMSPL is a major metabolite of SPL and both exert an anti-MR activity. The former belief was due to the use of nonspecific analytical methods leading to confusion of canrenone and other sulfur-containing metabolites [36-38].

A single intravitreal injection of 5% SPL-hexPLA polymer allowed a sustained release of spironolactone in rat eye up to one month, since therapeutic levels were found in the retina and RPE/ choroid/ sclera at day 31 with concentrations around 10 nM, 5-folds higher than 50 % of the inhibitory concentration (IC_{50}) of spironolactone which have been reported to be around 2

nM in the muscle [39, 40]. In ocular fluids, the concentration of spironolactone at day 3 and day 7 were respectively 0.55 µM and 0.43 µM, which are 215 to 275-folds higher than 50 % of the IC_{50} of spironolactone, respectively.

The *in vivo* biodistribution of spironolactone in the different ocular tissues following its release from the hexPLA polymer over time correlated with the release profile obtained *in vitro*; with high amounts observed in the first week (due to the burst release), followed by a gradual decrease in the last weeks (**Figure 7A**). This burst release of spironolactone was observed in all the ocular samples at Day 3, followed by a decrease in the amounts of spironolactone detected in the neuroretina, sclera-choroid-RPE complex and in the fluids at Day 7. In contrast, the amounts of spironolactone found in the anterior segment tissues, including the cornea and the iris, increased at day 7 due to the high clearance through the anterior pathway in the first week, as will be discussed later. At Day 31, spironolactone was only detected in the neuroretina and the sclera-choroid-RPE complex. This *in vitro-in vivo* correlation, comparable to a level D *in vitro-in vivo* correlation corresponding to an equivalent order of the release profile equations obtained *in vitro* and *in vivo*, suggests that the degradation process of the hexPLA polymer occurs by the only hydrolysis reaction instead of enzymatic reaction or a combination of both reactions.

In addition to spironolactone, its two main metabolites; canrenone and 7α-thiomethylspironolactone, were also detected in the ocular tissues suggesting the presence in the rat eye of enzymes, such as esterases and thiomethyltransferases, necessary for converting spironolactone to its major metabolites [41, 42]. The *in vivo* biodistribution profiles of these metabolites in ocular tissues **(Figures 7B, 7C**) were similar to the biodistribution profile of spironolactone. Interestingly, the biodistribution profile of spironolactone in the different ocular tissues following a single intravitreal injection of 5% spironolactone-hexPLA formulation was similar to the release profile observed after a single subcutaneous injection of 5% triptorelin-hexPLA. In this study, triptorelin plasma levels were detected for up to 6 months, with a higher rate of release during the first week, followed by constant plasma levels and finally a decrease from week 10 to the end of the study [25]. This study also showed a good *in vitro-in vivo* correlation of the release profile of the 5% triptorelin-hexPLA formulation, highlighting the robustness of the *in vitro* test used to evaluate the release profile and the sustained release properties of the hexPLA polymer.

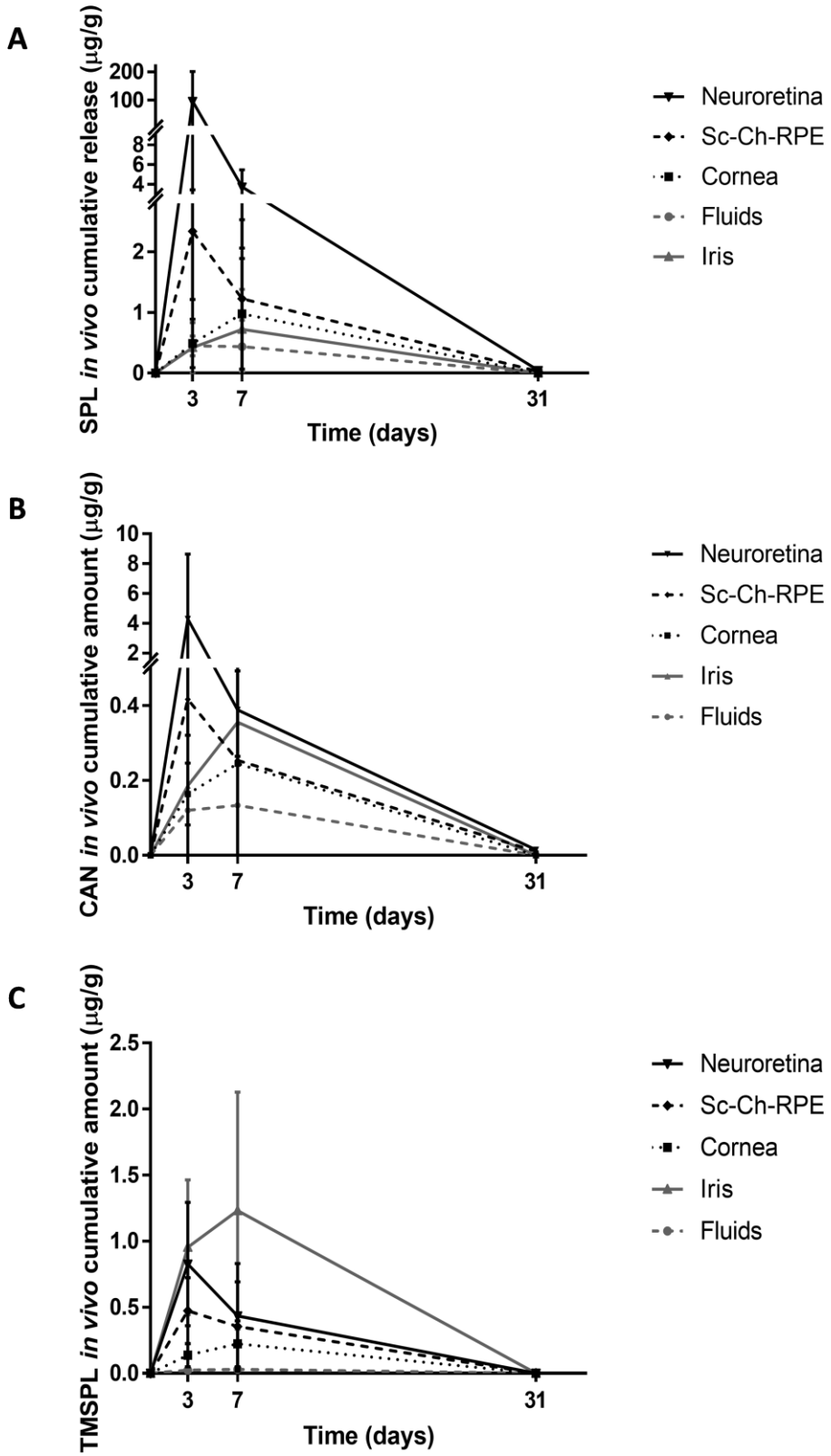

Figure 7. *in vivo* biodistribution of (A) spironolactone, (B) canrenone and (C) 7α-thiomethylspironolactone over time in ocular tissues following single intravitreal injection of 5% SPL-hexPLA. Fluids, aqueous and vitreous humour; Sc-Ch-RPE, Sclera-choroid-retinal pigment epithelium complex.

The biodistribution of spironolactone and its metabolites in ocular tissues showed that these compounds were cleared through both pathways, the anterior and the posterior routes. First, they were detected in cornea and in iris at days 3 and 7, suggesting a high clearance level through the anterior segment during the first week due to the high amounts of spironolactone released by the polymer in the posterior segment. Then, the clearance was mainly through the chorio-retinal route since all the compounds were absent in the anterior segment at day 31. This may be explained by lower amounts of SPL released into the posterior segment during the last weeks. It is well known that following intravitreal injection, drugs can be eliminated either by the anterior route or by the posterior route. The anterior route takes place by the diffusion of the drugs from the vitreous to the aqueous humor via the zonular spaces, then by elimination through the aqueous humor turnover. The posterior route takes place by drug permeation across the blood–retinal barrier via passive permeability (small molecular size, lipophilicity) or active transport mechanisms across these barriers [13-15, 17, 43].

Regardless of the highly interesting results obtained with the biodistribution study, we have encountered some limitations due to the animal model and the injection system used. In the rat eye, the volume of the vitreous is about 50 µL, and the lens occupies almost 50% of the volume of posterior segment leaving only a narrow crescent-shaped volume for the 5 uL-droplet of polymer to float [44]. This anatomical constraint could explain why 80% of the followed droplets were stuck to the lens at the end of the month of follow up. To confirm the tolerance of this formulation in the eye, a more suitable animal model such as rabbit, pig or monkey [43, 45, 46] should be used in future studies. In our study, even if the polymer was not perfectly floating in the vitreous during the whole study, the biodistribution study showed an *in vivo* release profile that correlated well with the one obtained *in vitro*, showing a sustained release of spironolactone from the hexPLA polymer for up to one month. On the other hand, the rat retina and particularly its vasculature is more comparable to the human retinal vasculature than the rabbit one. This is the reason why it was important to analyze the biodistribution of the formulation in the rat in this first study. Our next study will be performed in a model with eye dimensions closer to the human eye.

Regarding the injection technique, due to the viscous nature of the polymer, a trail of the polymer remained in the injection site when removing the needle, hindering the closure and healing of the injection site, as it is normally observed after intravitreal injection of aqueous solution. To overcome this limitation, a specific injection system adapted for viscous formulations should be used in further studies. After the penetration of the needle into the eye, this system should allow the release of the viscous formulation into the vitreous by propelling

the polymer droplet before the withdrawal of the needle. Despite the inflammatory reaction induced by the non-healed injection site, no retinal damage was observed in the other areas of the posterior segment showing that the polymer degradation products did not induce toxic effect on the retina. In further tolerance studies, the risk of visual disturbance due to the turbid polymeric droplet should be reduced, for instance by injecting the droplet in the inferior part of the vitreous, below the visual axis.

This study reports for the first time the application of a novel UHPLC-MS analytical method to quantify the amounts of spironolactone and its metabolites in ocular tissues. This sensitive analytical method allowed performing the *in vivo* biodistribution study of the 5% SPL-hexPLA. The results demonstrated that a single intravitreal injection of this biodegradable formulation allowed a sustained release of spironolactone, with therapeutic levels, into the posterior segment of the eye for at least one month. This release period could be modulated by modifying the concentration of spironolactone loaded in the hexPLA. These findings show that this spironolactone-loaded sustained release polymeric system, combined with an appropriate injection system, would be of interest to locally treat patients presenting chronic forms of CSCR and to improve their compliance by avoiding frequent injections.

Acknowledgements

ND and YNK acknowledge financial support from the Swiss Commission for Technology and Innovation (CTI Project 19086.1 PFLS-LS) and Apidel SA (Geneva, Switzerland). YNK would like to thank the University of Geneva, the Fondation Ernst and Lucie Schmidheiny and the Société Académique de Genève for providing financial support to enable the acquisition of the Waters Xevo® TQ-MS detector. The authors also thank the team of the histopathological laboratory and Catherine Martin from the Unit of Gene Therapy and Stem Cell Biology of the Fondation Asile des aveugles for technical support.

References

[1] A. Daruich, A. Matet, A. Dirani, E. Bousquet, M. Zhao, N. Farman, F. Jaisser, F. Behar-Cohen, Central serous chorioretinopathy: Recent findings and new physiopathology hypothesis, Prog. Retin. Eye Res. 48 (2015) 82-118.

[2] E. Bousquet, T. Beydoun, P.R. Rothschild, C. Bergin, M. Zhao, R. Batista, M.L. Brandely, B. Couraud, N. Farman, A. Gaudric, F. Chast, F. Behar-Cohen, Spironolactone for nonresolving central serous chorioretinopathy: A randomized controlled crossover study, Retina 35 (2015) 2505-2515.

[3] E. Bousquet, T. Beydoun, M. Zhao, L. Hassan, O. Offret, F. Behar-Cohen, Mineralocorticoid receptor antagonism in the treatment of chronic central serous chorioretinopathy: a pilot study, Retina 33 (2013) 2096-2102.

[4] M. Zhao, I. Celerier, E. Bousquet, J.C. Jeanny, L. Jonet, M. Savoldelli, O. Offret, A. Curan, N. Farman, F. Jaisser, F. Behar-Cohen, Mineralocorticoid receptor is involved in rat and human ocular chorioretinopathy, J. Clin. Invest. 122 (2012) 2672-2679.

[5] T.R. Herold, K. Rist, S.G. Priglinger, M.W. Ulbig, A. Wolf, Long-term results and recurrence rates after spironolactone treatment in non-resolving central serous chorio-retinopathy (CSCR), Graefes Arch. Clin. Exp. Ophthalmol. DOI 10.1007/s00417-016-3436-5(2016).

[6] T.R. Herold, K. Prause, A. Wolf, W.J. Mayer, M.W. Ulbig, Spironolactone in the treatment of central serous chorioretinopathy - a case series, Graefes Arch. Clin. Exp. Ophthalmol. 252 (2014) 1985-1991.

[7] E.K. Chin, D.R. Almeida, C.N. Roybal, P.I. Niles, K.M. Gehrs, E.H. Sohn, H.C. Boldt, S.R. Russell, J.C. Folk, Oral mineralocorticoid antagonists for recalcitrant central serous chorioretinopathy, Clin. Ophthalmol. 9 (2015) 1449-1456.

[8] Q. Ghadiali, J.J. Jung, S. Yu, S.N. Patel, L.A. Yannuzzi, Central serous chorioretinopathy treated with mineralocorticoid antagonists: A one-year pilot study, Retina 36 (2016) 611-618.

[9] E. Bousquet, M. Zhao, A. Ly, G. Leroux Les Jardins, B. Goldenberg, M.C. Naud, L. Jonet, B. Besson-Lescure, F. Jaisser, N. Farman, Y. De Kozak, F. Behar-Cohen, The aldosterone-mineralocorticoid receptor pathway exerts anti-inflammatory effects in endotoxin-induced uveitis, PLoS One 7 (2012) e49036.

[10] A. Odermatt, P. Arnold, F.J. Frey, The intracellular localization of the mineralocorticoid receptor is regulated by 11beta-hydroxysteroid dehydrogenase type 2, J. Biol. Chem. 276 (2001) 28484-28492.

[11] M. Zhao, F. Valamanesh, I. Celerier, M. Savoldelli, L. Jonet, J.C. Jeanny, F. Jaisser, N. Farman, F. Behar-Cohen, The neuroretina is a novel mineralocorticoid target: aldosterone up-regulates ion and water channels in Muller glial cells, FASEB J. 24 (2010) 3405-3415.

[12] J.L. Wilkinson-Berka, G. Tan, K. Jaworski, A.G. Miller, Identification of a retinal aldosterone system and the protective effects of mineralocorticoid receptor antagonism on retinal vascular pathology, Circ. Res. 104 (2009) 124-133.

[13] R. Gaudana, H.K. Ananthula, A. Parenky, A.K. Mitra, Ocular drug delivery, AAPS J 12 (2010) 348-360.

[14] A. Urtti, Challenges and obstacles of ocular pharmacokinetics and drug delivery, Adv Drug Deliv Rev 58 (2006) 1131-1135.

[15] E. Sakurai, H. Ozeki, N. Kunou, Y. Ogura, Effect of particle size of polymeric nanospheres on intravitreal kinetics, Ophthalmic Res. 33 (2001) 31-36.

[16] G. Gough, M. Szapacs, T. Shah, P. Clements, C. Struble, R. Wilson, Ocular tissue distribution and pharmacokinetic study of a small 13kDa domain antibody after intravitreal, subconjuctival and eye drop administration in rabbits, Exp. Eye Res. 167 (2017) 14-17.

[17] V. Agrahari, A. Mandal, V. Agrahari, H.M. Trinh, M. Joseph, A. Ray, H. Hadji, R. Mitra, D. Pal, A.K. Mitra, A comprehensive insight on ocular pharmacokinetics, Drug Deliv Transl Res 6 (2016) 735-754.

[18] U.B. Kompella, A.C. Amrite, R. Pacha Ravi, S.A. Durazo, Nanomedicines for back of the eye drug delivery, gene delivery, and imaging, Prog. Retin. Eye Res. 36 (2013) 172-198.

[19] A. Lambiase, S. Abdolrahimzadeh, S.M. Recupero, An update on intravitreal implants in use for eye disorders, Drugs Today (Barc) 50 (2014) 239-249.

[20] J. Wang, A. Jiang, M. Joshi, J. Christoforidis, Drug delivery implants in the treatment of vitreous inflammation, Mediators Inflamm. 2013 (2013) 780634.

[21] M.N. Yasin, D. Svirskis, A. Seyfoddin, I.D. Rupenthal, Implants for drug delivery to the posterior segment of the eye: A focus on stimuli-responsive and tunable release systems, J. Control. Release 196 (2014) 208-221.

[22] J.J. Kang-Mieler, C.R. Osswald, W.F. Mieler, Advances in ocular drug delivery: emphasis on the posterior segment, Expert Opinion on Drug Delivery 11 (2014) 1647-1660.

[23] W. Pearce, J. Hsu, S. Yeh, Advances in drug delivery to the posterior segment, Curr. Opin. Ophthalmol. 26 (2015) 233-239.

[24] H. Chen, Recent developments in ocular drug delivery, J. Drug Target. 23 (2015) 597-604.

[25] L.R. Asmus, J.C. Tille, B. Kaufmann, L. Melander, T. Weiss, K. Vessman, W. Koechling, G. Schwach, R. Gurny, M. Moller, In vivo biocompatibility, sustained-release and stability of triptorelin formulations based on a liquid, degradable polymer, J. Control. Release 165 (2013) 199-206.

[26] L.R. Asmus, J.P. Grimshaw, P. Richle, B. Eicher, D.M. Urech, R. Gurny, M. Moller, Injectable formulations for an intravitreal sustained-release application of a novel single-chain VEGF antibody fragment, Eur. J. Pharm. Biopharm. 95 (2015) 250-260.

[27] A. Daruich, A. Matet, A. Dirani, M. Gallice, L. Nicholson, S. Sivaprasad, F. Behar-Cohen, Oral mineralocorticoid-receptor antagonists: Real-life experience in clinical subtypes of nonresolving central serous chorioretinopathy with chronic epitheliopathy, Transl. Vis. Sci. Technol. 5 (2016) 2.

[28] R.P. Singh, J.E. Sears, R. Bedi, A.P. Schachat, J.P. Ehlers, P.K. Kaiser, Oral eplerenone for the management of chronic central serous chorioretinopathy, Int J Ophthalmol 8 (2015) 310-314.

[29] F. Pichi, P. Carrai, A. Ciardella, F. Behar-Cohen, P. Nucci, G. Central Serous Chorioretinopathy Study, Comparison of two mineralcorticosteroids receptor antagonists for the treatment of central serous chorioretinopathy, Int. Ophthalmol. DOI 10.1007/s10792-016-0377-2(2016).

[30] R. Gergely, I. Kovacs, M. Schneider, M. Resch, A. Papp, Z. Recsan, Z.Z. Nagy, M. Ecsedy, Mineralocorticoid Receptor Antagonist Treatment in Bilateral Chronic Central Serous Chorioretinopathy: A Comparative Study of Exudative and Nonexudative Fellow Eyes, Retina 37 (2017) 1084-1091.

[31] A. Daruich, A. Matet, A. Dirani, M. Gallice, L. Nicholson, S. Sivaprasad, F. Behar-Cohen, Oral Mineralocorticoid-Receptor Antagonists: Real-Life Experience in Clinical Subtypes of Nonresolving Central Serous Chorioretinopathy With Chronic Epitheliopathy, Transl. Vis. Sci. Technol. 5 (2016) 2.

[32] M. Zhao, E. Rodriguez-Villagra, L. Kowalczuk, M. Le Normand, M. Berdugo, R. Levy-Boukris, I. El Zaoui, B. Kaufmann, R. Gurny, I. Bravo-Osuna, I.T. Molina-Martinez, R. Herrero-Vanrell, F. Behar-Cohen, Tolerance of high and low amounts of PLGA microspheres loaded with mineralocorticoid receptor antagonist in retinal target site, J. Control. Release 266 (2017) 187-197.

[33] H. Dong, F. Xu, Z. Zhang, Y. Tian, Y. Chen, Simultaneous determination of spironolactone and its active metabolite canrenone in human plasma by HPLC-APCI-MS, J. Mass Spectrom. 41 (2006) 477-486.

[34] D.I. Sora, S. Udrescu, F. Albu, V. David, A. Medvedovici, Analytical issues in HPLC/MS/MS simultaneous assay of furosemide, spironolactone and canrenone in human plasma samples, J. Pharm. Biomed. Anal. 52 (2010) 734-740.

[35] M.F. Suyagh, P.L. Kole, J. Millership, P. Collier, H. Halliday, J.C. McElnay, Development and validation of a dried blood spot-LC-APCI-MS assay for estimation of canrenone in paediatric samples, J. Chromatogr. B 878 (2010) 769-776.

[36] J.M. Sandall, J.S. Millership, P.S. Collier, J.C. McElnay, Development and validation of an HPLC method for the determination of spironolactone and its metabolites in paediatric plasma samples, J. Chromatogr. B Analyt. Technol. Biomed. Life Sci. 839 (2006) 36-44.

[37] A.M. Kaukonen, P. Vuorela, H. Vuorela, J.P. Mannermaa, High-performance liquid chromatography methods for the separation and quantitation of spironolactone and its degradation products in aqueous formulations and of its metabolites in rat serum, J. Chromatogr. A 797 (1998) 271-281.

[38] L.E. Ramsay, J.R. Shelton, D. Wilkinson, M.J. Tidd, Canrenone--the principal active metabolite of spironolactone?, Br. J. Clin. Pharmacol. 3 (1976) 607-612.

[39] S.M. Garthwaite, E.G. McMahon, The evolution of aldosterone antagonists, Mol. Cell. Endocrinol. 217 (2004) 27-31.

[40] J.A. Chadwick, J.S. Hauck, J. Lowe, J.J. Shaw, D.C. Guttridge, C.E. Gomez-Sanchez, E.P. Gomez-Sanchez, J.A. Rafael-Fortney, Mineralocorticoid receptors are present in skeletal muscle and represent a potential therapeutic target, FASEB J. 29 (2015) 4544-4554.

[41] R.A. Keith, I. Jardine, A. Kerremans, R.M. Weinshilboum, Human erythrocyte membrane thiol methyltransferase. S-methylation of captopril, N-acetylcysteine, and 7 alpha-thio-spirolactone, Drug Metab. Dispos. 12 (1984) 717-724.

[42] J.R. Cashman, S. Pena, Canrenone formation via general-base-catalyzed elimination of 7 alpha-(methylthio)spironolactone S-oxide, Chem. Res. Toxicol. 2 (1989) 109-113.

[43] E.M. Del Amo, A. Urtti, Rabbit as an animal model for intravitreal pharmacokinetics: Clinical predictability and quality of the published data, Exp. Eye Res. 137 (2015) 111-124.

[44] O. Sha, W.H. Kwong, Postnatal Developmental Changes of Vitreous and Lens Volumes in Sprague-Dawley Rats, 2006.

[45] N.R. Miller, M.A. Johnson, T. Nolan, Y. Guo, A.M. Bernstein, S.L. Bernstein, Sustained neuroprotection from a single intravitreal injection of PGJ(2) in a nonhuman primate model of nonarteritic anterior ischemic optic neuropathy, Invest. Ophthalmol. Vis. Sci. 55 (2014) 7047-7056.

[46] P. Daull, C.A. Paterson, B.D. Kuppermann, J.S. Garrigue, A preliminary evaluation of dexamethasone palmitate emulsion: a novel intravitreal sustained delivery of corticosteroid for treatment of macular edema, J. Ocul. Pharmacol. Ther. 29 (2013) 258-269.

CHAPTER IV

Targeted delivery of spironolactone loaded nanomicelles to the pilosebaceous unit.

Naoual Dahmana[a], Thibault Mugnier[b], Doris Gabriel[b], Tatiana Favez[c], Laura Kowalczuk[c], Francine Behar-Cohen[c, d], Robert Gurny[a, b], Yogeshvar N. Kalia[a]

[a] School of Pharmaceutical Sciences, University of Geneva, University of Lausanne, CMU - 1 rue Michel Servet, 1211 Geneva 4, Switzerland.

[b] Apidel SA, 29 Quai du Mont Blanc, 1201 Geneva, Switzerland.

[c] Fondation Asile des Aveugles - Hôpital Ophtalmique Jules-Gonin, 15 Avenue de France, 1004 Lausanne, Switzerland.

[d] INSERM, UMRS 872 Team 17, Centre de Recherche des Cordeliers, 15 rue de l'Ecole de Médecine, 75006 Paris, France.

Manuscript in preparation.

Abstract

The aim of this work was to investigate the feasibility of using nanomicellar formulations of spironolactone (SPL) prepared using the biodegradable mPEG-dihexPLA copolymer for targeted delivery to the mineralocorticoid receptor (MR) in the skin. The first step involved the use of immunofluorescent labelling techniques to localize using the MR in skin. The results showed that the MR was mainly located in the pilosebaceous unit (PSU) and an interesting target since nanomicelles accumulate preferentially in appendageal structures. Biodistribution studies were performed using infinite and finite dose conditions demonstrated the delivery of therapeutic amounts of SPL to the epidermis and the upper dermis (up to depth of 400 µm) following topical application for 12 h of 0.1% SPL nanomicellar formulation (micelle diameter ~20 nm). Selective targeting of the PSU was demonstrated by comparing the amounts of SPL found in PSU-containing and PSU-free skin biopsies: SPL nanomicelles showed up to 5-fold higher delivery to the PSU containing biopsies. Delivery of SPL from 0.1% SPL nanomicellar solutions was compared to that from hydrogels – with the former showing a slightly higher selectivity for the PSU (1.3-fold higher). SPL was metabolized in the skin to canrenone; however, 7α-thiomethylspironolactone, the other active metabolite of SPL, was not detected. In conclusion, 0.1% SPL nanomicellar formulations enabled targeted follicular delivery of SPL, allowing site-specific antagonism of the MR, which is mainly localized in the PSU. Co-administration of this formulation during glucocorticoid (GC) therapy may be of clinical benefit for the treatment cutaneous delayed wound healing involving the overactivation of the MR by the GC. This formulation may also be considered as a promising strategy to treat the various pilosebaceous androgenic-related skin diseases including acne vulgaris, androgenic alopecia and hirsutism, since SPL is also a potent androgen antagonist.

Keywords: Spironolactone, polymeric micelles, pilosebaceous unit, transfollicular delivery, biodistribution, ultra-high performance liquid chromatography – mass spectrometry.

1. Introduction

Impaired cutaneous wound healing is a significant clinical problem encountered as a complication of certain chronic conditions such as diabetes as well as in patients under chronic glucocorticoid therapy [1]. Recent studies have elucidated the mechanism involved in the glucocorticoid-induced delayed wound healing and have attributed the cause to the off-target over activation of the mineralocorticoid receptor (MR) by the glucocorticoids [2-4].

Based on this observation, co-administration of a mineralocorticoid receptor antagonist, such as spironolactone (SPL) or its active metabolite canrenone (CAN), together with the glucocorticoids was suggested as a therapeutic strategy to block the off-target glucocorticoid binding to the MR. This hypothesis was tested *in vivo* in mice where the wounds treated with the combination of clobetasol, a potent glucocorticoid and canrenoate potassium, a water-soluble precursor of canrenone, showed a significant improvement in the wound closure compared to control (clobetasol + PBS) [5]. Moreover, a clinical trial conducted in 23 healthy volunteers showed a significant off-setting of the clobetasol-induced delayed wound healing of skin biopsies treated with spironolactone [6].

Given the positive results of the co-administration of a mineralocorticoid receptor antagonist to off-set the negative effect of the glucocorticoid therapy and the potential clinical benefits for patients under glucocorticoid therapy and suffering from wound healing abnormalities, we decided to address the unmet need and develop a spironolactone formulation for topical application to the skin.

Spironolactone is a poorly water-soluble (0.02 mg/mL) and potent MR antagonist. To enhance the aqueous solubility of SPL, we decided to use the micelle forming amphiphilic copolymer; methoxy-poly(ethylene glycol)-di-hexyl-substituted-poly(lactic acid), (mPEG-dihexPLA) which enabled to yield up to 2 mg/mL micellar solution of SPL, representing a 100-fold increase in aqueous solubility. This biodegradable and biocompatible diblock copolymer already showed interesting properties for topical delivery of poorly water-soluble compounds by enhancing their bioavailability in the skin and the cornea [7-11].

We have previously developed and characterized a 0.1% spironolactone nanomicellar solution based on mPEG-dihexPLA copolymer that showed a stability of at least 12 months at 5°C. The preclinical tolerability and efficacy of this formulation was assessed *in vivo* in rabbits in a corneal wound healing model where co-administration of this formulation off-set dexamethasone-induced corneal delayed wound healing [12].

In addition, there is no commercially available topical formulation of SPL. Lately, oral SPL has been increasingly used off-label to treat acne vulgaris, androgenic alopecia and hirsutism. However, oral administration of SPL to treat peripheric and localized diseases is not optimal since SPL is not selective to the MR and may also bind other steroid receptor leading to undesirable side effects associated to systemic exposure [13-15].

In this study, we first assessed the presence and localization of the MR in the skin using immunofluorescent labelling; these studies revealed that MR were principally present in the PSU. Recent investigations have shown a preferential accumulation of nanomicelles in the PSU, resulting in a topical, efficient treatment for diseases involving the hair follicle and the sebaceous glands such as acne vulgaris [10, 16]. Hence, developing a novel nanomicelle drug delivery system for topical delivery of SPL would allow site-specific targeting with potential for greater efficacy and reduced side effects. For a more patient-friendly dermatologic administration, the spironolactone nanomicellar solution was incorporated in a Carbopol® based hydrogel and *ex vivo* skin penetration following topical application was evaluated under both infinite and finite dose conditions. The safety of the composite nanomicellar hydrogels based on Carbopol® and mPEG-dihexPLA was already tested and showed no signs of toxicity following multiple topical application in healthy mice [9]. Following formulation development, an *ex vivo* biodistribution study was performed by quantifying the amount of spironolactone and its two main metabolites; 7α-thiomethylspironolactone and canrenone; as a function of skin depth using a validated UHPLC-ESI-MS analytical method. Follicular delivery of spironolactone nanomicelles was also investigated by quantifying the PSU and the PSU-free skin samples – in addition to quantification of the absolute amounts delivered, the delivery efficacies of the 0.1% spironolactone nanomicellar solution and hydrogel were compared.

2. Experimental

2.1. Materials

Methoxy-poly(ethylene glycol)-di-hexyl-substituted-poly(lactic acid),[17] (mPEG-dihexPLA, 5.5 kDa) was supplied by Apidel SA (Geneva, Switzerland). Spironolactone (SPL) was purchased from Zhejiang Langhua pharmaceutical Co., Ltd. (Zhejiang, China). 7α-thiomethylspironolactone (TMSPL) was purchased from TLC Pharmaceutical Standards Ltd. (Ontario, Canada). Canrenone (CAN) and 17α-methyltestosterone (MeT), used as an internal standard (IS), were purchased from Sigma-Aldrich (Buchs, Switzerland). Carbopol® Ultrez 10 was obtained from Lubrizol (Belgium). Millex® filters (Durapore PVDF, pore size 0.22 µm, diameter 13 mm) were purchased from Sigma-Aldrich (Buchs, Switzerland). Ultrapure water (H_2O, resistivity > 18 MΩ cm) was prepared using a Merck Millipore Milli-Q water purification system (Darmstadt, Germany). Methanol (MeOH, HPLC grade) was obtained from Fisher Scientific (Waltham, MA, USA) and formic acid (ULC/MS grade) from Biosolve (Dieuze, France). Trifluoroacetic acid was obtained from VWR (Dietikon, Switzerland). All other chemicals were at least of analytical grade. MR antibody (MABS496) and DAPI were obtained from Merck Millipore (Darmstadt, Germany).

2.2. Analytical methods

2.2.1. Quantification of spironolactone in the formulations using UHPLC-UV

An ultra-high performance liquid chromatography method with UV detection (UHPLC-UV) was developed to support the formulation development work. The liquid chromatographic system consisted of a Waters Acquity® UPLC® H-Class system (Baden-Dättwil, Switzerland) including a binary solvent manager, a sample manager and a column manager. The reverse phase chromatography was performed using a Waters XBridge® BEH C18 column (50 x 2.1 mm I.D., 2.5 µm) fitted with a Waters XBridge® BEH C18 VanGuard pre-column (5 x 2.1 mm I.D., 2.5 µm). The isocratic elution was carried out using a mobile phase consisting of 0.1% formic acid in H_2O:MeOH (30:70, v/v) with a flow rate of 0.45 mL/min and a runtime of 1 minute. Column temperature was held at 40°C and the sample manager was kept at room temperature. Injection volume was 10 µL and the UV detection of SPL was set at 240 nm. Calibration standards of SPL were prepared in methanol:water (1:1) mixture at 0.1, 0.2, 0.5, 1, 2, 5, and 10 µg/mL. Calibration curves were constructed by plotting the area of each analyte *versus* the concentration of each analyte. All the calibration curves were linear (R > 0.99). The limit of detection (LOD) and the limit of quantification (LOQ) of SPL were 0.1 µg/mL and 0.2 µg/mL, respectively. More information is provided in the supporting information (SI).

2.2.2. Quantification of spironolactone and its metabolites in the skin using UHPLC-ESI-MS

An ultra-high performance liquid chromatography coupled to mass spectrometry (UHPLC-ESI-MS) bioanalytical method was previously developed for the simultaneous detection and quantification of spironolactone (SPL) and its metabolites; 7α-thiomethylspironolactone (TMSPL) and canrenone (CAN), in biological samples. 17α-methyltestosterone (MeT) was used as internal standard. This method has been adapted and validated for the quantification of skin samples (see SI). Briefly, the liquid chromatographic system consisted of a Waters Acquity® ultra-performance liquid chromatography (UPLC®) system (Baden-Dättwil, Switzerland) including a binary solvent manager, a sample manager with an injection loop volume of 10 µL and a column manager. Reverse phase chromatographic separation of SPL, TMSPL, CAN and MeT was performed using a Waters XBridge® BEH C18 column (100 x 2.1 mm I.D., 2.5 µm) fitted with a Waters XBridge® BEH C18 VanGuard pre-column (5 x 2.1 mm I.D., 2.5 µm). The isocratic elution was carried out using a mobile phase consisting of 0.1% formic acid in H_2O:MeOH (50:50, v/v) with a flow rate of 0.3 mL/min and a runtime of 12 minutes. Column temperature was held at 50°C and the sample manager was kept at room temperature. Injection volume was set at 5 µL (partial loop injection mode). The mass spectrometry (MS) system consisted of a Waters XEVO® TQ-MS detector (Baden-Dättwil, Switzerland) fitted with a Z-spray electrospray ionization source. MS detection of the 4 compounds was performed using electrospray ionization in the positive-ion mode (ESI+) and the selected ion recording (SIR) using the pseudo-molecular ion of each compound as the parent ion (hydrogen adduct, $[M + H]^+$). The capillary voltage was set at 2.3 kV, and desolvation gas temperature and flow were maintained at 350 °C and 650 L/h, respectively. Identification and quantification of each analyte were carried on according to the mass-to-charge ratio (m/z) of the pseudo-molecular ion of each compound ($[M + H]^+$). Cone voltage optimal setting was 35 V and the pseudo-molecular parent ion corresponding to SPL/CAN, TMSPL and MeT have an *m/z* of 341.0, 389.0 and 303.0 respectively. SPL was detected with *m/z* of 341.0, which corresponds to the pseudo-molecular parent ion of CAN. This is due to the cleavage of the 7α-thioacetyl group of SPL during the electrospray evaporation and ionization process within the ESI source producing CAN. Dwell time was set at 5 ms for all the compounds. Data processing was performed using Waters MassLynx software version 4.1 (Milford, MA, USA). Calibration standards of SPL, TMSPL and CAN were prepared in porcine skin matrix at 5, 10, 20, 50, 200, 500 and 1000 ng/mL, and contained 100 ng/mL 17α-methyltestosterone as internal standard (IS). Calibration curves were constructed by plotting the ratio of the area of each analyte to the

area of the internal standard *versus* the ratio of the concentration of each analyte to the concentration of the internal standard. All calibration curves were linear (R > 0.99). The lower limit of quantification (LLOQ) of each analyte was 5 ng/mL. More information is provided in the SI.

2.3. Mineralocorticoid receptor labelling in the skin

Localization of the MR in the skin was assessed with immunofluorescent labelling. Skin biopsies were punched from the external part of fresh porcine ears obtained from a local slaughterhouse (CARRE; Rolle, Switzerland) then fixed in 4 mL of 4% paraformaldehyde in PBS during 1 h at room temperature followed by 3-times rinse in PBS. Samples were then cryoprotected using sucrose gradient solutions (10% then 20%) during 2 h at room temperature and finally left overnight in 30% sucrose solution at 5°C. The following day, samples were cryoembedded in OCT compound at -40°C during 45 s using the prestoCHILL (Milestone, Italy), cut into 5 µm serial sections (CryoStar NX70 Cryostat, Thermo Scientific) then mounted on glass slides and kept at -20°C until use. Prior to immunofluorescence labelling, skin sections were fixed using methanol for 10 min at -20°C then rinsed 3 times with PBS. Nonspecific protein binding was blocked using a blocking solution containing 5% Normal Goat Serum (NGS) and 0.3% Triton-X-100 in PBS for 1 h at 5°C then skin sections were incubated over night at 5°C with the MR primary antibody diluted 1:100 in 1% Bovine Serum Albumine (BSA) and 0.3% Triton-X-100 in PBS. After 3 rinsing cycles with PBS, skin sections were incubated with the secondary antibody (goat anti-mouse Alexa 488) diluted 1:2000 in 1% Bovine Serum Albumine (BSA) and 0.3% Triton-X-100 in PBS for 1 h at room temperature, away from light, then rinsed 3 times in PBS. DAPI was used as nuclear counterstain. Skin sections were incubated with DAPI (stock solution diluted 1:1000 in PBS) during 5 min at room temperature followed by 3 rinsing cycles in PBS. Finally, skin samples were mounted using a mounting medium (Mowiol®) and a cover slip then left to dry overnight at room temperature and away from light. Glass slides were stored at -20°C until imaging. All throughout the experiment, glass slides were placed in a humid plate to prevent dryness and covered with foil when incubated with secondary antibody.

2.4. Confocal microscopy

Imaging of the immunolabelled skin sections was performed using the Leica SP8 confocal laser scanning microscope (CLSM - Leica, Germany) equipped with a HC PL APO CS2 20×/0.75 immersion objective (Leica, Germany). Microscope settings are summarized in **Table 1**.

Table 1. Settings used for confocal microscopy.

Dye	Laser Type	λ Excitation	Laser Intensity	λ Emission	Detector	Gain	Pinhole
DAPI	Diode	405 nm	3.5%	480 nm	PMT (411-474 nm)	771	46.9 µm
Alexa 488	Diode	488 nm	9.7%	520 nm	HyD (493-557 nm)	100	50.8 µm

2.5. Spironolactone nanomicellar formulations

A concentrated spironolactone nanomicellar solution was prepared at 2 mg/mL using mPEG-dihexPLA copolymer. Briefly, 10 mg SPL and 400 mg mPEG-dihexPLA were dissolved in 1.5 mL acetone. Subsequently, this solution was added dropwise using a syringe pump (6 mL/h) to 5 mL of the aqueous phase; consisting of citrate buffer (20 mM, pH 5.5), under sonication (20 % amplitude, S 450 D, Branson, USA), then acetone was removed under reduced pressure (58°C, 180 mbar). Finally, the formulation was filtered through 0.22 µm PVDF filter into a sterilized vial and kept at 5°C. In parallel, a concentrated 1.6% (w/w) Carbopol® based hydrogel was prepared by dissolving 160 mg Carbopol® Ultrez 10 in 8 g MilliQ water, containing 4 mg benzalkonium chloride as a preservative. The pH was adjusted to 5.6 by dropwise addition of sodium hydroxide (10% solution) under magnetic stirring then the weight was adjusted to 10 g with MilliQ water. Finally, 0.1% (w/v) spironolactone nanomicellar solution and hydrogel were obtained by 1:1 (w/w) dilution of the 0.2% (w/v) spironolactone nanomicellar solution with MilliQ water and 1.6% (w/w) Carbopol® hydrogel, respectively. 3 g of 0.2% (w/v) spironolactone nanomicellar solution were weighed in a beaker and were added 3 g of either MilliQ water or 1.6% (w/w) Carbopol® hydrogel then the mix was homogenized by gentle stirring using a magnetic bar to yield a final 0.1% (w/v) spironolactone nanomicellar solution or hydrogel (0.8% (w/w) Carbopol®). Finally, formulations were characterized in terms of SPL dose, incorporation efficiency, micelle size, pH and viscosity. Final composition of the different formulations is indicated in **Table 2**.

Table 2. Composition of the different spironolactone nanomicellar formulations.

Formulation	[SPL]	[Citrate Buffer]	[mPEG-dihexPLA]	[Carbopol® Ultrez 10]
0.2% SPL nanomicellar solution	2 mg/mL	20 mM	80 mg/mL	-
0.1% SPL nanomicellar solution	1 mg/mL	10 mM	40 mg/mL	-
0.1% SPL nanomicellar hydrogel	1 mg/mL	10 mM	40 mg/mL	0.8%

2.6. Viscosity measurement

Viscosity was measured using the Haake® Mars® 40 rheometer fitted with a cone-plate measuring geometry (sensor C35/2° Ti – 35 mm diameter, cone-plate angle of 2°). Rheological measurements and data processing were performed with the RheoWin software. 400 µL hydrogel was deposited in the middle of the plate then the measurement was set in the rotary mode, with a shear rate of 4.3 s^{-1} over 30 s at 20 °C.

2.7. Size determination

The number weighted (d_n), the intensity weighted (Z-average, Z_{av}) hydrodynamic diameters and the polydispersity index (PDI) of the SPL micelles were measured using a Zetasizer Nano-ZS (Malvern Instruments, UK). SPL nanomicellar solutions were diluted and homogenized in MilliQ water to a final copolymer concentration of 20 mg/mL (1:1 for 0.1% concentration and 1:3 for the 0.2% concentration) then filled into disposable plastic cuvettes for analysis with back scattering light (173 degrees). Samples were equilibrated at 25°C before the first measurement.

2.8. Morphology visualisation

Micelles were visualized using transmission electron microscope (TEM, FEI Tecnai™ G2 Sphera, Oregon, USA). Briefly, the 0.1% nanomicellar solution was diluted 1:10 in MilliQ water, then 5 µL were deposited on a grid, left for 30 s and the excess was carefully wiped. Subsequently, one drop of 2% uranyl acetate was applied during 30 s to enhance the contrast and the excess was carefully removed. TEM magnification was set at 25000x.

2.9. *Ex Vivo* skin experiments

Ex vivo skin experiments were performed using Franz diffusion cells to evaluate the skin deposition and permeation of SPL following topical application of the 0.1% spironolactone nanomicellar formulations. All the experiments were performed according to the OECD guidelines [18].

2.9.1. Spironolactone skin deposition following topical application of spironolactone nanomicelles

Fresh porcine ears were obtained from a local slaughterhouse (CARRE; Rolle, Switzerland). After cleaning under running water, excessive hair was clipped then full thickness skin was harvested from the external part of the ear using a scalpel. Subsequently, skin biopsies were harvested using a 3.2 cm diameter punch then the underlying adipose tissue was excised using

the Thomas Stadie-Riggs tissue slicer to a final thickness of 1.0 ± 0.2 mm. Samples were stored until use for maximum 3 month at -20°C.

Before use, skin samples were thawed and rehydrated in PBS (10 mM, pH 7.4) during 15 min then mounted on Franz cells and fixed with a clamp. Consequently, the donor compartment (2 cm^2 contact surface area) was filled with the 0.1% SPL nanomicellar formulations (hydrogel, n=6; or solution, n=6) and left unoccluded. The experiment was performed in both finite dose (10 mg/cm^2) and infinite dose (200 mg/cm^2) conditions. The receptor compartment was filled with 10 mL PBS (10 mM, pH 7.4) containing 1% BSA to ensure sink conditions. Franz cells were placed in a water bath maintained at 32 ± 1°C then the experiment was run for 12 h where 1 mL buffer aliquots were withdrawn and replaced from the receiving compartment, through the arm, at 2, 4, 8 and 12 h to evaluate the drug permeation.

At the end of the experiment, Franz cells were carefully dismantled then skin samples were rinsed under running water and carefully wiped with tissue (3 cycles). Subsequently, the treated area was punched out using a 1.6 cm diameter punch then samples were snap-frozen in isopentane cooled in liquid nitrogen. Samples were then cut into 40 µm thickness serial sections (CryoStar NX70 Cryostat, Thermo Scientific) from the skin surface up to 400 µm skin depth then collected into eppendorfs containing 300 µL of the extraction solvent.

2.9.2. Investigation of the penetration pathway of the spironolactone nanomicelles

To evaluate the follicular delivery of SPL nanomicelles, another skin deposition experiment was performed as described above, then the deposition of SPL in skin samples containing the pilosebaceous unit (PSU) was quantified and compared to control samples, without the PSU (PSU-free). Briefly, porcine skin samples were prepared as described above except that samples were kept at full thickness to preserve the PSU integrity. Indeed, the hair follicle takes origin in the deepest dermis, sometimes even in the subcutaneous tissue with the hair bulb, then elongates through the dermis and the epidermis up to the skin surface with the hair shaft. Skin samples were placed in Franz cells then 0.1% SPL nanomicellar hydrogel (n=6) or solution (n=6) were applied on the skin in both infinite and finite dose conditions for each formulation. The experiment was run in the same conditions as above. After the 12 h experiment, skin samples were cleaned as mentioned above then skin biopsies containing the pilosebaceous unit (PSU, n=15) and control skin biopsies (PSU-free, n=15) were harvested using a 1 mm diameter punch and placed in eppendorfs containing 100 µL of the extraction solvent.

2.10. Extraction procedure

Skin slices, PSU and PSU-free skin samples obtained from the deposition studies above were placed in eppendorfs containing methanol:water (8:2) as extraction solvent and 100 ng/mL 17α-methyltestosterone as internal standard. Eppendorfs were then placed a shaking bath (150 min^{-1}) and left for extraction overnight at room temperature. The following day, samples were centrifuged (5000 rpm, 10 min) then the supernatant were quantified using the UHPLC-MS method. Validation of the extraction procedure is provided in the SI.

2.11. Statistical analysis

Statistics were calculated using SigmaPlot software. Results were statistically analysed using either *Student's t-test* or Mann-Whitney rank sum test. Data were expressed as the Mean ± SD. The level of significance was fixed at $\alpha=0.05$.

3. Results

3.1. Mineralocorticoid receptor labelling in the skin

The results of the immunofluorescence labelling confirmed the presence of MR in the porcine skin. MR was shown to be mainly located in the skin appendages with a high predominance in the hair follicles and in the epithelial cells of the eccrine sweat glands (**Figure 1**). The longitudinal sections of the hair follicles showed the presence of the MR in the hair bulb and in the inner and outer root sheaths. The outer root sheath is a stratified epithelium that is contiguous with the epidermis. Immunofluorescence was also detected in the epidermis and the dermis but with lower intensity compared to the hair follicle and sweat glands. In the dermis, the immunofluorescence signal may correspond to the MR localized in the endothelium of the vascular capillaries.

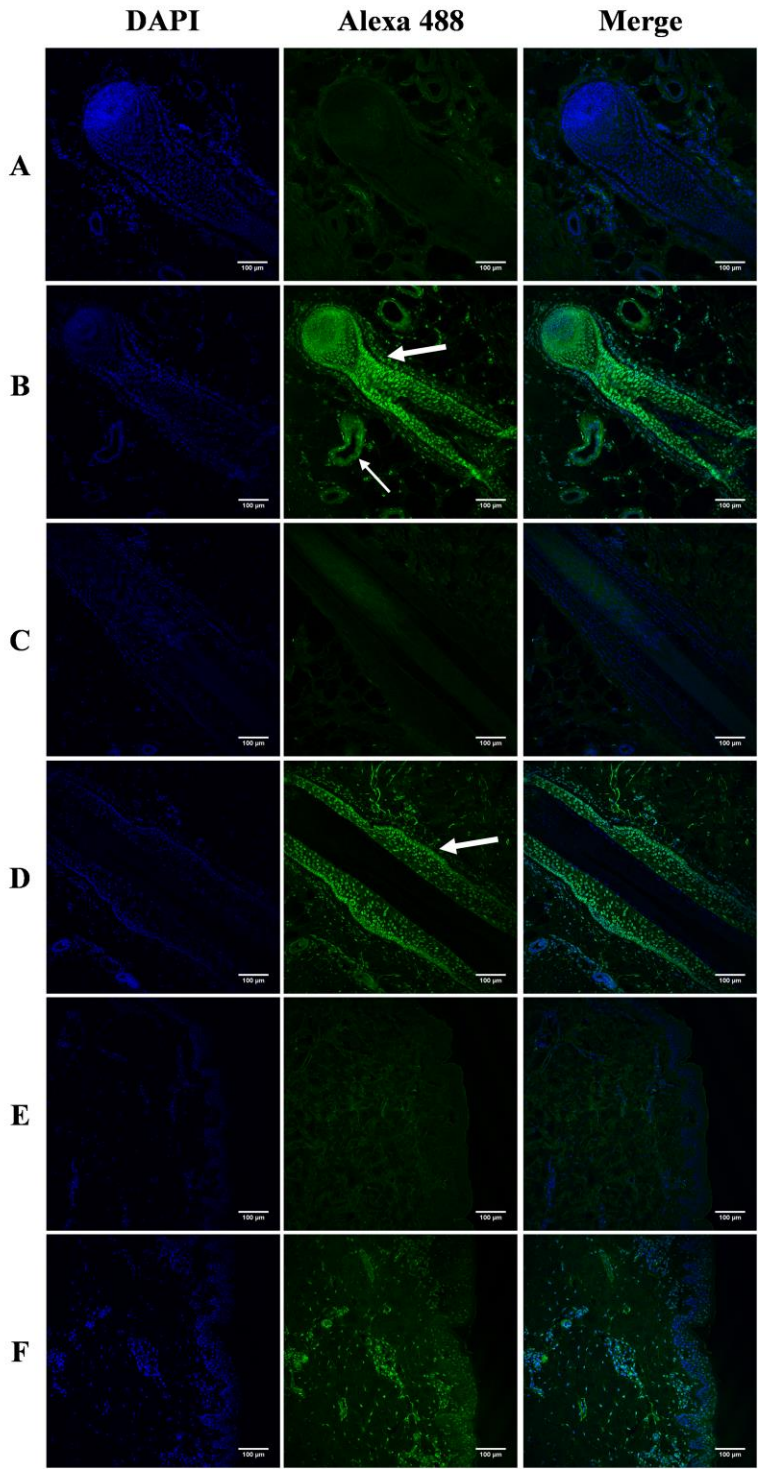

Figure 1. Localization of the mineralocorticoid receptor in porcine skin. A and B, longitudinal sections of the hair follicle with the hair bulb located in the deeper dermis. C and D, longitudinal sections of the hair follicle located in the mid-dermis. E and F, longitudinal sections of full thickness porcine skin. A, C and E, porcine skin incubated with Alexa 488 (control); B, D and F, porcine skin incubated with the MR antibody and Alexa 488. Thick arrows show the hair follicle; thin arrows show the eccrine sweat gland. Images obtained by CLSM (Leica SP8) under 20× objective lens.

3.2. Spironolactone nanomicellar formulations

Spironolactone was efficiently encapsulated in the mPEG-dihexPLA nanomicelles at 2.00 ± 0.11 mg/mL with 100.15 ± 0.11% incorporation efficiency. After 1:1 (w/w) dilution in MilliQ water, SPL concentration was found to be 0.96 ± 0.03 mg/mL. Importantly, nanomicelles size after dilution remained identical to the size found with the concentrated solution which was in the range of 20 nm (**Table 3**). TEM showed the spherical shape of the nanomicelles (**Figure 2**).

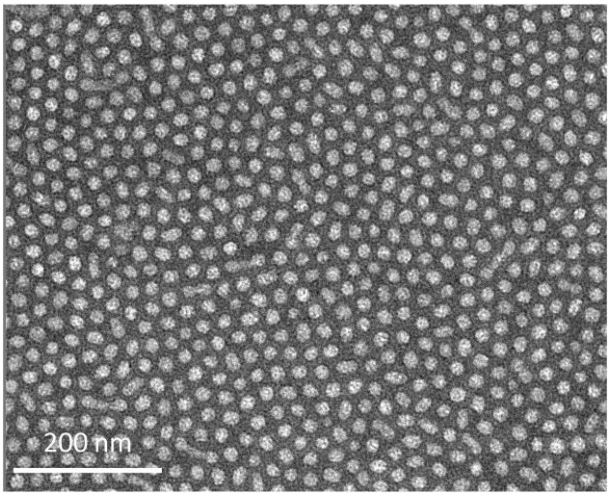

Figure 2. Morphology of 0.1% spironolactone nanomicelles. Mean size of 20 nm.

Dilution of the 0.2% spironolactone nanomicellar solution 1:1 (w/w) in the concentrated 1.6% Carbopol® hydrogel yield to the formation of a composite hydrogel with a final Carbopol® concentration of 0.8%. The unloaded hydrogel was transparent, SPL loaded nanomicellar solution and hydrogel were slightly turbid due to the colloidal suspension formed by the nanomicelles (see SI). The viscosity of the concentrated 1.6% Carbopol® hydrogel was 70 Pa. s, once diluted with the concentrated nanomicellar solution, the viscosity drops to 20 Pa. s which is suitable for topical application. Indeed, the hydrogel is easily spreadable on the skin and evaporate quickly without leaving any sticky residue. pH of the hydrogels remained identical before and after dilution and was 5.6 which is optimal for skin application. SPL concentration in the 0.1% SPL nanomicellar hydrogel was found to be 0.98 ± 0.01 mg/mL. The integrity of the SPL nanomicelles following mixing with the concentrated 1.6% Carbopol® hydrogel was assessed using Nile Red-loaded nanomicelles (see SI).

All the formulations were stable in terms of concentration, pH, viscosity and micelles size for at least 1 month at 5°C (see SI). All formulations characteristics are summarized in **Table 3**.

Table 3. Characteristics of the formulations.

Formulation	[SPL] (mg/mL)	pH	Viscosity (Pa. s)	d_n (nm)	Z_{av} (nm)	PDI
0.2% SPL nanomicellar solution	2.00 ± 0.11	5.5	-	21	43	0.2
0.1% SPL nanomicellar solution	0.96 ± 0.03	5.7	-	21	43	0.2
0.1% SPL nanomicellar hydrogel	0.98 ± 0.01	5.6	20	21*	43*	-

*: Extrapolated size of the nanomicelles from the solution to the hydrogel based on the integrity test performed using Nile Red-loaded nanomicelles (see SI).

3.3. Spironolactone skin deposition and biodistribution

Ex vivo skin topical application of 0.1% SPL nanomicellar formulations during 12 h resulted in the deposition of therapeutic amounts of SPL in the epidermis and the upper dermis (up to 400 µm) in both infinite and finite dose conditions (**Figure 3**).

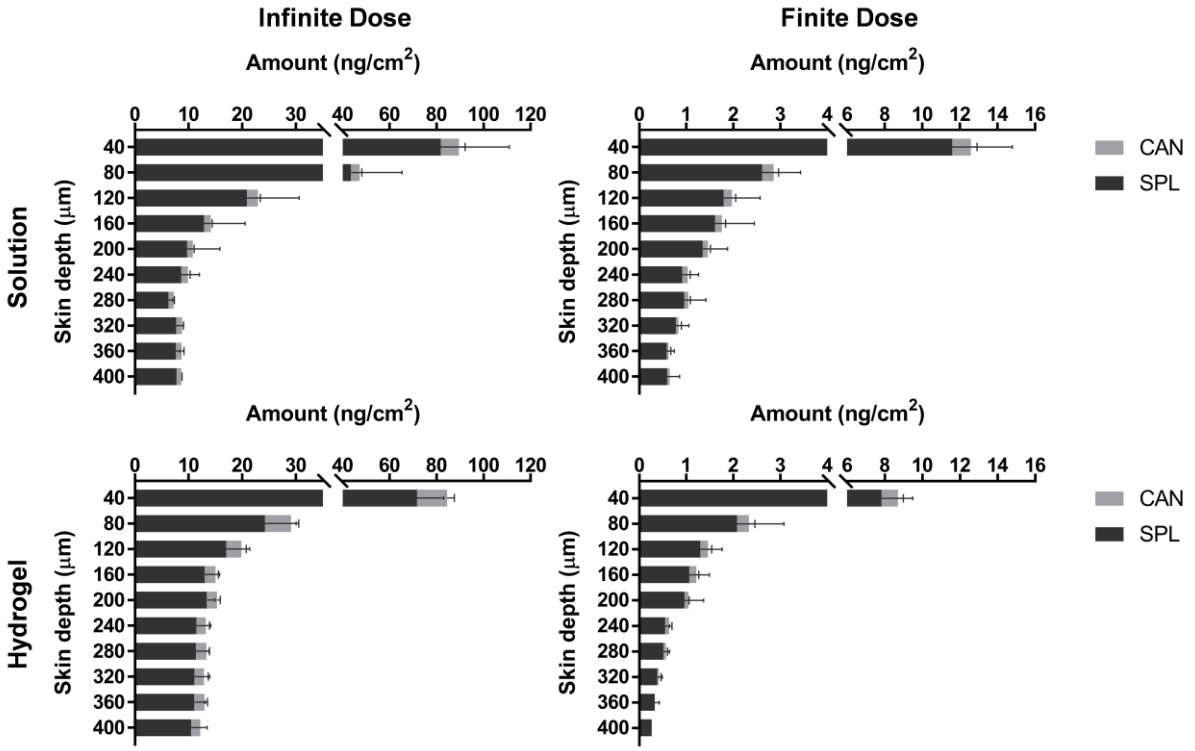

Figure 3. Spironolactone and canrenone amounts deposited in the epidermis and the upper dermis of porcine skin following topical application of 0.1% spironolactone nanomicellar solution and hydrogel in infinite and finite dose conditions. CAN, canrenone, SPL, spironolactone. Narrow head error bars, standard deviation of spironolactone amounts; large head error bars, standard deviation of canrenone amounts.

Regardless the formulation form and the amount applied, we can note the identical biodistribution profile with higher concentration at the surface of the skin and a gradual decrease in the amount delivered along the skin depth (**Figure 3**). We can also note the 10-fold decrease in the amount of SPL delivered to the skin when we compare infinite *versus* finite dose. This may be explained by the 20-fold decrease in the amount of the formulation applied to the skin surface between infinite and finite dose (200 mg/cm^2 *vs.* 10 mg/cm^2).

Interestingly, *ex vivo* topical application of 0.1% SPL nanomicellar formulations to porcine skin resulted in the formation of the metabolite canrenone, however the other active metabolite, 7α-thiomethylspironolactone was not detected **(Figure 3**).

Comparison of the delivery efficiency of SPL to the skin achieved with both 0.1% SPL nanomicellar hydrogel and solution showed no significant difference between the amounts of SPL found in the epidermis (up to 160 µm skin depth) following topical application in both infinite (125.86 ± 21.84 *vs.* 159.04 ± 57.77 ng/cm^2, respectively) and finite (12.26 ± 3.22 *vs.* 17.62 ± 5.03 ng/cm^2, respectively) doses. However, in the upper dermis (160-400 µm skin depth), the hydrogel delivered significantly higher amounts compared to the solution in infinite dose conditions (68.74 ± 13.02 *vs.* 47.68 ± 11.23 ng/cm^2, respectively; $p<0.001$). In the contrary, the solution delivered significantly higher amounts of SPL to the upper dermis compared to the hydrogel in finite dose conditions (5.17 ± 1.81 *vs.* 3.01 ± 0.76 ng/cm^2, respectively; $p=0.042$).

Comparison of the amounts of CAN formed in the skin following topical application of the 0.1% SPL nanomicelles showed no significant difference between the solution and hydrogel except in the upper dermis with infinite dose conditions (11.04 ± 3.71 *vs.* 6.39 ± 1.33 ng/cm^2, respectively; $p<0.001$) which is expected given the higher amounts of SPL found in the upper dermis after application of the 0.1% SPL nanomicellar hydrogel in infinite dose compared to the solution.

Quantification of the receiver compartment showed no drug permeation through the skin after 12 h topical application of the 0.1% SPL micellar formulations at finite dose which mimics the real use conditions. However, application of 0.1% SPL micellar solution and hydrogel to porcine skin at infinite dose led to the permeation of 354.57 ± 79.18 and 443.98 ± 134.23 ng/cm^2, respectively, after 12 h skin exposure to the formulations. CAN was also detected in the receiver compartment after 12 h topical application of 0.1% SPL micellar solution and hydrogel, at 15.49 ± 3.52 and 20.24 ± 6.42 ng/cm^2, respectively.

3.4. Spironolactone follicular deposition

Figure 4 shows typical skin biopsies obtained by punching out the pilosebaceous unit (PSU) and the PSU-free samples following topical application of the 0.1% SPL nanomicellar formulations.

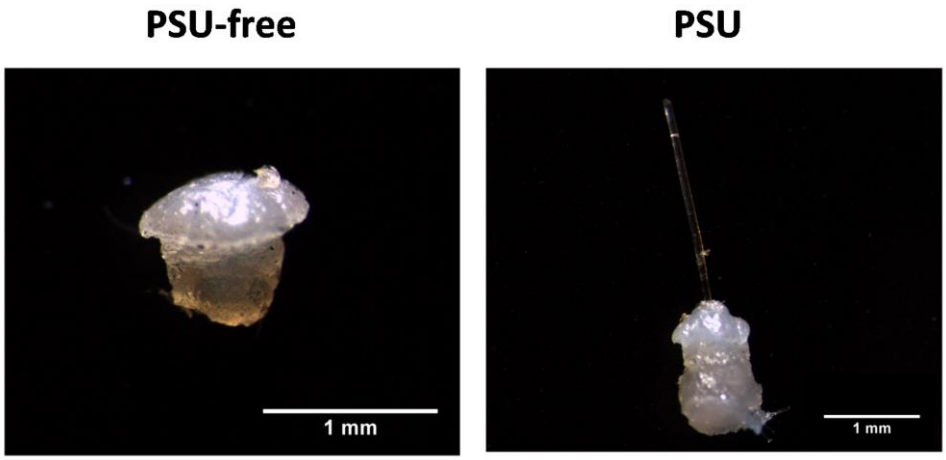

Figure 4. Typical skin biopsies obtained after punching out the pilosebaceous unit (PSU) and skin samples without the PSU (PSU-free).

Comparison between the amounts of SPL deposited in the skin samples containing or not the PSU showed significantly higher amounts of SPL found in the PSU-containing skin samples following topical application of the 0.1% SPL nanomicellar hydrogel and solution, in both infinite and finite dose conditions (**Figure 5**).

The amounts of SPL deposited in the PSU skin samples were 3-folds higher than the PSU-free skin samples after topical application of the 0.1% SPL nanomicellar solution at both infinite (4.97 ± 1.20 *vs.* 1.56 ± 0.45 ng/mm^2, respectively; $p<0.001$) and finite (0.72 ± 0.21 *vs.* 0.24 ± 0.06 ng/mm^2, respectively; $p<0.001$) dose conditions. This difference was even 5-folds higher after topical application of the 0.1% SPL nanomicellar hydrogel at both infinite (3.67 ± 0.82 *vs.* 0.70 ± 0.26 ng/mm^2, respectively; $p<0.001$) and finite (0.54 ± 0.18 *vs.* 0.10 ± 0.03 ng/mm^2, respectively; $p<0.001$) dose conditions (**Figure 5**).

CAN amounts found in the PSU skin samples were 2-folds higher compared to the PSU-free skin samples after topical application of 0.1% SPL micellar solution at infinite (0.73 ± 0.15 *vs.* 0.45 ± 0.11 ng/mm^2, respectively; $p<0.001$) and finite (0.13 ± 0.05 *vs.* 0.06 ± 0.02 ng/mm^2, respectively; $p<0.001$) doses. Topical application of the 0.1% SPL micellar hydrogel also led to 2-fold higher CAN amounts found in the PSU skin samples compared to the PSU-free skin samples at infinite (0.51 ± 0.10 *vs.* 0.28 ± 0.10 ng/mm^2, respectively; $p<0.001$) and finite (0.10 ± 0.03 *vs.* 0.05 ± 0.02 ng/mm^2, respectively; $p<0.001$) doses (**Figure 5**).

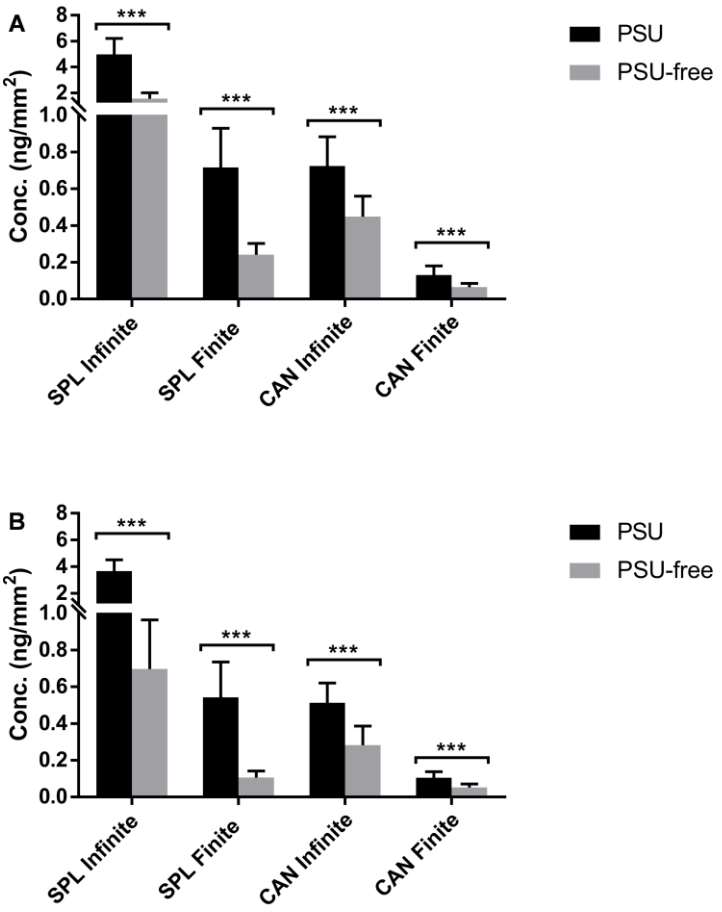

Figure 5. Spironolactone (SPL) and canrenone (CAN) deposition in the pilosebaceous unit (PSU) and the PSU-free skin biopsies following topical application of A, 0.1% SPL nanomicellar solution; B, 0.1% SPL nanomicellar hydrogel in both infinite and finite dose conditions. ***, $p<0.001$.

4. Discussion

4.1. Localization of the mineralocorticoid receptor in the skin

Despite our extensive research, we could only find one study localizing the MR in the skin [19]. In contrast, many recent studies have reported the emerging roles of the MR in the skin physiology and importantly in the cutaneous wound healing. Hence, and in the frame of our project leading to develop SPL formulation to target the MR in the skin, we needed to first identify our target within the skin to better design the drug delivery system.

This is the first study demonstrating the presence and the localization of the MR in porcine skin using immunofluorescence labelling. Indeed, Kenouch *et al.* assessed the presence of the MR in human skin using *in situ* hybridization and immunohistochemistry [19]. Their findings were consistent with our results since they also have reported the localisation of the MR in the hair

follicle (HF) and the sweat glands (SwG). They also reported the presence of the MR in the sebaceous glands (SbG) and the epidermis, which was not obvious in our results. Our findings show that MR is predominantly expressed in the HF and the SwG.

The presence of MR in the sweat glands is not surprising since MR and aldosterone regulate fluid secretion and electrolyte homeostasis through activation of the Na^+-K^+-ATPase during the sudation process [20, 21]. MR was found to be exactly located in the epithelial cells of the eccrine sweat glands.

Our results showing the predominant localization of the MR in the HF presents a great advantage for us in terms of formulation development and targeted drug delivery. Indeed, we have previously established the penetration pathway of the mPEG-dihexPLA nanomicelles following topical application to the skin using both qualitative and quantitative techniques. First, visualization of skin samples using a CLSM following topical application of Nile Red-labelled mPEG-dihexPLA micelles showed a preferential accumulation of the NR-labelled copolymer around the hair follicle [7]. Second, this was also verified quantitatively by comparing the amounts of the drug delivered to the PSU-containing *versus* PSU-free skin samples using UHPLC-MSMS analytical methods which showed a 2-fold higher delivery to the PSU-containing skin samples [10]. These findings consolidate our strategy of using mPEG-dihexPLA nanomicelles as carriers to deliver SPL to the skin.

4.2. SPL delivery to the epidermis and the upper dermis following topical application of the nanomicelles

The biodistribution study showed that the viscosity of the formulation does not affect the deposition efficiency to the epidermis layer of the skin. Albeit, the hydrogel was significantly more efficient ($p<0.001$) in the delivery to the upper dermis in infinite dose and the solution was significantly more efficient ($p<0.05$) in delivery to the upper dermis in finite dose.

Regardless of the delivery efficiency, both the solution and the hydrogel allow the delivery of therapeutic amounts of SPL up to 400 µm skin depth and to the PSU and PSU-free skin samples after application of both finite and infinite doses of 0.1% SPL micelles. However, given the higher amounts found in the PSU, we suppose that the therapeutic effect will be mostly exerted in the PSU. Spironolactone IC_{50} is reported to be around 2 nM in the muscle; [22-24] the biodistribution study showed that the nanomicelles could deliver spironolactone to the upper dermis up to 150-folds higher amounts than the IC_{50} with the micellar hydrogel and up to 250-folds higher amounts with the micellar solution, even in finite dose conditions.

Moreover, the metabolite CAN also contribute to the antagonism of the MR and was detected up to 400 µm skin depth and in the PSU and PSU-free skin samples. Interestingly, and unlike our findings following *in vivo* topical application of the 0.1% SPL nanomicelles to rabbit cornea, 7α-thiomethylspironolactone (TMSPL) was not detected in porcine skin following *ex vivo* topical application of 0.1% SPL nanomicelles [12]. This may be due to local organ physiological variability, such as enzymes expression (esterases, S-methyltransferases), between the cornea and the skin resulting in difference in the metabolization of SPL. Also, 0.1% SPL nanomicelles were instilled up to 6 six times daily during 5 days to the right eye of the rabbits, hence, TMSPL may be occurring only following multiple dosing. Finally, the difference in SPL metabolism may be due to the different conditions (*ex vivo vs. in vivo)* and the different models used (pig *vs.* rabbit). TMSPL and CAN are both active metabolites of SPL. Recent studies reported that TMSPL is the main active metabolite of SPL contrasting what was previously thought which was due to the use of non-specific analytical methods leading to confusing CAN and the other thiol-containing metabolites [25]. Metabolization of SPL occurs first via deacetylation catalysed by esterases forming the 7α-thiospironolactone (TSPL) intermediate metabolite. TSPL then undergoes S-methylation catalysed by the thio-methyltranserase (TMT) forming 7α-thiomethylspironolactone [26]. Some studies reported that canrenone is formed via sulfoxide elimination of the thioester S-oxide group from 7α-thiomethylspironolactone S-oxide via non-enzymatic pathway leading to removal of the sulfur moiety [27]. Weather TMSPL could be detected only *in vivo* remains to be investigated.

SPL is unlikely to reach to systemic circulation *in vivo* following topical application to the skin since SPL did not permeate to the receiving chamber in finite dose conditions. The permeation observed with infinite dose conditions may be explained by the combination of the high amounts applied and the thickness of the skin used. Indeed, for the biodistribution study, the skin used was sliced to ~800 µm thickness. At this thickness the subcutaneous tissue and part of the dermis is removed, and as we have already mentioned, the hair follicle penetrates the skin even down to the subcutaneous tissue. Hence, the process of slicing may have altered the integrity of the PSU by cutting the hair follicle resulting in the formation of a canal communicating between the donor and the receiver compartments. As we have demonstrated that the nanomicelles were mainly accumulating in the PSU, probably forming a depot in the canal of the HF, therefore we can easily imagine the nanomicelles flowing through this canal especially after topical application of infinite dose of the 0.1% SPL nanomicelles.

4.3. Targeted follicular delivery of SPL nanomicelles

0.1% SPL nanomicelles have shown to preferentially target the hair follicle with up to 5-folds higher amounts of SPL delivered to the PSU compared to the PSU-free skin biopsies. These finding are in accordance with our previous studies where topical application of retinoic acid mPEG-dihexPLA based nanomicelles showed a 2-folds higher delivery to the PSU compared to the PSU-free skin samples, and adapalene TPGS based nanomicelles showed up to 4.5-folds higher delivery to the PSU compared to the PSU-free skin samples [7, 10, 16].

The solution delivered 1.3-folds higher amounts of SPL to the PSU compared to the hydrogel in both infinite (4.97 ± 1.20 *vs.* 3.67 ± 0.82 ng/mm^2, respectively; p=0.001) and finite (0.72 ± 0.21 *vs.* 0.54 ± 0.18 ng/mm^2, respectively; p=0.001) doses. This may be explained by the different rheological behaviour of both forms with the solution having more facility to penetrate and flow through the follicular duct compared to the more viscous hydrogel. Nevertheless, both forms allowed the delivery of therapeutic amounts of SPL to the target site, i.e. the MR located in the hair follicle.

4.4. The transfollicular drug delivery route

Transfollicular administration route has been recently the object of many studies, especially with the advent of nanotechnologies as topical drug delivery. Transfollicular delivery has many advantages. First, in terms of site-specific drug delivery to target the pilosebaceous unit-associated disorders such as acne vulgaris, alopecia areata and hirsutism, providing a higher therapeutic efficacy and minimizing the side effects due to systemic exposure. Second, by providing a penetration shunt pathway and a shortcut to circumvent to the stratum corneum barrier and improving the drug bioavaibility in the epidermis and dermis following topical application [28-30].

Indeed, the hair follicle is an invagination and a continuity of the epidermis extending deep into the dermis, providing a larger contact area of the skin available for drug permeation. Moreover, the stratum corneum lining the infundibular part of the hair follicle (the upper part) is more permeable to substances allowing to bypass the cutaneous stratum corneum which plays the role of skin barrier [28-30].

Moreover, many studies reported that after topical application of particulate formulations, substances penetrate through the HF orifice, accumulate in the HF duct and form a reservoir that may act as sustained release and provide a continuous diffusion of the substances to the

follicular and the perifollicular cells and even reach the viable skin strata by lateral diffusion [28, 30, 31].

4.5. Promising clinical applications of the transfollicular delivery of SPL nanomicelles

The pilosebaceous unit is considered as the endocrine organ of the skin as it expresses different steroid receptors and synthetizes various hormones. Indeed, all the steroid receptors have been found expressed in the skin including androgen, estrogen, progesterone, glucocorticoid and mineralocorticoid receptors. This makes it an interesting target for the treatment of the numerous hormones-related skin and hair conditions including acne vulgaris, seborrhea, androgenic alopecia and hirsutism [32-36].

Another established target of spironolactone with therapeutic efficacy is the androgen receptor which is also located in the PSU, mainly in the sebocytes of the sebaceous gland and the dermal papilla of the hair follicle [37]. Androgens mediate sebocyte proliferation, sebum production and hair growth; their excess results in various skin and hair conditions such as acne vulgaris, seborrhea, androgenic alopecia and hirsutism [38].

In most of the patients suffering from androgen-related skin and hair conditions, the circulating androgen levels were found to be normal. The cutaneous hyperandrogenism characterizing these skin and hair diseases is reported to be due to *in situ* overexpression of the androgenic enzymes such as 5α-dihydrotestosterone (5α-DHT) and the hyperresponsiveness of the androgen receptor (AR). Hence, the importance of developing a local and site-specific drug delivery system for the treatment of these diseases for better efficacy and safety [39].

Acne is mostly due to excess of sebum production by the sebaceous glands through androgen stimulation, mainly by 5α-dihydrotestosterone, the potent reduced form of testosterone catalysed by 5α-reductase present in the skin. SPL, with its anti-androgenic activity, competitively inhibits 5α-DHT from binding to the androgen receptor thus decreasing sebum production. Several studies have reported the efficacy of the use of SPL to treat acne in patients [15, 39-44].

Hirsutism is the presence of excessive hair growth affecting mostly women and is most often caused by increased production of androgens. Hence, oral SPL was also used to treat hirsutism and significantly showed decreased hair growth [14, 45].

Androgenic alopecia, characterized by hair loss and affects mostly men, is also due to excessive production of androgens. SPL was used to treat androgenic alopecia and results showed

decreasing androgen production within the sebaceous glands and blocking the androgen receptor in dermal papillae [45-47].

In addition to these potential clinical applications, transfollicular delivery may be exploited to target the stem cells located in the bulge region of the HF which could provide opportunities for the treatment of wound healing and inflammatory skin diseases [29-31].

Finally, in addition to the site-specific management of MR-mediated cutaneous wound healing, 0.1% SPL nanomicelles may be used for the treatment of AR-mediated skin diseases.

5. Conclusion

We have successfully developed 0.1% spironolactone nanomicellar formulations for topical application to the skin that enable the delivery of therapeutic amounts of spironolactone to the epidermis and the upper dermis. Our results showed a transfollicular delivery of SPL nanomicelles allowing the site-specific targeting of the mineralocorticoid receptor located, as we have demonstrated, in the hair follicle and hence offset the glucocorticoid off-target agonism of the mineralocorticoid receptor responsible of the cutaneous delayed wound healing. These findings may be of considerable clinical relevance since patients may benefit from a co-administration of 0.1% spironolactone nanomicelles to manage glucocorticoid-induced side effects on wound healing and still benefit from the anti-inflammatory effects of the glucocorticoids. Our results showed the *ex vivo* metabolism of spironolactone to canrenone following topical application of 0.1% spironolactone micelles to porcine skin. Interestingly, the other active metabolite of spironolactone, 7α-thiomethylspironolactone, was not detected, contrasting our findings following *in vivo* topical application of 0.1% spironolactone micelles to rabbit cornea in a corneal wound healing model. *In vivo* application of this formulation in a cutaneous wound healing model may help understand this variability. Finally, the targeted transfollicular delivery of the 0.1% spironolactone nanomicellar formulations may be extended to other clinical applications such as androgen-mediated skin and hair diseases including acne vulgaris, androgenic alopecia and hirsutism.

6. Supporting information

6.1. Validation of the UHPLC-UV analytical method

The UHPLC-UV analytical method was developed to support the development of spironolactone (SPL) formulations and follow their stability. This method was validated according to the ICH guidelines.

6.1.1. Linearity

Calibration standards of SPL were prepared in methanol:water (1:1) mixture at 0.1, 0.2, 0.5, 1, 2, 5, and 10 µg/mL. Calibration curves were constructed by plotting the area of each analyte versus the concentration of each analyte (**Figure S1**).

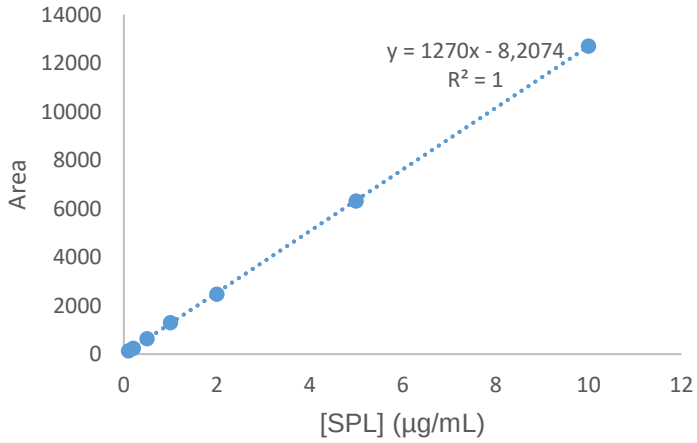

Figure S1. Calibration curve of spironolactone in methanol:water (1:1) mixture.

6.1.2. Limit of determination - Limit of quantification

Limit of detection (LOD), the lowest concentration of SPL that could be detected in a sample, was calculated using the following equation:

$$\mathrm{LOD} = 3\,\frac{\mathrm{SD}}{\mathrm{S}}$$

where SD is the standard deviation of the response based on the standard deviation of the y-intercept of the regression line and S is the slope of the calibration curve.

Limit of quantification (LOQ), the lowest concentration of SPL that could be quantified in a sample, was calculated using the following equation:

$$\mathrm{LOQ} = 10\,\frac{\mathrm{SD}}{\mathrm{S}}$$

SD and S are the same as described for calculation of the LOD.

Method characteristics are summarized in **Table S1**.

Table S1. UHPLC-UV method characteristics for spironolactone detection and quantification.

	SPL
Range (µg/mL)	0.1 – 10.0
R	1
LOD (µg/mL)	0.1
LOQ (µg/mL)	0.2

6.2.Validation of the UHPLC-MS bioanalytical method for skin application

A UHPLC-MS bioanalytical method for the quantification of spironolactone (SPL) and its metabolites – 7α-thiomethyspironolactone (TMSPL) and canrenone (CAN) – was previously developed and validated for ocular applications. The suitability of this method for skin application was validated in terms of specificity and linearity of the signal as a function of analyte concentration in porcine skin matrix. This method was validated according to the FDA guidelines. The lower limit of quantification (LLOQ) of the different analytes in the skin matrix was also determined.

6.2.1. Skin matrix

Porcine skin was harvested from the external surface of porcine ears obtained immediately after sacrifice of the animals at a local slaughterhouse. Skin samples with an area of 2 cm^2 were punched out (1.6 cm diameter punch), rinsed in phosphate buffered saline (PBS) then cut into small pieces and placed in a vial containing 4 mL MeOH:H_2O (8:2) and left for extraction overnight under agitation at room temperature. The following day, samples were centrifuged at 4 000 rpm for 20 minutes and the supernatants were collected, pooled to be used for the preparation of standard calibration curves.

6.2.2. Specificity

The specificity of the method was verified with regards to possible interferences between the endogenous component of porcine skin and the analytes. **Figure S2** and **Figure S3** show that the endogenous peaks of porcine skin matrix are clearly separated from the peaks of the different analytes.

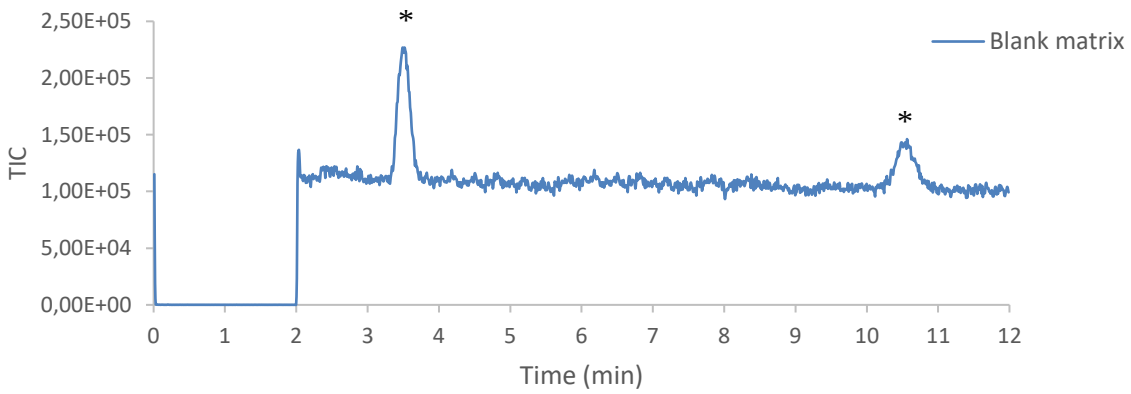

Figure S2. Typical chromatogram of blank porcine skin matrix. *, endogenous peaks of porcine skin matrix.

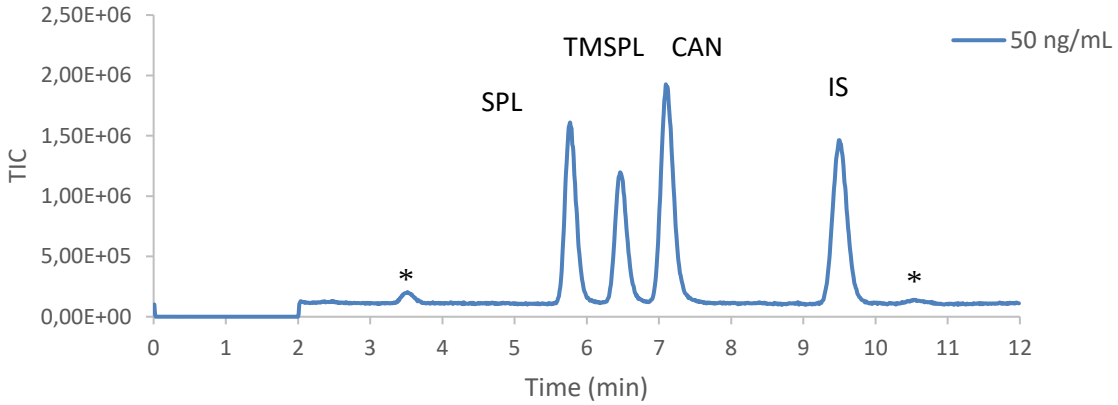

Figure S3. Typical chromatogram of porcine skin matrix spiked with a mixture of spironolactone (SPL), 7α-thiomethylspironolactone (TMSPL) and canrenone (CAN) at 50 ng/mL. IS, internal standard. *, endogenous peaks of porcine skin matrix.

6.2.3. Linearity in skin matrix

Calibration standards containing SPL, TMSPL and CAN were prepared in skin matrix at 5, 10, 20, 50, 200, 500 and 1000 ng/mL. The internal standard 17α-methyltestosterone (IS) was added to each calibration standard at 100 ng/mL. Calibration curves were constructed by plotting the ratio of the area of each analyte to the area of the internal standard versus the ratio of the concentration of each analyte to the concentration of the internal standard (**Figures S4-S6**). All the calibration curves were linear ($R > 0.99$).

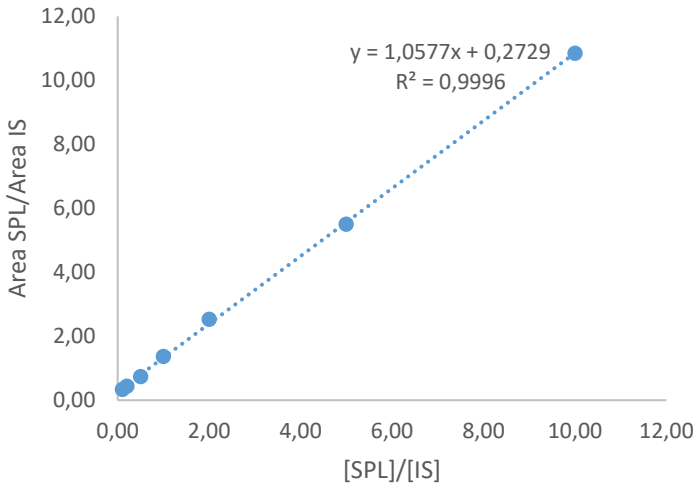

Figure S4. Calibration curve of spironolactone in porcine skin matrix

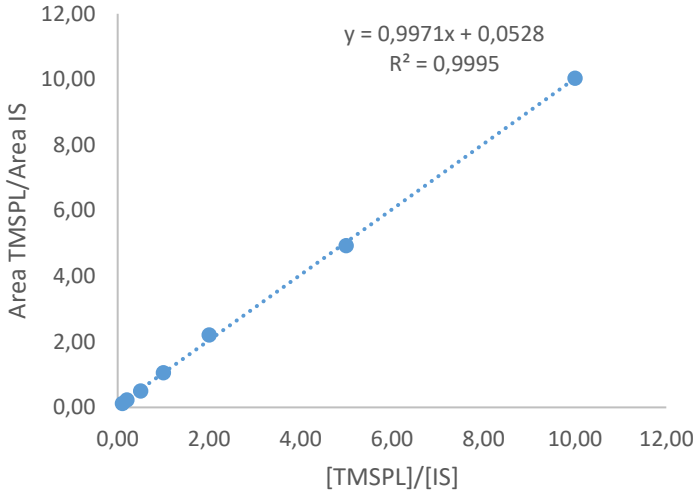

Figure S5. Calibration curve of 7α-thiomethylspironolactone in porcine skin matrix.

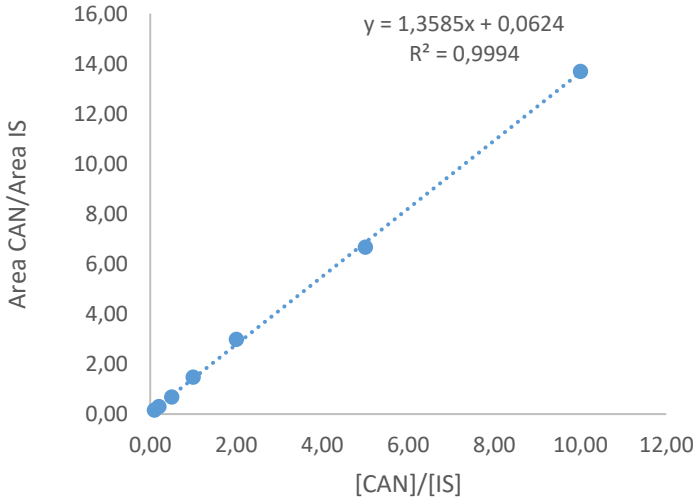

Figure S6. Calibration curve of canrenone in porcine skin matrix.

6.2.4. Lower Limit of quantification

The lower limit of quantification (LLOQ) was determined by calculating the signal-to-noise ratio for each analyte and assessing at least five times higher area obtained with the lowest calibration standard (5 ng/mL, n=5) when compared to a blank sample consisting of a blank skin matrix. The LLOQ of each analyte was found to be 5 ng/mL. UHPLC-MS Method characteristics are summarized in **Table S2**.

Table S2. UHPLC-MS method characteristics for the detection and quantification of spironolactone (SPL), 7α-thiomethyspironolactone (TMSPL) and canrenone (CAN).

	SPL	TMSPL	CAN
Range (ng/mL)	5 - 1000	5 - 1000	5 - 1000
R	0.9998	0.9997	0.9997
LLOQ (ng/mL)	5	5	5

6.3.Extraction method

The extraction procedure was validated using porcine skin (n=3) spiked with different amounts of SPL, TMSPL and CAN. 20 µL of a mixture containing SPL, TMSPL and CAN at either 10, 40 or 100 µg/mL in acetone was applied to the skin and left to evaporate (i.e. resulting in deposition of 0.2, 0.8 or 2 µg of each API on the skin surface). Acetone is a lipid solvent which partially lyses the epithelium of the skin allowing the compounds to spread in the tissue. After acetone evaporation, skin samples were cut into small pieces, placed in vials containing 4 mL MeOH:H_2O (8:2) and 100 ng/mL IS (MeT) then left for extraction overnight at room temperature under agitation. The following day, samples were centrifuged at 8 000 rpm for 20 minutes and the supernatants collected for analysis. The extraction efficiency (expressed as a percentage recovery, **Table S3**) was estimated by calculating the recovered amount to the spiked amount as displayed in the following equation:

$$\%\ \text{Extraction Efficiency} = \frac{\text{Recovered Amount}}{\text{Spiked Amount}} \times 100\%$$

Table S3. Extraction efficiencies for SPL, TMSPL and CAN from porcine skin.

Spiked amount (µg)	Recovered amount (µg) ± SD and % recovery ± SD					
	SPL	%	TMSPL	%	CAN	%
0.2	0.22±0.02	110.5±11.1	0.23±0.02	115.4±8.2	0.19±0.01	95.5±4.1
0.8	0.81±0.04	101.0±4.5	0.74±0.05	92.7±6.0	0.82±0.01	102.0±1.2
2	2.09±0.10	104.6±4.8	1.99±0.09	99.3±4.3	2.02±0.02	100.9±0.8

6.4.Stability of spironolactone nanomicellar formulations

6.4.1. 0.1% SPL nanomicellar formulations

0.1% SPL micellar formulations (**Figure S7**) met the requirement for a dermatological application in terms of pH and viscosity and were stable for at least one month at 5°C (**Table S4**).

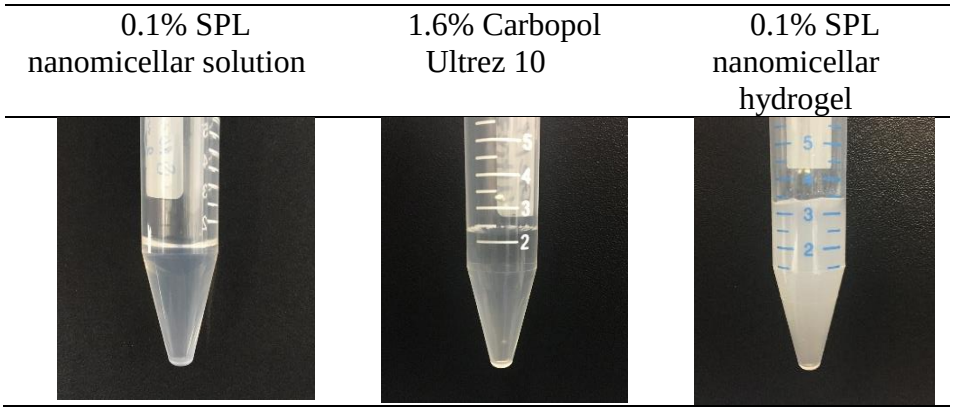

Figure S7. Visual aspect of the different formulations.

Table S4. Characterization and stability of the 0.1% spironolactone nanomicellar formulations.

	0.1% SPL nanomicellar solution		0.1% SPL nanomicellar hydrogel	
	T=0	T4 weeks	T=0	T4 weeks
Concentration (mg/mL)	0.96	0.92	0.98	0.94
pH	5.7	5.6	5.6	5.6
Micelle size (nm)	21	19	~20*	~20*
Viscosity (Pa.s)	-	-	20	21

* nanomicelles size was not directly measured in the hydrogel.

To assesse the stability of the nanomicelles upon dilution in the hydrogel, we have incorporated Nile Red in mPEG-dihexPLA nanomicelles and assesses visually their stability by following the color of the hydrogel and the precipitation of Nile Red.

Briefly, 70 µg Nile Red and 50 mg mPEG-dihexPLA were dissolved in 1.5 mL acetone. Subsequently, this solution was added dropwise using a syringe pump (6 mL/h) to 5 mL of the aqueous phase; consisting of citrate buffer (34 mM, pH 5.5), under sonication (20 % amplitude, S 450 D, Branson, USA), then acetone was removed under reduced pressure (58°C, 180 mbar). Finally, the formulation was filtered through 0.22 µm PVDF filter into a sterilized vial. In parallel, a concentrated 1% (w/w) Carbopol® based hydrogel was prepared by dissolving 100 mg Carbopol® Ultrez 10 in 8 g MilliQ water, containing 4 mg benzalkonium chloride as a preservative. The pH was adjusted to 5.5 by dropwise addition of sodium hydroxide (10%

solution) under magnetic stirring then the weight was adjusted to 10 g with MilliQ water. Finally, Nile Red nanomicellar hydrogel was prepared by mixing 1:1 (w/w) the concentrated Nile Red nanomicelles with the concentrated hydrogel.

Nile Red loaded nanomicelles showed stability for at least 1 year at 5°C, suggesting that mPEG-dihexPLA nanomicelles remain stable upon dilution in the Carbopol® hydrogel (**Figure S8**).

Figure S8. Aspect of the Nile Red nanomicellar hydrogel.

Acknowledgements

ND and YNK acknowledge financial support from the Swiss Commission for Technology and Innovation (CTI Project 19086.1 PFLS-LS) and Apidel SA (Geneva, Switzerland). YNK would like to thank the University of Geneva, the Fondation Ernst and Lucie Schmidheiny and the Société Académique de Genève for providing financial support to enable the acquisition of the Waters Xevo® TQ-MS detector. We would also like to thank Dr Christoph Bauer and Jérôme Bosset from the Bioimaging Center of the University of Geneva for their precious advice with TEM and CLSM.

References

[1] S. Werner, R. Grose, Regulation of wound healing by growth factors and cytokines, Physiol. Rev. 83 (2003) 835-870.

[2] N. Farman, E. Maubec, B. Poeggeler, J.E. Klatte, F. Jaisser, R. Paus, The mineralocorticoid receptor as a novel player in skin biology: beyond the renal horizon?, Exp. Dermatol. 19 (2010) 100-107.

[3] J. Boix, L.M. Sevilla, Z. Saez, E. Carceller, P. Perez, Epidermal mineralocorticoid receptor plays beneficial and adverse effects in skin and mediates glucocorticoid responses, J. Invest. Dermatol. DOI 10.1016/j.jid.2016.07.018(2016).

[4] H. Schacke, W.D. Docke, K. Asadullah, Mechanisms involved in the side effects of glucocorticoids, Pharmacol. Ther. 96 (2002) 23-43.

[5] V.T. Nguyen, N. Farman, E. Maubec, D. Nassar, D. Desposito, L. Waeckel, S. Aractingi, F. Jaisser, Re-epithelialization of pathological cutaneous wounds is improved by local mineralocorticoid receptor antagonism, J. Invest. Dermatol. 136 (2016) 2080-2089.

[6] E. Maubec, C. Laouenan, L. Deschamps, V.T. Nguyen, I. Scheer-Senyarich, A.C. Wackenheim-Jacobs, M. Steff, S. Duhamel, S. Tubiana, N. Brahimi, S. Leclerc-Mercier, B. Crickx, C. Perret, S. Aractingi, B. Escoubet, X. Duval, P. Arnaud, F. Jaisser, F. Mentre, N. Farman, Topical mineralocorticoid receptor blockade limits glucocorticoid-induced epidermal atrophy in human skin, J. Invest. Dermatol. 135 (2015) 1781-1789.

[7] M. Lapteva, K. Mondon, M. Moller, R. Gurny, Y.N. Kalia, Polymeric micelle nanocarriers for the cutaneous delivery of tacrolimus: a targeted approach for the treatment of psoriasis, Mol. Pharm. 11 (2014) 2989-3001.

[8] M. Lapteva, V. Santer, K. Mondon, I. Patmanidis, G. Chiriano, L. Scapozza, R. Gurny, M. Moller, Y.N. Kalia, Targeted cutaneous delivery of ciclosporin A using micellar nanocarriers and the possible role of inter-cluster regions as molecular transport pathways, J. Control. Release 196 (2014) 9-18.

[9] D. Gabriel, T. Mugnier, H. Courthion, K. Kranidioti, N. Karagianni, M.C. Denis, M. Lapteva, Y. Kalia, M. Moller, R. Gurny, Improved topical delivery of tacrolimus: A novel composite hydrogel formulation for the treatment of psoriasis, J. Control. Release 242 (2016) 16-24.

[10] M. Lapteva, M. Moller, R. Gurny, Y.N. Kalia, Self-assembled polymeric nanocarriers for the targeted delivery of retinoic acid to the hair follicle, Nanoscale 7 (2015) 18651-18662.

[11] C. Di Tommaso, J.L. Bourges, F. Valamanesh, G. Trubitsyn, A. Torriglia, J.C. Jeanny, F. Behar-Cohen, R. Gurny, M. Moller, Novel micelle carriers for cyclosporin A topical ocular delivery: in vivo cornea penetration, ocular distribution and efficacy studies, Eur. J. Pharm. Biopharm. 81 (2012) 257-264.

[12] N. Dahmana, T. Mugnier, D. Gabriel, V. Kaltsatos, T. Bertaim, F. Behar-Cohen, R. Gurny, Y.N. Kalia, Topical Administration of Spironolactone-Loaded Nanomicelles Prevents Glucocorticoid-Induced Delayed Corneal Wound Healing in Rabbits, Mol. Pharm. 15 (2018) 1192-1202.

[13] B.M. Afzali, E. Yaghoobi, R. Yaghoobi, N. Bagherani, M.A. Dabbagh, Comparison of the efficacy of 5% topical spironolactone gel and placebo in the treatment of mild and moderate acne vulgaris: a randomized controlled trial, Journal of Dermatological Treatment 23 (2012) 21-25.

[14] J. Brown, C. Farquhar, O. Lee, R. Toomath, R.G. Jepson, Spironolactone versus placebo or in combination with steroids for hirsutism and/or acne, Cochrane Database Syst. Rev. DOI 10.1002/14651858.CD000194.pub2(2009) CD000194.

[15] H.R. Kelidari, M. Saeedi, Z. Hajheydari, J. Akbari, K. Morteza-Semnani, J. Akhtari, H. Valizadeh, K. Asare-Addo, A. Nokhodchi, Spironolactone loaded nanostructured lipid carrier gel for effective treatment of mild and moderate acne vulgaris: A randomized, double-blind, prospective trial, Colloids Surf. B. Biointerfaces 146 (2016) 47-53.

[16] S.G. Kandekar, S. Del Rio-Sancho, M. Lapteva, Y.N. Kalia, Selective delivery of adapalene to the human hair follicle under finite dose conditions using polymeric micelle nanocarriers, Nanoscale DOI 10.1039/c7nr07706h(2017).

[17] T. Trimaille, K. Mondon, R. Gurny, M. Moller, Novel polymeric micelles for hydrophobic drug delivery based on biodegradable poly(hexyl-substituted lactides), Int. J. Pharm. 319 (2006) 147-154.

[18] OECD, OECD Guideline for the testing of chemicals - Skin absorption: *in vitro* method, DOI (2004) 428.

[19] S. Kenouch, M. Lombes, F. Delahaye, E. Eugene, J.P. Bonvalet, N. Farman, Human skin as target for aldosterone: coexpression of mineralocorticoid receptors and 11 beta-hydroxysteroid dehydrogenase, J. Clin. Endocrinol. Metab. 79 (1994) 1334-1341.

[20] R.C. Kern, J.D. Foster, D.Z. Pitovski, Mineralocorticoid (type I) receptors in the olfactory mucosa of the mammal: studies with [3H]aldosterone and the anti-mineralocorticoid spironolactone, Chem. Senses 22 (1997) 141-148.

[21] H. Sasano, K. Fukushima, I. Sasaki, S. Matsuno, H. Nagura, Z.S. Krozowski, Immunolocalization of mineralocorticoid receptor in human kidney, pancreas, salivary, mammary and sweat glands: a light and electron microscopic immunohistochemical study, J. Endocrinol. 132 (1992) 305-310.

[22] D.A. Sica, Pharmacokinetics and pharmacodynamics of mineralocorticoid blocking agents and their effects on potassium homeostasis, Heart Fail. Rev. 10 (2005) 23-29.

[23] S.M. Garthwaite, E.G. McMahon, The evolution of aldosterone antagonists, Mol. Cell. Endocrinol. 217 (2004) 27-31.

[24] J.A. Chadwick, J.S. Hauck, C.E. Gomez-Sanchez, E.P. Gomez-Sanchez, J.A. Rafael-Fortney, Gene expression effects of glucocorticoid and mineralocorticoid receptor agonists and antagonists on normal human skeletal muscle, Physiol. Genomics 49 (2017) 277-286.

[25] L.E. Los, S.M. Pitzenberger, H.G. Ramjit, A.B. Coddington, H.D. Colby, Hepatic metabolism of spironolactone. Production of 3-hydroxy-thiomethyl metabolites, Drug Metab. Dispos. 22 (1994) 903-908.

[26] R.A. Keith, I. Jardine, A. Kerremans, R.M. Weinshilboum, Human erythrocyte membrane thiol methyltransferase. S-methylation of captopril, N-acetylcysteine, and 7 alpha-thio-spirolactone, Drug Metab. Dispos. 12 (1984) 717-724.

[27] J.R. Cashman, S. Pena, Canrenone formation via general-base-catalyzed elimination of 7 alpha-(methylthio)spironolactone S-oxide, Chem. Res. Toxicol. 2 (1989) 109-113.

[28] F. Rancan, A. Vogt, Getting under the skin: what is the potential of the transfollicular route in drug delivery?, Ther. Deliv. 5 (2014) 875-877.

[29] A. Patzelt, J. Lademann, Drug delivery to hair follicles, Expert Opin Drug Deliv 10 (2013) 787-797.

[30] V.M. Meidan, M.C. Bonner, B.B. Michniak, Transfollicular drug delivery--is it a reality?, Int. J. Pharm. 306 (2005) 1-14.

[31] S. Hansen, C.M. Lehr, Transfollicular delivery takes root: the future for vaccine design?, Expert Rev Vaccines 13 (2014) 5-7.

[32] W.C. Chen, C.C. Zouboulis, Hormones and the pilosebaceous unit, Dermatoendocrinol. 1 (2009) 81-86.

[33] C.C. Zouboulis, The skin as an endocrine organ, Dermatoendocrinol. 1 (2009) 250-252.

[34] D. Deplewski, R.L. Rosenfield, Role of hormones in pilosebaceous unit development, Endocr. Rev. 21 (2000) 363-392.

[35] C.C. Zouboulis, Human skin: an independent peripheral endocrine organ, Horm. Res. 54 (2000) 230-242.

[36] J. Reichrath, The skin is a fascinating endocrine organ, Dermatoendocrinol. 1 (2009) 195-196.

[37] R. Choudhry, M.B. Hodgins, T.H. Van der Kwast, A.O. Brinkmann, W.J. Boersma, Localization of androgen receptors in human skin by immunohistochemistry: implications for the hormonal regulation of hair growth, sebaceous glands and sweat glands, J. Endocrinol. 133 (1992) 467-475.

[38] C.C. Zouboulis, W.C. Chen, M.J. Thornton, K. Qin, R. Rosenfield, Sexual Hormones in Human Skin, Horm. Metab. Res. 39 (2007) 85-95.

[39] M.G. Mercurio, D.S. Gogstetter, Androgen physiology and the cutaneous pilosebaceous unit, J. Gend. Specif. Med. 3 (2000) 59-64.

[40] E. Berardesca, P. Gabba, G. Ucci, G. Borroni, G. Rabbiosi, Topical spironolactone inhibits dihydrotestosterone receptors in human sebaceous glands: an autoradiographic study in subjects with acne vulgaris, Int. J. Tissue React. 10 (1988) 115-119.

[41] B.M. Afzali, E. Yaghoobi, R. Yaghoobi, N. Bagherani, M.A. Dabbagh, Comparison of the efficacy of 5% topical spironolactone gel and placebo in the treatment of mild and moderate acne vulgaris: a randomized controlled trial, J Dermatolog Treat 23 (2012) 21-25.

[42] J. Lademann, H. Richter, U.F. Schaefer, U. Blume-Peytavi, A. Teichmann, N. Otberg, W. Sterry, Hair follicles - a long-term reservoir for drug delivery, Skin Pharmacol. Physiol. 19 (2006) 232-236.

[43] J. Lademann, F. Knorr, H. Richter, U. Blume-Peytavi, A. Vogt, C. Antoniou, W. Sterry, A. Patzelt, Hair follicles--an efficient storage and penetration pathway for topically applied substances. Summary of recent results obtained at the Center of Experimental and Applied Cutaneous Physiology, Charite - Universitatsmedizin Berlin, Germany, Skin Pharmacol. Physiol. 21 (2008) 150-155.

[44] J. Lademann, H. Richter, A. Teichmann, N. Otberg, U. Blume-Peytavi, J. Luengo, B. Weiss, U.F. Schaefer, C.M. Lehr, R. Wepf, W. Sterry, Nanoparticles--an efficient carrier for drug delivery into the hair follicles, Eur. J. Pharm. Biopharm. 66 (2007) 159-164.

[45] B.M. Burke, W.J. Cunliffe, Oral spironolactone therapy for female patients with acne, hirsutism or androgenic alopecia, Br. J. Dermatol. 112 (1985) 124-125.

[46] R.N. Shamma, M.H. Aburahma, Follicular delivery of spironolactone via nanostructured lipid carriers for management of alopecia, International journal of nanomedicine 9 (2014) 5449-5460.

[47] D.A. Adamopoulos, M. Karamertzanis, S. Nicopoulou, A. Gregoriou, Beneficial effect of spironolactone on androgenic alopecia, Clin. Endocrinol. (Oxf.) 47 (1997) 759-760.

CONCLUSIONS AND OUTLOOK

In recent years, many researchers have investigated the abnormalities related to the consequences of over-activation of the mineralocorticoid receptor and the subsequent diseases including delayed cutaneous/corneal wound healing and central serous chorioretinopathy. Their work has been fruitful and has helped to elucidate potential disease mechanisms and the hypothesis that use of mineralocorticoid receptor antagonists could be an effective therapeutic strategy. However, mineralocorticoid receptor antagonists are only available for oral and parenteral delivery (Aldactone®, Inspra®, Soldactone®; Pfizer, Switzerland). Thus, they are given orally off-label for the treatment of central serous chorioretinopathy where high doses are needed to achieve a therapeutic effect in the eye leading to high systemic exposure and subsequent side effects. Likewise, mineralocorticoid receptor antagonists have been shown to off-set the glucocorticoid-induced delayed cutaneous wound healing; however, there is no available spironolactone formulation for topical delivery.

To address this unmet medical need, we have aimed to develop novel safe and efficient formulations for a site-specific delivery of the potent mineralocorticoid receptor antagonist, spironolactone, using polymeric micelles for topical delivery to the eye and to the skin and a biodegradable sustained release polymer for intravitreal injection to the eye. The safety and efficacy of these formulations for the treatment of delayed wound healing and central serous chorioretinopathy were evaluated.

The bio-analytical method developed and validated for the detection and quantification of spironolactone and its active metabolites was crucial for the success of the project. Indeed, this method was used to quantify spironolactone and its metabolites in the biological tissues and fluids obtained from the treated animals and from the *ex vivo* samples. The method enabled us to characterize spironolactone metabolism in the different tissues and correlate the physiological effect observed with the concentrations of the parent compound and active metabolites present.

Encapsulation of spironolactone in the mPEG-dihexPLA micelles led to a 100-fold increase in aqueous solubility with a preliminary stability for at least 1 year at 5°C. The safety of this formulation following topical instillation and its efficacy in off-setting the dexamethasone-induced corneal delayed wound healing makes this formulation of great clinical interest in ophthalmology. Successful translation of these preclinical results to the clinical practice could improve therapeutic outcomes for glucocorticoid-treated patients since topical instillation of the spironolactone micelles might counter the impaired wound healing associated with routine glucocorticoid therapy.

The targeted delivery of the hydrogel form of the 0.1% spironolactone micelles to the pilosebaceous unit enables the site-specific antagonism of the mineralocorticoid receptor located in the hair follicle. Spironolactone micelles hence constitute a promising candidate for the treatment of delayed cutaneous wound healing, including chronic diabetic wounds. Nevertheless, *in vivo* studies are needed to confirm the efficacy of the spironolactone micelles to improve the cutaneous delayed wound healing.

The targeted delivery of spironolactone to the pilosebaceous unit by the micelles paves the way to many other therapeutic areas where spironolactone could be beneficial. Indeed, many other hormonal receptors are located in the pilosebaceous unit, including the androgen receptor. Spironolactone being a potent androgen antagonist; topical administration of spironolactone may be of interest for other clinical applications such as for the treatment of androgen-mediated skin and hair diseases including acne vulgaris, androgenic alopecia and hirsutism.

Intravitreal injection of spironolactone incorporated in a biodegradable sustained release polymer (hexPLA) to the rat's eye enabled a prolonged delivery, for at least one month, of spironolactone to the retina and the choroid where the mineralocorticoid receptor is located. Our next studies will be performed in a model with eye dimensions closer to the human eye. This formulation combined with an appropriate injection system, would be of interest to treat patients suffering from chronic forms of central serous chorioretinopathy, improving their compliance by avoiding frequent injections.

PUBLICATIONS

Received: 30 November 2017 | Revised: 20 April 2018 | Accepted: 4 May 2018

DOI: 10.1002/bmc.4287

RESEARCH ARTICLE

WILEY Biomedical Chromatography

Development and validation of a fast and sensitive UHPLC-ESI-MS method for the simultaneous quantification of spironolactone and its metabolites in ocular tissues

Naoual Dahmana[1] | Doris Gabriel[2] | Robert Gurny[1,2] | Yogeshvar N. Kalia[1]

[1] School of Pharmaceutical Sciences, University of Geneva, University of Lausanne, Lausanne, Switzerland

[2] Apidel SA, Geneva, Switzerland

Correspondence
Yogeshvar N. Kalia, School of Pharmaceutical Sciences, University of Geneva, University of Lausanne, Lausanne, Switzerland.
Email: yogi.kalia@unige.ch

Funding information
Kommission für Technologie und Innovation, Grant/Award Number: 19086.1 PFLS-LS

Abstract

Glucocorticoids are a mainstay for the treatment of immune-mediated conditions and inflammatory diseases. However, their chronic use causes numerous side-effects including delays in corneal and cutaneous wound healing. This is attributed to off-target agonism of the mineralocorticoid receptor, which can be reduced by co-administration of a mineralocorticoid receptor antagonist such as spironolactone. The aim of this study was to develop a fast, selective and sensitive UHPLC-ESI-MS method for the simultaneous quantification of spironolactone, its active metabolites (7α-thiomethylspironolactone and canrenone), the latter's water-soluble prodrug potassium canrenoate and the synthetic glucocorticoid, dexamethasone, in corneal samples (17α-methyltestosterone served as an internal standard). A one-step extraction procedure using MeOH–H_2O (1:1) was validated and employed to recover the analytes from the corneal tissue. Extracts were centrifuged and the supernatant analyzed under isocratic conditions. Compounds were detected using selected ion recording mode. The method satisfied US Food and Drug Administration guidelines with respect to selectivity, precision and accuracy and displayed linearity from 5 to 1000 ng/mL for all of the analytes. The lower limit of quantitation of the method was 5 ng/mL, making it sufficiently sensitive for quantification of the analytes in samples from *in vivo* studies.

KEYWORDS

7α-thiomethylspironolactone, canrenone, potassium canrenoate, spironolactone, ultra-high performance liquid chromatography tandem mass spectrometry

1 | INTRODUCTION

Spironolactone (SPL; Figure 1a) is a synthetic mineralocorticoid receptor (MR) antagonist that competes with the endogenous hormone aldosterone to bind to the MR (Sica, 2005). It is indicated for the treatment of (a) primary and secondary hyperaldosteronism and hypokalaemia, (b) edematous conditions such as nephrotic syndrome and ascites and (c) cardiovascular conditions such as congestive heart failure and essential hypertension (Dong, Xu, Zhang, Tian, & Chen, 2006; Sandall, Millership, Collier, & McElnay, 2006; Sica, 2005).

To date, it has proved difficult to establish a direct relationship between the extent of the pharmacological effect exerted by SPL and its concentration since the molecule undergoes rapid and extensive metabolism via different pathways—including deacetylation, *S*-methylation and dethioacetylation. Two of its principal metabolites, 7α-thiomethylspironolactone (TMSPL; Figure 1b) and canrenone (CAN; Figure 1c; Sandall, Millership, Collier, & McElnay, 2006), have biological activity in their own right and exert a pharmacological effect. Indeed, for many years, CAN was believed to be the sole active metabolite of SPL and responsible for most of its pharmacological

Abbreviations: CAN, canrenone; CANK, potassium canrenoate; DXM, dexamethasone; MeOH, methanol; MeT, 17α-methyltestosterone; MR, mineralocorticoid receptor; SIR, selected ion recording; SPL, spironolactone; TMSPL, 7α-thiomethylspironolactone.

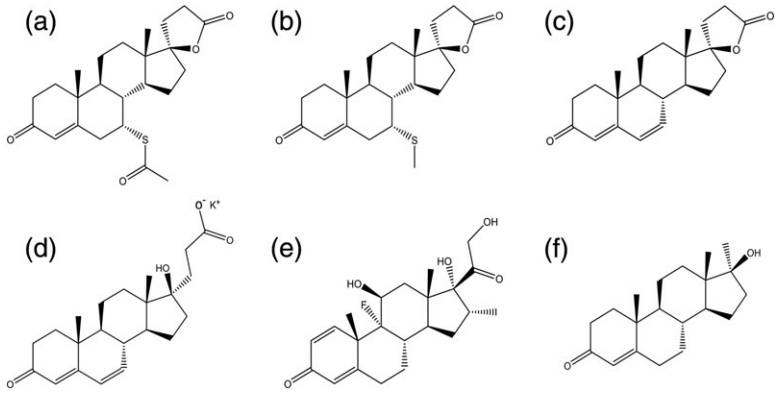

FIGURE 1 Chemical structures of (a) spironolactone, (b) 7α-thiomethylspironolactone, (c) canrenone, (d) potassium canrenoate, (e) dexamethasone and (f) 17α-methyltestosterone, internal standard

activity. This assumption was due to the use of nonspecific analytical methods, such as fluorometric detection (Ramsay, Shelton, Harrison, Tidd, & Asbury, 1976) that overestimated CAN concentrations in plasma, because of the co-determination of other fluorescing sulfur-containing SPL metabolites such as TMSPL. The use of more specific HPLC methods, capable of distinguishing between the metabolites, confirmed that CAN plasma levels were lower than previously thought (Dahlof, Lundborg, Persson, & Regardh, 1979). As a result, it is now considered that both metabolites contribute to the anti-mineralocorticoid effects of SPL (Kaukonen, Vuorela, Vuorela, & Mannermaa, 1998; Sandall, Millership, Collier, & McElnay, 2006). Some studies have even suggested that TMSPL is the main active metabolite in humans owing to its higher affinity for renal MR and since its plasma concentrations were higher than those of CAN (Kaukonen, Vuorela, Vuorela, & Mannermaa, 1998; Los, Pitzenberger, Ramjit, Coddington, & Colby, 1994; H. W. Overdiek, Hermens, & Merkus, 1985a; Sandall, Millership, Collier, & McElnay, 2006).

Recent reports have pointed to new therapeutic applications for SPL (and its active metabolites); for example, it is being increasingly prescribed "off-label" in ophthalmology for the treatment of central serous chorioretinopathy (Bousquet et al., 2015; Chin et al., 2015; Daruich et al., 2016; Ghadiali, Jung, Yu, Patel, & Yannuzzi, 2016; Herold, Prause, Wolf, Mayer, & Ulbig, 2014; Herold, Rist, Priglinger, Ulbig, & Wolf, 2017; Salehi, Wenick, Law, Evans, & Gehlbach, 2015; van Dijk et al., 2016), which involves the accumulation of fluid under the retina and can result in retinal detachment and vision impairment. Other studies have suggested that concomitant administration of MR antagonists might offset glucocorticoid-induced delays in cutaneous wound healing (Farman et al., 2010; Maubec et al., 2015; Nguyen et al., 2016). This led to the hypothesis that SPL and its metabolites might also be able to counter the deleterious effects of glucocorticoids on corneal lesions and the delayed wound healing process and so create a new therapeutic application in ophthalmology.

It was decided to test this hypothesis with an *in vivo* study (Dahmana et al., 2018); however, this required the development of a sophisticated analytical method able to quantify the biodistribution not only of SPL and its active metabolites (TMSPL and CAN), but also of potassium canrenoate (CANK; Figure 1d), a water-soluble CAN prodrug that is of particular clinical interest since it can be administered intravenously (and was used as a control in the *in vivo* study) and dexamethasone (a potent glucocorticoid that was used to induce the delayed wound healing; DXM, Figure 1e).

Although several HPLC methods have been reported for the separation and quantification of SPL and/or its metabolites, none satisfied all of the requirements of the *in vivo* study. Some protocols did not enable the simultaneous determination of SPL and its active metabolites, TMSPL and CAN (Dong, Xu, Zhang, Tian, & Chen, 2006; Sora, Udrescu, Albu, David, & Medvedovici, 2010; Suyagh et al., 2010); others either lacked sensitivity (limits of quantification >10 ng/mL) or the runtime was excessively long, ranging from 11 to 36 min, making them unsuitable for routine or high-throughput sample management (Abosehmah-Albidy, York, Wong, Losowsky, & Chrystyn, 1997; Jankowski, Skorek-Jankowska, & Lamparczyk, 1996; Kaukonen, Vuorela, Vuorela, & Mannermaa, 1998; J. W. Overdiek, Hermens, & Merkus, 1985b; Sandall, Millership, Collier, & McElnay, 2006; Sherry, O'Donnell, & Colby, 1986). Furthermore, none of the methods included the simultaneous quantification of CANK and DXM.

Therefore, the aim of the present investigation was to develop and to validate a fast, selective and sensitive analytical method for the simultaneous quantification of spironolactone, its two main metabolites (TMSPL and CAN), potassium canrenoate and dexamethasone concentrations in the cornea that could be used in the planned *in vivo* study. To normalize the matrix effect of the biological tissue, 17α-methyltestosterone (MeT; Figure 1f) was used as an internal standard (IS).

2 | EXPERIMENTAL

2.1 | Chemicals and reagents

Spironolactone was purchased from Zhejiang Langhua Pharmaceutical Co. Ltd (Zhejiang, China). 7α-Thiomethylspironolactone was purchased from TLC Pharmaceutical Standards Ltd (Ontario, Canada). Canrenone, potassium canrenoate and MeT were obtained from Sigma-Aldrich (Buchs, Switzerland). Dexamethasone was purchased from Tianjin TianMao Technology Development Corp. Ltd (Tianjin, China). Ultrapure water (H_2O) was obtained from a Milli-Q® water purification system (resistivity >18 MΩ cm) from Merck Millipore (Darmstadt, Germany). Methanol (MeOH, HPLC grade) was obtained from Fisher Scientific (Waltham, MA, USA) and formic acid (ULC/MS grade) from Biosolve (Dieuze, France). All other chemicals were at least of analytical grade.

2.2 | Liquid chromatography set-up

The liquid chromatographic system consisted of a Waters Acquity® ultra-performance liquid chromatography (UPLC®) core system (Baden-Dättwil, Switzerland), including a binary solvent manager, a sample manager with an injection loop volume of 10 µL and a column manager. The reverse-phase chromatographic separation of the analytes (SPL, CAN, TMSPL, CANK and DXM) and the internal standard (MeT; IS) was performed using a Waters XBridge® BEH C_{18} column (50 × 2.1 mm i.d., 2.5 µm) fitted with a Waters XBridge® BEH C_{18} VanGuard pre-column (5 × 2.1 mm i.d., 2.5 µm). Isocratic elution was carried out using a mobile phase consisting of 0.1% formic acid in H_2O:MeOH (48:52, *v*/v) with a flow rate of 0.45 mL/min and a runtime of 5 min. Column temperature was kept at 40°C and the sample manager was at room temperature. Injection volume was set at 5 µL (partial loop injection mode).

2.3 | Mass spectrometry system

The mass spectrometry (MS) system consisted of a Waters XEVO® TQ-MS detector (Baden-Dättwil, Switzerland) fitted with a Z-spray electrospray ionization source. MS detection of the six compounds was performed using electrospray ionization in the positive-ion mode (ESI+) and selected ion recording (SIR) using the pseudo-molecular ion of each compound as the parent ion (hydrogen adduct, $[M + H]^+$). Capillary voltage was set at 2.3 kV, desolvation gas temperature and flow were maintained at 350°C and 650 L/h, respectively, and cone temperature was set at 150°C. Analyte-specific MS parameters were tuned and determined by infusing each compound individually at 1 µg/mL in MeOH–H_2O (1:1) at a flow rate of 5 µL/min. Cone voltages and dwell time were optimized to obtain the best peak intensity for each compound. Data processing was performed using Waters MassLynx software version 4.1.

2.4 | Preparation of the corneal matrix

Freshly enucleated porcine eyes were obtained from a local slaughterhouse. After cleaning the eye globes, the corneas were harvested and rinsed in phosphate-buffered saline. Each cornea was then cut into small pieces in a vial containing 2 mL MeOH–H_2O (1:1) and left for extraction overnight under agitation at room temperature. The following day, samples were centrifuged at 12,000 rpm for 20 min, then supernatants were collected and pooled. Fifty corneas harvested from different animals were used to prepare the corneal matrix.

The corneal matrix solution was used to assess the specificity of the method and evaluate the matrix effect. Calibration standards and quality control samples were also prepared in the corneal matrix solution.

2.5 | Preparation of stock solutions, calibration standards and quality control samples

A stock solution of each compound (SPL, TMSPL, CAN, CANK, DXM and MeT) was prepared at 1 mg/mL in methanol. All stock solutions were freshly prepared prior to each analysis except for TMSPL and CAN—for these substances, the stock solutions were stored at −20°C. A working solution was then prepared by mixing SPL, TMSPL, CAN, CANK and DXM stock solutions at 10 µg/mL in corneal matrix (prepared as described above). This solution was further diluted in corneal matrix to obtain the intermediate working solutions at 1 and 0.1 µg/mL, which served to prepare the calibration standards. A working solution of the IS was also prepared at 1 µg/mL by appropriate dilution of the stock solution in corneal matrix.

Calibration standard samples were prepared in corneal matrix by suitable dilution of the working solutions to the desired concentration in the range 5–1000 ng/mL. The appropriate volume of the IS working solution was then used to spike the calibration standard samples so as to obtain a final IS concentration of 100 ng/mL.

Quality control samples were prepared in the same way at 10, 100 and 500 ng/mL in corneal matrix. All of the working solutions, calibration standards and quality control samples were prepared and diluted in corneal matrix in such a way that the final composition in terms of matrix component remained equivalent in each sample at the different analyte concentrations.

2.6 | Method validation

The method was validated according to US Food and Drug Administration (2001) and ICH guidelines with respect to selectivity and specificity, accuracy and precision, linearity and sensitivity (lower limit of quantification, LLOQ). In addition, the matrix effect of the cornea was evaluated, the extraction procedure of the analytes from the cornea was validated and sample stability was assessed.

2.6.1 | Selectivity and specificity

The selectivity of the method was verified by analyzing a sample containing a mixture of the six analytes (SPL, TMSPL, CAN, CANK, DXM and the IS) in MeOH–H_2O (1:1) at different concentrations, in the range 5–1000 ng/mL, and assessing peak separation and baseline resolution.

The specificity of the method was investigated in two steps. First, the specificity was assessed with respect to signal interferences between the respective SIR signals of the different analytes, where each analyte was injected individually at 100 ng/mL in MeOH–H_2O (1:1) and the resulting signals were compared with the signal obtained after injection of the mixture of the six analytes at the same concentration. Second, the specificity was verified with respect to the endogenous compounds present in the porcine cornea to confirm the absence of interference between their peaks and the peaks of the different analytes. For that, a blank sample of the corneal matrix (obtained as described in Section 2.4) was analyzed and compared with another corneal matrix sample spiked with the six analytes at 100 ng/mL.

2.6.2 | Matrix effect evaluation

Ion suppression/enhancement owing to a matrix effect was investigated by comparing the signal obtained from the five analytes (SPL, TMSPL, CAN, CANK and DXM) at 50 ng/mL prepared in a standard solution of MeOH–H_2O (1:1) vs the signal obtained of the same five analytes prepared at the same concentration in corneal matrix. All of the samples contained IS at 100 ng/mL. The matrix effect was

evaluated by calculating the matrix factor and the IS normalized matrix factor using the following equations:

$$\text{Percentage matrix factor} = \frac{\text{Analyte area}_{\text{spiked matrix}}}{\text{Analyte area}_{\text{standard solution}}} \times 100\% \quad (1)$$

$$\text{Percentage IS normalized matrix factor} = \frac{\text{Matrix factor}_{\text{Analyte}}}{\text{Matrix factor}_{\text{IS}}} \times 100\% \quad (2)$$

(when the percentage matrix factor is 100%, it means the absence of matrix effect; <100%, means ion suppression; >100% means ion enhancement).

2.6.3 | Linearity

Calibration standards were prepared by spiking the analytes at known concentrations in porcine corneal matrix obtained as described in Section 2.4. The concentrations were selected to cover the range of the concentrations expected to be found in the biological samples, i.e. from 5 to 1000 ng/mL. Eight calibration standards containing 100 ng/mL IS (MeT) were prepared at 5, 10, 20, 50, 100, 200, 500 and 1000 ng/mL ($n = 5$) in porcine corneal matrix as described in Section 2.5.

To standardize the matrix effect of the cornea, calibration curves of each analyte (SPL, TMSPL, CAN, CANK and DXM) were constructed by plotting the relative peak area, i.e. the ratio between the peak area of each analyte to the peak area of the IS (MeT), vs the concentration of each analyte to the known concentration of the IS (100 ng/mL, equation (1)). This method was also used for further sample quantification such as the quality control samples.

$$\text{Concentration of analyte} = \left(\frac{\text{Concentration of IS}}{\text{Slope}}\right) \times \left(\frac{\text{Area of analyte}}{\text{Area of IS}} - \text{Intercept}\right) \quad (3)$$

The slope and the intercept were calculated from the calibration curve obtained the same day as each analysis. The acceptance criterion for the linearity of a calibration curve was a correlation coefficient (R) of at least 0.99 and an RSD <15% at each calibration standard (<20% at LLOQ).

2.6.4 | Sensitivity (LLOQ)

The LLOQ was determined by calculating the signal-to-noise ratio for each analyte and assessing an area at least five times higher obtained with the lowest calibration standard (5 ng/mL, $n = 5$) of each analyte (SPL, TMSPL, CAN, CANK and DXM) when compared with a blank sample consisting of a blank corneal matrix and verifying accuracy and precision at the LLOQ.

2.6.5 | Accuracy and precision

Accuracy and precision were determined by measuring the intra-day and inter-day recovery and variability of each analyte (SPL, TMSPL, CAN, CANK and DXM) at three different concentrations over 3 days. Samples were prepared by spiking the corneal matrix containing 100 ng/mL IS with a mixture of the five analytes (SPL, TMSPL, CAN, CANK and DXM) at 10, 100 and 500 ng/mL ($n = 5$).

Accuracy (expressed as a percentage recovery) for each analyte was calculated as the ratio of the measured concentration, calculated using the calibration curve obtained on the same day of analysis, with the actual (spiked) concentration, as shown in the following equation:

$$\text{Percentage recovery} = \frac{\text{Measured concentration}}{\text{Actual concentration}} \times 100\% \quad (4)$$

Intra-day accuracy was evaluated by calculating the percentage recovery of measurements of the same concentration obtained from five independent determinations during the same day. Inter-day accuracy was evaluated by calculating the percentage recovery of measurements of the same concentration obtained from 10 independent determinations over 2 days and 15 independent determinations over 3 days.

Intra-day precision was evaluated by calculating the relative standard deviation (RSD) of measurements of the same concentration obtained from five independent determinations during the same day. Inter-day precision was evaluated by calculating the relative standard deviation of measurements of the same concentration obtained from 10 independent determinations over 2 days and 15 independent determinations over 3 days.

2.6.6 | Extraction procedure

The efficiency of the extraction procedure to recover the different analytes from the cornea was evaluated and validated using porcine cornea samples, obtained as explained in Section 2.4. Corneas ($n = 3$ per concentration) were spiked with 10 µL of an acetone solution containing a mixture of SPL, TMSPL, CAN, CANK and DXM at 10, 40 or 100 µg/mL then left to evaporate (i.e. resulting in deposition of 100, 400 or 1000 ng of each analyte in the cornea). Acetone is a lipid solvent which partially lyses the epithelium of the cornea, allowing the compounds to spread in the tissue. After acetone evaporation, the corneas were carefully cut into small pieces, placed in vials containing 2 mL MeOH–H_2O (1:1) and 100 ng/mL IS then left under agitation overnight (~12 h) for extraction at room temperature. Subsequently, samples were centrifuged at 12,000 rpm for 20 min and the supernatants collected for analysis.

The extraction efficiency (expressed as a percentage) was estimated by calculating the recovered amount to the spiked amount as displayed in the following equation:

$$\text{Percentage extraction efficiency} = \frac{\text{Recovered amount}}{\text{Spiked amount}} \times 100\% \quad (5)$$

2.6.7 | Sample stability

Stability of the stock solutions of TMSPL and CAN at 1 mg/mL stored at −20°C was tested at 10 µg/mL by comparing the IS normalized area obtained from the stored solutions to that obtained from the freshly prepared solutions with acceptable difference being ±10% and RSD no more than 10%. Stock solutions of the other analytes and the corneal matrix solution were prepared freshly prior to each analysis. Validation of the extraction procedure was also used to test the stability of the analytes in contact with the corneal matrix.

2.7 | Statistical analysis

Data are expressed as means ± SD. The Grubbs test was used to test for outliers (none were found).

3 | RESULTS AND DISCUSSION

3.1 | Method development

The chromatographic separation of the analytes (SPL, its metabolites TMSPL and CAN, prodrug CANK and DXM) and the IS (MeT) within a reasonable runtime was the most challenging part of the method development. This was especially so with respect to the separation of SPL and its two active metabolites, TMSPL and CAN, owing to their very similar chemical structures. Chromatographic conditions were optimized to obtain the best peak resolution, intensity and shape within the shortest possible runtime.

For this purpose, various conditions including column chemistry and temperature, mobile phase composition and flow rate, injection volume and runtime were varied and optimized. First, a Waters Acquity UPLC® BEH C_{18} column (50 × 2.1 mm i.d., 1.7 µm) was tested but this did not enable the separation of SPL and its metabolites within a relatively short runtime. Interestingly, that was achieved with a Waters XBridge® BEH C_{18} column (50 × 2.1 mm i.d., 2.5 µm). The only difference between the Acquity® and XBridge® columns is the particle size, which is smaller in the former; although this should enable better selectivity, in our case, the XBridge® column proved to be more selective. Separation of SPL, its metabolites, CANK, DXM and the IS was achieved with a mobile phase consisting of 0.1% formic acid in H_2O–MeOH (48:52, *v*/v) with a flow rate of 0.45 mL/min. It was noted that isocratic elution resulted in a better separation of the analytes. These experiments enabled the best chromatographic conditions to be selected and these were used for the subsequent validation of the analytical method.

To maximize the MS signal of the parent ion of the six analytes, some instrument parameters were optimized. Because most of the analytes are protonated at the low pH of the mobile phase, electrospray ionization in the positive mode was selected over the negative mode for better sensitivity. Identification and quantification of each analyte were carried out according to the mass-to-charge ratio (*m/z*) of the pseudo-molecular ion of each compound (hydrogen adduct, $[M + H]^+$). Multiple reaction monitoring detection is accepted as being more specific than the SIR detection mode; however, as demonstrated by the validation of this method described below, the SIR mode was able to provide the necessary sensitivity and specificity for quantification of the samples to be analyzed in this study.

The pseudo-molecular parent ion *m/z* corresponding to DXM, CANK, SPL/CAN, TMSPL and MeT were 393.1, 359.1, 341.0, 389.0 and 303.0, respectively. SPL was detected with an *m/z* of 341.0, which corresponds to the pseudo-molecular parent ion of CAN. This is due to the cleavage of the 7*α*-thioacetyl group of SPL during the electrospray evaporation and ionization process within the ESI source producing CAN. This was reported by Sora, Udrescu, Albu, David, and Medvedovici (2010) and Vlase, Imre, Muntean, Achim, and Muntean (2011). However, the SPL signal can be easily distinguished from the CAN signal since their retention times are 2.4 and 3.0 min, respectively. The capillary voltage was set at 2.3 kV and the optimal cone voltage settings were 15 V for DXM, 32 V for CANK and 35 V for SPL, TMSPL, CAN and MeT. Dwell time was set at 5 ms for all the compounds except for DXM at 328 ms to enhance the sensitivity. The specific detection settings for each of the six compounds are presented in Table 1.

3.2 | Method validation

3.2.1 | Selectivity and specificity

As mentioned previously, multiple reaction monitoring mode is reported to be more specific because of the use of a unique parent-to-daughter transition for the detection of each analyte; however, in this study, we showed that we can achieve sufficient specificity using SIR mode. Individual injection of the standard solution of each analyte in MeOH–H_2O (1:1) showed no interference (Figure 2a–f). Injection of a standard solution containing a mixture of the six compounds at 100 ng/mL in MeOH–H_2O (1:1) confirmed the good peak separation and resolution (Figure 2g).

The inter-day relative standard deviations (RSD) of the retention times were < 2% for all the compounds (Table 2). Any minor shift (~0.05 min) in the retention time of the six analytes always followed the same trend, i.e. all peaks shifted either to shorter or longer retention times and hence did not affect the peak separation and resolution.

Analysis of a blank corneal matrix sample (Figure 3a) and a spiked sample with the six compounds (Figure 3b) showed no interference between the corneal matrix components and the analytes since the endogenous substances from the cornea eluted much earlier (t = 0.34 min) than the analytes, confirming the specificity of this method for the identification of DXM, CANK, SPL, TMSPL, CAN and MeT (IS) in the corneal matrix.

TABLE 1 Specific MS parameters for the detection of each analyte

Analyte [M]	$[M + H]^+$	Cone voltage (V)	Dwell time (s)
Dexamethasone	393.1	15	0.328
Potassium canrenoate	359.1	32	0.005
Spironolactone	341.0	35	0.005
7*α*-Thiomethylspironolactone	389.0	35	0.005
Canrenone	341.0	35	0.005
17*α*-Methyltestosterone (IS)	303.0	35	0.005

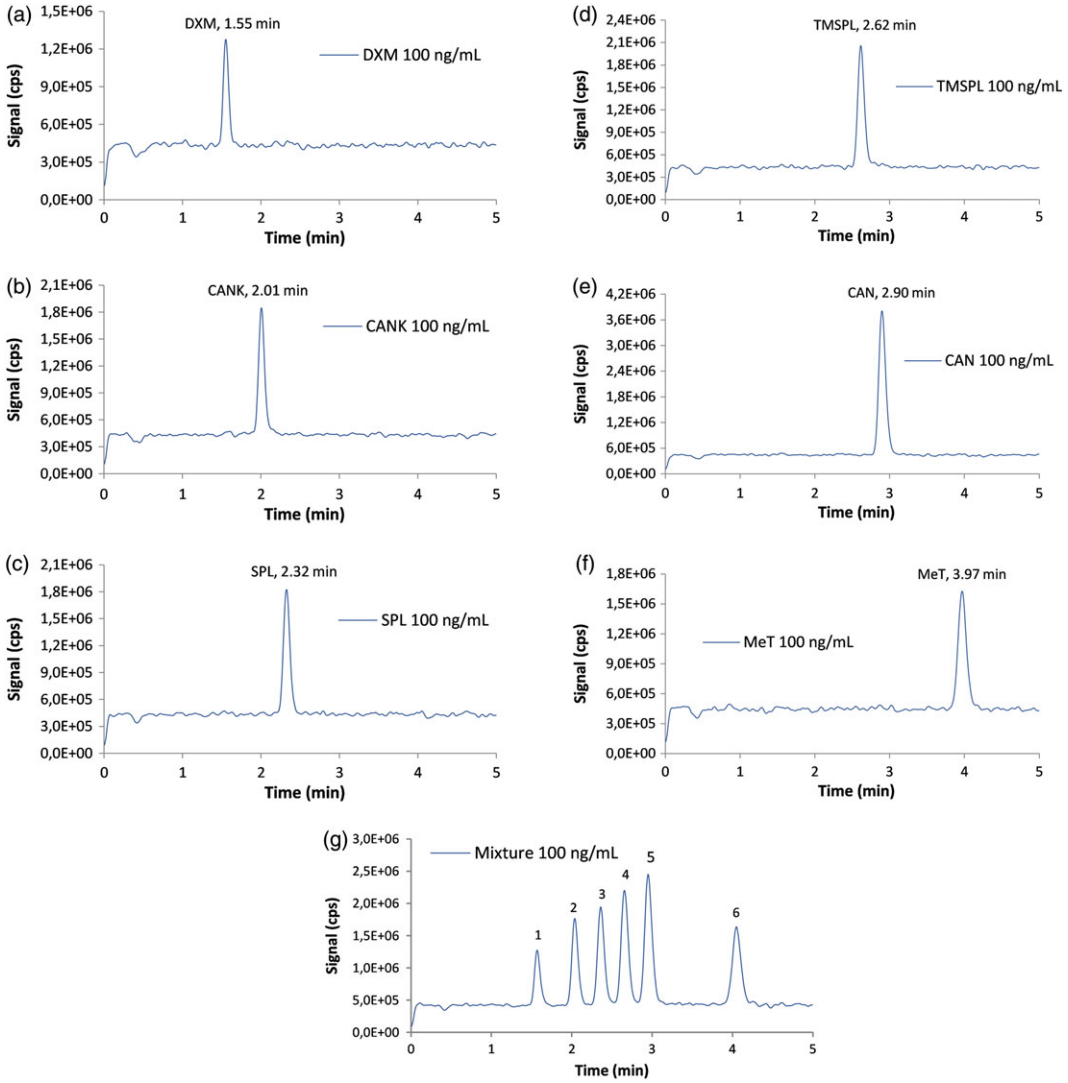

FIGURE 2 Selected ion recording (SIR) trace of each analyte at 100 ng/mL in methanol–water (1:1). (a) Dexamethasone, DXM; (b) potassium canrenoate, CANK; (c) spironolactone, SPL; (d) 7α-thiomethylspironolactone, TMSPL; (e) canrenone, CAN; (f) 17α-methyltestosterone, MeT; and (g) SIR trace of a mixture with all six analytes at 100 ng/mL in methanol–water (1:1). 1, DXM; 2, CANK; 3, SPL; 4, TMSPL; 5, CAN and 6, MeT

TABLE 2 Retention time (t_R) of each analyte

Analyte	Inter-day mean t_R (min)	RSD
Dexamethasone	1.56 ± 0.01	0.8
Potassium canrenoate	2.03 ± 0.02	1.1
Spironolactone	2.35 ± 0.03	1.2
7α-Thiomethyspironolactone	2.64 ± 0.03	1.0
Canrenone	2.93 ± 0.03	1.2
17α-Methyltestosterone (IS)	4.02 ± 0.06	1.5

Values are given as mean ± SD of 20 determinations.

3.2.2 | Matrix effect

Matrix effect was observed for the six analytes (Table 3). All of the analytes, including the internal standard (IS), underwent ion suppression to a relatively similar extent with percentage matrix factors ranging from 80.4 to 84.2% and RSD from 0.6 to 5.5%. IS-normalized matrix factors ranged from 97.3 to 102.0% and RSD from 2.3 to 4.9%, supporting the choice of MeT as the internal standard.

3.2.3 | Linearity

The method showed linearity over the concentration range of 5–1000 ng/mL for all of the analytes with the RSD of the calibration standards from the nominal concentration ranging from 0.6 to 9.1 (from 8.0 to 9.7 at LLOQ), which is consistent with US Food and Drug Administration guidelines. Moreover, all the calibration curves showed an excellent correlation ($r > 0.99$) between the IS-normalized peak area and the IS-normalized concentration of each analyte within the test range. Typical equations of the calibration curves of each analyte are displayed in Table 4.

3.2.4 | Sensitivity (LLOQ)

The LLOQ of each analyte (DXM, CANK, SPL, TMSPL and CAN) was determined to be 5 ng/mL since the signal-to-noise ratio of each

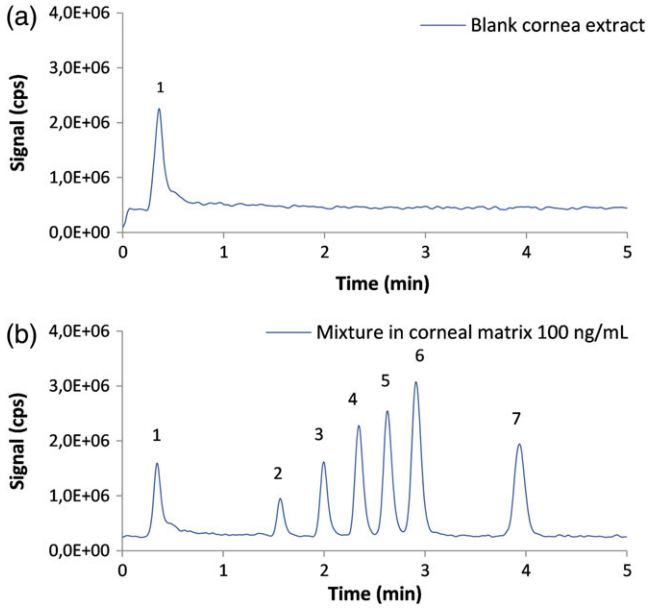

FIGURE 3 SIR trace of (a) blank porcine corneal matrix and (b) porcine corneal matrix spiked with the six analytes at 100 ng/mL. 1, Porcine corneal matrix peak; 2, dexamethasone; 3, potassium canrenoate; 4, spironolactone; 5, 7α-thiomethylspironolactone; 6, canrenone; 7, 17α-methyltestosterone (internal standard)

analyte, i.e. the areas obtained from each analyte vs the areas obtained from the blank corneal matrix sample, ranged from 9.6 to 42.9 with RSD ranging from 4.2 to 17.2%, which satisfied the US Food and Drug Administration guidelines (Table 5). Accuracy and precision were also verified at 5 ng/mL for all the analytes since all intra- and inter-day recovery values (94.6–107.1%) and RSD values (3.0–11.0%) were within the acceptable range as described in the US Food and Drug Administration guidelines for the LLOQ (Table 5). Thus, the method was considered to be sufficiently sensitive for the quantification of DXM, CANK, SPL, TMSPL and CAN in the corneal matrix.

3.2.5 | Accuracy and precision

Results of intra- and inter-day accuracy and precision of the method for the determination of the different analytes are shown in Table 6. For intra-day measurements, the mean recoveries (accuracy) were within the range of 85.7–103.3% and RSD (precision) ranged from 0.6 to 9.2%. For inter-day measurements, the mean recoveries were within the range of 93.8–103.3% and the RSD ranged from 1.0 to 11.0%. All intra- and inter-day recovery values (85.7–103.3%) and RSD values (0.6–11.0%) were within the acceptable range as described in the US Food and Drug Administration guidelines.

3.2.6 | Extraction procedure

Given the high water content of the cornea (70–80% in the stroma), MeOH–H_2O (1:1) mixture was used as the extraction solvent to improve the extraction efficiency and to enable the simultaneous extraction of the six analytes from the cornea. The mean recovery percentages of the different analytes from the cornea ranged from 91 ± 8% to 107 ± 5% at three different concentrations. The only exception was CAN spiked at 100 ng where the percentage recovery was 116 ± 1%. Recovered concentrations and extraction efficiency (percentage recovery) of each analyte are presented in Table 7. The convenience and simplicity of this one-step extraction method made it ideal for routine sample analysis.

3.2.7 | Sample stability

Results of the stability study of the stock solutions of TMSPL and CAN at 1 mg/mL stored at −20°C showed stability over a period of at least 6 months since the IS normalized areas of each analyte after 6 months were within ±10% of the IS normalized areas obtained from the freshly prepared stock solutions (5.5 ± 0.0 and 5.8 ± 0.1 for TMSPL; 8.8 ± 0.0 and 9.3 ± 0.2 for CAN, for the freshly prepared stock solutions and after storage, respectively). RSD ranged from 0.4 to 2.2. Validation of the extraction procedure also confirmed the stability of the

TABLE 3 Matrix factor (MF) and IS normalized matrix factor of each analyte

Analyte	MF (%)	RSD (%)	IS normalized MF (%)	RSD (%)
Dexamethasone	82.9 ± 3.1	3.7	100.4 ± 4.2	4.2
Canrenoate potassium	80.4 ± 1.4	1.8	97.3 ± 2.3	2.3
Spironolactone	82.6 ± 3.6	4.3	100.0 ± 4.4	4.4
7α-Thiomethylspironolactone	83.4 ± 4.6	5.5	101.0 ± 5.0	4.9
Canrenone	84.2 ± 2.9	3.4	102.0 ± 3.2	3.2
17α-Methyltestosterone (IS)	82.6 ± 0.5	0.6	-	-

Values are given as mean ± SD of five determinations.

TABLE 4 Linearity range and typical equation of each analyte

Analyte	Linearity range (ng/mL)	Typical equation	R
Dexamethasone	05–1000	y = 0.2908x + 0.0262	1.000
Potassium canrenoate	05–1000	y = 0.5373x + 0.0118	1.000
Spironolactone	05–1000	y = 0.7387x + 0.0679	1.000
7α-Thiomethylspironolactone	05–1000	y = 0.5805x + 0.0495	1.000
Canrenone	05–1000	y = 0.9911x + 0.0912	1.000

y is the ratio between the peak area of each analyte to the peak area of the IS (17α-methyltestosterone); *x* is the ratio of the concentration of each analyte to the known concentration of the IS (100 ng/mL).

TABLE 5 Signal-to-noise (S/N), accuracy and precision (intra-day, inter-day 1 and 2) at the lower limit of quantification (LLOQ = 5 ng/mL) of each analyte

	S/N		Intra-day			Inter-day 1			Inter-day 2		
	Area LLOQ / Area Blank	RSD (%)	Measured concentration (ng/mL)	RSD (%)	Recovery (%)	Measured concentration (ng/mL)	RSD (%)	Recovery (%)	Measured concentration (ng/mL)	RSD (%)	Recovery (%)
DXM	9.6 ± 1.7	17.2	5.1 ± 0.5	10.2	102.9	5.1 ± 0.6	11.0	101.8	5.0 ± 0.5	11.0	99.4
CANK	12.0 ± 1.9	15.7	5.2 ± 0.5	9.0	103.9	5.4 ± 0.5	8.5	107.1	5.1 ± 0.5	9.5	101.7
SPL	19.3 ± 1.9	9.9	4.7 ± 0.5	10.1	94.7	5.2 ± 0.5	8.9	104.2	5.2 ± 0.5	9.3	103.5
TMSPL	36.2 ± 1.5	4.2	5.1 ± 0.2	3.0	102.9	5.2 ± 0.5	9.6	104.6	5.1 ± 0.5	8.9	102.0
CAN	42.9 ± 5.4	12.6	4.7 ± 0.5	10.0	94.6	5.0 ± 0.4	7.6	99.3	5.0 ± 0.4	8.8	100.5

DXM, Dexamethasone; CANK, potassium canrenoate; SPL, spironolactone; TMSPL, 7α-thiomethylspironolactone; CAN, canrenone.

Values are given as mean ± SD of 5 determinations for S/N and intra-day accuracy and precision, 10 determinations for inter-day 1 and 15 determinations for inter-day 2.

six analytes in the presence of the corneal matrix since they were left in contact with the corneal matrix overnight (~12 h) before they were recovered.

3.3 | Novelty of the method

As far as we are aware, there is no available validated UHPLC–MS method in the literature allowing the simultaneous detection and quantification of spironolactone and its main metabolites, TMSPL and CAN, in corneal tissues, within a relatively short runtime of 5 min. Indeed, recent LC–MS/MS methods have been published for the quantification of spironolactone and its metabolite, CAN, in human plasma but these methods did not include TMSPL (Dong, Xu, Zhang, Tian, & Chen, 2006; Lee, An, Kim, Shim, & Lee, 2015; Sora, Udrescu, Albu, David, & Medvedovici, 2010; van der Nagel, Versmissen, Bahmany, Gelder, & Koch, 2017; Vlase, Imre, Muntean, Achim, & Muntean, 2011) and the runtimes were relatively long (> 10 min; Dong, Xu, Zhang, Tian, & Chen, 2006; Sora, Udrescu, Albu, David, & Medvedovici, 2010; Takkis et al., 2017). Including TMSPL in the analytical method is of great importance, especially now that it is recognized as being one of the main active metabolites of spironolactone (Kaukonen, Vuorela, Vuorela, & Mannermaa, 1998; Sandall, Millership, Collier, & McElnay, 2006; Sora, Udrescu, Albu, David, & Medvedovici, 2010) and contributes significantly to the pharmacological effects observed (Kaukonen, Vuorela, Vuorela, & Mannermaa, 1998; Los, Pitzenberger, Ramjit, Coddington, & Colby, 1994; H. W. Overdiek, Hermens, & Merkus, 1985a; Sandall, Millership, Collier, & McElnay, 2006). The method described here enables a more complete characterization of the biotransformation of spironolactone in the cornea, and hence allows better understanding of the relative contributions of the different molecules to the underlying mechanism of action of spironolactone and its metabolites as mineralocorticoid receptor antagonists.

4 | CONCLUSION

To the best of our knowledge, this is the first analytical method developed and validated allowing the simultaneous quantification of spironolactone and its two main metabolites, i.e. TMSPL and CAN, potassium canrenoate and dexamethasone in ocular tissues. The sensitivity of this UHPLC-ESI-MS method enables quantification of concentrations <10 ng/mL with a relative short runtime of 5 min. In addition, the method brings real advantages in terms of high-throughput features given the one-step extraction method combined with a "one-shot" analysis of each sample since all of the analytes are detected and quantified simultaneously within 5 min, which constitutes a real time-saving when analyzing a large number of samples. This method was applied *in vivo* to quantify the corneal penetration and biotransformation of mineralocorticoid receptor antagonists following multiple topical instillation and to relate the concentrations to the observed pharmacological effects (Dahmana et al., 2018). That study showed that co-administration of a mineralocorticoid receptor antagonist together with the glucocorticoid countered the glucocorticoid-induced corneal delayed wound healing with a higher potency of spironolactone over potassium canrenoate. Finally, it should be

TABLE 6 Intra- and inter-day precision and accuracy of the method for each analyte

	Intra-day			Inter-day 1			Inter-day 2		
Theoretical (true) concentration (ng/mL)	Measured concentration (ng/mL)	RSD (%)	Recovery (%)	Measured concentration (ng/mL)	RSD (%)	Recovery (%)	Measured concentration (ng/mL)	RSD (%)	Recovery (%)
DXM									
10	9.9 ± 0.9	9.2	98.9	10.1 ± 0.9	8.5	100.7	10.2 ± 1.0	10.0	102.1
100	98.8 ± 1.5	1.5	98.8	96.4 ± 3.0	3.1	96.4	97.2 ± 3.4	3.5	97.2
500	511.0 ± 3.1	0.6	102.2	505.3 ± 5.8	1.2	101.1	513.6 ± 13.7	2.7	102.7
CANK									
10	8.6 ± 0.2	2.5	85.7	9.5 ± 1.0	10.0	95.3	9.6 ± 1.1	11.0	96.1
100	98.2 ± 1.0	1.0	98.2	95.3 ± 2.0	2.1	95.3	96.8 ± 4.6	4.8	96.8
500	502.7 ± 6.8	1.3	100.5	494.2 ± 6.2	1.3	98.8	502.2 ± 16.0	3.2	100.4
SPL									
10	9.1 ± 0.4	4.2	90.8	9.4 ± 0.5	5.0	93.8	9.5 ± 0.5	5.2	94.8
100	99.1 ± 1.2	1.2	99.1	97.3 ± 2.4	2.5	97.3	98.1 ± 3.1	3.2	98.1
500	516.7 ± 4.4	0.9	103.3	509.0 ± 4.9	1.0	101.8	516.6 ± 12.4	2.4	103.3
TMSPL									
10	9.5 ± 0.4	4.6	94.7	9.7 ± 0.8	8.1	97.3	9.6 ± 0.8	8.2	95.7
100	99.3 ± 2.1	2.1	99.3	96.8 ± 3.3	3.4	96.8	97.6 ± 3.3	3.3	97.6
500	515.2 ± 3.0	0.6	103.0	507.0 ± 7.5	1.5	101.4	514.8 ± 11.1	2.2	103.0
CAN									
10	8.7 ± 0.4	4.1	87.5	9.6 ± 0.6	6.3	95.7	9.5 ± 0.5	5.7	95.4
100	99.2 ± 2.1	2.1	99.2	96.8 ± 3.0	3.1	96.8	97.9 ± 3.7	3.8	97.9
500	516.1 ± 4.8	0.9	103.2	508.7 ± 7.2	1.4	101.7	515.4 ± 12.0	2.3	103.1

Values are given as means ± SD of five determinations for intra-day, 10 determinations for inter-day 1 and 15 determinations for inter-day 2.

TABLE 7 Recovered amounts and extraction efficiency of the different analytes after extraction from the corneas

Spiked amount (ng)	DXM	CANK	SPL	TMSPL	CAN
Recovered amount (ng)					
100	96 ± 10	99 ± 6	96 ± 4	103 ± 5	116 ± 1
400	428 ± 21	395 ± 25	365 ± 32	370 ± 32	406 ± 18
1000	982 ± 42	1028 ± 33	939 ± 48	981 ± 26	1039 ± 33
Extraction recovery (%)					
100	96 ± 10	99 ± 6	96 ± 4	103 ± 5	116 ± 1
400	107 ± 5	99 ± 6	91 ± 8	92 ± 8	101 ± 5
1000	98 ± 4	103 ± 3	94 ± 5	98 ± 3	104 ± 3

Values are given as mean ± SD of three different corneas spiked with the same amount of analytes at each concentration level.

possible to adapt the method for use with other biological matrices such as the skin to investigate the interplay between glucocorticoids and mineralocorticoid antagonists following different loco-regional applications and so develop novel pharmaceutical formulations.

ACKNOWLEDGMENTS

N.D. and Y.N.K. acknowledge financial support from the Swiss Commission for Technology and Innovation (CTI Project 19086.1 PFLS-LS) and Apidel SA (Geneva, Switzerland). Y.N.K. would like to thank the University of Geneva, the Fondation Ernst and Lucie Schmidheiny and the Société Académique de Genève for providing financial support to enable the acquisition of the Waters Xevo® TQ-MS detector.

ORCID

Yogeshvar N. Kalia http://orcid.org/0000-0001-9049-5489

REFERENCES

Abosehmah-Albidy, A. Z., York, P., Wong, V., Losowsky, M. S., & Chrystyn, H. (1997). Improved bioavailability and clinical response in patients with chronic liver disease following the administration of a spironolactone: beta-cyclodextrin complex. *British Journal of Clinical Pharmacology*, *44*(1), 35–39.

Bousquet, E., Beydoun, T., Rothschild, P. R., Bergin, C., Zhao, M., Batista, R., … Behar-Cohen, F. (2015). Spironolactone for nonresolving central serous chorioretinopathy: A randomized controlled crossover study. *Retina*, *35*(12), 2505–2515.

Chin, E. K., Almeida, D. R., Roybal, C. N., Niles, P. I., Gehrs, K. M., Sohn, E. H., … Folk, J. C. (2015). Oral mineralocorticoid antagonists for

recalcitrant central serous chorioretinopathy. *Clinical Ophthalmology*, *9*, 1449–1456.

Dahlof, C. G., Lundborg, P., Persson, B. A., & Regardh, C. G. (1979). Re-evaluation of the antimineralocorticoid effect of the spironolactone metabolite, canrenone, from plasma concentrations determined by a new high-pressure liquid-chromatographic method. *Drug Metabolism and Disposition*, *7*(2), 103–107.

Dahmana, N., Mugnier, T., Gabriel, D., Kaltsatos, V., Bertaim, T., Behar-Cohen, F., … Kalia, Y. N. (2018). Topical administration of spironolactone-loaded nanomicelles prevents glucocorticoid-induced delayed corneal wound healing in rabbits. *Molecular Pharmaceutics*, *15*(3), 1192–1202.

Daruich, A., Matet, A., Dirani, A., Gallice, M., Nicholson, L., Sivaprasad, S., & Behar-Cohen, F. (2016). Oral mineralocorticoid-receptor antagonists: Real-life experience in clinical subtypes of nonresolving central serous chorioretinopathy with chronic epitheliopathy. *Translational Vision Science and Technology*, *5*(2), 2.

Dong, H., Xu, F., Zhang, Z., Tian, Y., & Chen, Y. (2006). Simultaneous determination of spironolactone and its active metabolite canrenone in human plasma by HPLC-APCI-MS. *Journal of Mass Spectrometry*, *41*(4), 477–486.

Farman, N., Maubec, E., Poeggeler, B., Klatte, J. E., Jaisser, F., & Paus, R. (2010). The mineralocorticoid receptor as a novel player in skin biology: beyond the renal horizon? *Experimental Dermatology*, *19*(2), 100–107.

Ghadiali, Q., Jung, J. J., Yu, S., Patel, S. N., & Yannuzzi, L. A. (2016). Central serous chorioretinopathy treated with mineralocorticoid antagonists: A one-year pilot study. *Retina*, *36*(3), 611–618.

Herold, T. R., Prause, K., Wolf, A., Mayer, W. J., & Ulbig, M. W. (2014). Spironolactone in the treatment of central serous chorioretinopathy—a case series. *Graefes Archive of Clinical and Experimental Ophthalmology*, *252*(12), 1985–1991.

Herold, T. R., Rist, K., Priglinger, S. G., Ulbig, M. W., & Wolf, A. (2017). Long-term results and recurrence rates after spironolactone treatment in non-resolving central serous chorio-retinopathy (CSCR). *Graefes Archive of Clinical and Experimental Ophthalmology*, 255(2), 221–229.

International Conference on Harmonization of Technical Requirements for Registration of Pharmaceuticals for Human Use (2005). Validation of Analytical Procedures: Text and Methodology Q2 (R1).

Jankowski, A., Skorek-Jankowska, A., & Lamparczyk, H. (1996). Simultaneous determination of spironolactone and its metabolites in human plasma. *Journal of Pharmaceutical and Biomedical Analysis*, *14*(8–10), 1359–1365.

Kaukonen, A. M., Vuorela, P., Vuorela, H., & Mannermaa, J. P. (1998). High-performance liquid chromatography methods for the separation and quantitation of spironolactone and its degradation products in aqueous formulations and of its metabolites in rat serum. *Journal of Chromatography A*, *797*(1–2), 271–281.

Lee, J.-H., An, T.-G., Kim, S. J., Shim, W.-S., & Lee, K.-T. (2015). Development of liquid chromatography tandem mass spectrometry method for determination of spironolactone in human plasma: application to a bioequivalence study of Daewon Spiracton tablet® (spironolactone 50 mg). *Journal of Pharmaceutical Investigation*, *45*(6), 601–609.

Los, L. E., Pitzenberger, S. M., Ramjit, H. G., Coddington, A. B., & Colby, H. D. (1994). Hepatic metabolism of spironolactone. Production of 3-hydroxy-thiomethyl metabolites. *Drug Metabolism and Disposition*, *22*(6), 903–908.

Maubec, E., Laouenan, C., Deschamps, L., Nguyen, V. T., Scheer-Senyarich, I., Wackenheim-Jacobs, A. C., … Farman, N. (2015). Topical mineralocorticoid receptor blockade limits glucocorticoid-induced epidermal atrophy in human skin. *Journal of Investigative Dermatology*, *135*(7), 1781–1789.

van der Nagel, B. C. H., Versmissen, J., Bahmany, S., van Gelder, T., & Koch, B. C. P. (2017). High-throughput quantification of 8 antihypertensive drugs and active metabolites in human plasma using UPLC-MS/MS. *Journal of Chromatography B: Analytical Technology in Biomedicine and Life Sciences*, *1060*, 367–373.

Nguyen, V. T., Farman, N., Maubec, E., Nassar, D., Desposito, D., Waeckel, L., … Jaisser, F. (2016). Re-epithelialization of pathological cutaneous wounds is improved by local mineralocorticoid receptor antagonism. *Journal of Investigative Dermatology*, *136*(10), 2080–2089.

Overdiek, H. W., Hermens, W. A., & Merkus, F. W. (1985a). New insights into the pharmacokinetics of spironolactone. *Clinical Pharmacological Therapy*, *38*(4), 469–474.

Overdiek, J. W., Hermens, W. A., & Merkus, F. W. (1985b). Determination of the serum concentration of spironolactone and its metabolites by high-performance liquid chromatography. *Journal of Chromatography B*, *341*, 279–285.

Ramsay, L., Shelton, J., Harrison, I., Tidd, M., & Asbury, M. (1976). Spironolactone and potassium canrenoate in normal man. *Clinical Pharmacological Therapy*, *20*(2), 167–177.

Salehi, M., Wenick, A. S., Law, H. A., Evans, J. R., & Gehlbach, P. (2015). Interventions for central serous chorioretinopathy: A network meta-analysis. *Cochrane Database of Systematic Reviews*, *12*, CD011841. https://doi.org/10.1002/14651858.CD011841.pub2

Sandall, J. M., Millership, J. S., Collier, P. S., & McElnay, J. C. (2006). Development and validation of an HPLC method for the determination of spironolactone and its metabolites in paediatric plasma samples. *Journal of Chromatography B*, *839*(1–2), 36–44.

Sherry, J. H., O'Donnell, J. P., & Colby, H. D. (1986). Separation of spironolactone and its biologically active sulfur-containing metabolites by high-performance liquid chromatography. *Journal of Chromatography B*, *374*, 183–190.

Sica, D. A. (2005). Pharmacokinetics and pharmacodynamics of mineralocorticoid blocking agents and their effects on potassium homeostasis. *Heart Failure Reviews*, *10*(1), 23–29.

Sora, D. I., Udrescu, S., Albu, F., David, V., & Medvedovici, A. (2010). Analytical issues in HPLC/MS/MS simultaneous assay of furosemide, spironolactone and canrenone in human plasma samples. *Journal of Pharmaceutical and Biomedical Analysis*, *52*(5), 734–740.

Suyagh, M. F., Kole, P. L., Millership, J., Collier, P., Halliday, H., & McElnay, J. C. (2010). Development and validation of a dried blood spot-LC-APCI-MS assay for estimation of canrenone in paediatric samples. *Journal of Chromatography B*, *878*(9–10), 769–776.

Takkis, K., Aro, R., Kõrgvee, L.-T., Varendi, H., Lass, J., Herodes, K., & Kipper, K. (2017). Signal enhancement in the HPLC-ESI-MS/MS analysis of spironolactone and its metabolites using HFIP and NH4F as eluent additives. *Analytical and Bioanalytical Chemistry*, *409*(12), 3145–3151.

US Food and Drug Administration. (2001). Guidance for Industry: Bioanalytical Method Validation. Rockville, MD.

van Dijk, E. H., Nijhoff, M. F., de Jong, E. K., Meijer, O. C., de Vries, A. P., & Boon, C. J. (2016). Central serous chorioretinopathy in primary hyperaldosteronism. *Graefes Archive of Clinical and Experimental Ophthalmology*, *254*(10), 2033–2042.

Vlase, L., Imre, S., Muntean, D., Achim, M., & Muntean, D.-L. (2011). Determination of spironolactone and canrenone in human plasma by high-performance liquid chromatography with mass spectrometry detection. *Croatica Chemica Acta*, *84*(3), 361–366.

How to cite this article: Dahmana N, Gabriel D, Gurny R, Kalia YN. Development and validation of a fast and sensitive UHPLC-ESI-MS method for the simultaneous quantification of spironolactone and its metabolites in ocular tissues. *Biomedical Chromatography*. 2018;e4287. https://doi.org/10.1002/bmc.4287

molecular pharmaceutics

Article

Cite This: Mol. Pharmaceutics 2018, 15, 1192−1202

Topical Administration of Spironolactone-Loaded Nanomicelles Prevents Glucocorticoid-Induced Delayed Corneal Wound Healing in Rabbits

Naoual Dahmana,[†] Thibault Mugnier,[‡] Doris Gabriel,[‡] Vassilios Kaltsatos,[§] Thierry Bertaim,[§] Francine Behar-Cohen,[⊥,¶] Robert Gurny,[†,‡] and Yogeshvar N. Kalia*[,†]

[†]School of Pharmaceutical Sciences, University of Geneva & University of Lausanne, CMU - 1 rue Michel Servet, 1211 Geneva 4, Switzerland

[‡]Apidel SA, 29 Quai du Mont Blanc, 1201 Geneva, Switzerland

[§]CEVA Santé Animal, 10 Avenue de la Ballastière, 33500 Libourne, France

[⊥]Fondation Asile des Aveugles, Hôpital Ophtalmique Jules-Gonin, 15 Avenue de France, 1004 Lausanne, Switzerland

[¶]INSERM, UMRS 872 Team 17, Centre de Recherche des Cordeliers, 15 rue de l'Ecole de Médecine, 75006 Paris, France

Supporting Information

ABSTRACT: The objective was to investigate whether mineralocorticoid receptor antagonism using a novel topical micellar formulation of spironolactone could prevent glucocorticoid-induced delayed corneal wound healing in New Zealand white rabbits. Spironolactone micelles (0.1%, w/v) with a mean number weighted diameter of 20 nm were prepared using a pegylated copolymer (mPEG-dihexPLA) and showed a preliminary stability of at least 12 months at 5 °C. Preclinical studies in New Zealand white rabbits demonstrated that the 0.1% spironolactone micellar formulation was well-tolerated since no reaction was observed in the cornea following multiple daily instillation over 5 days. As expected, the preclinical studies also confirmed that dexamethasone significantly delayed epithelial wound healing as compared to untreated control (percentage re-epithelialization after day 4: 84.6 ± 13.9% versus 99.5 ± 1.0% for the control, $p < 0.05$). However, the addition of the 0.1% spironolactone micellar formulation significantly improved the extent of re-epithelialization, countering the dexamethasone induced delayed wound healing with a percentage re-epithelialization that was statistically equivalent to the control (96.9 ± 7.3% versus 99.5 ± 1.0%, $p > 0.05$). The biodistribution study provided insight into the ocular metabolism of spironolactone and hence the relative contributions of the parent molecule and its two principal metabolites, 7α-thiomethylspironolactone and canrenone, to the observed pharmacological effects. Comparison of the efficacies of spironolactone and potassium canrenoate (a water-soluble precursor of canrenone) in overcoming the dexamethasone-induced delayed wound healing confirmed that the former had greater efficacy. The results pointed to the greater potency of 7α-thiomethylspironolactone over canrenone as a mineralocorticoid receptor antagonist, which explained its superior ability in countering the glucocorticoid-induced overactivation that was responsible for the delayed wound healing. In conclusion, the preliminary results supported the above-mentioned hypothesis suggesting that coadministration of mineralocorticoid receptor antagonists to patients under glucocorticoid therapy might prevent the deleterious effects of glucocorticoids on complex corneal wound healing processes.

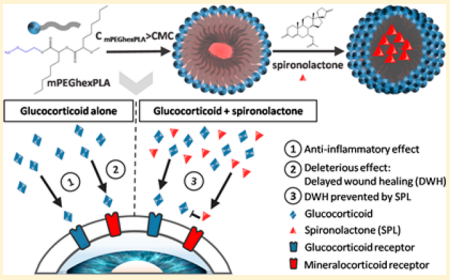

KEYWORDS: *glucocorticoids, corneal wound healing, spironolactone, polymeric micelles, in vivo preclinical study, ultrahigh performance liquid chromatography, mass spectrometry*

INTRODUCTION

Impaired wound healing is a significant clinical problem encountered as a complication of certain chronic conditions such as diabetes, sickle cell disease, Cushing syndrome, and also in patients receiving prolonged glucocorticoid therapy.[1,2] Impaired corneal wound healing is a major concern in ophthalmology since it can cause chronic infection and ulceration resulting in corneal opacity and scarring responsible for major visual disturbance that may ultimately lead to blindness.[3,4]

Wound healing is a complex and highly organized process that encompasses successive and overlapping stages including inflammation, granular tissue formation and re-epithelialization, new matrix formation, and collagen accumulation. The whole process is tightly controlled by a precise and complex interplay of various factors involving cells, growth factors, cytokines, and

Received: November 17, 2017
Revised: February 2, 2018
Accepted: February 4, 2018
Published: February 4, 2018

DOI: 10.1021/acs.molpharmaceut.7b01028
Mol. Pharmaceutics 2018, 15, 1192−1202

components of the extracellular matrix.[1,2,5−8] While wound healing follows a uniform pattern all over the body, local specificities exist resulting from tissue-specific differences, for example, lack of vessels in the cornea compared to the skin.[8] The critical feature of wound healing is the restoration of the epithelial barrier. Re-epithelialization in the cornea is a key step in preventing abnormal healing and subsequent impaired vision.[6] During this process, corneal epithelial cells proliferate at the wound edge, migrate to cover the lesioned area, and differentiate to form the new tissue. Absence of cell migration is related to the clinical phenotype of chronic nonhealing wounds. When total re-epithelialization is achieved, the barrier is restored and the eye is again protected from external infections.[2,3,5,6,8]

Synthetic glucocorticoids (GC) are among the most widely prescribed drugs in the world. They are given systemically or topically to treat a wide number of inflammatory and autoimmune diseases, allergies, and ocular disorders. In ophthalmology, GC are currently used to prevent and treat postoperative ocular inflammation, graft rejection, and corneal neovascularization; they are also indicated for the treatment of many ocular surface disorders including dry eye.[2,7,9,10] While the pleiotropic anti-inflammatory effects of GC reduce cytotoxic and pro-angiogenic cytokines and metalloproteinase expression,[11] they are also associated with delayed wound healing.[2,8,12] Several *in vivo* studies have reported that the use of GC such as dexamethasone resulted in delayed corneal wound healing in rabbits.[4,7,13,14] More significantly, GC treatment also leads to reduced and delayed wound re-epithelialization in humans.[15] In a clinical trial, 42 patients who received topical prednisolone phosphate were found to re-epithelialize more slowly than the placebo group.[4]

GC bind to the glucocorticoid receptor (GR), but they can also bind with high affinity to the closely related mineralocorticoid receptor (MR); both receptors are expressed in the corneal epithelium. Recent studies have reported that, in the skin, delayed wound healing might be due to illicit occupancy of the MR by GC. In mineralocorticoid-sensitive tissues like the kidney, GC are inactivated by the enzyme 11β-hydroxysteroid dehydrogenase type II (HSD2), thereby preventing their binding to MR, which is therefore selectively activated by aldosterone, the endogenous mineralocorticoid (MC) that binds to the MR and is responsible for sodium homeostasis.[2,9,12,16−18] However, tissues where HSD2 activity is low such as skin, eye, heart, and neurons are susceptible to off-target GC binding to the MR.

Given that the MR might be overactivated by GC in tissues where HSD2 activity is low, the use of a MR antagonist (MRA) was proposed as a potential therapeutic strategy to overcome the negative impact of GC treatment on wound healing. This hypothesis was verified in several studies: (i) in cultured human skin explants where clobetasol-induced epidermal atrophy was significantly limited by the MRA, potassium canrenoate, and eplerenone;[2,9] (ii) in mice where potassium canrenoate significantly improved clobetasol-induced delayed wound healing;[2] and (iii) in healthy volunteers, where local coadministration of the MRA, spironolactone, with clobetasol significantly improved the clobetasol-induced impairment of skin wound closure.[9] Spironolactone is a potent MRA, which competes with aldosterone to bind to the MR, and is marketed mainly as a diuretic (potassium-sparing) for the treatment of congestive heart failure, essential hypertension and various oedematous conditions.[19,20] Spironolactone is pharmacologically active, but it also exerts its effect via two main metabolites: 7α-thiomethylspironolactone and canrenone.[21−23]

The objective of the present study was to investigate whether, as in the case of the skin, GC-induced delayed corneal wound healing could be reversed by MR antagonists. To test this hypothesis, a novel micellar formulation of spironolactone (0.1%, w/v) was developed and characterized for topical ocular administration and then evaluated to determine whether it was possible to counter the impaired corneal wound healing induced by dexamethasone in New Zealand white rabbits. It was decided to compare the results to those observed after topical application of a lower concentration micellar formulation of spironolactone (0.01%, w/v) and a formulation containing the water-soluble prodrug, potassium canrenoate (0.1%, w/w), which is a precursor of canrenone. To provide an insight on the role played by the different aforementioned molecules in the process of re-epithelialization, an analytical method allowing the simultaneous quantification of spironolactone and its two main metabolites; 7α-thiomethylspironolactone and canrenone; potassium canrenoate and dexamethasone was developed and validated. Although aqueous solutions are the most suitable and convenient dosage form for topical delivery to the eye, spironolactone has a very low aqueous solubility (0.02 mg/mL). Therefore, methoxy-poly(ethylene glycol)-dihexyl-substituted-poly(lactic acid) (mPEG-dihexPLA) diblock copolymer was used to prepare spironolactone micelles to increase its aqueous solubility. This biodegradable self-assembling copolymer has proven safety in rabbits and enhanced drug bioavailability following topical application to the eye.[24−26]

EXPERIMENTAL SECTION

Materials. Methoxy-poly(ethylene glycol)-dihexyl-substituted-poly(lactic acid)[27] (mPEG-dihexPLA, 5.5 kDa, Scheme 1A) was supplied by Apidel SA (Geneva, Switzerland).

Scheme 1. Chemical Structure of (A) mPEG-dihexPLA Copolymer and (B) Spironolactone

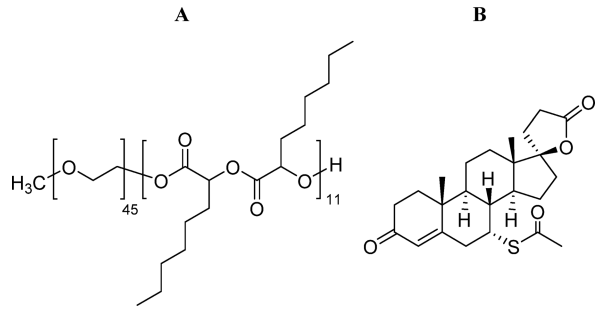

Spironolactone (SPL, Scheme 1B) was purchased from Zhejiang Langhua Pharmaceutical Co., Ltd. (Zhejiang, China). 7α-Thiomethylspironolactone (TMSPL) was purchased from TLC Pharmaceutical Standards Ltd. (Ontario, Canada). Canrenone (CAN), potassium canrenoate (CANK), and 17α-methyltestosterone (MeT), used as an internal standard (IS), were purchased from Sigma-Aldrich (Buchs, Switzerland). Dexamethasone (DXM) was purchased from Tianjin TianMao Technology Development Corp. Ltd. (Tianjin, China). Maxidex (dexamethasone 0.1% suspension, Alcon) was purchased from a local pharmacy. Sodium chloride was obtained from Hänseler AG (Herisau, Switzerland). Ultrapure water (H_2O, resistivity >18 MΩ cm) was prepared

DOI: 10.1021/acs.molpharmaceut.7b01028
Mol. Pharmaceutics 2018, 15, 1192−1202

using a Merck Millipore Milli-Q water purification system (Darmstadt, Germany). Methanol (MeOH, HPLC grade) was obtained from Fisher Scientific (Waltham, MA, USA) and acetonitrile (ACN, HPLC grade) and formic acid (ULC/MS grade) from Biosolve (Dieuze, France). Acetone Chromasolv (HPLC grade) was purchased from Sigma-Aldrich (Buchs, Switzerland), and trifluoroacetic acid was obtained from VWR (Dietikon, Switzerland). All other chemicals were at least of analytical grade. Millex filters (Durapore PVDF, pore size 0.22 μm, diameter 13 mm) were purchased from Sigma-Aldrich (Buchs, Switzerland). Ten milliliter sterile eye drop vials were purchased from Müller + Krempel AG (Bülach, Switzerland).

Analytical Methods. *HPLC Methods.* HPLC methods were developed to support formulation development and stability studies of both spironolactone micelles and the potassium canrenoate solution.

Quantification of Spironolactone by HPLC-UV. Spironolactone quantification was performed on an Agilent 1100 HPLC using a reversed phase column (YMC basic, 250 mm × 3.0 mm, 5 μm) heated to 40 °C. The method employed a gradient of acetonitrile and water containing 0.1% trifluoroacetic acid: the acetonitrile percentage was increased from 40% to 80% over 5 min, kept constant for 3 min, and then decreased to 40% within half a minute. The mobile phase flow rate was 1.0 mL/min and the UV detector was set to 238 nm.

Quantification of Potassium Canrenoate by HPLC-UV. Potassium canrenoate quantification was performed on an Agilent 1100 HPLC using a reversed phase column (YMC basic, 250 mm × 3.0 mm, 5 μm) heated to 40 °C. The mobile phase consisted of acetonitrile containing 0.1% trifluoroacetic acid (A) and water containing 0.1% trifluoroacetic acid (B). The analysis was carried out in isocratic mode with 55% eluent A and 45% eluent B. The mobile phase flow rate was 1.0 mL/min and the UV detector was set to 286 nm.

UHPLC−MS Method. A UHPLC−MS analytical method was developed and validated to enable the simultaneous quantification of the different analytes in the rabbit corneas obtained from the *in vivo* study. Briefly, the liquid chromatographic system consisted of a Waters Acquity ultra performance liquid chromatography (UPLC) system (Baden-Dättwil, Switzerland) including a binary solvent manager, a sample manager with an injection loop volume of 10 μL, and a column manager. The reversed phase chromatographic separation of the six compounds was performed on a Waters XBridge BEH C18 column (50 mm × 2.1 mm I.D., 2.5 μm) fitted with a Waters XBridge BEH C18 Vanguard precolumn (5 mm × 2.1 mm I.D., 2.5 μm). The elution was carried out in isocratic mode with a mobile phase consisting of 0.1% formic acid in H_2O/MeOH (48/52, v/v) with a flow rate of 0.45 mL/min and a run time of 5 min. Column temperature was held at 40 °C, and sample manager temperature was kept at room temperature. Injection volume was set at 5 μL. The mass spectrometry (MS) system consisted of a Waters XEVO TQ-MS detector (Baden-Dättwil, Switzerland) fitted with a Z-spray electrospray ionization source. MS detection of the six compounds was performed using electrospray ionization in the positive mode (ESI+) and selected ion recording (SIR) using the pseudomolecular ion of each compound as the parent ion (hydrogen adduct, $[M + H]^+$). The capillary voltage was set at 2.3 kV, and desolvation gas temperature and flow were maintained at 350 °C and 650 L/h, respectively. The specific MS parameters for each analyte were tuned and determined by infusing each compound individually at 1 μg/mL in MeOH:H_2O (1:1) at a flow rate of 5 μL/min. Identification and quantification of each analyte were carried out according to the mass-to-charge ratio (m/z) of the pseudomolecular ion of each compound (hydrogen adduct, $[M + H]^+$). Cone voltage optimal settings were 15 V for DXM, 32 V for CANK, and 35 V for SPL, TMSPL, CAN, and MeT. The pseudomolecular parent ion corresponding to DXM, CANK, SPL/CAN, TMSPL, and MeT had an m/z of 393.1, 359.1, 341.0, 389.0, and 303.0, respectively. Dwell time was set at 5 ms for all the compounds except for DXM at 328 ms. Data processing was performed using Waters MassLynx software version 4.1 (Baden-Dättwil, Switzerland).

Calibration standards at 10, 20, 50, 100, 200, 500, and 1000 ng/mL were prepared in a corneal matrix obtained from porcine corneas extracted in MeOH:H_2O (1:1). All calibration curves were linear ($r^2 > 0.99$). The limit of detection (LOD) and the limit of quantification (LOQ) for each analyte are summarized in Table 1.

Table 1. Limit of Determination (LOD) and Limit of Quantification (LOQ) of Each Analyte in Corneal Matrix

analyte	LOD (ng/mL)	LOQ (ng/mL)
dexamethasone	5.4	16.3
potassium canrenoate	2.4	7.2
spironolactone	3.8	11.4
7α-thiomethyspironolactone	1.3	3.9
canrenone	2.9	8.8

Development and Optimization of Spironolactone Micellar Formulation. Spironolactone loaded micelles (0.1%, w/v) were prepared using mPEG-dihexPLA copolymer at different SPL:copolymer ratios: 1:20, 1:40, and 1:60. Two buffers were also evaluated: citrate buffer (10 mM, pH 5.5) and PBS (10 mM, pH 7.4). Formulations were prepared at a batch size of 10 mL. Briefly, 10 mg of spironolactone was dissolved in 2 mL of acetone. Then 200, 400, or 600 mg of mPEG-dihexPLA, corresponding respectively to 1:20, 1:40, or 1:60 SPL:copolymer ratios, was added to the acetone solution containing SPL and dissolved. Subsequently, this solution was added dropwise using a syringe pump (6 mL/h) under sonication (20% amplitude, S 450 D, Branson, USA) to 10 mL of the aqueous phase, consisting of either citrate buffer (10 mM, pH 5.5) or PBS (10 mM, pH 7.4). Then acetone was removed under reduced pressure (58 °C, 180 mbar, Buchi Rotavapor R-210, Switzerland). Finally, the osmolarity was adjusted to 270−300 mOsm with NaCl and the formulations filtered under a laminar flow hood through 0.22 μm PVDF filters into sterilized vials and kept at 5 °C. Formulations were characterized in terms of concentration, drug loading, incorporation efficiency, and micelle size. Micelles were also visualized using transmission electron microscope (TEM, FEI Tecnai G2 Sphera, Oregon, USA). Briefly, the micellar formulation was diluted 1:10 in Milli-Q water, then 5 μL was deposited on a grid, left for 30 s, and the excess was carefully wiped. Subsequently, one drop of 2% uranyl acetate was applied during 30 s to enhance the contrast, and the excess was carefully removed. TEM magnification was set at 25 000×.

Determination of Drug Content and Incorporation Efficiency. Spironolactone content was quantified by HPLC-UV. Aliquots from spironolactone micellar formulations were diluted with acetonitrile (1:10) prior to HPLC analysis. Drug loading and incorporation efficiency were calculated using the following equations:

DOI: 10.1021/acs.molpharmaceut.7b01028
Mol. Pharmaceutics 2018, 15, 1192−1202

$$\text{Drug Loading (mg/g)} = \frac{\text{Mass of drug incorporated in micelles (mg)}}{\text{Mass of copolymer used (g)}} \quad (1)$$

$$\text{Incorporation Efficiency (\%)} = \frac{\text{Actual drug loading}}{\text{Target drug loading}} \times 100 \quad (2)$$

Size Determination. The intensity weighted (Z-average, Z_{av}) and the number weighted (d_n) hydrodynamic diameters and the polydispersity index (PDI) of the micelles were measured by dynamic light scattering using the Zetasizer Nano-ZS (Malvern Instruments, UK). SPL micellar solutions were diluted 1:1 in Milli-Q water and filled into disposable plastic cuvettes for analysis with back scattering light (173 degrees).

Preparation and Characterization of the Formulations Used *in Vivo*. *Spironolactone Micellar Formulations (0.1% and 0.01%, w/v).* Spironolactone loaded micelles (0.1%, w/v) were prepared at a batch scale of 14 mL. Briefly, 616 mg of mPEG-dihexPLA and 15.4 mg of spironolactone were dissolved in 2 mL of acetone. The organic phase was added dropwise (6 mL/h) to the aqueous phase (10 mM citrate buffer, 0.7% NaCl, pH 5.5) under sonication (20% amplitude, S 450 D, Branson, USA). Subsequently, acetone was removed under reduced pressure (58 °C, 180 mbar, Buchi Rotavapor R-210, Switzerland). This formulation was prepared with 10% excess (by weight) to counterbalance the amount of SPL and mPEG-dihexPLA lost in the syringe during the formulation process. The 0.01% (w/v) SPL concentration was obtained by 1:10 dilution of the 0.1% SPL micelles in the aqueous phase. Finally, formulations were filtered through 0.22 μm PVDF filters and stored in sterile eye drop vials. Spare aliquots from both formulations were kept for stability testing.

Potassium Canrenoate Solution (0.1%, w/w). Potassium canrenoate solution (0.1%, w/w) was prepared by dissolving 50 mg potassium canrenoate in 50 g of aqueous buffer (5 mM phosphate buffer, 0.9% NaCl, pH 8.0). This solution was filtered through 0.22 μm PVDF filters and stored in sterile eye drop vials. Spare aliquots were kept for stability testing of the formulation.

***In Vivo* Tolerability and Efficacy Study in Rabbits.** *Animals.* Fifty male albino New Zealand rabbits, weighing approximately 2.3−3.0 kg, were included in the study (Iris Pharma, France). Animals were housed individually in standard cages, under identical environmental conditions. The temperature was kept at 15−21 °C, and the relative humidity was >45%. Rooms were continuously ventilated (≥15 air volumes per hour). Temperature and relative humidity were continuously controlled and recorded. Animals were routinely exposed (in-cage) to a 10−200 lx light in a 12-h light/dark cycle (from 7:00 a.m. to 7:00 p.m.). Animals had enrichment and free access to food (150 g/day) and were allowed water *ad libitum*. All animals were healthy and free of clinically observable ocular abnormalities throughout the study. All animals were treated according to the Directive 2010/63/EU, The European convention on the protection of animals used for scientific purposes, and to the Association for Research in Vision and Ophthalmology (ARVO) Statement for the use of animals in ophthalmic and visual research. The studies were approved by the local veterinary authority for animal experimentation (French governmental platform APAFIS, authorization number 20160212659386).

Induction of Corneal Wounds. Animals were anesthetized by intramuscular injection of a ketamine-xylazine mixture. Then a drop of 0.4% oxybuprocaine was topically applied for local anesthesia. In addition, buprenorphine (20 μg/kg) was administered, by subcutaneous injection, 30 min prior to wound induction to prevent pain. A scalpel handle was used to keep the right eye out of orbit, then the corneal epithelium was completely removed using a scalpel blade. De-epithelialization was monitored by fluorescein staining. Finally, eyes were washed with physiological saline and swabbed with a dry cotton tip applicator to remove cellular debris.

Study Design. Animals were randomized into five treatment groups as presented in Table 2. Each group included 10 rabbits,

Table 2. Treatment Received Per Animal Group

group	rabbit no.	left eye	right eye
1	01−10	control	0.1% spironolactone micelles + 0.1% dexamethasone
2	11−20	control	0.01% spironolactone micelles + 0.1% dexamethasone
3	21−30	control	0.1% potassium canrenoate solution + 0.1% dexamethasone
4	31−40	control	PBS
5	41−50	control	0.1% dexamethasone

and the animals were instilled in the right eye every 1.50 ± 0.15 h using an eye-dropper, three times daily on Day 0, six times daily from Day 1 to Day 4, and once on Day 5.

Groups 1, 2, and 3. Animals received the formulations containing the mineralocorticoid receptor antagonist (0.1% spironolactone micelles, 0.01% spironolactone micelles, and 0.1% potassium canrenoate solution, respectively): 1 drop (∼35 μL) of the formulation, then 5 min later, 1 drop of 0.1% dexamethasone (Maxidex).

Group 4 (Positive Control). Animals received only PBS (control): 2 drops of PBS with 5 min interval between each administration.

Group 5 (Negative Control). Animals received 1 drop of PBS, then 5 min later, 1 drop of 0.1% dexamethasone (Maxidex).

On Day 5, 30 min after the last assessment of tolerability, animals received the last instillation (1 drop in the right eye). Subsequently, rabbits were euthanized, both eyes were enucleated, and corneas were harvested and stored at −80 °C until analysis.

Ocular Tolerability. An ophthalmoscope was used for accurate examination of the conjunctiva, cornea, and iris. Both eyes of each rabbit were examined using the ophthalmoscope during the pretest period (baseline), then once daily after the last administration of the day from Day 0 to Day 4. The observations were scored using the Draize scale (Table S1).

Corneal Wound Healing. The size of the corneal wound was evaluated using the fluorescein test, immediately after ocular debridement and once a day before the first instillation. A baseline was recorded before the de-epithelialization (Table S2). One drop of fluorescein was instilled to the right (lesioned) eye, and then the cornea was illuminated with blue light. Images of the corneal lesion (area stained by fluorescein) were taken using a CCD camera and analyzed using image J software. Percentage of re-epithelialization was calculated as follows:

DOI: 10.1021/acs.molpharmaceut.7b01028
Mol. Pharmaceutics 2018, 15, 1192−1202

Table 3. Characterization of Different Formulations of Spironolactone

buffer	formulation name	ratio[a]	target [SPL][b] (mg/mL)	[SPL] ± SD (mg/mL)	target DL[c] (mg/g)	actual DL ± SD (mg/g)	IE[d] ± SD (%)	size (nm) d_n	Z_{av}	PDI
citrate	A20	1:20	1	0.49 ± 0.01	50.0	24.5 ± 0.5	49.0 ± 1.0	13	53	0.2
	A40	1:40	1	0.89 ± 0.00	25.0	22.3 ± 0.1	89.1 ± 0.2	17	50	0.2
	A60	1:60	1	0.85 ± 0.01	16.7	14.2 ± 0.1	84.8 ± 0.7	16	50	0.2
PBS	B20	1:20	1	0.45 ± 0.02	50.0	22.4 ± 1.0	44.8 ± 2.0	31	55	0.2
	B40	1:40	1	0.73 ± 0.00	25.0	18.2 ± 0.1	72.9 ± 0.3	25	56	0.2
	B60	1:60	1	0.84 ± 0.01	16.7	14.0 ± 0.1	83.6 ± 0.6	19	52	0.2

[a]Spironolactone/copolymer ratio. [b]Spironolactone concentration. [c]Drug loading. [d]Incorporation efficiency.

$$\%\ \text{Re-epithelialization (Day } x) = \%\ \text{Wounded Area(Day 0)} - \%\ \text{Wounded Area(Day } x) \quad (3)$$

Animal Sacrifice and Sampling. At the end of the measurement period, animals were euthanized by an intracardiac injection of overdosed pentobarbital following anesthesia by intramuscular injection of ketamine-xylazine mixture. This method is one of the recommended methods for euthanasia by the European authorities. Immediately after euthanasia, both eyes were enucleated, and corneas were dissected and stored at −80 °C until analysis.

Extraction and Quantification of the Drugs in the Cornea. The extraction method of the drugs from the cornea was validated prior to use. The 50 treated and 50 control corneas stored at −80 °C were thawed at room temperature, weighed, and ground manually into small pieces, which were placed in a glass vial containing 1 mL of MeOH/H_2O (1:1) and 100 ng/mL internal standard (IS, 17α-methyltestosterone). The vials were left under stirring at 300 rpm overnight for extraction. The following day, samples were centrifuged during 20 min at 12 000 rpm, and the supernatants were quantified using the validated UHPLC−MS method.

Statistical Analysis. Statistical analysis on the percentage re-epithelialization of the corneas in the rabbits from the different groups was performed using Kruskal−Wallis one-way analysis of variance on ranks followed by Student−Newman−Keuls posthoc analysis. Statistical analysis on the mean concentrations found in the left and right corneas was performed using Student *t* test or Mann−Whitney rank sum test.

RESULTS

Spironolactone Micelles Formulation and Optimization. The incorporation efficiency of SPL in the mPEG-dihexPLA micelles varied according to the SPL:copolymer ratio and was also influenced by the buffer used. Overall, the formulation containing SPL and mPEG-dihexPLA copolymer at a ratio of 1:40 and citrate buffer (buffer A; 10 mM, pH 5.5) as the aqueous phase (Formulation A40) achieved the best incorporation efficiency of 89.1 ± 0.2% corresponding to a drug loading of 22.3 ± 0.1 mg/g (Table 3). In the case of PBS (buffer B; 10 mM, pH 7.4), the highest incorporation efficiency, of 83.6 ± 0.6%, was achieved with SPL:copolymer ratio of 1:60 (Formulation B60) corresponding to a drug loading of 14.0 ± 0.1 mg/g (Table 3). The difference of ∼5% in incorporation efficiency may have been due to the different ionic strengths of the buffer solutions (citrate buffer, 50 mM; PBS buffer, 167 mM). The intensity weighted micelle diameters (Z_{av}) for Formulation A40 and B60 were 50 and 52 nm, respectively, and the corresponding number weighted micelle diameters (d_n) were 17 and 19 nm (PDI = 0.2) (Table 3). The spherical and homogeneous aspect of the spironolactone loaded micellar nanocarriers are clearly discerned in Figure 1.

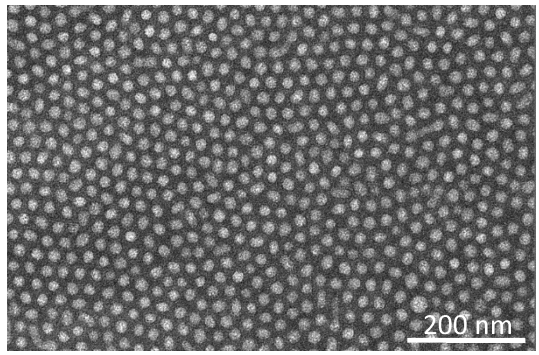

Figure 1. Transmission electron microscopy (TEM) image of the optimized 0.1% spironolactone loaded micelles.

The stability of Formulations A40 and B60 was monitored during one month at 5 °C. Results showed that Formulation A40 remained stable over one month with respect to the concentration, pH and osmolarity versus 2 weeks for Formulation B60. Micelle size was stable over a period of one month after storage at 5 °C for both formulations (d_n, Z_{av}, and PDI were 19 nm, 62 nm, and 0.2, respectively, for Formulation A40 and 25 nm, 55 nm, and 0.2, respectively, for Formulation B60). Formulation A40 was optimized to achieve 100% incorporation efficiency corresponding to a SPL concentration of 1 mg/mL. During the formulation development, it was noticed that a small amount of SPL and mPEG-dihexPLA was lost in the syringe during addition to the aqueous solution. To correct for this loss, it was decided to prepare the formulations with 10% excess (by weight) of spironolactone and mPEG-dihexPLA, corresponding to the amount lost during the formulation process. Given the higher incorporation efficiency and the superior stability, Formulation A40 was selected as the lead formulation to be used in further studies.

Characterization of Formulations Used *in Vivo*. The stability of the 0.01% and 0.1% spironolactone micellar formulations was assessed over 12 months at 5 °C. Concentration, pH, and micelle size remained perfectly stable over the 12 month period. The stability of the 0.1% potassium canrenoate solution was assessed over 24 days at 5 °C, to ensure product stability for the duration of the animal study. Results showed that the concentration and pH remained stable over the desired study period. Formulation characteristics are summarized in Table 4.

DOI: 10.1021/acs.molpharmaceut.7b01028
Mol. Pharmaceutics 2018, 15, 1192−1202

Table 4. Characterization of Formulations Used During *in Vivo* Study

formulation	conc.[a] ± SD (mg/mL)	pH	size (nm) d_n	Z_{av}	PDI
0.1% spironolactone micelles	1.03 ± 0.00	5.5	20	48	0.2
0.01% spironolactone micelles	0.10 ± 0.00	5.5	26	49	0.2
0.1% potassium canrenoate solution	0.95 ± 0.00	8.0	-	-	-

[a]Measured concentration of spironolactone or potassium canrenoate.

Tolerability and Efficacy Study in New Zealand White Rabbits. *Ocular Tolerability.* Results of the ocular examinations of the animals on Day 4 are reported per treatment group in Table 5. Conjunctival redness, chemosis, discharge, iritis, and corneal opacities were scored according to the Draize scale (Table S1). Most of the ocular reactions observed were slight and transient and were not attributed to the treatment since they are commonly observed in the de-epithelialization model. No ocular reaction was observed on Day 5 for all groups except for one animal treated with 0.1% dexamethasone alone (Group 5), which still displayed a slight conjunctival redness (score 1 on a scale of 0 to 3), a mild chemosis (score 2 on a scale of 0 to 4) associated with a moderate discharge (score 2 on a scale of 0 to 3). Indeed, this animal still exhibited a marked corneal re-epithelialization defect on Day 5 (−42.6%), this having possibly contributed to a persistent ocular reaction.

Corneal Wound Healing. A significant beneficial effect of the 0.1% spironolactone micelles on corneal re-epithelialization was observed from Day 4. The mean percentages of re-epithelialization achieved on Day 4 according to the treatment received are shown in Figure 2.

As expected, re-epithelialization of the wounded corneas treated with 0.1% DXM (Maxidex) was delayed compared to the corneas treated with PBS alone (control). In this model, we expected a two-fold delay in the healing of the wounded corneas treated with 0.1% DXM, compared to control, on Day 2 or 3. This difference was observed on Day 3 with a percentage wounded area of 21.2 ± 9.2% for the animals treated with 0.1% DXM versus 9.3 ± 8.3% for the animals treated with PBS in the control group, which validated the model used in this study (Table S2).

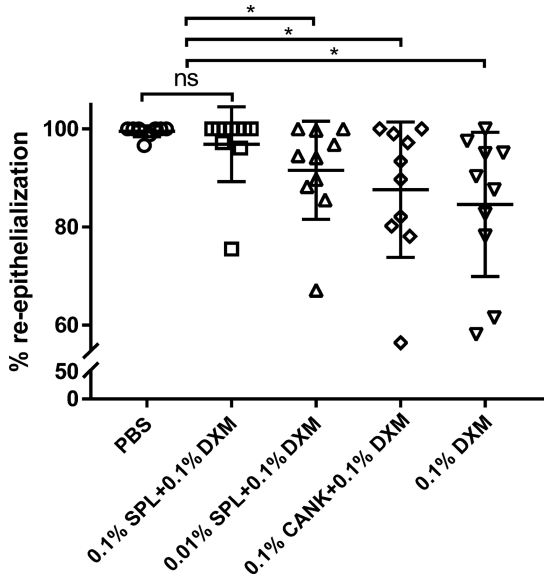

Figure 2. Mean percentage of re-epithelialization of the corneal wounds per treatment group at Day 4. Bars represent means, errors bars represent standard deviation. *P*-values were calculated using Kruskal−Wallis one-way analysis of variance on ranks followed by Student−Newman−Keuls posthoc analysis test; ns, nonsignificant difference ($p > 0.05$); ∗, significant difference ($p < 0.05$). SPL, spironolactone; DXM, dexamethasone; CANK, potassium canrenoate.

After multiple topical administration of 0.1% SPL micelles together with 0.1% DXM, a significant suppression of the dexamethasone-induced corneal delayed wound healing was observed on Day 4 with a mean percentage of re-epithelialization of 96.9 ± 7.3% versus 84.6 ± 13.9% with 0.1% DXM alone ($p < 0.05$). Moreover, the percentage re-epithelialization achieved with coadministration of 0.1% SPL micelles with 0.1% DXM was statistically equivalent ($p > 0.05$) to the positive control (PBS treatment alone, 99.5 ± 1.0%). Thus, 0.1% SPL micelles seemed to completely compensate the negative impact of 0.1% DXM on corneal re-epithelialization (Figure 2).

After multiple topical administrations of 0.01% SPL micelles or 0.1% CANK solution together with 0.1% DXM, a trend toward a reduction in the negative impact of DXM on re-epithelialization was observed. Although the mean extents of re-

Table 5. Ocular Observations of Animals on Day 4[a]

	0.1% SPL micelles + 0.1% DXM	0.01% SPL micelles + 0.1% DXM	0.1% CANK solution + 0.1% DXM	PBS	0.1% DXM
conjunctival redness	*1/3*[c] 1/10	*1/3*[c] 2/10	*1/3*[c] 5/10	[b]	*1/3*[c] 4/10
chemosis	*1/4* 1/10	[b]	[b]	[b]	*2/4* 1/10
discharge	[b]	[b]	*1−2/3* 5/10	[b]	*2/3* 1/10
iritis	[b]	[b]	*1/2*[c] 2/10	[b]	[b]
corneal opacities	[d]	*Intensity: 1/4* *Area: 1−2/4* 4/10	*Intensity: 1−2/4* *Area: 1−4/4* 10/10	*Intensity: 1/4* *Area: 1/4* 5/10	*Intensity: 1/4* *Area: 1/4* 4/10

[a]Score (*italic*) and number of animals concerned. [b]No reaction was observed. [c]Observation of the right treated eye. [d]Corneal opacities were observed but not scored. Conjunctival redness, conjunctival hyperemia; chemosis, swelling of the bulbar conjunctiva; discharge, mucus, pus or excessive tearing from the eye; iritis, inflammation of the iris; corneal opacities, loss of the cornea transparency. Scoring according to the Draize scale. SPL, spironolactone; CANK, potassium canrenoate; DXM, dexamethasone.

DOI: 10.1021/acs.molpharmaceut.7b01028
Mol. Pharmaceutics 2018, 15, 1192−1202

epithelialization of the wounded area observed upon cotreatment with either 0.01% SPL micelles or 0.1% CANK solution remained higher than 0.1% DXM alone at Day 4 (91.6 ± 9.5% and 87.6 ± 13.1%, respectively versus 84.6 ± 13.9%), these differences were not statistically significant ($p > 0.05$). Therefore, in this model and with these study conditions, effects on re-epithelialization of 0.01% SPL micelles and 0.1% CANK solution treatments did not appear as evident as was the case for 0.1% SPL micelles (Figure 2).

Biodistribution and Quantification of Drugs in Cornea. Group 1:0.1% Spironolactone Micelles + 0.1% Dexamethasone (Maxidex). Multiple ocular instillation of 0.1% SPL micelles and 0.1% DXM to the right eyes of 10 animals during 5 days resulted in the detection in the right corneas of spironolactone and its metabolites, 7α-thiomethylspironolactone, and canrenone, with mean concentrations of 7802 ± 4387 ng/g, 114 ± 82 ng/g, and 809 ± 180 ng/g, respectively. Dexamethasone was also detected in the right corneas with a concentration of 3233 ± 2190 ng/g (Figure 3A). Interestingly, SPL and its metabolites were also detected in the left (control) corneas of all the animals instilled with 0.1% SPL micelles and 0.1% DXM with mean concentrations of 7406 ± 3040 ng/g, 95 ± 75 ng/g, and 651 ± 177 ng/g, respectively, for SPL, TMSPL, and CAN. There was no significant difference in their mean concentrations found in the treated corneas compared to the control corneas ($p > 0.05$). However, unlike the aforementioned molecules, DXM was not detected in the left corneas (Figure 3A).

Group 2:0.01% Spironolactone Micelles + 0.1% Dexamethasone (Maxidex). Multiple ocular instillation of 0.01% SPL micelles and 0.1% DXM to the right eyes of 9 animals (according to Grubbs test, rabbit number 18 was an outlier and was then excluded from the data analysis of Group 2) during 5 days resulted in the detection of SPL in the right corneas with a mean concentration of 715 ± 488 ng/g, that is, 10-fold less than the mean concentration found with 0.1% SPL micelles (7802 ± 4387 ng/g, Figure 3B). The metabolites, TMSPL and CAN, were also detected, at concentrations of 36 ± 25 ng/g and 168 ± 57 ng/g, respectively, as was DXM (4542 ± 3428 ng/g). As for the 0.1% SPL formulation, SPL and its metabolites were also detected in the left corneas of all the animals instilled with 0.01% SPL micelles and 0.1% DXM at concentrations of 1148 ± 864 ng/g, 37 ± 19 ng/g, and 122 ± 77 ng/g, respectively, for SPL, TMSPL, and CAN (no significant difference in the mean concentrations found in the treated and control corneas, $p > 0.05$). As for the animals in Group 1, DXM was not detected in the left corneas (Figure 3B).

Group 3:0.1% Potassium Canrenoate Solution + 0.1% Dexamethasone (Maxidex). Multiple ocular instillations of 0.1% CANK solution and 0.1% DXM to the right eyes of 10 animals during 5 days allowed the detection in the right corneas of potassium canrenoate and canrenone at 13 440 ± 6346 ng/g and 8596 ± 3097 ng/g, respectively, whereas dexamethasone was detected at 5004 ± 2376 ng/g (Figure 3C). CANK and CAN were also detected in the left corneas at 1672 ± 739 ng/g and 6349 ± 2379 ng/g, respectively, with a significant difference compared to the right corneas ($p < 0.05$). Unlike in the right corneas, mean concentration of CAN was higher than that of CANK; as for Groups 1 and 2, DXM was not detected in the left corneas (Figure 3C).

Group 4: PBS (Positive Control). No drug was detected in the corneas obtained from the PBS treated animals (Figure S4).

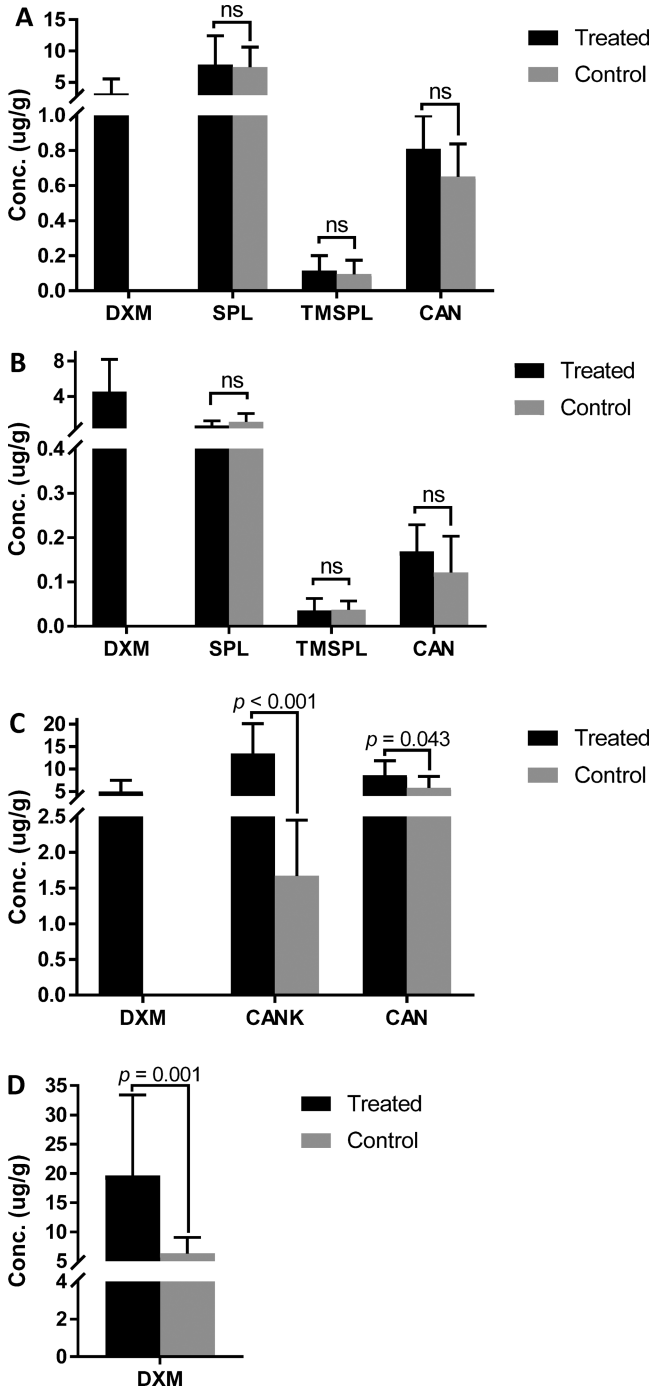

Figure 3. Mean concentrations of the drugs and metabolites found in the right (treated) and left (control) corneas after 5-days multiple instillation of (A) 0.1% spironolactone micelles followed by 0.1% dexamethasone ($n = 10$), (B) 0.01% spironolactone micelles followed by 0.1% dexamethasone ($n = 9$), (C) 0.1% potassium canrenoate solution followed by 0.1% dexamethasone ($n = 10$), and (D) 0.1% dexamethasone ($n = 10$). *P*-values are obtained with Student *t* test; ns, nonsignificant difference ($p > 0.99$). DXM, dexamethasone; SPL, spironolactone; TMSPL, 7α-thiomethyspironolactone; CAN, canrenone; CANK, potassium canrenoate.

Group 5:0.1% Dexamethasone (Maxidex, Negative Control). Multiple ocular instillations of 0.1% DXM to the right eyes of 10 animals during 5 days resulted in the detection of dexamethasone in the right corneas at 19 651 ± 13 032 ng/g. Interestingly, unlike in Groups 1−3, DXM was also detected in

DOI: 10.1021/acs.molpharmaceut.7b01028
Mol. Pharmaceutics 2018, 15, 1192−1202

Table 6. Mean Concentrations of Spironolactone (SPL), 7α-Thiomethyspironolactone (TMSPL), and Canrenone (CAN) Found in Treated Corneas at Day 5 and Their Corresponding Percentage of Re-epithelialization at Day 4, Following Multiple Instillation of 0.1% SPL Micelles (n = 10), 0.01% SPL Micelles (n = 9), or 0.1% Potassium Canrenoate (CANK) Solution (n = 10)

	mean concentration in the treated corneas ± SD (ng/g)			
	SPL	TMSPL	CAN	re-epithelialization ± SD (%)
0.1% SPL micelles	7802 ± 4387	114 ± 82	809 ± 180	96.9 ± 7.3
0.01% SPL micelles	715 ± 488	36 ± 25	168 ± 57	91.6 ± 9.5
0.1% CANK solution	-	-	8596 ± 3097	87.6 ± 13.1

the left corneas at 6337 ± 2603 ng/g (Figure 3D) albeit with a significant difference compared to the right corneas ($p < 0.05$).

Typical chromatograms obtained from the analysis of both corneas from each group are provided in the Supporting Information (Figures S1–S5).

DISCUSSION

The results of the *in vivo* study showed a good tolerability of the 0.1% spironolactone micelles following multiple topical instillation into rabbit eye. More interestingly, 0.1% spironolactone micelles showed a significant beneficial effect on the dexamethasone-induced delayed corneal wound healing.

Comparison of the mean SPL concentrations found in the corneas treated either with 0.1% or 0.01% SPL micelles showed a 10-fold difference (7802 ± 4387 ng/g versus 715 ± 488 ng/g, respectively), which is consistent with the 10-fold difference in the applied dose. These results show that there is a correlation between the applied SPL dose and the amount quantified in the corneas pointing to the controlled delivery of SPL by the micelles. In addition to the quantification of the drugs in the corneas, the biodistribution study provided information on their metabolism in the eye, and to a certain extent, on their mechanism of action. Indeed, multiple topical instillation of spironolactone to the eye resulted in the detection of its two main metabolites, that is, 7α-thiomethylspironolactone and canrenone, confirming the presence of thioesterase and thiol methyltransferase activity in the rabbit eye. The detection of canrenone after multiple topical instillation of potassium canrenoate confirmed the *in situ* conversion of canrenoate to canrenone via lactonization of the γ-hydroxy acid group and so confirming the presence of paraoxonase enzyme (PON) in the rabbit eye.

Mineralocorticoid Receptor Antagonists Improved Re-epithelialization. Table 6 summarizes the mean concentrations of SPL, TMSPL, and CAN found in the right (treated) corneas following multiple topical instillation of 0.1% SPL micelles, 0.01% SPL micelles, or 0.1% CANK solution and their corresponding mean percentage of re-epithelialization. The mean percentage of re-epithelialization obtained with 0.1% SPL micelles was superior and significantly different from that obtained with 0.01% SPL micelles and 0.1% CANK solution ($p < 0.05$); however, there was no significant difference in the mean percentage of re-epithelialization obtained between the latter two groups ($p > 0.05$). The highest CAN concentration level was found in the corneas treated with 0.1% CANK solution; however, these corneas had the lowest percentage of re-epithelialization, suggesting that CAN is not the main metabolite involved in the mineralocorticoid receptor antagonism. The mean percentages of re-epithelialization achieved with 0.1% and 0.01% SPL micelles were higher, supporting the higher potency of TMSPL over CAN as a mineralocorticoid receptor antagonist and evidencing its ability to counter-act the GC side effects and thus improve wound healing.

These findings are consistent with previously published data where (i) Corvol et al.[28] pointed out the importance of the C_7 side chain for MR antagonism and reported a 10-fold lower affinity of CAN for the MR as compared to SPL (and its sulfur-containing metabolite, TMSPL), and a very low affinity of CANK for the MR since the negative charge of the carboxylate hinders binding to the receptor as there is no compensatory positive charge in the vicinity; (ii) Sutanto et al.[29] reported the higher potency of SPL as compared to CANK in terms of MR antagonism with half maximal inhibitory concentrations (IC_{50}) of 4.9 nM and >1000 nM, respectively.

Detection of Drugs and Their Metabolites in Contralateral Eye. During this study, animals received the different treatments only in their right eye, the contralateral (control) eye was kept as a control. Interestingly, after multiple instillation of the different treatments, SPL, CANK, and their metabolites were detected in the control corneas of all the treated animals. More interestingly, DXM was only detected in the control corneas of the animals that did not receive any MR antagonist (Group 5).

It has been reported that unilateral ocular drug administration leads to its detection in the contralateral eye,[30−33] and this was explained in two different ways. The first involves a local nonhematogenous route where a direct passage from one eye to another can occur, especially in rats and lagomorphs, by interorbital communication either via lymphatic spread or via the lacrimal duct system with retrograde flow into the uninstilled eye.[31] Indeed, a previous study confirmed, clinically and histologically, the conjunctival cross-transfer of an antigen in rabbits using labeled human serum albumin.[32] In another study, iontophoresis of glucocorticoids into rat eyes resulted in the observation of GC effects in the contralateral eye at levels much higher than those deemed compatible with systemic passage.[33] The second explanation involves the hematogenous route, which involves the return of the drug to the eyes through the general circulation. Indeed, after topical instillation of a drug, there are two main pathways of entry into the anterior segment: (i) across the cornea and (ii) across the conjunctiva. When the drug is crossing the conjunctiva, a fraction of the drug will be lost into the conjunctival blood circulation and the rest will diffuse into the sclera before reaching the heavily vascularized choroid, where another part is also cleared into the general circulation. The possibility of external contact transfer of the molecules from one eye to another with the rabbit paw was excluded regarding the equivalent concentrations of SPL and its metabolites found in both eyes in all the animals.

Another interesting observation was the comparison between the concentrations found in the treated eye versus the contralateral eye following the different treatments and molecules administered. Indeed, in Group 1 and 2,

DOI: 10.1021/acs.molpharmaceut.7b01028
Mol. Pharmaceutics 2018, 15, 1192−1202

concentrations of SPL, TMSPL, and CAN in the treated and control corneas were statistically equivalent; however, DXM was only detected in the treated corneas. In Group 3, concentrations of CANK and CAN in the treated and control corneas were statistically different (13.44 ± 6.35 μg/g vs 1.67 ± 0.74 μg/g and 8.60 ± 3.10 μg/g vs 5.84 ± 2.38 μg/g for CANK and CAN, respectively; Student *t* test). It should be noted that the mean concentration of CANK is higher than CAN in the treated eye, whereas the opposite is the case for the contralateral eye. CANK once administered is available in the body as canrenoic acid, which is in equilibrium with its metabolite, canrenone. Indeed, the γ-hydroxy acid on the C_{17} of CANK is converted by cyclization to the γ-lactone present in CAN by the paraoxonase enzyme (PON). Our findings confirm the presence of PON in the rabbit eye; however, the higher mean concentration of CAN compared to CANK found in the contralateral eye suggests that PON in the plasma or other tissues play a significant role in the biotransformation of CANK to CAN, resulting in the higher levels of CAN found in the contralateral eye. As in Group 1 and 2, DXM was only detected in the treated corneas of Group 3.

Mineralocorticoid Receptor Antagonists Prevented Dexamethasone Binding to MR. In Group 5, unlike in Groups 1−3, DXM was detected in both the treated and control corneas, although levels in the control corneas were significantly lower (p = 0.001). Interestingly, DXM mean concentration in the treated corneas was found to be at least four-fold higher in the absence of any MR antagonist (19.65 ± 13.03 μg/g vs 3.23 ± 2.19 μg/g, 4.54 ± 3.43 μg/g, and 5.00 ± 2.38 μg/g for Group 5, 1, 2, and 3, respectively). These findings demonstrate that DXM binding to the MR was prevented by the presence of a MR antagonist (SPL, TMSPL, CAN, or CANK). This can be explained by the saturation of MR by the MR antagonist (SPL, TMSPL, CAN, or CANK) in Groups 1−3, leading to a lower occupancy of the MR by DXM, which is consequently quickly eliminated given its relative short plasma half-life (estimated at 1.9 h in rabbit cf. 1.4, 13.8, and 16.5 h, respectively, for SPL, TMSPL, and CAN).[34−36] Moreover, Rafestin-Oblin et al.[37,38] reported a higher affinity of SPL to MR (K_d = 3.6 nM) compared to DXM (K_d = 10 nM) and Stokes et al.[39] reported that the MR concentration in the human corneal epithelium and endothelium is three-times higher than the GR concentration. Given the above, the four-fold higher DXM concentrations found in the treated corneas and its detection only in the contralateral corneas of the animals in Group 5 might be explained by the fact that in this case, there was no competition to bind to MR since there were no MR antagonists. Thus, the mean DXM concentration found in Group 5 was the sum of DXM bound to GR and to MR, whereas the mean concentrations found in Group 1, 2, and 3 corresponded to the unique fraction of DXM bound to GR. These findings confirm (i) the increased off-target occupancy of MR by DXM in the absence of a MR antagonist and (ii) the resulting delayed wound healing when considering the percentage of re-epithelialization obtained with Group 5. Finally, the results support the rationale of using MR antagonist coadministration in conjunction with a prolonged GC therapy to prevent the delayed wound healing side-effects associated with GC.

In future studies, blood samples will also be taken to quantify the systemic exposure following a topical administration to better understand the roles of hematogenous and non-hematogenous drug transport to the contralateral eye.

CONCLUSION

A stable spironolactone micellar formulation (0.1%, w/v) for topical administration was developed and tested in New Zealand white rabbits *in vivo* with respect to tolerability and efficacy in a corneal wound healing model. The formulation was safe and showed beneficial effects on corneal wound management, that is, the use of spironolactone micelles countered the delayed wound healing caused by the glucocorticoid therapy. This is the first study showing that MR antagonism can efficiently prevent the glucocorticoid-induced delay in corneal wound re-epithelialization, providing evidence that MR activation by glucocorticoids prevents corneal epithelial growth, differentiation or migration.

Mineralocorticoid receptor antagonism may exert beneficial effects through modulation of several mechanisms known to be induced by mineralocorticoid receptor activation such as activation of monocyte/macrophage and polymorphonuclear leukocyte as well as expression of metalloproteinases and pro-fibrotic molecules.[11,17,40] Mineralocorticoid receptors could also directly influence the expression of ion channels such as ENAC and therefore influence epithelial cell migration.[41] Additional studies are required to better dissect the exact mechanisms of the effects we have observed *in vivo*.

Successful translation of these preclinical results to the clinic could improve therapeutic outcomes for glucocorticoid-treated patients since topical instillation of the spironolactone micelles might counter the impaired wound healing associated with routine glucocorticoid therapy.

ASSOCIATED CONTENT

Supporting Information

The Supporting Information is available free of charge on the ACS Publications website at DOI: 10.1021/acs.molpharmaceut.7b01028.

Description of ocular tolerance evaluation, corneal re-epithelialization over time, and chromatograms obtained from analysis of corneas (PDF)

AUTHOR INFORMATION

Corresponding Author

*E-mail: Yogi.Kalia@unige.ch. Phone: +41 22 379 3355. Fax: +41 22 379 3360.

ORCID

Yogeshvar N. Kalia: 0000-0001-9049-5489

Notes

The authors declare no competing financial interest.

ACKNOWLEDGMENTS

N.D. and Y.N.K. acknowledge financial support from the Swiss Commission for Technology and Innovation (CTI Project 19086.1 PFLS-LS) and Apidel SA (Geneva, Switzerland). We also acknowledge the support from CEVA Animal Health (Libourne, France) for the *in vivo* study. Y.N.K. would like to thank the University of Geneva, the Fondation Ernst, and Lucie Schmidheiny and the Société Académique de Genève for providing financial support to enable the acquisition of the Waters Xevo TQ-MS detector.

ABBREVIATIONS

CAN, canrenone; CANK, potassium canrenoate; DXM, dexamethasone; GC, glucocorticoid; GR, glucocorticoid

DOI: 10.1021/acs.molpharmaceut.7b01028
Mol. Pharmaceutics 2018, 15, 1192−1202

receptor; MC, mineralocorticoid; mPEG-dihexPLA, methoxy-poly(ethylene glycol)-dihexyl-substituted-poly(lactic acid); MR, mineralocorticoid receptor; MRA, mineralocorticoid receptor antagonist; PBS, phosphate-buffered saline; SPL, spironolactone; TEM, transmission electron microscopy; TMSPL, 7α-thiomethylspironolactone; UHPLC−MS, ultra-high performance liquid chromatography−tandem mass spectroscopy

REFERENCES

(1) Werner, S.; Grose, R. Regulation of wound healing by growth factors and cytokines. *Physiol. Rev.* **2003**, *83* (3), 835−70.

(2) Nguyen, V. T.; Farman, N.; Maubec, E.; Nassar, D.; Desposito, D.; Waeckel, L.; Aractingi, S.; Jaisser, F. Re-epithelialization of pathological cutaneous wounds is improved by local mineralocorticoid receptor antagonism. *J. Invest. Dermatol.* **2016**, *136* (10), 2080−9.

(3) Park, S. C.; Kim, J. H. Effect of steroids and nonsteroidal anti-inflammatory agents on stromal wound healing following excimer laser keratectomy in rabbits. *Ophthalmic Surg. Lasers* **1996**, *27*, S481−6.

(4) Srinivasan, M.; Lalitha, P.; Mahalakshmi, R.; Prajna, N. V.; Mascarenhas, J.; Chidambaram, J. D.; Lee, S.; Hong, K. C.; Zegans, M.; Glidden, D. V.; McLeod, S.; Whitcher, J. P.; Lietman, T. M.; Acharya, N. R. Corticosteroids for bacterial corneal ulcers. *Br. J. Ophthalmol.* **2009**, *93* (2), 198−202.

(5) Adams, S.; Valchanova, R. S.; Munz, B. RIP2: a novel player in the regulation of keratinocyte proliferation and cutaneous wound repair? *Exp. Cell Res.* **2010**, *316* (5), 728−36.

(6) Liu, M.; Saeki, K.; Matsunobu, T.; Okuno, T.; Koga, T.; Sugimoto, Y.; Yokoyama, C.; Nakamizo, S.; Kabashima, K.; Narumiya, S.; Shimizu, T.; Yokomizo, T. 12-Hydroxyheptadecatrienoic acid promotes epidermal wound healing by accelerating keratinocyte migration via the BLT2 receptor. *J. Exp. Med.* **2014**, *211* (6), 1063−78.

(7) Kadmiel, M.; Janoshazi, A.; Xu, X.; Cidlowski, J. A. Glucocorticoid action in human corneal epithelial cells establishes roles for corticosteroids in wound healing and barrier function of the eye. *Exp. Eye Res.* **2016**, *152*, 10−33.

(8) Hashizume, N.; Saika, S.; Okada, Y.; Miyamoto, T.; Shimizu, K.; Ohnishi, Y. Effects of antiinflammatory drugs on migration of the rabbit corneal epithelium. *J. Cataract Refractive Surg.* **2001**, *27* (9), 1499−502.

(9) Maubec, E.; Laouenan, C.; Deschamps, L.; Nguyen, V. T.; Scheer-Senyarich, I.; Wackenheim-Jacobs, A. C.; Steff, M.; Duhamel, S.; Tubiana, S.; Brahimi, N.; Leclerc-Mercier, S.; Crickx, B.; Perret, C.; Aractingi, S.; Escoubet, B.; Duval, X.; Arnaud, P.; Jaisser, F.; Mentre, F.; Farman, N. Topical mineralocorticoid receptor blockade limits glucocorticoid-induced epidermal atrophy in human skin. *J. Invest. Dermatol.* **2015**, *135* (7), 1781−9.

(10) Sarchahi, A. A.; Maimandi, A.; Tafti, A. K.; Amani, M. Effects of acetylcysteine and dexamethasone on experimental corneal wounds in rabbits. *Ophthalmic Res.* **2007**, *40* (1), 41−8.

(11) De Paiva, C. S.; Corrales, R. M.; Villarreal, A. L.; Farley, W. J.; Li, D. Q.; Stern, M. E.; Pflugfelder, S. C. Corticosteroid and doxycycline suppress MMP-9 and inflammatory cytokine expression, MAPK activation in the corneal epithelium in experimental dry eye. *Exp. Eye Res.* **2006**, *83* (3), 526−35.

(12) Stojadinovic, O.; Lindley, L. E.; Jozic, I.; Tomic-Canic, M. Mineralocorticoid Receptor Antagonists-A New Sprinkle of Salt and Youth. *J. Invest. Dermatol.* **2016**, *136* (10), 1938−41.

(13) Petroutsos, G.; Guimaraes, R.; Giraud, J. P.; Pouliquen, Y. Corticosteroids and corneal epithelial wound healing. *Br. J. Ophthalmol.* **1982**, *66* (11), 705−8.

(14) Fagerholm, P. Wound healing after photorefractive keratectomy. *J. Cataract Refractive Surg.* **2000**, *26* (3), 432−47.

(15) Wang, A. S.; Armstrong, E. J.; Armstrong, A. W. Corticosteroids and wound healing: clinical considerations in the perioperative period. *Am. J. Surg.* **2013**, *206* (3), 410−7.

(16) Youm, J. K.; Park, K.; Uchida, Y.; Chan, A.; Mauro, T. M.; Holleran, W. M.; Elias, P. M. Local blockade of glucocorticoid activation reverses stress- and glucocorticoid-induced delays in cutaneous wound healing. *Wound Repair Regen.* **2013**, *21* (5), 715−22.

(17) Farman, N.; Nguyen, V. T. A novel actor in skin biology: the mineralocorticoid receptor. *Exp. Dermatol.* **2016**, *25* (1), 24−5.

(18) Boix, J.; Sevilla, L. M.; Saez, Z.; Carceller, E.; Perez, P. Epidermal mineralocorticoid receptor plays beneficial and adverse effects in skin and mediates glucocorticoid responses. *J. Invest. Dermatol.* **2016**, *136*, 2417.

(19) Sica, D. A. Pharmacokinetics and pharmacodynamics of mineralocorticoid blocking agents and their effects on potassium homeostasis. *Heart Failure Rev.* **2005**, *10* (1), 23−9.

(20) Ferrario, C. M.; Schiffrin, E. L. Role of mineralocorticoid receptor antagonists in cardiovascular disease. *Circ. Res.* **2015**, *116* (1), 206−13.

(21) Dong, H.; Xu, F.; Zhang, Z.; Tian, Y.; Chen, Y. Simultaneous determination of spironolactone and its active metabolite canrenone in human plasma by HPLC-APCI-MS. *J. Mass Spectrom.* **2006**, *41* (4), 477−86.

(22) Sandall, J. M.; Millership, J. S.; Collier, P. S.; McElnay, J. C. Development and validation of an HPLC method for the determination of spironolactone and its metabolites in paediatric plasma samples. *J. Chromatogr. B: Anal. Technol. Biomed. Life Sci.* **2006**, *839* (1−2), 36−44.

(23) Kaukonen, A. M.; Vuorela, P.; Vuorela, H.; Mannermaa, J. P. High-performance liquid chromatography methods for the separation and quantitation of spironolactone and its degradation products in aqueous formulations and of its metabolites in rat serum. *J. Chromatogr. A* **1998**, *797* (1−2), 271−81.

(24) Di Tommaso, C.; Bourges, J. L.; Valamanesh, F.; Trubitsyn, G.; Torriglia, A.; Jeanny, J. C.; Behar-Cohen, F.; Gurny, R.; Moller, M. Novel micelle carriers for cyclosporin A topical ocular delivery: in vivo cornea penetration, ocular distribution and efficacy studies. *Eur. J. Pharm. Biopharm.* **2012**, *81* (2), 257−64.

(25) Di Tommaso, C.; Torriglia, A.; Furrer, P.; Behar-Cohen, F.; Gurny, R.; Moller, M. Ocular biocompatibility of novel Cyclosporin A formulations based on methoxy poly(ethylene glycol)-hexylsubstituted poly(lactide) micelle carriers. *Int. J. Pharm.* **2011**, *416* (2), 515−24.

(26) Di Tommaso, C.; Valamanesh, F.; Miller, F.; Furrer, P.; Rodriguez-Aller, M.; Behar-Cohen, F.; Gurny, R.; Moller, M. A novel cyclosporin a aqueous formulation for dry eye treatment: in vitro and in vivo evaluation. *Invest. Ophthalmol. Visual Sci.* **2012**, *53* (4), 2292−9.

(27) Trimaille, T.; Mondon, K.; Gurny, R.; Moller, M. Novel polymeric micelles for hydrophobic drug delivery based on biodegradable poly(hexyl-substituted lactides). *Int. J. Pharm.* **2006**, *319* (1−2), 147−54.

(28) Corvol, P.; Claire, M.; Oblin, M. E.; Geering, K.; Rossier, B. Mechanism of the antimineralocorticoid effects of spirolactones. *Kidney Int.* **1981**, *20* (1), 1−6.

(29) Sutanto, W.; de Kloet, E. R. Mineralocorticoid receptor ligands: biochemical, pharmacological, and clinical aspects. *Med. Res. Rev.* **1991**, *11* (6), 617−39.

(30) Maurice, D. M.; Mishima, S. Ocular Pharmacokinetics. In *Pharmacology of the Eye*; Sears, M. L., Ed.; Springer Berlin Heidelberg: Berlin, Heidelberg, 1984; pp 19−116.

(31) Jensen, P. R.; Aronson, S. B.; Pollycove, M.; Yamamoto, E. Mechanisms of host response in the eye. 3. Interocular protein transfer. *Arch. Ophthalmol.* **1967**, *77* (6), 814−7.

(32) Jensen, P.; Pollycove, M.; Aronso, S. B.; Yamamoto, E. Radioisotopic measurements of protein transfer between the eyes. *Invest. Ophthalmol. Vis. Sci.* **1964**, *3* (6), 676.

(33) Behar-Cohen, F.; Parel, J. M.; Pouliquen, Y.; Thillaye-Goldenberg, B.; Goureau, O.; Heydolph, S.; Courtois, Y.; De Kozak, Y. Iontophoresis of dexamethasone in the treatment of endotoxin-induced-uveitis in rats. *Exp. Eye Res.* **1997**, *65* (4), 533−45.

(34) Stokes, P. E.; Stoll, P. M.; Schluger, J. H.; Lasley, B. Hypercortisolemia decreases dexamethasone half-life in rabbit. *J. Psychiatr. Res.* **2002**, *36* (6), 423−8.

DOI: 10.1021/acs.molpharmaceut.7b01028
Mol. Pharmaceutics 2018, 15, 1192−1202

(35) Maron, B. A.; Leopold, J. A. Mineralocorticoid receptor antagonists and endothelial function. *Curr. Opin Investig. Drugs* **2008**, *9* (9), 963−9.
(36) Beyer, J.; Bierl, A.; Peters, F. T.; Maurer, H. H. Screening procedure for detection of diuretics and uricosurics and/or their metabolites in human urine using gas chromatography-mass spectrometry after extractive methylation. *Ther. Drug Monit.* **2005**, *27* (4), 509−20.
(37) Rafestin-Oblin, M. E.; Lombes, M.; Couette, B.; Baulieu, E. E. Differences between aldosterone and its antagonists in binding kinetics and ligand-induced hsp90 release from mineralocorticosteroid receptor. *J. Steroid Biochem. Mol. Biol.* **1992**, *41* (3−8), 815−21.
(38) Rafestin-Oblin, M. E.; Lombes, M.; Lustenberger, P.; Blanchardie, P.; Michaud, A.; Cornu, G.; Claire, M. Affinity of corticosteroids for mineralocorticoid and glucocorticoid receptors of the rabbit kidney: effect of steroid substitution. *J. Steroid Biochem.* **1986**, *25* (4), 527−34.
(39) Stokes, J.; Noble, J.; Brett, L.; Phillips, C.; Seckl, J. R.; O'Brien, C.; Andrew, R. Distribution of glucocorticoid and mineralocorticoid receptors and 11beta-hydroxysteroid dehydrogenases in human and rat ocular tissues. *Invest. Ophthalmol. Vis. Sci.* **2000**, *41* (7), 1629−38.
(40) Jaisser, F.; Farman, N. Emerging Roles of the Mineralocorticoid Receptor in Pathology: Toward New Paradigms in Clinical Pharmacology. *Pharmacol. Rev.* **2016**, *68* (1), 49−75.
(41) Yang, H. Y.; Charles, R. P.; Hummler, E.; Baines, D. L.; Isseroff, R. R. The epithelial sodium channel mediates the directionality of galvanotaxis in human keratinocytes. *J. Cell Sci.* **2013**, *126* (9), 1942−51.

DOI: 10.1021/acs.molpharmaceut.7b01028
Mol. Pharmaceutics 2018, 15, 1192−1202

PRESENTATIONS

1. Oral presentations

Controlled release polymer for ocular intravitreal delivery of spironolactone: *in vitro* characterization and *in vivo* tolerance in rats. Naoual Dahmana, Laura Kowalczuk, Doris Gabriel, Francine Behar-Cohen, Robert Gurny, Yogeshvar N. Kalia.

4th Conference on Innovation in Drug Delivery: site specific drug delivery – Nice (France) – 2016.

Topical delivery of spironolactone nanocarriers prevents dexamethasone-induced delayed corneal wound healing. Naoual Dahmana, Thibault Mugnier, Doris Gabriel, Vassilios Kaltsatos, Thierry Bertaim, Francine Behar-Cohen, Robert Gurny, Yogeshvar N. Kalia.

11th World Meeting on Pharmaceutics, Biopharmaceutics and Pharmaceutical Technology – Granada (Spain) – 2018.

2. Poster presentations

Development of micellar formulations of spironolactone for topical treatment of eye diseases - Naoual Dahmana, Doris Gabriel, Laura Kowalczuk, Francine Behar-Cohen, Robert Gurny, Yogeshvar N. Kalia.

ISOPT Clinical – Berlin (Germany) – 2015.

Targeted nanocarrier-mediated ocular delivery of spironolactone to improve corneal wound healing: Demonstrating tolerability and efficacy in New Zealand rabbits. Naoual Dahmana, Thibault Mugnier, Doris Gabriel, Vassilios Kaltsatos, Thierry Bertaim, Francine Behar-Cohen, Robert Gurny, Yogeshvar N. Kalia.

European Nanomedicine Meeting – London (United Kingdom) – 2017.

Targeted nanocarrier-mediated ocular delivery of spironolactone to improve corneal wound healing: Demonstrating tolerability and efficacy in New Zealand rabbits. Naoual Dahmana, Thibault Mugnier, Doris Gabriel, Vassilios Kaltsatos, Thierry Bertaim, Francine Behar-Cohen, Robert Gurny, Yogeshvar N. Kalia.

Swiss Science Pharma Day – Bern (Switzerland) – 2017.

Targeted delivery of spironolactone loaded nanomicelles to the pilosebaceous unit for the treatment of cutaneous delayed wound healing. Naoual Dahmana, Thibault Mugnier, Doris Gabriel, Tatiana Favez, Francine Behar-Cohen, Robert Gurny, Yogeshvar N. Kalia.

11th World Meeting on Pharmaceutics, Biopharmaceutics and Pharmaceutical Technology – Granada (Spain) – 2018.

REMERCIEMENTS

J’adresse ma profonde gratitude à mon directeur de thèse, Prof. Yogeshvar N. Kalia, pour avoir supervisé ce travail, de m’avoir accueillie dans son équipe et de m’avoir permis d’effectuer mon doctorat dans d’aussi bonnes conditions. Yogi, merci pour votre disponibilité permanente et vos discussions et critiques scientifiques ; vous m’avez poussé à donner le meilleur de moi-même. Merci également de m’avoir permis de participer à des conférences internationales aussi intéressantes.

Je souhaiterais aussi adresser mes remerciements les plus chaleureux au Prof. Robert Gurny, sans qui ce projet n’aurait pas vu le jour. Robert, merci d’avoir cru en moi et de m’avoir fait confiance. Merci de m’avoir donné l’opportunité de travailler avec des collaborations aussi enrichissantes, de m’avoir challengé pour donner le meilleur de moi-même et de m’avoir transmis votre passion pour les sciences pharmaceutiques. Merci pour votre disponibilité permanente et votre soutien sans faille.

Je tiens aussi à remercier Prof. Francine Behar-Cohen de m’avoir accueillie dans son laboratoire à l’Hôpital ophtalmique Jules-Gonin, de m’avoir permis d’y effectuer des expériences enrichissantes et pour sa contribution clinique.

Je remercie également les membres du jury (par ordre alphabétique) ; Prof. Eric Allémann, Dr. Grégoire Schwach et Prof. Bernard Verrier d’avoir accepté d’évaluer mon travail de thèse.

J’aimerais aussi exprimer mes remerciements les plus sincères à mes collègues avec qui j’ai travaillé en étroite collaboration, pour leur contribution inestimable à ce projet. Doris, merci pour ton aide au labo et ton enthousiasme permanent ; Laura, merci pour ton aide précieuse avec les études *in vivo* et ta pêche d’enfer ! Thibault merci pour ton aide avec les micelles et les fous rires au labo. Hervé, merci pour ton aide technique précieuse.

Je remercie également l'équipe du laboratoire d'histopathologie et de l'unité de thérapie génique et de biologie des cellules souches de la Fondation Asile des aveugles en particulier Helga Motta, Catherine Martin et Tatiana Favez pour leur soutien technique.

Je remercie la Commission Suisse pour la Technologie et l'Innovation (CTI) pour le soutien financier et CEVA Santé Animale (Libourne, France) pour avoir contribué aux études précliniques.

Je remercie aussi Prof. Eric Allémann de m’avoir donné accès aux instruments du département Technologie pharmaceutique, ainsi que Dr. Christoph Bauer et Jérôme Bosset du Centre de bio-imagerie de l'Université de Genève pour leur aide précieuse en microscopie.

Je tiens aussi à remercier vivement mes collègues de l'Ecole de Pharmacie de l'Université de Genève, notamment les membres et ex-membres du groupe FAPER. Julie, merci pour ton amitié, ton soutien infaillible et les fous rires partagés ! César, merci pour ton aide précieuse avec les appareils analytiques et ton bel esprit d'équipe ; Maria, merci pour ton aide avec les expériences avec la peau et ton esprit créatif. Un grand merci à toute l'équipe : Vasundhara, Gisela, Si, Mayank, Somnath, Verena, Yvonne, Jonathan, Aditya, Maria Sebastian mais aussi l'équipe FABIP notamment Elinam, Francesca et Hesham ; pour ces belles années passées ensemble. Merci à tous de m'avoir aidé, de près ou de loin, et d'avoir créé un environnement de travail aussi agréable ; c'était un plaisir de venir travailler chaque matin et de partager des bons moments ensemble en dehors du labo. Je n'oublierai pas les éclats de rires qu'on échangeait pendant les pauses café.

Je remercie également mes collègues d'Apidel SA qui ont beaucoup contribué pour que ce projet voie le jour ; un grand merci à Alan, Victoria et Vitalia.

Enfin, je n'aurais pas pu accomplir cette thèse sans l'aide et le soutien de mes amies et de ma famille ; un grand merci à Lydia, Margarita, Nawal et Linda qui ont toujours su trouver les mots pour me donner la force quand j'en avais le plus besoin.